ALLFORSK AVH
Department of Physics
N-7055 Dragvoll, NORWAY

THE MARITIME TURBULENT WIND FIELD MEASUREMENTS AND MODELS

Final report for the Statoil Joint Industry Project

Contract No. 7916
Project No. 209 ALLFORSK-AVH

Project coordinator:

Odd Jan Andersen, Statoil, IGT
Stavanger, NORWAY

Executed by:

Tore Heggem, Jørgen Løvseth,
Knut Mollestad and Svein Erik Aasen
Department of Physics and ALLFORSK
University of Trondheim

Odd Jan Andersen
Statoil, IGT

Work sponsored by

**Amoco Norway Oil Company - Conoco Norway Inc. - Elf Aquitaine Norge A/S
Exxon Production Research Company - A/S Norske Shell - Norsk Hydro
Saga Petroleum A/S**

April 1991

TABLE OF CONTENTS

EXECUTIVE SUMMARY

EXECUTIVE SUMMARY

Data basis

The report summarizes results from analysis of multilevel wind and air/sea temperature data recorded with sampling rate 0.85 Hz at two sites of very good exposure to maritime wind:

- Sletringen: One 45 m mast at islet (max terrain height 4 m).
  Period: March 1988 - May 1989 (Phases 1 and 2);
- Skipheia: Three masts (100. 100 and 45 m) landbased on western Frøya.
  Period: November 1988 - May 1989 (Phase 2).

Data quality

Data quality has been assured by:

- Careful calibration of the sensors before the measurements and maintenance of the sensors and measurement system during the measurement period;
- Careful mounting of the sensors 2 - 2.5 m from the mast (towards W at Sletringen) to avoid mast distortion;
- Doubling of wind speed sensors at each height at Skipheia and automatic choice of upwind sensor to avoid mast distortion;
- Daily datacontrol during the measurement period;
- Control of the distributions against the raw data to identify measurement errors.

Data recovery and wind conditions

During the Phase 2 period several hurricanes and severe lightening reduced the data recovery:

- Sletringen: 68%
- Skipheia: 76%

Strong winds (> 15 m/s) were maritime. mainly confined to the sector S - W. Reference wind speeds (10 m. 1 h) were less than 20 m/s during Phase 1 and exceeded 20 m/s for 35 cases during Phase 2.

Lapse rate ranged from strongly stable to:

- Strongly unstable during Phase 1;
- Slightly unstable during Phase 2.

Non-neutral conditions were found to prevail even for strong winds.

Data sets

Based on plots of reference wind speed, wind direction and lapse rate, 3 data sets were defined for strong wind speeds ($>$ 15 m/s):

- Quasi-stationary (QS);
- Partially quasi-stationary (PQS);
- Full data set (FD).

Data analysis

The data were analyzed according to the assumptions that

- The boundary layer structure is determined by the 2 independent 1 h mean quantities
  - reference wind speed;
  - lapse rate or air-sea temperature difference.

- The turbulent timeseries is adequatly described as the original timeseries subject to removal of the 1 h moving average timeseries. This definition of turbulence implies
  - eliminated synoptic energy;
  - modulated mesoscale (1.5 h to 15 min) energy;
  - conserved high frequency energy ($<$ 13 min).

Thus, the dynamic maritime wind field description is significant for wind fluctuations with period less than 13 min only.

Also, for the analysis, the basic input to the parameterization process was plots of the mean and standard-deviation of the quantities in question versus

- Lapse rate for classes of reference wind speed;
- Reference wind speed for classes of lapse rate.

The calculation of local Richardson number or Monin-Obukhov length scale from experimental data may imply some numerical instability problems. Even so, a local Richardson number formulation was investigated as an alternative to lapse rate.

The static maritime boundary layer

The 1 h mean profiles

1. The thermal structure at Skipheia is more complex and quite different from the more well-defined structure at Sletringen.
2. Lapse rate is necessary to give a good description of the structure of the static maritime wind field. Air-sea temperature difference can be used as a good alternative.
3. The wind speed profile is better described by a logarithmic than by a power law. The logarithmic description is independent of data set (QS, PQS, FD).
4. Although Richardson number and lapse rate are equally good in describing the QS og PQS data sets, the results indicate that the Richardson number is less useful for the FD data set.
5. For SW winds, the wind speed profiles are essentially equal at Sletringen and Skipheia. Thus, the Sletringen description can be assumed valid up to 100 m.
6. For heights above 10 m, the wind speed gradient
   - Is relatively large for stable conditions;
   - Decreases significantly with lapse rate for near neutral conditions;
   - Is relatively small for unstable conditions;
   - Increases with reference wind speed, particularly for unstable conditions.
7. For the highest refence wind speeds (> 26 m/s), the wind speed gradient differs from that observed for lower wind speeds. This increases the uncertainty when extrapolating the results to design reference wind speed conditions.
8. The NPD recommendation for the 1 h mean wind speed profile is slightly conservative compared to the present results. The difference between the two seems to decrease with reference wind speed (note, however, the above (7) extrapolation problem).

Reference gusts

The following conclusions apply to gust durations in the range 1 sec. to 10 min.:

1. The mean gust description is the same for the QS, PQS and FD data sets and can be extrapolated to design reference wind speed conditions.
2. The mean gust is independent of lapse rate.
3. Short gusts increase more slowly with height than the longer ones.
4. The NPD recommendation significantly overestimates mean gusts for heights above 20 - 30 m and underestimates slightly the gusts below these levels.

5. The gust distribution is Gaussian up to moderate gust values. For larger gust values the distribution falls off exponentially at a rate more slowly than the Gaussian distribution.
6. The gust distribution depends strongly on lapse rate.
7. Extrapolation to design reference wind speed conditions is not recommended for the gust distribution parameters.

Turbulence intensity

1. Turbulence intensity varies with height according to a power law with exponent - 0.22.
2. For reference wind speeds exceeding 18 m/s the turbulence intensity increases slowly with reference wind speed and is independent of lapse rate.
3. For less than gale force reference wind speeds the turbulence intensity increases with lapse rate and combines the NPD recommendation and results from British sector (West Sole) in the limits of strongly unstable and stable conditions, respectively.
4. The description of the mean turbulence intensity is independent of data set (QS, PQS. FD).
5. On normal paper the cumulative distribution of turbulence intensity is represented by two straight lines. The clockwise angle between the two branches of this curve decreases with reference wind speed and increases with lapse rate and height.
6. More data are needed to firmly establish the distribution parameters for turbulence intensity and their functional dependence on reference wind speed, lapse rate and height.

Wind direction fluctuations

1. Typically. the wind direction for maritime wind is very stable with fluctuations of the order 5 - 10°. Large changes reflect the passage of synoptic pressure systems. The most dramatic observed change of the mean wind direction was 85° in 100 s for gale force wind.
2. The 1 h maximum of the mean wind direction fluctuation for some subperiod is denoted the wind direction gust for that subperiod. The frequency distribution of these gusts is found to be asymmetric with a tail towards large gust values. The cumulative distribution is characterized by
   - A wind speed independent median value of some 5° for a 10 min subperiod increasing to 15° for 3.5 s;
   - Approximate representation by separate error functions below and above the median point with corresponding standard deviations of 1.5° and 9°.

3. The distribution of the standard deviation of the wind direction fluctuations is similar to the distribution described above (2). The cumulative distribution is characterized by
   - a median value of some 5^{o} which increases from stable to unstable conditions;
   - separate error function behaviour below and above the median point with the corresponding standard deviations being 1^{o} and 4^{o}.

The dynamic maritime windfield

1. The analysis of both one point turbulence spectra and two point coherence and phase spectra were based on ensemble averaging in intervals of reference wind speed, lapse rate, frequency, height and wind direction (for coherence and phase for horisontal separation).
2. During the process of fitting algebraic expressions to the observed spectra, a weight function is adopted with the properties of being
   - Independent of lapse rate;
   - Zero for frequencies below 1/(10 min);
   - Effectively reduced for frequencies higher than 0.065 Hz in order to reduce high frequency influence on the spectral parameter estimates.

One point turbulence spectra

1. The basic functional form adopted for the spectral function represents a slight generalization relative to most forms found in literature.
2. The recommended spectral function is a sum of two basic terms:
   - The first is independent of lapse rate and has a Kaimal shape with height dependent amplitude;
   - The second is independent of height and has a lapse rate dependent shape which is broader than the Kaimal spectrum.
3. Whereas Monin-Obukhov scaling is not adopted, the lapse rate dependency is expressed by a modified Richardson number.
4. A cross-over point is found at 0.01 Hz, particularly in the Skipheia data:
   - For higher frequencies, stable conditions contain more turbulent energy than unstable conditions.
   - For lower frequencies, unstable conditions are by far the most energetic.
5. The Harris spectrum, which is recommended by the NPD, will not adequately describe the spectral function.
6. At higher elevations the spectrum is effectively described by the non-Kaimal term. For neutral and unstable conditions this term gives a rather broad spectrum. The

present description corresponds generally to both broader and flatter spectra than most or all earlier published parameterizations.

7. The spectrum depends on reference wind speed according to a power law with exponent 3.

Coherence for vertical separation

1. Coherence for vertical (and horizontal) separation is adequately described by an extension of Davenport's exponential decay model.
2. Stability dependence is important for low frequencies (< 0.02 Hz), only. In this frequency range, coherence increases with increasing instability.
3. The coherence length increases with height and decreases slowly with vertical separation.
4. The coherence description differs only slightly and apparantly not systematically between Skipheia and Sletringen.

Coherence for horizontal separation

1. For longitudinal separation, coherence decreases with increasing instability. For lateral (and vertical) separation, the coherence increases with increasing instability.
2. The ratio of longitudinal to lateral (or vertical) coherence length decreases with frequency. These ratios are large (6 - 25) in accordance with Taylor's hypothesis and depend strongly on lapse rate.
3. Because of the above (2) large ratios, it is very difficult to isolate the longitudinal coherence when analyzing experimental data.
4. Coherence increases with height.

Phase differences for vertical separation

1. Contrary to the typical picture of constant phase along straight lines, the present description corresponds to curved lines. The angle to the horizontal plane increases with height and is somewhat smaller than indicated by earlier studies.
2. Phase differences depend weakly on lapse rate. This dependency is insignificant for strong wind.
3. Phase differences vary with height according to a power law with exponent - 0.6.
4. Phase differences show a strong non-linear dependency on frequency and reference wind speed.

Phase differences for horizontal separation

1. The longitudinal phase difference description agrees with Taylor's hypothesis: The turbulence structures are transported with the mean wind field.
2. The longitudinal phase difference is independent of lapse rate.

1. INTRODUCTION

The purpose of the project reported here is to obtain a better data base for the fluctuations of the maritime wind field in time and space. A special objective has been to provide a better basis for calculating the wind loads on wind sensitive offshore structures with fundamental frequencies of the order of 0.01 Hz.

During Phase 1 (Heggem et al., 1989, hereafter referred to as P1) of this project, measurements were carried out at the islet of Sletringen, which is situated some 1 km west of the larger island Frøya. Frøya protrudes like a wedge out towards the Norwegian sea off the coast of Trøndelag. As described in the P1-report, measurements at Sletringen are thought to be very representative for maritime conditions, provided the wind direction is in the maritime sector, defined to run from 160° (S-SE) through south, west and north to 40° (N-E). The Sletringen station has one mast of height 45 m based 4 m above MSL. Wind speed data are recorded at 5 levels from 5 to 46 m, temperature data at 5 and 45 m and in the sea, and wind direction at 45 m. The P1 measurements were made in the period February 23 - November 11 1988.

The Phase 2 (P2) measurements, which are reported here, started at Sletringen on November 12, as a continuation of the P1 program. In addition, the Phase 2 program includes measurements at the station Skipheia near Titran on Frøya. These measurements started on November 28 1988. The P2 measurements were terminated on May 15 1989. The Skipheia station was originally built as part of the Norwegian wind energy program. It consists of three masts placed in a triangle, two of height 100 m separated by a distance 78.9 m, and one of height 45 m at a distance of 187.1 m from the center point between the other two. The locations of the stations are shown on the maps in Fig. 2.1 - 2.4 in the next chapter. The sensor configuration is described in Sec. 2.1.

Data are recorded with a frequency of 0.85 Hz corresponding to 512 measurements every 10 minutes. The particular value of the logging frequency has been chosen to suit the use of fast Fourier technique (FFT) in the analysis. Data are grouped into time series of 40 min length, which are stored as separate files. The files can be linked together during analysis, giving a contiguous time series of any length - limited of course by down periods of the instrumentation.

The virtue of the Skipheia station is of course the three masts, making it possible to study correlations in horizontal as well as vertical direction. The foundations of the three masts are approximately 20 m above MSL. Towards south (approximately perpendicular to the local shoreline), the distance to the sea is 300 - 600 m, to the west and north, some 2 km. There are no trees in the neighbourhood, and the surface is mostly marshy or rocky, with ondulations not too different from rough sea. Close to the shorelines, there are however some cliffs of 5 to 10 m height.

Experimental results from the two stations are presented separately and compared. It is generally found that wind speed profiles, one point spectra and cross spectra for vertical separation from the two stations agree well in the overlapping height region in a wind direction sector from 180° to 240°. This sector contains about 40% of the data for wind

speed > 10 m/s. Using the Sletringen station as a reference, the Skipheia data are judged to be representative for maritime conditions in this restricted sector.

Chapter 2 presents a more detailed description of the Skipheia station and the recording system. The station at Sletringen is the same as during P1. A detailed description was given in the P1-report, and will not be repeated here. The procedures for sensor calibration and maintenance are discussed as well, together with the extensive quality control of the data at all stages of the process.

A survey of the data is presented in Chapter 3. This includes time-series of 1 h mean values of wind speed at 10 m, wind direction and lapse rate (temperature gradient). Frequency plots and tables of these quantities are presented as well. The shadowing effect from mast No. 2 at Skipheia is demonstrated by a plot of the 1h mean wind speed for a pair of wind speed sensors (east and west at 10 m height) versus wind direction.

The static maritime wind field is discussed in Chapter 4, based on observed time series of 1 hour length. Data are presented for the mean wind profile, the gust profile, the turbulence intensity and the distribution properties of the wind speed fluctuations. Maximum values and standard deviations of wind direction fluctuations are also discussed. The studies of fluctuations are based on wind data from which the synoptic and mesoscale trend has been removed. This is done by defining the fluctuation as the difference between the measured value at a time t and the running 1 hour mean, calculated in the window [t-½h, t+½h], for the quantity in question. Trend removal was not applied in the P1-report as far as the static maritime wind field is concerned. The profiles and the shape of the distributions are discussed as functions of wind speed and atmospheric stability. The fluctuation distributions are in general found to be asymmetric around the median point, with a "tail" towards large fluctuations. The asymmetry is most pronounced for unstable atmospheric conditions.

In Chapter 5, the dynamic behaviour of the wind is discussed. The spectra of wind speed describe the frequency distribution of turbulent energy in the wind field, and are calculated by a fast Fourier transform (FFT) of the measured timeseries using T = 40 minutes as the basic period. Trends in the data are removed as mentioned above, but here by subtracting the running mean over a period T. Trends may otherwise give spurious contribution to the low frequency part of this spectrum. The representativity of the results are discussed in some detail. The one point spectra are parameterized as an extension of the P1-work, and the dependence on wind speed and lapse rate is explicitly modelled. In addition, correlations in vertical and horizontal direction are discussed. The coherence is modelled as a function of separation, wind speed and lapse rate, and the phase lag is estimated.

Finally, in the last part of the report, a "User's guide" is given, with worked examples demonstrating the use of central formulae and graphs.

2. DESCRIPTION OF THE STATION AND THE RECORDING SYSTEM

In this section the instrumentation and dataflow at the two measurement stations is described. Sletringen was the main station in Phase-1 of this project, and has not been modified. A detailed description of the station at Sletringen is given in the Phase-1 report. The station at Skipheia is described in some detail with respect to the sensor mounting and data acquisition system. Finally, a summary of the measurement period and the data recovery is found in Section 2.3.

2.1 Site and instrumentation

The maps in Figures 2.1, 2.2, 2.3 and 2.4 show the locations of the stations and the sensor masts. Table 2.2 and Fig. 2.6 shows the positions and orientations of the masts at Skipheia. The directions and distances between the masts are shown in the figure. The two 100m masts, M2 and M4, are placed on a low hill 20 meters above MSL, and roughly 600 meters from the sea. The 45m mast, M3, based 22 meters above MSL, is placed on a neighbouring hill closer to the sea. The map in Fig. 2.4 gives an impression of the topography in the close surroundings, which is typical for the western part of Frøya. The mast at Sletringen is 4 km to the west of the station at Skipheia.

Wind speed sensors are placed at the heights 11 m, 21 m, 41 m and 101 m in the two 100 m masts. In addition there are wind speed sensors at 72 m in M2. Pairs of sensors are mounted on supports in opposite directions in the two masts at all heights below the top. The shadowing and speed up effects from the mast structure is avoided by always choosing data from the sensor on the upwind side. The distance from the mast edge to the sensor cup is 2.6 meters. Details for the mounting assembly are shown in Fig. 2.7. Table 2.2 gives a list of all the sensors with the heights and orientations relative to the mast. The computer programs will select a sensor as the upwind sensor if the wind direction is within a sector of $\pm 90°$ of the orientation direction, and only the upwind sensor will normally be used in the analyses. At the top of M2 and M4 there are a single wind speed sensor, direction sensor and a lightning-rod. Even a small shading effect on the wind speed sensor from the lightning-rod has been seen in a narrow sector. This was found to be a serious problem for the spectra of fluctuations, but is not a serious problem for the mean value profiles. In the more slender M3 the sensors are mounted 1 meter to the west from the mast at the heights 11 m, 21 m and 46 m, and there is no sensor doubling. This will give a noticeable shading effect for easterly winds.

Wind direction sensors are placed at the top of all masts and at 41 m in M2. Normally only one of the direction sensors will be used.

Air temperature sensors are mounted in M4 at 10 m, 40 m, 99 m and in a small separate mast at 0.2 m and 2.0 m. In addition the temperature in the ground has been measured. However, these 3 latter temperature measurements are not included in the Phase 2 program. The calculations of lapse rate are primarily based on data from the sensors at 40 m and 99 m.

The sensors at Skipheia are of the same types as the sensors at Sletringen. All the wind speed sensors are cup anemometers made by Vaisala. They have a distance constant of 1.5 m, the value of which has been checked in a separate project. They give a frequency signal as output, with 14 pulses per revolution. The wind speed is determined by counting pulses from the sensors, the frequency being proportional to the wind speed.

The wind direction sensors are Met-One 022 bivane sensors. The output is an analogue voltage. Because the vertical directions is not required in this project, only the horizontal direction has been recorded.

All temperature sensors are thermistors with negative temperature coefficients. They are shielded from radiation and ventilated by a fan. The thermistors are individually calibrated to detect temperature differences of 0.01 - 0.02 K.

2.2 Data acquisition system

The data acquisition system at Skipheia is placed in a barrack between the masts. Data from Sletringen are transmitted via a radio link to Skipheia. The receiver antenna is placed in M4.

The acquisition system at Skipheia is similar to the system at Sletringen described in the Phase 1 report. Fig. 2.5 shows the data acquisition system at Skipheia. Sampling frequency is 0.85 Hz, corresponding to a sampling time of 1.17 sec. The recording method of counting pulses described above gives a resolution of 0.085 m/s for wind speed. At Skipheia the wind direction signals are converted from analogue voltages to frequencies. Both the wind speed and direction are then determined by counting pulses. This may produce a spurious value for the direction signal each time North is passed (normally the direction of the gap in the potentiometer). However, this is not a significant problem for calculating the mean direction for 10 minutes (or longer). Data filtering methods to handle the problem with respect to the fluctuation distributions are described in Sec. 4.6.1. The voltage to frequency conversion is done to provide a good shield when the signal is sent through an optical link. The function of this link is to inhibit overvoltage to enter the computer system. The thermistor signals are not converted to pulses because of the limited accuracy of the converter circuits. They are shielded and protected against surges, and fed via a multiplexer to a high quality voltmeter, which is interfaced to the computer.

The data logging is controlled by a DEC Falcon single board computer (SBC), with the programs in EPROMS. It will restart immediately after a power failure. A watch-dog system ensures restart in case of "hang-up". An uninterruptable power supply will keep the system operating for about 8 hours after a mains failure. This system will, however, only save the 10 minutes values for mean, maximum, minimum and variance.

A Micro-VAX computer at Skipheia reads all the data from Sletringen and Skipheia. Via telephone lines (DATAPAK), the Micro-VAX computer can be controlled from Trondheim, and selected data can be transferred. Most of the data have been transferred by streamer tape to Trondheim.

2.3 Data recovery

During the first part of the measurement period (December - February) the weather conditions were extreme with several hurricanes and abnormal lightning activity. This caused a lot of problems in keeping the stations operative. The mains power supply at Frøya had several failure periods, lasting from hours to days. In addition the lightning made some damage to the equipment. At Sletringen the junction-box in the mast was torn off by the waves on December 22th, and the heavy sea did not allow transport to the islet until the end of January. The radio-link from Sletringen to Skipheia also had some malfunctions. Even though some of the hurricanes were lost, a lot of periods with extreme weather conditions were recorded.

With both Skipheia and Sletringen operating, we have about 40 sensors. It is rather unlikely that all the sensors will work all the time. Periods with sensor failures have been logged, and data from faulty sensors are excluded from the analyses.

Table 2.1 **The levels above mean sea level and the NGO coordinates for the bases of the masts at Skipheia.**
The NGO coordinates are given in meters relative to a grid in the NGO coordinate system (axis no. 2).

Mast	X-coordinate	Y-coordinate	Base level
Mast 2	631.277,75	-2.074,80	19.3
Mast 3	631.118,42	-2.133,71	22.2
Mast 4	631.322,89	-2.139,52	20.1

Table 2.2 **Sensor overview. Shorthand specification of observed parameter, sensor description, height above ground level and orientation of the mounting bar.**

The descriptions are the ones used in the plot legends with some deviations. "W" and "E" are abbreviations for west and east.

Physical parameter	Description	Height[m]	Orientation
Skipheia:			
Wind Speed	'M2 100m'	101.0	"top"
Wind Speed	'M2W 70m'	72.0	300°
Wind Speed	'M2W 40m'	41.0	300°
Wind Speed	'M2W 20m'	20.5	300°
Wind Speed	'M2W 10m'	11.0	300°
Wind Speed	'M2E 70m'	72.0	120°
Wind Speed	'M2E 40m'	41.0	120°
Wind Speed	'M2E 20m'	20.5	120°
Wind Speed	'M2E 10m'	11.0	120°
Wind Speed	'M4 100m'	101.0	"top"
Wind Speed	'M4W 40m'	41.0	250°
Wind Speed	'M4W 20m'	20.5	250°
Wind Speed	'M4W 10m'	11.0	250°
Wind Speed	'M4E 40m'	41.0	70°
Wind Speed	'M4E 20m'	20.5	70°
Wind Speed	'M4E 10m'	11.0	70°
Wind Speed	'M3 45m'	41.0	270°
Wind Speed	'M3W 20m'	20.5	270°
Wind Speed	'M3W 10m'	11.0	270°
Horizontal Wind Dir	'Dir M2 100m'	100.0	"top"
Horizontal Wind Dir	'Dir M2W 40m'	41.0	210°
Horizontal Wind Dir	'Dir M4 100m'	100.0	"top"
Horizontal Wind Dir	'Dir M3 45m'	45.0	"top"
Air Temperature	'Temp M4 100m'	99.0	
Air Temperature	'Temp M4 70m'	71.0	
Air Temperature	'Temp M4 40m'	40.0	
Air Temperature	'Temp M4 10m'	10.0	
Air Temperature	'Temp 2m'	2.0	
Air Temperature	'Temp 0.2m'	0.2	
Air Temperature	'Temp grnd.'	0.0	
Sletringen:			
Wind Speed	'SLE 46m'	46.0	"top"
Wind Speed	'SLE 42m'	42.0	270°
Wind Speed	'SLE 20m'	20.5	270°
Wind Speed	'SLE 10m'	10.5	270°
Wind Speed	'SLE 5m'	5.5	270°
Horizontal Wind Dir	'Dir SLE 46m'	45.0	"top"
Air Temperature	'Temp SLE 45m'	45.0	
Air Temperature	'Temp SLE 5m'	4.6	
Sea Temperature	'Temp SLE sea	-5.0	

2.4 Data quality and instrument calibration

The whole experimental setup for the measurements in this project was designed for obtaining high quality data. The main steps in this process are

1. Choice of high quality sensors.
2. Careful calibration or calibration verification of the sensors.
3. Careful mounting of the sensors to avoid that e.g. obstacles in the air stream would produce misleading readings.
4. Efforts to ensure noiseless and accurate electronic recording of sensor signals at the correct times.
5. Careful maintenance of the sensors and the recording system.
6. Daily check of the system and data output during the measurement phase.
7. Continued check of data quality during all steps of data treatment.

Some aspects of this have already been discussed in the previous sections.

During the measurements, the system performance was checked on all working days. By logging onto the Frøya MicroVax from Trondheim and starting a local program, mean, maximum and minimum values for the last 10 min period and instant values for all sensors at the selected station were displayed on the terminal screen in Trondheim. To a trained eye, most types of sensor malfunctioning would be rather easily apparent.

We will below briefly describe the calibration and maintenance procedures of the sensors, and some aspects of the continuous check of the data during the treatment process.

2.4.1 Calibration and maintenance of wind speed sensors

The dynamic and static response of the wind speed sensors which were used in this project, Vaisala WAA 12 and Vaisala WAA 15, were tested in the wind tunnel at The Norwegian Institute of Technology in Trondheim. Some sensors of the type Met One 010B, which were used in earlier projects, were tested at the same time. All three instrument types are anemometers with good time response, and represent high quality wind speed sensors used by research institutions for precise measurements.

It was confirmed that the distance constant of the tested instruments was $D = 1.5$ m for both acceleration and deceleration, in agreement with the manufacturers' specifications. The corresponding time constant is

$$\tau = D / u,$$

where u is the wind speed. This means e.g. $\tau = 0.1$ s for $u = 15$ m/s. If the wind speed jumps from one level to another level, the deviation between the instrument reading and the true value is reduced by a factor 1/e for each time increment τ. With the present logging period of 1.17 s, and the focus on high wind speeds, the time response of the sensors is sufficiently fast for all practical purposes for this project.

The absolute calibration of the three wind speed sensor types was also checked. They were found to give the same reading of wind speed within 0.5 %, which was the stability limit of the wind tunnel, over the whole wind speed range. The absolute calibration of the instruments did agree with the wind tunnel instrumentation at 20 m/s. For lower wind speeds, a deviation was found between the tunnel instruments and the anemometers, varying roughly as u^{-2}, and amounting to some 3% at u = 10 m/s. Because the absolute calibration of two of these anemometer types had been checked and found satisfactory at an earlier test, and because there was no apparent reason to expect a deviation of this type for the anemometers in the low wind speed region, the discrepancy was ascribed to a problem with the wind tunnel Pitot tube instrumentation. This discrepancy is in any case of minor interest to the present project which emphasises the high wind speed region where all the instrumentation agreed.

With respect to change in sensitivity with use, the bearings are the critical part of the anemometers, according to our experience. Worn bearings will introduce a threshold wind speed below which the anemometer will not turn, and the readings will be too low in the low wind speed region immediately above. A wind speed distribution from an instrument with worn bearings will therefore show a spike at zero wind speed, whereas the distribution from a good instrument starts from zero and increases proportionally to wind speed. The bearings in our anemometers were routinely changed after every 6 month of use, in order to keep this problem away. As deviations due to bearing problems usually decrease as u^{-2} with wind speed, they would also be of little importance in the high wind speed region.

In the parameterization of the wind speed profile, the difference between wind speed at height z and at reference height z_r = 10 m is used as a basis of parameterization. Irregularities of the order of 1 % in the speed measurements will cause deviations of the order of 10 % in the profile parameters. If systematic irregularities of this type were present, they would easily be seen in the plots, but were never observed.

At Sletringen, we have wind speed sensors at 46 and 42 m height. From the wind speed profile parameterizations discussed in Sec. 4.2.3, it follows that the higher sensor is expected to show a value some 1 % larger than that of the lower one. Differences in agreement with this were always found in the daily inspections during the measurement phase as well as in the data treatment phase. Values from the pairs of sensors mounted at the same height at Skipheia, were also always found to be consistent, when possible shading effects were taken into account.

Provided good maintenance, and noiseless recording, it is our experience that the types of anemometers used give very reliable readings. The most "dangerous" source of error will be shading or acceleration effects introduced by nearby elements in the wind flow. The sensor doubling, and 2.6 m mounting distance from the masts, are precautions to avoid such effects. As discussed in Sec. 5.3.1, turbulence measurements at the top sensor at Skipheia were disturbed by an upwind lightening rod (essentially due to wind direction fluctuations, affecting the "with" and "against" wind sides of the anemometer differently), but the mean wind speed values are not thought to be seriously affected.

2.4.2 Calibration and maintenance of wind direction and temperature sensors

Most commercially available wind direction sensors seem to be intended for measurements with $\pm$ 10° accuracy, which is usually sufficient. In particular, means are usually lacking for an accurate orientation of the sensor housing, which is necessary for a correct absolute direction measurement.

In the present project, the absolute calibration of the wind direction sensors was made by pointing the wind vanes to a set of specified directions and comparing the readings to the direction values calculated from the precisely determined positions of the masts and coordinates obtainable from topographical maps. The operational accuracy of the direction measurements in the present project is probably of the order of 5°. The need for accurate knowledge of the wind direction relative to the inter mast orientation became evident during the analysis of two point coherence data, and an accuracy of about 1° will be aimed for in a future project.

The thermistor temperature sensors were individually calibrated to fit a 3 parameter nonlinear temperature-voltage curve, with r.m.s. deviation typically less than 0.005 K over the range -15 to 25 °C. A very stable temperature bath with a high accuracy thermal calibration sensor (HP 2804A Quartz Thermometer) was used for this. Some uncertainties are introduced in the mounting and switching of the temperature sensors, and the operational accuracy may not be better than a few hundredth of a degree. In a future project, the temperature sensors will be duplicated at each height to get a better operational check on the temperature measurements. Temperature measurements with this precision in open air conditions are known to be very difficult.

2.4.3 Check of data quality in the analysis phase

The body of raw data from the Phase 1 and 2 projects amount to approximately half a billion values, and it is of course impossible to verify that all values represent a correct measurement with respect to the physical phenomenon in question. Two types of errors will be difficult to establish during the measurement process:

1. Those appearing as very rare events
2. Small amplitude disturbances

An example of the former type is the occurrence of spikes with a rate of the order 10^{-6} for some of the sensors during the Phase 2 measurements. However, they were readily identified in the analysis phase when extreme value data were examined, and eliminated as discussed in Sec. 4.1.1. An example of the second type is the additional turbulence introduced by the lightning rods, which was identified during the comparison of spectra from various heights and direction sectors.

In general, all statistical distributions have been compared to all available circumstantial evidence to examine if they look "reasonable". Extreme fluctuations are listed and dated in auxiliary output from the analysing programmes. A check of the

original time series will usually reveal if the fluctuation in question correspond to a real event. Thus the most extreme fluctuations in wind direction discussed in Sec. 4.6.2, were found to be associated with the special time series discussed in Sec. 4.6.1.

3. DATA SURVEY

In this chapter, hourly mean values of wind speed, wind direction and lapse rate (- dT/dz) are presented. The main idea is to give an impression of the type of weather in the period.

3.1 Time series of 1-h mean values

Fig. 3.1.1 shows time series of the 1-h mean values of wind speed at 10 m height, wind direction and lapse rate for the Sletringen station for November 1988. In Figs. 3.1.2 - 3.1.7 corresponding data are shown for both stations for the subsequent months of December 1988 through May 1989 are presented. Periods with no data are indicated by vertical lines to/from the bottom border of the graphs. Note that the direction data are presented on a scale from -180 to 360 degrees, to enable a continuous curve for zero crossings. Direction values on the plot differing by 360° are of course physically identical. Data for the Skipheia station are from mast 2 (M2), and speed values for the upwind sensor are always chosen according to the procedure discussed in Sec. 2.1. The lapse rate for the stations is calculated as

$$\gamma = [T(z_1) - T(z_2)]/ (z_2 - z_1) \qquad (1)$$

where z_1/z_2 are 40/100 m for the Skipheia station and 5/45 m for Sletringen. The highest pair of temperature sensors are chosen for Skipheia. These sensors are least disturbed by heating/cooling of the ground, and are therefore thought to be most relevant for maritime conditions.

As seen from the graphs, wind direction, and, by part, temperature data are not available from Sletringen during the period December 9 to March 2. This is due to the extremely difficult maintenance situation at this station, as discussed in Chapter 2.

Data which are considered suspect are not included in the presentations in this section or in the analysis in chapter 4 and 5. A table containing definitions of "bad" or "down" periods for the individual sensors are consulted by the plotting and analysing programs for this purpose. At the Skipheia station, a substitution scheme for the direction sensors is defined. When at least one sensor is operating, direction will therefore be defined. The direction sensors contain a potentiometer, and have higher failure rate than the other sensors.

The highest wind speed values were recorded on December 22 just before the mains supply of the stations broke down. A time serie for this case of the 10-min values for Sletringen is shown in Fig. 3.1.8. At 46 m, a maximum value of 45 m/s was observed. This time series is from casette data recorded at Sletringen. This station operated 4 h longer than the Skipheia station, until a wave washed away the cables.

The second highest peak in wind speed values occurred on February 15 1989. A time series of 10 min values for selected wind speed sensors at both Sletringen and

Skipheia is shown in Fig. 3.1.9. It is seen that the wind speed series at the two stations follow each other rather closely. We return to a more detailed comparison of the two stations in Chapters 4 and 5.

3.2 Distributions of 1-h mean values

Because of the problems with the recording of wind direction at Sletringen, the distributions presented in this section are based on data from Sletringen for the period November 12 1988 through December 1, and on data from Skipheia in the period December 2 through May 15 1989.

The relative distribution of 1 h mean wind speed at 10 m and 40 m (exact values are 10.5/11 m and 42/41 m at Sletringen/Skipheia, respectively) is presented in Fig. 3.2.1. In stead of presenting the data by a histogram, curves are drawn through the centered fractional values in successive bins of size 1 m/s (the sum of the fractional values is normalized to 1).

The relative distribution of wind direction is shown in Fig. 3.2.2. Normalized curves for wind speeds higher than 5, 10 and 15 m/s are also shown. For strong winds, there is a very dominant peak in the S-W direction. The traditional winter peak corresponding to easterly winds is nearly absent.

The relative distribution of lapse rate is shown in Fig. 3.2.3 for wind speeds higher than 10 and 15 m/s. The data are strongly peaked at neutral atmospheric stability (lapse rate $\simeq$ 10 K/km). Compared to P1, there are higher frequencies of stable and neutral atmospheric stability. In Table 3.1.1 is shown the distribution of the P2 data in wind speed and lapse rate classes.

The effects of shadowing and speed up caused by the mast are demonstrated in Fig. 3.2.4, where the average value of wind speed for the period 01.12.88-15.05.89 in sectors of 10° width is shown versus direction for the west and east sensor at 10 m height, Skipheia. The shadowing effects are most important for the 100 m masts, which have a relative high solidity. In the Sletringen mast, the shadowing sector will coincide with the direction of wind from the light-house area, where the wind is heavily perturbed in any case. By choosing the upwind sensor in the 100 m masts at Skipheia, no significant perturbation is expected.

Table 3.2.1 **The number of observed 1 h mean values in wind speed and lapse rate classes.**

The wind speed is observed at 10 m height. The data are from Sletringen in the period 88.11.12-88.12.01 and from Skipheia 88.12.02-89.05.15. The mid-value for each class is indicated. The size of the lapse rate classes is 5 K/km in the range $-5 < \gamma < 15$ K/km, otherwise 10 K/km. The size of the speed classes is 2 m/s.

U	Lapse rate γ (= -dT/dz) in K/km										
(m/s)	-30.0	-20.0	-10.0	-2.5	2.5	7.5	12.5	20.0	30.0	40.0	Sum
1.0	2	3	4	5	20	20	37	10	5	2	108
3.0	15	14	23	27	61	91	124	54	5	0	414
5.0	37	58	77	56	61	99	103	40	2	0	533
7.0	73	68	51	28	26	66	119	56	0	0	487
9.0	26	60	44	21	29	49	114	82	0	0	425
11.0	1	20	57	13	23	39	124	133	6	0	416
13.0	0	3	30	29	22	17	94	77	10	0	282
15.0	0	0	1	12	16	44	52	39	1	0	165
17.0	0	0	4	10	12	23	19	15	0	0	83
19.0	0	0	0	3	16	5	8	11	0	0	43
21.0	0	0	0	0	1	2	9	7	0	0	19
23.0	0	0	0	0	0	0	2	5	0	0	7
25.0	0	0	0	0	0	4	1	1	0	0	6
27.0	0	0	0	0	0	0	3	0	0	0	3
29.0	0	0	0	0	0	0	0	0	0	0	0
31.0	0	0	0	0	0	0	0	0	0	0	0
33.0	0	0	0	0	0	0	0	0	0	0	0
35.0	0	0	0	0	0	0	0	0	0	0	0
37.0	0	0	0	0	0	0	0	0	0	0	0
39.0	0	0	0	0	0	0	0	0	0	0	0
Sum	154	226	291	204	287	459	809	530	29	2	2991

4. STATIC MARITIME WIND

4.1 Introduction

Based on the data from the stations Sletringen and Skipheia, the present chapter examines the properties of maritime turbulent wind in terms of the wind description normally assumed relevant for offshore structures which are sensitive to static wind load. The following properties are discussed

* the 1 hour mean wind profile
* the gust profile for several gust durations and the gust distribution characteristics
* the 1 hour standard deviation of turbulent wind fluctuations and its distribution

However, before going into discussions concerning these aspects of the maritime wind field, a brief review is required of the climatology of the coastal areas off Trøndelag, of the procedures adopted for the examination of the data quality (Section 4.1.1) and of the particular data selection applied in the study (Section 4.1.2).

As discussed in the final report of the Phase 1 project (Heggem et. al 1989), data from the Sletringen station with wind direction in the sector from 160° to 40° through north, are likely to be very representative for maritime conditions. When the wind approaches the Skipheia station, some modifications are expected to be introduced by the rough land surface. From west to north, the distance to the sea is some 3 km, (see Fig. 2.2, Chapter 2). The western Frøya landscape is gently rolling, with a rocky or marchy surface. There are no trees or bushes which are expected to influence the terrain roughness. The possible topographical effects are discussed in view of comparison between data from the two stations.

During the Phase 1 of the present project the atmosphere was often found to be thermally unstable (lapse rate 20-30 K/km) even during strong winds. This was due to frequent outbreaks during the Phase 1 period of cold air masses, often of polar origin, flowing over a relatively warm sea (the coastal current off Trøndelag is a branch of the Gulf stream). With respect to cooling, the sea is a very stiff heat reservoir, practically speaking with zero internal thermal resistance and infinite heat capacity, and the sea surface temperature will remain unchanged during such cold air outbreaks leading to unstable atmospheric conditions.

The conditions over land are different. In the case of constant incoming ambient air temperature, an equilibrium situation will be established which depends on the ground surface properties, the below surface ground temperature and the downward radiative fluxes. Over land, the heat flux can be significantly reduced and even reversed if the radiation balance is negative. This is usually the case if the sky is clear and the downward shortwave radiative fluxes are small. In a turbulent flow the air parcels are moving up and down all the time. Over land the effective mixing associated with mechanical turbulence will tend to produce a neutral boundary layer even in the presence of a heat flux.

Due to the large scale turbulence and the organized convection regimes over the sea, the air flow will consist of layers with different potential temperature. Thus, even if the heat flux is significantly changed as the air flows from sea to land, thermally driven turbulence may persist for some time over land in addition to the mechanical one. The relevance of lapse rate measurements at Skipheia for winds in the sectors from W to NE may therefore be questionable. We will return to these questions when discussing the individual distributions in the next sections.

4.1.1 Elimination of "spikes"

During Phase 1, "spikes", or single measurement values which are more or less obviously wrong, were not a problem at all (except for a period in September 1988 when a discriminator in the electronics system was inoperative; these data were excluded from analysis). During Phase 2, some 100 spikes have been identified and excluded, amounting to a spike rate of the order of 10^{-6}. The errors were mainly located to certain sensors. The erroneous data were flagged and omitted from the analysis. After this process, the affected sensors show the same type of 1.15 s gust-values as the other sensors, indicating that the chosen procedure was adequate.

A preliminary examination showed that spikes occurred singly. The search procedure was therefore based on examination of three successive wind speed values x_1, x_2 and x_3, and then advancing one value and starting anew. The relative deviation of x_2 from the mean of the neighbours

$$g_3 = (x_2 - m)/m \qquad m = (x_1 + x_3)/2 \tag{1}$$

and the relative differences between successive values,

$$g_2 = (x_2 - x_1)/[(x_2 + x_1)/2] \tag{2}$$

were calculated and used as a basis for identification and elimination of spikes. Some examples of g-distributions are shown in Fig. 4.1.1. Note that some local irregularities for small values of the g in the curves are caused by the finite resolution in the wind speed values. The g_3-distributions are seen to be more narrow, and g_3 was consequently chosen as basis for the exclusion of spikes. Both distributions were found to fit approximately to the formula

$$f(g) = f_0 \exp[-(g/\gamma)^q] \tag{3}$$

A summary of characteristic values f_0, γ and q, together with the value of g_3 used to exclude the x_2 as "wild", is given in Table 4.1.1. Because the value of q is in the range 1.0 - 1.5 and therefore well below 2.0, all the distributions are far from being Gaussian.

Table 4.1.1 Examples of the shape parameters of the distribution f(g), Eq. (4.1.3), used to fit single point distributions, and the value g_{3x} used to define the "spikes".

Station & height	Var.	γ	q	g_{ix}
Sletringen 46 m	g_2	0.038	1.40	-
- 46 m	g_3	0.028	1.45	0.30
- 20 m	g_3	0.034	1.41	0.35
- 10 m	g_3	0.046	1.36	0.40
- 5 m	g_3	0.070	1.52	0.45
Skipheia 100 m	g_2	0.031	1.01	-
- 100 m	g_3	0.023	1.01	0.30
- 70 m	g_3	0.027	1.38	0.30
- 40 m	g_3	0.034	1.36	0.30
- 20 m	g_3	-	-	0.35
- 10 m	g_3	0.058	1.46	0.40

4.1.2 Definition of quasi stationary periods

In the Appendix report to the reports from the Phase 2 project, Aasen (1989), plots of time series of 10 min. mean values of wind speed at 10 m, wind direction and lapse rate are presented for both stations for all days when at least one value of the 1-hour mean speed at 10 m, u_{ref}, exceeds 15 m/s. On the basis on these plots, a set of quasi stationary (QS) periods were selected according to the criteria

* $u_{ref} \geq 15$ m/s
* Constant or slowly varying values of the running 1 hour mean wind speed and wind direction. Some fluctuations around a well defined mean value or trend were allowed, in particular lapse rate fluctuations of the order of 10K/km were tolerated.

Large lapse rate fluctuations are sometimes found during periods which are quasi stationary with respect to wind speed and wind direction. A second set of "partly" quasi stationary (PQS) periods was therefore selected (including the QS-periods) without restrictions on the lapse rate fluctuations. For details, the reader is referred to the Appendix report. Data for these 2 types of selected periods, and data for the complete period, were treated separately in the analysis which are reported in the following sections.

4.2 The 1 hour mean wind profile

To describe the variation of the mean wind speed with height, two alternative approaches are found in the literature, the theoretically based logarithmic law, and the more empirical power law. As we shall see below, they are quite closely related. In the unmodified form, none of the laws provide a satisfactory fit to the data. Based on the logarithmic formalism, we have however developed a parameterization which fits the data quite well. The model can be used to make a reasonable prediction of the wind speed up to about 100 m height from data at 10 m.

4.2.1 Discussion of the logarithmic and power law parameterizations

The logarithmic law is based on the governing boundary layer equations and dimensional arguments. The general form is

$$u(z) = (u_*/\kappa) [\ln(z/z_0) - \psi_m(z/L)] \quad (1)$$

where z is the height above surface level, u_* is the friction velocity, κ is the Von Karmans constant which usually is assumed to have the value 0.4. The roughness length, z_0 is for calm sea conventionally assumed to be 0.1 mm increasing to 1 mm for rough sea. ψ_m is some function of the ratio z/L, L being the Monin-Obukhov length, which has to be determined empirically for different stability conditions. Both argument (through L) and functional form are stability dependent. For neutral lapse rate ($L = \infty$) ψ_m vanishes, and the pure logarithmic profile is supposed to be valid,

$$u(z) = (u_*/\kappa) \ln(z/z_0) \quad (2)$$

From this relation the quantities u_* and z_0 can be determined from the observed profile at neutral conditions. By introducing $z_r = 10$ m and $u_r = u(z_r)$, Eq. (2) may formally be rewritten as

$$u(z) = u_r [1 + \alpha \ln(z/z_r)] \quad (3)$$

where $\alpha = u_*/\kappa u_r$. For the objectives of the present study, the change of reference level from z_0 to z_r is quite relevant. In the Phase 1 report, it was found convenient to adopt Eq. (3) rather than Eq. (1) as the basis for describing the wind profile. The main argument was that a generalized parameter $\alpha(u_r, dT/dz, z/z_r)$ can be determined from the observations in a numerically stable way.

For neutral conditions (subscript n), the "standard" parameters in Eq. (2) are given in terms of α and the reference speed u_r as

$$z_0 = z_r \exp[-(1/\alpha_n)] \quad (4)$$

$$u_{*n} = \kappa \alpha_n u_r \tag{5}$$

The "rough sea" value of z_0 = 1 mm corresponds to α = 0.108. Experimentally, quite small values can however be found for α even for near neutral conditions. From Eq. (4) it is seen that $(1/z_0)$ is "doubly" divergent when $\alpha_n \to 0$. Therefore z_0 is a numerically awkward quantity to use directly to parameterize the wind speed profile. The parameter α is simply related to the velocity ratio

$$\alpha = [u(z)/u_r - 1]/\ln(z/z_r) \tag{6}$$

which is the quantity of primary interest. In the next section, we will therefore use Eq. (3) as a basis for describing the wind profile for all stability classes, and parameterize α in terms of height, wind speed and lapse rate.

The power law appears to be a purely phenomenological description in terms of dimensionless quantities. This law is numerically stable and provides an alternative convenient description of the mean wind profile. This law can be written as

$$u(z) = u_r (z/z_r)^p \tag{7}$$

The first two terms in a series expansion of this expression will correspond to the logarithmic law with p = α. The higher order terms indicate that for a given wind shear at the reference level, the power law predicts a stronger increase with height than the logarithmic law. The wind speed height gradient, or wind shear, is given by the two laws under discussion as

$$du/dz = \alpha u_r/z \qquad \text{simple logarithmic law} \tag{8}$$

$$du/dz = p\, u(z)/z \qquad \text{power law} \tag{9}$$

confirming that the power law predicts a stronger increase of the wind speed with height than the logarithmic law. As we shall see in the next section, the wind speed increase with height at Sletringen is found to be smaller than indicated by either of these laws. As already indicated, we will therefore use the logarithmic law as a basis for the description.

The correction term $\psi_m(z/L)$ in the logarithmic profile, Eq. (1), was briefly discussed in the Phase 1 report (see e.g. Panofsky and Dutton (1986) for a more extensive treatment). The argument z/L may be expressed as a function of the local Richardson number Ri defined by

$$Ri = g\,(dT/dz + \gamma_d)/[\,T\,(du/dz)^2] \tag{10}$$

where γ_d is the dry adiabatic lapse rate (9.8 K/km). At Sletringen the air temperature was measured at two heights, 5 and 45 m, only. Therefore only a mean value of dT/dz

between these levels is available. Consequently, a bulk form only of the Richardson number can be calculated. If we choose the wind speed sensors closest to the air temperature sensors, and replace differentials by the corresponding finite difference quotients, an estimate for Ri can be found using the sensors at 5 and 45 or 46 m. This "bulk" or average value.

$$Ri_b = \frac{g}{T}\left(\frac{T(z_1) - T(z_2)}{z_1 - z_2} + \gamma_d\right)\left(\frac{z_1 - z_2}{u(z_1) - u(z_2)}\right)^2 \qquad (11)$$

is probably close to a true value at the geometrical mean $z_b = 15$ m of the heights involved. Using these quantities to evaluate the Monin-Obukhov length L by the formulae recommended by Panofsky and Dutton (1986), the argument z/L is related to Ri_b by

$$\begin{aligned} z/L &= Ri_b\, z/z_b && \text{Unstable air, } -dT/dz > \gamma_d \\ z/L &= Ri_b\, z/[z_b\,(1 - 5\,Ri_b)] && \text{Stable air, } -dT/dz < \gamma_d \end{aligned} \qquad (12)$$

The critical assumption with respect to the z-dependence of the above relation is that the measurement heights at Sletringen are within the constant flux layer for stationary flow. In that case L is independent of height, and the assumption

$$R_i = R_{ib} \text{ at } z = z_b$$

will imply Eq. (12).

The Monin-Obukhov length L is defined by

$$1/L = -\kappa\, g\, H_0/(T_0\, C_P\, u_*^3) \qquad (13)$$

where H_0 is eddy flux of sensible heat, T_0 is the surface temperature and C_P is the heat capacity at constant pressure. Because $-H_0$ increases monotonically with the potential temperature gradient $d\theta/dz = dT/dz + \gamma_d$, 1/L will do the same. However, plots of the logarithmic height coefficient α versus Ri_b (see Section 4.2.2) show a systematic behaviour for the well-defined, quasi stationary data only. The plots of α versus lapse rate do however show a systematic trend for all data selections.

A further problem is that z_0 appearing in Eq. (1) will generally depend on stability - as well as the wind speed - for maritime conditions. From Eq. (1), the surface stress $\tau = \rho\, u_*^2$ (equal to the momentum transfer) is given as

$$\tau = \rho\, \kappa^2\, u^2/[\ln(z/z_0) - \psi_m(z/L)]^2 \qquad (14)$$

where ρ is the air density. The stress is seen to increase with wind speed and decreasing stability. Increasing surface stress is expected to cause an increase in z_0 (Eq. (14) even implies a positive feedback). Typically, a relation on the form

$$z_0 = \text{const. } u_*^2 \tag{15}$$

is assumed, i.e. the maritime roughness length is proportional to the surface stress.

From Eqs. (1) and (6) it follows that

$$\alpha = \chi \{1 - [\psi_m(z/L) - \psi_m(z_r/L)]/\ln(z/z_r)\} / [1 - \chi \psi_m(z_r/L)] \tag{16}$$

where $\chi = 1/\ln(z_r/z_0)$ (for neutral conditions, $\alpha = \chi$). Because both χ and ψ depend on stability, and because of the problems already mentioned in determining L, we will (see Sec. 4.2.3) parameterize α directly against lapse rate and wind speed, rather than going through the above conventional formalism (Eqs. 1, 13 and 16), which seems hard to apply in our case.

4.2.2 Presentation of the experimental data

All experimental values presented in this section are 1 h mean values. Composite quantities are calculated in terms of the 1h mean values of the basic quantities.

In all the following scatter plots, the range along the horizontal axis is divided into some 20 intervals. The points shown represent the mean value in each interval of the quantity in question, and are plotted at the midpoint of the interval. The bars through the points indicate the scatter, and correspond to $\pm$ the square root of the average variance of the values used to calculate the mean value. The bars are given a small tilt in order not to overlap for points separated in the vertical direction. Points without a bar usually represent single events. If the particular interval has no events, nothing is plotted. We return to the interpretation of the graphs below.

Plots of the logarithmic law height coefficient α (as defined by Eq. (6)) versus reference wind speed are shown in Fig. 4.2.1 for Sletringen and mast M2 at Skipheia. All data, without lapse rate classification, are included. This graph therefore contains somewhat more data than graphs which require lapse rate data. This is due to the smaller recovery of such data. The values of α are calculated from pairs of 1h mean wind speed values at the indicated heights.

The data presented in Fig. 4.2.1 show a large variance, in particular, that is true for the Skipheia data. We shall see below that the variance of the Sletringen data is reduced when the data are classified according to lapse rate. Originally, it was hoped that missing temperature data at one station could be replaced by data from the other. A plot of the mean values and the mean values $\pm$ standard deviation of the lapse rate -dT/dz for various height intervals at Skipheia (evaluated as the temperature difference divided by the corresponding height difference) versus the lapse rate at Sletringen is shown in Fig. 4.2.2. Unfortunately, the correlation is only modest. The best correlation with Sletringen values is seen for the 70/40 m pair of temperature sensors at Skipheia, although the scatter is also here very large. This pair was therefore selected to replace missing Sletringen values (see

discussion below). The data for the logarithmic coefficient α with lapse rate replacements are not shown in the plots, but are briefly discussed below.

A scatter plot of α versus lapse rate for Sletringen is shown in Fig. 4.2.3 for four classes of reference wind speed $u_r > 10$ m/s. The curves shown will be discussed in the next section. In Fig. 4.2.4 and 4.2.5, corresponding plots are shown for selected sets of quasi stationary (QS) and partly quasi stationary (PQS) data (Sec. 4.1.2) for three classes of reference wind speed $u_r > 14$ m/s. For the classification used in these plots, the difference is small between the quasi stationary data and the complete set of data. The advantage of this latter set is that it is representative of all observed conditions, and therefore provides a wider range of wind speed values. If the same sets of data in addition include events for which missing Sletringen lapse rate values have been replaced by concurrent 70/40 Skipheia values as explained above, some 20 % more events are included, with a higher fraction at high wind speeds. However, the trend is in any case very much the same in corresponding classes, independent of data set selection.

In Figs. 4.2.6-8, scatter plots of α versus reference wind speed are shown for four classes of lapse rate for the same sets of data as discussed in the preceding paragraph. Again, the trends in the data are pretty much independent of data set selection.

Scatter plots of α versus the bulk estimate of the Richardson number Ri_b, as defined by Eq. (11), are shown in Figs. 4.2.9-11 for the three sets of Sletringen data. For wind speeds below 18 m/s several noticeable features should be observed:

* α versus lapse rate is well defined for all 3 data sets (Figs. 4.2.3-5) and can be represented by the same functional form. For the wind speed ranges represented, this is also seen to be the case for the α versus Ri_b relations in the QS and PQS data sets, but not in the full data set (Figs. 4.2.9-11, note the different Ri_b scales and an additional wind speed class for the full data set).
* The range of Ri_b values in the plots is from -0.60 to 0.40 for the full data set in the wind speed class $10 < u_r < 14$ m/s (QS and PQS data sets are not defined for $u_r < 15$ m/s, and are not shown). Note that $Ri_b > 0.2$ is incompatible with the stable branch of the empirical relation (12), which is valid for turbulent flow. In the next class, $14 < u_r < 18$ m/s, the range in Ri_b is from -0.15 to 0.07 for the QS and PQS data, and -0.20 to 0.15 for the full data set. Compared to the QS and PQS data sets, a principally new feature appears in the full data set: A maximum in the α versus Ri_b relationship.
* For stable conditions and moderate wind speeds, the scatter in α values is very large.

The values of Ri_b entering in the plots are calculated from experimental values at 5 and 45 (46) m height by Eq. (11). To demonstrate the interrelation between Ri_b and α, we will express the Richardson number in terms of α. From Eqs. (10) and (8), we can write

$$Ri = \frac{g}{T}\,\theta_z\,\frac{z^2}{\alpha^2\,u_r^2}$$

where $\theta_z = dT/dz + \gamma_d$ is the potential temperature gradient. (This is essentially also a bulk estimate of Ri, the only difference from Eq. (11) is that du/dz is evaluated from the 46/10 m values.) If σ_α / α were small, σ_α being the standard deviation of α, an approximate estimate for the standard deviation of Ri would be

$$\sigma_{Ri} = [\,4\,(Ri\;\sigma_\alpha/\alpha)^2 + (Ri\;\sigma_{\Theta z}/\Theta_z)^2]^{1/2}$$

From Fig. 4.2.3 it is seen that σ_α/α is typically 0.4 in the stable range of the lowest wind speed class for the full set of data. This indicates that σ_{Ri}/Ri is of the order 1, and this is also expected to be the case for Ri_b evaluated by Eq. (11). Thus, when the values of Ri_b are calculated from experimental data by Eq. (11), the uncertainty in the result will be a sum of uncertainties due to the θ_z and α terms.

In addition, due to the nonlinearity, symmetric fluctuations in α will tend to shift the value of Ri upwards. This is in particular apparent near the upper end of the Ri_b scale in Fig. 4.2.9, where the large values of Ri_b are due to small values of α, giving the α versus Ri_b plot a maximum at Ri_b values somewhat below 0.2 for the two lowest wind speed classes. This maximum is clearly seen in the full data set only.

For strongly stable conditions and moderate wind speed, the turbulence tends to decay. The eddy viscosity is reduced, and the wind speed profile is easily perturbed, giving rise e.g. to gravity effects. Instationarities, as low laying jets, will experience very little damping. Or to quote Panofsky and Dutton (1983), p. 145: "Measurements in stable air are difficult, and the assumptions used in the surface layer tend to break down; hence, different investigators obtain different results". The critical value of Ri_b, beyond which instationarities will dominate, is 0.2, as indicated by the empirical formula (12). Our experimental results for strongly stable conditions and moderate wind speeds are good illustrations of these points.

A stability indicator as the Richardson number is meaningful for stationary flow only, according to boundary layer theory. Lapse rate enters the boundary layer equations directly in the buoyancy term, and is under all circumstances of direct importance. Thus, because γ is also empirically the best classifier of the data, we have chosen γ rather than Ri as the primary independent variable in addition to u_r.

In Fig. 4.2.1, we presented plots of α versus reference wind speed for both Sletringen and Skipheia. The data were not classified according to lapse rate. By introducing such a classification (Figs. 4.2.3 to 4.2.8) it was shown that the variance in the Sletringen data was reduced. As will be shown below this conclusion was not found valid for the Skipheia data. Plots of α versus reference wind speed for four classes of lapse rate is shown for the complete data set in Fig. 4.2.12, and for the QS data set in Fig. 4.2.13. In contrast to the Sletringen data, there are no clear trends. This negative conclusion is independent of the particular temperature sensors used to calculate the lapse rate, including

the ones at Sletringen. As can be seen from the Appendix report (Aasen, 1989), the lapse rate at Skipheia is very often different from the one at Sletringen, and a more detailed study of the data show that the lapse rate at Skipheia will very often vary significantly with height. As an example time series of temperature and lapse rate for March 16-17 1989 for both Sletringen and various sensors at Skipheia are shown in Fig. 4.2.14. The general conclusion is that even when the thermal structure of the atmosphere is stationary at Sletringen, the situation at Skipheia is generally not stationary. The reason for this lack of stationarity at Skipheia is not well understood. However, the influence from the ground on the lower air layers, varying with the radiation balance, and a remanent strong maritime influence on the upper layers is likely to produce a complex temperature profile there.

A plot of α versus wind direction is shown for both stations in Fig. 4.2.15 for reference wind speed $u_r > 15$ m/s. More than 90 % of the data is in the sector 180° - 300°. Half of the data at Skipheia are found between 200° and 240°, and in this sector, with a rather short distance to the ocean (100-500 m), the height variation of α is seen to be rather small and "Sletringen like". In the W - NW direction, where the distance to the ocean is of the order of 3 km, α seems to increase with height, which is somewhat difficult to understand. But it could conceivably be due to the buildup of a new internal boundary layer associated with the land topography, and that this process is causing the strongest retardation of the winds at lower heights.

This picture is confirmed by Fig 4.2.16, where the ratio of wind speed at Skipheia to wind speed at Sletringen is shown for selected sensors versus direction. In the sector [180°,240°], a ratio around 1 is observed for the pairs of sensors from 10 to 40 m at approximately the same height, and a "normal" value around 1.1 for the 100/46 pair. A scatter plot of α versus wind speed with the same stability classification as used for the Sletringen data, is shown in Fig. 4.2.17 for wind direction in this restricted sector. Although Fig. 4.2.17 clearly shows a larger variance and a more noisy picture at Skipheia as compared to Sletringen (Fig. 4.2.6), the results of the two preceding plots are confirmed: The wind in the sector [180°,240°] seems to show the same height dependence as the wind at Sletringen, and in the height range 10 - 40 m, the wind speed is the same at the two stations. In this sector, the Skipheia data can therefore be used to extend the Sletringen results to heights up to 100 m.

In Fig. 4.2.18-20, the coefficient α versus the air-sea temperature difference is shown for the three sets of Sletringen data, with the same selection of wind speed classes as used above. The curves are discussed below, and can be seen to give a fairly good description of the data.

4.2.3 Parameterization of the experimental data

The experiences from the preceding sections can be summarized as follows:

Information about atmospheric stability is required to provide an adequate description of the 1h mean wind speed profile. Classification of the data according to lapse rate or air-sea temperature difference gives a reasonable description even in the non-stationary cases.

This is not the case if the Richardson number is used to describe atmospheric stability, because then the data for stationary conditions only can be parameterized. We have therefore chosen to describe the profile in terms of the reference wind speed and the lapse rate.

From the plots of α versus lapse rate for the smallest wind speed class (Figs. 4.2.3-5), we can see that when the lapse rate increases from negative (stable) values, a transition takes place with a strong variation of the profile through the neutral region. For the highest wind speed class, the corresponding variation in the profile is small. Thus, well above a transitional wind speed region, the change of α (or the wind speed height gradient) from stable to unstable conditions is very small, well below it is large. The value of the transitional speed will depend on height. A similar transition in the variation of α with wind speed is found (Figs.4.2.6-8) for unstable conditions (large values of the lapse rate), although the lower part of this transition is not well covered in our graphs. We shall assume that these effects will factorize, and that they can be described by the same transitional function.

In addition to these transitional effects, more continuous effects may be seen as well: A slow increase in the value of α with wind speed (which in the classical terms can be interpreted as an increase of the roughness length with wind speed) and a general decrease of α with increasing atmospheric stability.

A general formula which is capable of describing this composite behaviour is

$$\alpha = \alpha_0 + \alpha_u u_r - \alpha_\gamma \gamma - \alpha_s \, sig(\gamma,\gamma_s,\gamma_d) \, sig(u_r,u_{rs},u_{rd}) \qquad (17)$$

$$\gamma = - dT/dz$$

$$sig(x,x_s,d) = 1/\{1 + exp[- (x-x_s)/d]\} \qquad (18)$$

The sigmoid function, $sig(x,x_s,d)$ has been introduced to describe a "soft" step function. It increases from 0 to 1 with a value 0.5 for $x=x_s$, where the derivative has a maximum value of 0.25/d. Thus the width of the transitional region is 4d.

A similar parameterization of the transitional region was introduced by Heggem et al. (1989) (note that a printing error is present in Eq. (3.2.15 & 16) of that report, the term $z^{0.5}$ should read $(z/z_r)^{0.5}$).

By fitting Eq. (17) to the data, the values for the coefficients were found to be:

$$\alpha_0 = 0.10 \qquad \alpha_u = 0.001 \text{ s/m} \qquad \alpha_\gamma = 0.0002 \text{ km/K} \qquad \alpha_s = 0.06$$

$$\gamma_s = 6 \text{ K/km} \qquad \gamma_d = 3.0 \text{ K/km} \qquad u_{rd} = -0.2 \, u_{rs} \qquad (19)$$

$$u_{rs} = u_{rs0} + u_{rs1} \ln(z/z_r) \qquad u_{rs0} = 8.2 \text{ m/s} \qquad u_{rs1} = 4.0 \text{ m/s}$$

Note that units m/s and K/km are assumed for wind speed and lapse rate respectively.

No attempt was made to fit the 5/10 data. We do not claim that these values are the final ones, but they do give a reasonable fit to the bulk of the data. There is a special problem in determining the value of α_s, because the low end part of the transition in u_r was

not included in the plots. Moreover it is not unlikely that the transitional wind speed will depend on the lapse rate, because it represents a point where mechanically and thermally induced turbulence are about the same size.

In the graphs, values of α are presented for a range in one of the variables (either reference wind speed u_r or lapse rate γ). The corresponding curves (Eqs. (17) together with (19)) are based on fit to the mean values of α in each interval, using the value of u_r or γ at the midpoint of the interval. If a weighted mean for the actual data had been used instead, this would have given slightly different values. This is most important for the α versus lapse rate curves, because the dependence on wind speed is rather strong. The effect can explain some of the deviations in Figs. 4.2.3-6 for large values of the lapse rate.

Apart from the values of the coefficients, the model itself is of course open for discussion too. There could e.g. be a second order term in the reference wind speed. Indeed, wind speed events in the range 26 - 28 m/s shown in Fig. 4.2.1 do indicate such a behaviour. There are only 6 events in this region, and lapse rate data for these are not available. Because the data below 26 m/s do not indicate a second order term in u_r, it has not been included.

The curves in Figs. 4.2.18-20 of α versus the air-sea temperature difference were based on fit to a formula similar to Eq. (17), except that the lapse rate is now replaced by the temperature difference Δ.

$$\alpha = \alpha_0 + \alpha_u u_r + \alpha_t \Delta - \alpha_s \, \mathrm{sig}(\Delta,\Delta_s,\Delta_d) \, \mathrm{sig}(u_r,u_{rs},u_{rd})$$
$$\Delta = T_{air} - T_{sea} \qquad (20)$$

Most of the coefficients are given by Eqs. (19). For the new ones, the following values were used,

$$\alpha_t = 0.001 \ K^{-1}. \quad \Delta_s = -0.25 \ K \quad \Delta_d = -1.0 \ K \qquad (21)$$

The fit seems reasonable with this parameterization too.

The variation of the ratio $u(z)/u_r$ with height based on our parameterization - Eq. (3) combined with Eqs.(17-19) and (20-21) - is shown in Fig. 4.2.21, and compared to a curve (full line) based on $\alpha = 0.15$ (value proposed by the Norwegian Petroleum Directory). Curves are presented for two values of the reference wind speed, 20 and 30 m/s. The latter value represents an extrapolation from our measurements. One should however bear in mind that the highest values presented in Fig. 4.2.1 for the interval $26 < u_r < 28$ m/s, do show a deviation from the trend for the wind speed region below 26 m/s. Because the events above 26 m/s are so few (a total of 6), they do not represent statistically significant evidence of a change in trend.

4.3 Trend removal considerations

Generally, the wind process is composed of the components

* a synoptic mean value
* a synoptic and/or a mesoscale trend
* the field of turbulent fluctuations

For the purpose of the present and the following sections, the trend component will have to be removed. The field of turbulent fluctuations is defined as the residual component and will therefore depend on the method applied for this removal.

The basic assumption adopted is that the turbulent fluctuations are reasonably well-defined for given synoptic mean values of wind speed and lapse rate. The trend of the latter quantities reflects the speed and the particular stage of development of the travelling synoptic pressure system in which the time series in question is embedded. It is believed that these system characteristics disturb our understanding of the boundary layer relationships we are dealing with.

The fact that the slow synoptic trend is generally non-linear, requires a synoptic wind speed definition which takes this into account. Within the framework of the present static maritime wind discussion, the definition to be adopted is that of the 1 h running mean $U_{syn}(t)$.

The time series of wind u(t) in the time interval

$$[t_0 - T/2,\ t_0 + T/2],\quad T = 60 \text{ min}$$

centered at time t_0, is associated with a synoptic time series

$$U_{syn}(z,t) = (1/T) \int_{t-T/2}^{t+T/2} u(z,t')dt' , \qquad t \in [t_0-T/2,\ t_0+T/2] \qquad (1)$$

a basic mean wind speed defined for every hour,

$$U_{mean}(z.t_0) = U_{syn}(z.t_0) \qquad (2)$$

and a turbulent time series

$$u'(z.t) = u(z,t) - U_{syn}(z.t) \qquad (3)$$

Note that both this series and the series $U_{syn}(t)$ will generally contain modulated mesoscale components (15 min - 1.5 hour) if mesoscale weather systems are typical in the area. The fact that discontinuities are not present in the QS and PQS series will reduce this problem significantly for these series.

The ratio of the hourly standard deviation of the wind fluctuations, Eq.(3), to the hourly mean value of the wind speed, U_{mean}, is defined as turbulence intensity, and is further discussed in Section 4.5. Gusts are in the next section defined as the maximum mean wind speed of duration $T_i << 1$ hour. The ratio of the gust to the coincident running mean U_{syn} is called the gust factor, and is believed to be a slowly varying function. In modelling the statistics of gust factors and turbulence intensity, the associated hourly mean values of reference wind speed and lapse rate will be used.

4.4 The gust profile

4.4.1 Introduction

The gust of duration T_i for each hour is defined to be the maximum value of the running subinterval mean $<u>_{Ti}$ found during the hour. The actual subintervals selected in this investigation are 3.51 s (three logging periods), 15 s, 1 min and 10 min. The mean value in the subinterval is calculated in a sliding window, i.e. as the mean of the appropriate number of contiguous loggings, running through the whole time series, and advancing the starting point of the window one logging at a time. These maximum mean values, or gusts of duration T_i, for each 1 hour period are recorded.

The position of the gust, t_g, is defined as the mid-point of the window when the gust is recorded.

The gust factor for the subinterval T_i may be defined as the ratio between the gust value and the 1 h running mean, $U_{syn}(z,t_g)$, Eq. (4.3.1),

$$G_i(z) = \text{Max}(<u(z)>_{Ti})_{1h} / U_{syn}(z,t_g) \qquad (1)$$

Normalization with the 1 h running mean centered at time t_g, rather than the hourly mean value, will ensure that the effects of a linear trend will disappear. To see this, consider the artificial case with a linearly increasing wind speed with no fluctuations. The maximum wind speed would then be recorded at the end of the 1 hour interval. With the definition (1), a gust factor of 1 would be recorded, as is reasonable for a situation with no fluctuations. Division by the 1 hour mean value would on the other hand give a gustfactor dependent on the trend, which we wanted to remove.

However, the quantity to be studied further in this investigation is the ratio between the gust value and the running 1 h mean of the reference wind speed,

$$G_{ri}(z) = \text{Max}(<u(z)>_{Ti})_{1h} / U_{syn}(z_r,t_g) = G_i(z)\, U_{syn}(z,t_g) / U_{syn}(z_r,t_g) \qquad (2)$$

This quantity will be referred to as the reference gust factor. As indicated in the above equation, the reference gust factor equals the ordinary gust factor times a profile factor.

Of importance for practical purposes is the probability that the gust factor will exceed some value. To investigate this problem, information is required about the statistical distribution of gust factors. We shall see in the next section that the distribution is dependent on atmospheric stability. For the stable atmosphere, the distribution is approximately Gaussian. For neutral and unstable conditions, the distribution is still Gaussian for small and intermediate values of the gustfactor, but for large values the distribution is best described by an exponential tail joining the Gaussian. Therefore, the experimental distributions presented in the next section have been fitted to the following frequency function,

$$f(G) = \begin{cases} N \exp[-(G-\alpha)^2/2\sigma^2] & G - \alpha < D = \sigma^2/\delta \\ N \exp[-(G-\alpha-D/2)/\delta] & G - \alpha > D \end{cases} \qquad (3)$$

Both the function f(G) and its derivative satisfies the requirement of being continuous across the juncture point D. The physical interpretation of the parameters is rather obvious. σ is the width (standard deviation) of the Gaussian part and δ is the decay-length of the exponential tail. For a pure Gaussian distribution ($\delta = 0$), α will be the mean and median value of the gust factor; with an exponential tail, there will be correction terms which have to be calculated numerically. N is a normalization factor defined by the requirement

$$1 = \int_1^\infty f(G)\, dG$$

For practical purposes, the lower limit can be taken as $-\infty$, and from Eq. (3), N can be expressed explicitly by the error function erf as

$$N = \delta^{-1}\{ \pi^{1/2} y [1 + \mathrm{erf}(y)] + \exp(-y^2)\}^{-1} \qquad y = 2^{-1/2}\sigma/\delta$$
$$\mathrm{erf}(y) = 2\pi^{-1/2} \int_0^y \exp(-x^2)\, dx \qquad (4)$$

The determination of the best fit values of α, σ and δ is done from the cumulative distributions using the corresponding cumulative probability function

$$F(G) = \int_1^G f(x)\, dx \qquad (5)$$

The Norwegian Petroleum Directorate (NPD) has suggested a reference gust factor of the form

$$G_{ri}(z) = U(z,T_i) / u_r = 1 + a \ln(z/z_r) - b \ln(T_i/3600) \qquad (6)$$

to describe the variation of the gust wind $U(z,T_i)$ with height z, gust interval T_i and 1 hour mean wind speed u_r at $z = z_r = 10$ m. In the next section this formula is used as a starting point to describe the variation of the mean (for given z, u_r and stability γ) gust wind and the parameter α introduced in Eq. (3) with z, u_r and γ. Because short gusts increase more slowly with height than the longer ones, the parameterization scheme which has been adopted as an alternative to Eq. (6) also includes a cross term dependent on height z and gust duration T_i.

4.4.2 Experimental results

The quasi stationary and nearly quasi stationary data show within the statistical uncertainties the same behaviour as the complete set of data. Consequently, mean values of the gust factor and the shape parameters of the distribution have been determined from the full set of data. Therefore the results presented in this section are valid even during periods with changing weather patterns and represent the complete data set. This also implies that the gust structure is determined by atmospheric stability and reference wind speed rather than by large scale weather phenomena.

Plots of the mean value and standard deviation of the reference gust factors versus lapse rate are shown in Fig. 4.4.1 for the height 46 m at Sletringen. Data for the 4 selected gust lengths are displayed in 4 intervals of reference wind speed, 10-14, 14-18, 18-22, and $u_r > 22$ m/s. In Figs. 4.4.2-4, corresponding plots are shown for the heights 42, 20 and 10 m. In Figs. 4.4.5-8, scatter plots of the same data sets are shown versus reference wind speed. The curves shown in the Figs. 4.4.1-8 are based on the following formula

$$<G_{ri}> = \{0.97 + 0.10 \ln(z/z_r) + [-0.05 + 0.0055 \ln(z/z_r)] \ln(T_i/T)\} \cdot [1 + 0.004 (u_r-10)] + 0.2 \, sig(u_r,10.,-5) \, sig(\gamma,10,3) \quad (7)$$

where γ is the lapse rate, T_i length of the gust interval, T = 1 h and $sig(x,x_s,d)$ is the sigmoid function defined in Eq. (4.2.18). Units m/s and K/km are understood for the quantities with dimension velocity and thermal gradient, respectively. The main features apparent from Figs. 4.4.1-8 and Eq. (7) are:

* The lapse rate dependence is not very important for the mean value of the gust factor for wind speeds exceeding 10 m/s, and the importance decreases with wind speed. As we shall see below, the lapse rate dependence is mainly manifesting itself through the exponential tail in the gustfactor distribution.
* The dependence on height decreases with the length of the gust interval, meaning that the short gusts increase more slowly with height (approximately as $0.06 \ln(z/z_r)$ for 3.5 s) than the longer ones (approximately as $0.09 \ln(z/z_r)$ for 10 min) and the mean wind speed (approximately as $0.10 \ln(z/z_r)$).
* A slow increase of the reference gust factor with wind speed is indicated.

As already indicated, the frequency function of the gustfactor appears to be approximately Gaussian for small to intermediate values. In the following, the cumulative distributions will therefore be shown as "normal" plots, where the range along the vertical axis corresponds to $\pm$ 3 standard deviations, or probabilities from 0.0013 to 0.9987. A plot of an ideally normally distributed quantity would give a straight line. The extreme nonlinearity of the vertical axis should be noted.

Cumulative distributions of the observed reference gust factor without reference to stability class are shown for reference wind speed intervals 14-18 m/s and 18-22 m/s in

Figs. 4.4.9-12 for the heights 46, 42, 20 and 10 m. For practical applications, these are probably the most interesting distributions, since lapse rate data are normally not easily available. The fitted curves are based on Eq. (3). The shape parameters depend on the height z and the maximum point α of the distribution, and can approximately be described by the following ad hoc 3 factor formula

$$\sigma = \sigma_\gamma [\alpha - \sigma_r - \sigma_z \ln(z/z_r)] [\sigma_0 + \sigma_1 \ln(z/z_r)]$$
$$\delta = \delta_\gamma [\alpha - \delta_r - \delta_z \ln(z/z_r)] [\delta_0 + \delta_1 \ln(z/z_r)] \qquad (8)$$

The multipliers σ_γ and δ_γ will generally depend on lapse rate, but are in this case ("natural" data for all lapse rate classes) set equal to unity. The second factor describes the dependence on the length of the gust interval in terms of the most probable reference gust factor α. Note that the α-dependence is modified by z-dependent terms. The last factor takes care of the remaining z-dependence. The parameters were fitted for the heights 46 and 10 m and interval lengths $T_1 = 3.5$ s and $T_4 = 600$ s. For the intermediate values of z and T_i, the general logarithmic parameterization Eq. (8) was assumed. The following values were then found in the two wind speed ranges

$14 < u_r < 18$ m/s:

$$\alpha = 0.957 + 0.116 \ln(z/z_r) - 0.0463 \ln(T_i/T) + 0.0076 \ln(z/z_r) \ln(T_i/T)$$
$$\sigma_r = 0.70 \quad \sigma_z = 0.135 \quad \delta_r = 0.70 \quad \delta_z = 0.203$$
$$\sigma_0 = 0.05 \quad \sigma_1 = 0.014 \quad \delta_0 = 0.19 \quad \delta_1 = 0.108 \qquad (9)$$

$18 < u_r < 22$ m/s:

$$\alpha = 0.956 + 0.130 \ln(z/z_r) - 0.0512 \ln(T_i/T) + 0.0089 \ln(z/z_r) \ln(T_i/T)$$
$$\sigma_r = 0.80 \quad \sigma_z = 0.135 \quad \delta_r = 0.80 \quad \delta_z = 0.169$$
$$\sigma_0 = 0.066 \quad \sigma_1 = 0.023 \quad \delta_0 = 0.18 \quad \delta_1 = 0.102 \qquad (10)$$

As an example, for 15 s gusts at 46 m height and a reference wind speed of 20 m/s, the above set of parameter values together with Eq. (8) will yield the values

$$\alpha = 1.36 \quad \sigma = 0.035 \quad \delta = 0.1 \quad D = 0.01$$

for the basic parameters to be used in Eq. (3). Thus the exponential tail will indeed play a dominating role. This is also apparent from the graphs.

Cumulative distributions of the reference gust factor for stable, neutral and unstable lapse rate for the reference wind speed range $14 < u_r < 18$ m/s are shown in Figs. 4.4.13-16 for the heights 46, 42, 20 and 10 m at Sletringen. The 3 stability classes correspond to lapse rate values $\gamma < 5$, $5 < \gamma < 15$ and $\gamma > 15$ K/km. In Figs. 4.4.17-20 the same sets of plots are shown for the wind speed range $18 < u_r < 22$ m/s. The

values of α for the set of curves shown are given in Table 4.4.2. They can approximately be fitted by the type of formula given in Eqs. (9) and (10) for α, but the coefficients will depend on stability, and curvature effects are also apparent. The values of the stability multipliers σ_γ and δ_γ used are given in Table 4.4.1. the shape parameters σ and δ are then determined by Eq. (8) with the coefficients given by Eq. (9) or (10), lines 2 or 3. Because the stability dependent parameterization is of limited practical importance in any case, it has been omitted.

The parameters - including the α - for neutral conditions are however given by Eqs. (8-10) with $\sigma_\gamma = \delta_\gamma = 1$ with reasonable accuracy, and this set is recommended for general use. Extrapolation to higher wind speed can probably be done with some care, but is generally not recommended, as the variation of the shape parameters is rather intricate. For the wind speed ranges covered, the decay length δ of the exponential tail decreases with wind speed, whereas the standard deviation σ and maximum point α for the Gaussian part increase.

The probability that the reference gust factor will exceed some specified value is of interest for design purposes. This probability is defined from the frequency function Eq. (3) as (cmp. Eq. (4))

$$p(G>G_p) = \int_{G_p}^{\infty} f(G')\, dG' \tag{11}$$

For small values of p when G is in the exponential region, $G > \alpha + \sigma^2/\delta$ (cmp. Eq. (3)), the integral in Eq. (11) can be evaluated analytically. This allows Eq.(11) to be inverted to give the limiting reference gust factor G_{rp} as a function of the exceedance probability p as

$$G_{rp} = \alpha + \sigma^2/2\delta + \delta \ln(N\delta/p) \tag{12}$$

Based on the parameter values defined by Eqs. (3), (4), (8) and (11), plots of G_{rp} are shown for p = 0.01 and 0.001 in Fig. 4.4.21 for reference wind speed u_r = 20 m/s. Comparing the experimental cumulative distributions for the reference gust factor for the two speed ranges covered, it can be seen that the limiting reference gust factor seems to decrease slowly with wind speed for small values of p, corresponding to values of the cumulative probability F = 1 - p close to 1. It is then conservative to assume that the limiting gustfactor calculated for u_r = 20 m/s and shown in Fig. 4.4.21, will also be valid at u_r = 30 m/s.

The dependence of the limiting gust factor on probability can rather easily be inter- or extrapolated if the logarithmic dependence on p defined by Eq. (12) is noticed. The values corresponding to probabilities p_1 and p_2 are simply related by

$$G_r(p_2) = G_r(p_1) + \delta \ln(p_1/p_2) \tag{13}$$

As is apparent from Figs. 4.4.9-20, the experimental data are found in the ranges

$u_r < 22$ m/s and $p > 0.01$. Therefore, higher wind speeds and smaller probabilities will represent extrapolations from the experimental basis.

The Norwegian Petroleum Directorate (NPD) has proposed the following general formula for the reference gust factor

$$G_{ri}(z,Ti) = 1 + 0.15 \ln(z/z_r) - 0.051 \ln (T_i/T), \qquad T = 3600 \text{ s} \tag{14}$$

A comparison between this formula and the present recommendation for the mean reference gust factor, Eq. (7), is shown in Fig. 4.4.22 for 3 values of the lapse rate, γ = 0, 10 and 20 K/km, and for reference wind speed u_r = 20 and 30 m/s. Eq. (7) gives higher values of the reference gust factor for heights close to 10 m, but implies a smaller increase with height, giving a cross-over point where the two parameterizations are approximately equal at $z \simeq 15$ m for u_r = 20 m/s and at $z \simeq 25$ m for u_r = 30 m/s. The spread due to variation of the lapse rate is not very important compared to the disagreement in the height variation.

Table 4.4.1. Lapse rate multipliers σ_γ and δ_γ used in conjunction with Eqs. (9) and (10) to determine the curves shown in Figs. 4.4.13-20.

Lapse rate (K/km)	$14 < u_r < 18$ m/s		$18 < u_r < 22$ m/s	
	σ_γ	δ_γ	σ_γ	δ_γ
$-20 < \gamma < 5$ (Stable)	1.00	0.50	1.00	0.42
$5 < \gamma < 15$ (Neutral)	1.00	1.00	1.00	1.00
$15 < \gamma < 30$ (Unstable)	1.80	1.25	1.00	1.00

Table 4.4.2. The value of α in Eq. (3) (the reference gust factor value for which the distribution peaks) used to calculate the curves shown in Figs. 4.4.13-20.

Height	Atm Stab\T	$14 < u_r < 18$ m/s				$18 < u_r < 22$ m/s			
		3.5 s	15 s	60 s	600 s	3.5 s	15 s	60 s	600 s
46 m	Sta	1.414	1.367	1.295	1.210	1.450	1.390	1.350	1.240
	Neu	1.380	1.340	1.280	1.193	1.415	1.370	1.340	1.227
	Uns	1.380	1.345	1.300	1.200	1.405	1.355	1.315	1.210
42 m	Sta	1.400	1.350	1.280	1.197	1.435	1.385	1.330	1.220
	Neu	1.370	1.333	1.270	1.182	1.405	1.360	1.315	1.215
	Uns	1.380	1.340	1.285	1.190	1.390	1.345	1.300	1.200
20 m	Sta	1.333	1.285	1.210	1.120	1.390	1.330	1.245	1.135
	Neu	1.325	1.272	1.210	1.115	1.365	1.310	1.245	1.140
	Uns	1.340	1.295	1.225	1.128	1.350	1.295	1.230	1.135
10 m	Sta	1.295	1.232	1.142	1.047	1.330	1.250	1.165	1.060
	Neu	1.280	1.215	1.145	1.040	1.320	1.245	1.170	1.060
	Uns	1.295	1.235	1.165	1.060	1.300	1.250	1.170	1.070

4.5 Turbulence intensity

The turbulence intensity is in this investigation defined as the 1 h r.m.s. value of the difference between the instantaneous wind speed and the 1 h running mean of the wind, divided by the 1 h mean wind speed for the period, or

$$I = \sigma_u(z)/U_{mean}(z) = \{<[u(z,t) - U_{syn}(z,t)]^2>_{1h}\}^{1/2} / U_{mean} \quad (1)$$

where U_{mean} and U_{syn} are defined by Eq. (4.3.2) and (4.3.1), respectively.

For the purposes of this section, the quasi stationary and partly quasi stationary data were examined separately, but within statistical uncertainties they showed the same behaviour as the complete set of data. Thus, the present results are valid for the complete set of data.

Plots for the observed mean and standard deviation of turbulence intensity versus lapse rate are shown in Fig. 4.5.1 for the heights 5, 10, 20, 42 and 46 m at Sletringen. Data are displayed separately for 4 intervals of reference wind speed, 10-14, 14-18, 18-22 and $u_r > 22$ m/s. In Fig. 4.5.2, similar plots versus reference wind speed are shown for the same sets of data for 4 lapse rate classes, $\gamma < 0$, 0-10, 10-20 and $\gamma > 20$ K/km. The curves shown in Figs. 4.5.1-2 are based on the following ad hoc formula

$$I = 0.085\ (z/z_r)^{-.22} + 0.0019\ u_r + 0.12\ sig(u_r,12,-2)\ sig(\gamma,15,3) \quad (2)$$

where γ is the lapse rate, $sig(x,x_s,d)$ is the sigmoid function defined in Eq. (4.2.18) and units m/s or K/km are understood for the variables. The main properties of the mean value of the turbulence intensity indicated from Figs. 4.5.1-2 and incorporated in Eq. (2), are that I

* decreases with height
* increases slowly with wind speed for stable conditions.
  For unstable conditions: decreases with wind speed for moderate wind speeds and increases with wind speed for strong wind speeds.
* increases with lapse rate, the increase being pronounced for reference wind speeds less than 12 m/s, only.

The height dependence is in this case better described by a power law with negative exponent than by the logarithmic parameterizations used for mean wind speed and gust. The increase with wind speed has been modelled to be independent of height - and determined by the regression coefficients for the three highest sensors. The sensor at 10 m actually shows a somewhat higher increase and the one at 5 m a lower one. As in the earlier sections, the sigmoid function was found practical in modelling the lapse rate dependence. The variation for reference wind speeds below 10 m/s was not examined. Due to the lapse rate dependence, the data for unstable to neutral conditions show a minimum for reference wind speeds in the region 16 - 18 m/s. For reference wind speeds

above 20 m/s, there is effectively no dependence on lapse rate, and the mean value of the turbulence intensity is in this case well described by the first two terms in Eq. (2), giving only a u_r- and z-dependence.

Normal plots of the cumulative distributions for the turbulence intensity for stable, neutral and unstable conditions and for the heights 46, 42, 20 10 and 5 m are shown in Fig. 4.5.3 and 4.5.4 for reference wind speed in the range 14-18 and 18-22 m/s, respectively. The three stability classes correspond to lapse rate values $\gamma < 5$, $5 < \gamma < 15$ and $\gamma > 15$ K/km. These distributions show the same characteristic features as the cumulative distributions of the reference gust factor shown in the previous section. Especially for the wind speed range 14-18 m/s, there is a characteristic change of slope between the lower and upper half of each plot, most pronounced for neutral and unstable conditions. The variation within each section may well be fitted by a straight line. A somewhat better description is obtained from fit to a distribution function on the form

$$f(I) = N \{\exp(- d_1^2/2 - d_1)/\sigma_1 + \exp(- d_2^2/2 + d_2)/\sigma_2\}/[\exp(-d_1) + \exp(d_2)]$$
$$d_k = (I-I_0)/\sigma_k \quad k = 1, 2 \tag{3}$$

rather than the function introduced in the previous section. In Eq. (3), the transition between standard deviations σ_1 and σ_2 is described by using as weighting factor the exponential function with argument being linear in the normalized deviations d_1 and d_2. Weighting in addition with $1/\sigma_1$ and $1/\sigma_2$ ensures that the two regions are about equal in terms of cumulative probability. N is a normalization factor defined by the requirement of

$$\int_0^\infty f(I)\, dI = 1$$

The curves shown in Figs. 4.5.3-4 are based on Eq. (3) with the following z-dependence of the parameters

$$I_0 = I_{0r} + I_{0z} (z/z_r)^{-0.5} \tag{4}$$

$$\sigma_k = \sigma_{kr} + \sigma_{kz} \ln(z/z_r) \quad k = 1, 2 \tag{5}$$

The values of the basic parameters determined by a fit to the data are given in Table 4.5.1. The amount of data in the wind speed range 18-22 m/s is insufficient to give a precise determination of the parameters (or the type of the distribution function), and the results should only be considered as indicative. But the asymmetry in the distribution function above and below the median point is really striking for neutral and unstable conditions in the range $14 < u_r < 18$ m/s, and more so for increasing height. With increasing wind speed, the asymmetry is reduced.

Table 4.5.1 Parameters used in conjunction with Eqs. (3-5) to determine the curves shown in Figs. 4.5.3-4.

a) $14 < u_r < 18$ m/s

Lapse rate	Stability	I_{0r}	I_{0z}	σ_{1r}	σ_{1z}	σ_{2r}	σ_{2z}
$\gamma < 5$ K/km	Stable	0.057	0.050	0.009	-0.0015	0.011	0.0015
$5 < \gamma < 15$ K/km	Neutral	0.060	0.050	0.009	-0.0015	0.029	0.0045
$\gamma > 20$ K/km	Unstable	0.067	0.050	0.012	0	0.041	0.0030

b) $18 < u_r < 22$ m/s

Lapse rate	Stability	I_{0r}	I_{0z}	σ_{1r}	σ_{1z}	σ_{2r}	σ_{2z}
$\gamma < 5$ K/km	Stable	0.065	0.053	0.009	0	0.016	0.003
$5 < \gamma < 15$ K/km	Neutral	0.070	0.050	0.009	0	0.023	0.0015
$\gamma > 20$ K/km	Unstable	0.070	0.050	0.009	0	0.023	0.0015

4.6 Wind direction fluctuations

4.6.1 Introduction. Discussion of general properties and special events

The wind direction is generally very stable for maritime conditions. This may be seen from Appendix report no. 1, where time series of wind direction, based on 10 min mean values, are shown for all days having at least one occurrence of reference wind speed greater than 15 m/s. However, in conjunction with rapid changes of the general level of wind speed, there may also be large changes of wind direction. These changes can be of the order of 90°. Usually, these regime changes evolve during one to a couple of hours.

In a time series of wind direction data, where the elements are mean values over some time interval in the range 1 s to 10 min, the median difference between neighbouring elements is close to 1.5°, independent of interval length and wind speed. This conclusion applies to the full data set, and illustrates the general stability of wind direction for maritime conditions.

The basic time series of direction raw data from Sletringen represent close to instantaneous values of the sensor output (sampling time 0.05 s), but the mechanical inertia of the sensor will cause some smoothing with respect to very rapid fluctuations. The effective time constant decreases with wind speed, and is not known precisely. For wind speeds above 15 m/s, it is of the order of 0.1 s. The Skipheia raw data represent mean values of the sensor output for the basic logging period.

In Figs. 4.6.1 and 4.6.2, two of the more dramatic examples of wind direction time series are shown, together with the time series of the 10 m wind speed. Data for the basic 1.16 s period are plotted. In the first case, the reference wind speed increases from a level of about 5 m/s to 25 m/s during 40 min. This is associated with a change of wind direction of 60° over a period of 15 min. In the following 60 min period, a slow decrease is observed, and the total effective change becomes 40°. During the preceding 2 h period, a change of approximately 70° had taken place at low wind speeds, making the maximal change in a 2 h period about 120° (cmp. Appendix report for 11-Nov-1988). In the second case, a change of wind direction of 120° takes place during 35 min, while the reference wind speed is reduced from around 17 m/s to 8 m/s. A jump of some 50° is seen to take place in 40 s with wind speeds around 15 m/s . By far the most dramatic example of wind direction change at high wind speed is shown in Fig. 4.6.3a, where a change of some 85° takes place in 85 s, while the 10 m wind speed is reduced from about 18 m/s to 13 m/s. The most dramatic 5 min period of the same event is shown with better time resolution in Fig. 4.6.3b. A running 1 min average will switch from a level of 252° to 325°, or 73°, in less than 2 min.

Apart from these events due to a sudden change of wind regime, the general picture is that the wind direction is rather stable with fluctuations of a few degrees. But all frequency probability distributions are found to be asymmetric, with large excursions much more probable than indicated by a normal distribution based on small scale fluctuations. We will return to this problem in the sections below.

4.6.2 Maximum fluctuation of wind direction in 1 hour periods

Following the discussion of wind speed gusts in Sec. 4.4. wind direction fluctuations are defined relative to the running 1 h mean wind direction. which is defined in analogy with Eq. (4.3.1) as

$$\Theta_{syn}(t) = (1/T) \int_{t-T/2}^{t+T/2} \theta(t')dt' \qquad (1)$$

Mean values of wind direction over a set of subintervals T_i. will be compared to $\Theta_{syn}(t)$. and are defined correspondingly as

$$\langle\Theta(t)\rangle_{Ti} = (1/T) \int_{t-T_i/2}^{t+T_i/2} \theta(t')dt' \qquad (2)$$

The actual subintervals selected in this investigation are 1.17 s (one logging period). 3.51 s (three logging periods). 15 s. 1 min and 10 min. The mean value in the subinterval is calculated in a sliding window. running through the whole time series. and advancing the starting point of the window one logging at a time.

The maximum direction fluctuation. D_i. for the subperiod T_i is defined as the maximum absolute value of the difference between the subinterval mean and the running 1 h mean.

$$D_i = \text{Max}\{|\langle\Theta\rangle_{Ti} - \Theta_{syn}|\} \qquad (3)$$

The maxima are recorded for each 1 hour period and each subinterval.

Wind direction is normally defined in the interval [0. 360°]. For the calculation of mean values and fluctuations. a time series without cycle shifts is needed. For that purpose. an auxiliary continuous time series is defined by adding/subtracting 360°. This time series will in general fall outside the normal angular interval. The calculation of mean values is then in practical terms unambiguous. because wind direction changes of the order of 180° have not been observed for the averaging periods in question for reference wind speed exceeding 10 m/s. The direction sensors do give a signal which switches abruptly from the maximum value to zero as the full cycle point is passed. Some averaging is involved in recording this signal for each logging period. and spurious values can arise due to the cycle passage. A special filtering procedure is therefore applied near this change-over point. and dubious values are rejected. As wind directions around north. where this problem arises. are rather rare. this is not a serious problem in practice. An example of a 360°/0° crossing

is shown in Fig. 4.6.2. All the fluctuation calculations were found to proceed smoothly past this crossing, as well as the few other $360^0/0^0$ crossings that are of relevance.

Cumulative distributions of the maximum wind direction fluctuations are shown in Fig. 4.6.4 for reference wind speed in the ranges $10 < u_{ref} < 14$ m/s and $u_{ref} > 14$ m/s. respectively. The data shown are from Sletringen, and are not resolved with respect to lapse rate. The distributions are presented as normal plots. The curves shown for the upper wind speed interval represent the asymmetric frequency probability distribution introduced in Sec. 4.5, which in this case can be written as

$$f(D) = N \{\exp(-d_1^2/2)\exp(-d_1)/\sigma_1 + \exp(-d_2^2/2)\exp(d_2)/\sigma_2\}/[\exp(-d_1) + \exp(d_2)] \quad (4)$$
$$d_k = (D - D_{0i})/\sigma_k, \quad k = 1,2$$

where the index i refers to fluctuation duration. N is a normalization factor, σ_1 and σ_2 are the standard deviation for the parts below and above the approximate median point (of the corresponding cumulative distribution) D_{0i}, respectively. The first term gets most weight when $D < D_{0i}$, and the second when $D > D_{0i}$. The standard deviations used in the fit in Fig. 4.6.4 are

$$\sigma_1 = 1.5^o, \quad \sigma_2 = 9^o$$

The values of the parameters D_{0i} depends on the time interval T_i considered, and were found to be

T_i/s	1.17	3.51	15	60	600
D_{0i}/degr.	15.5	12.5	8.0	6.0	3.5

It can be shown from Eq. (4) that the most likely maximum wind direction deviation of duration T_i is slightly below the value of D_{0i}, listed in the above table.

The value of the maximum fluctuation during a 1 h period is seen to depend strongly on the averaging time interval. For reference wind speeds above 14 m/s, the values in the basic time series are normally less than 20^o from the 1 h running average, and the deviation of the 1 min running mean from the 1 h running mean is normally less than 10^o. The frequency distributions are very asymmetric around the median points, with a ratio of 6 between the standard deviations for the two parts, as defined by Eq. (4). The most extreme events are associated with the time series shown in Fig. 4.6.1-3.

4.6.3 Standard deviation of wind direction

The r.m.s. values of the wind direction fluctuations from the 1 h running mean have been calculated for each 1 h period. We call this quantity the standard deviation. Cumulative distributions of this quantity for the Sletringen data are shown as normal plots in Fig. 4.6.5 for the reference wind speed ranges (m/s) [10. 14] and [14. 25] and the lapse rate ranges (K/km). [-10.0. 2.5] (stable). [2.5. 17.5] (neutral) and [17.5, 40.0] (unstable conditions). There is a modest lapse rate dependence. The observations in the higher wind speed range were fitted to the asymmetric distribution defined in Eq.(4). The curves shown correspond the standard deviations (for the standard deviation distributions)

$$\sigma_1 = 1.0^{\circ}, \quad \sigma_2 = 4.0^{\circ}$$

and "median" values D_0 of

$D_0 = 2.5^{\circ}$ for stable conditions

$D_0 = 4.0^{\circ}$ for near neutral conditions

$D_0 = 5.0^{\circ}$ for unstable conditions

The most likely value of the standard deviation is slightly below the corresponding value of D_0 listed above.

The statistical basis for the stable data is rather poor. Again. the distributions imply that small values of the r.m.s. wind direction fluctuations represent the normal situation. but the "tail" make higher values more probable than a simple normal distribution would indicate. As might be expected. the direction fluctuations are highest for unstable conditions.

5. DYNAMIC MARITIME WIND

5.1 Introduction

In Chapter 4 of the present report a description of maritime turbulent wind was established for features of the wind process which are relevant for offshore structures in general

* the 1 hour mean wind profile;
* the gust profile;
* the turbulence intensity profile.

Whereas these aspects of the wind process represent bulk or integral properties of wind, more detailed information is needed for structures which are dynamically sensitive to wind

* spectral energy density for turbulence providing a measure of the kinetic energy associated with turbulent eddies as a function of frequency;
* correlation and coherence in 3 dimensions providing a measure of the eddy dimensions as functions of frequency;
* phase relationships providing a measure of eddy shape as a function of frequency.

Similarly to the analysis of Chapter 4, the present analysis emphasizes that this information shall be parameterized relative to the synoptic state of the atmosphere as given by

* the reference wind speed;
* some bulk measure of air mass stability.

In the study special attention is given to wind speed fluctuations in the frequency range around 0.01 Hz (90-120 sec) which is the range containing the characteristic frequencies of typical floating, compliant offshore production systems.

Following the discussion of wind gusts and turbulence intensity in Chapter 4, the concept of moving average is adopted in order to define the turbulent time series for the given synoptic context. However, the present discussion differs from that of Chapter 4 in several ways:

* During the measurements the sampling frequency was 0.85 Hz (= 512/10 min). Also the FFT-method requires a number of data points in the time series which is equal to some integer power of 2. Therefore the basic length of the time series used to establish the individual spectra is now 40 min corresponding to 2048 data points (no resampling procedure has been adopted to obtain 60 min time series).

* The time series obtained from the raw data by removing the 40 min moving average is used as a basis to obtain the spectral coefficients. This time series still contains residual modulated mesoscale components. Methods to eliminate these components, and the general relation between the spectral coefficients obtained from the 40 min time series and the true ones obtainable in principle from an uninterrupted time series are discussed in the next section.

The number of good quality 40 min time series in wind speed classes available from the two stations for the present study of dynamic maritime wind is given below. Note that for Skipheia, this table contains both the number for the extended as well as the restricted maritime sector.

Mean wind speed (m/s)	# 40 min series		
	Sletringen	Skiph. 160-400	Skiph. 180-240
10 - 15	556	785	302
15 - 20	173	227	99
20 - 25	22	40	20
25 - 30	-	6	5

5.2 Definition of turbulence

Suppose that the basic function of time is given as

$$u(t) = A_0 + \sum_{m=1}^{\infty} \left(A_m \cos(\omega_m t) + B_m \sin(\omega_m t) \right) \qquad (1)$$

If the synoptic value of this function, defined as a moving average over a time T, viz.

$$u_{SYN}(t) = \frac{1}{T} \int_{t-T/2}^{t+T/2} u(t')dt'$$

is subtracted from the original function, it may be shown that the resulting function $u_{res}(t)$ becomes

$$u_{res}(t) = \sum_{m=1}^{\infty} \left(1 - \frac{\sin x_m}{x_m} \right) \left(A_m \cos(\omega_m t) + B_m \sin(\omega_m t) \right) \qquad (2)$$

where

$$x_m = \frac{\omega_m \cdot T}{2} \equiv \frac{\pi \cdot T}{\tau_m}$$

Note that the modulating function

$$F_M = 1 - \frac{\sin x_m}{x_m}$$

depends strongly on T. $F_M(T,\tau_m)$ is shown versus τ_m in Fig. 5.2.1 for T = 40 min. From Fig. 5.2.1 it is seen that the function $u_{res}(t)$

* is effectively filtered for the slowly varying synoptic components with period longer than 1 - 1.5 hour;
* is effectively not changed with respect to components with period equal to or smaller than 10 min.;
* contains mesoscale components with period in the range 10 min $< \tau_m <$ 1.5 hour which are moderately to strongly affected by the averaging process.

From these conclusions it follows that the components which have been removed are the ones being responsible for the synoptic trend. However, the somewhat faster variations associated with mesoscale processes are still present in a modified form. Fortunately, the components of particular interest for the present study are not influenced.

As mentioned, the wind is experimentally sampled N = 2048 times in the periods T = 40 min. A discrete Fourier series, corresponding to the finite time resolution 1/T, is given by

$$u^{**}(t) = \sum_{n=1}^{N/2} [a_n \cos(\omega_n t) + b_n \sin(\omega_n t)], \quad \omega_n = 2\pi n/T \tag{3a}$$

The mean term is omitted, as it does not enter in the turbulence evaluation (strictly speaking, only the sin term can be evaluated for n = N/2). The coefficients a_n,b_n can be evaluated from A_n,B_n. If u^{**} is assumed to represent u_{res} in the interval [-T/2,T/2], the relations are

$$a_n = \cos(\pi \cdot n) \cdot 2 \sum_{m=1}^{\infty} \left(1 - \frac{\sin x_m}{x_m}\right) \cdot B_m \cdot \frac{x_m \cdot \sin x_m}{x_m^2 - (\pi \cdot n)^2}$$

$$b_n = \cos(\pi \cdot n) \cdot 2\pi \cdot n \sum_{m=1}^{\infty} \left(1 - \frac{\sin x_m}{x_m}\right) \cdot A_m \cdot \frac{\sin x_m}{x_m^2 - (\pi \cdot n)^2} \tag{3b}$$

The weight functions

$$F_{A1} = \frac{\pi \cdot n \cdot \sin x_m}{x_m^2 - (\pi \cdot n)^2} \quad \text{and} \quad F_{A2} = \frac{x_m \cdot \sin x_m}{x_m^2 - (\pi \cdot n)^2}$$

are shown in Fig. 5.2.2 versus τ_m for n = 40 corresponding to T/n = 1 min.

The real wind spectrum is continuous, and the spectral coefficients A_m,B_m should be replaced with spectral density functions $A(\omega_m)$,$B(\omega_m)$. Therefore the above sums are integrals with a contributing range centered at $\omega_m = \pi\, n$. Thus, it follows that if the continuous spectrum is reasonably smooth, then the main contribution to a_n, b_n is from A_m, B_m when $\omega_n \simeq \omega_m$ or from the corresponding continuous functions $A(\omega_n)$,$B(\omega_n)$. This is approximately valid even for small values of n, as the modulating function $F_M = 1$ for $\omega_m = \omega_n$. However, both the variation of F_M and the relative width of the frequency region contributing during summation (or integration) increase for small n values.

Based on this discussion it is concluded that the three lowest terms in n shall be rejected because they provide an inaccurate description of the true spectrum. This will limit the spectrum to periods less than 13 min, meaning in addition that mesoscale contributions are excluded. It is therefore concluded that the modified inverse-Fourier transform

$$u_{turb}(t) = \sum_{n=4}^{N/2} [a_n \cos(\omega_n t) + b_n \sin(\omega_n t)] \tag{4}$$

will have the properties of

* having zero mean value;
* containing no synoptic or mesoscale energy and corresponding trend;
* describing adequately the components of turbulence which are of primary interest for the present study;
* containing the components of the original time series which are expected to depend primarily on the synoptic state. Thus, these components are expected to be invariant to change of the trend for a given synoptic state.

An example of the series u(t), $u_{syn}(t)$, $u_{res}(t)$ and $u_{turb}(t)$ is shown in Fig. 5.2.3.

In the next sections, an estimate of a_n,b_n is obtained for each sensor and period by performing an FFT on the sampled wind speed time series with the moving average value removed. These experimental estimates of discrete sets of spectral coefficients are related to the true spectral functions $A(\omega)$,$B(\omega)$ the same way as discussed above. However, when the N spectral coefficients are calculated from an N point time series by FFT, aliasing effects may be important. If the signal being sampled contains components with frequencies $f > f_N = N/2T$, f_N being the Nyquist frequency, then the energy associated with these components is mapped into the frequency region $[0,f_N]$ in addition to the true one. In particular, a component at frequency f in the region $[f_N,2f_N]$ is mapped to $f-f_N$. The wind speed spectra being discussed in the following are calculated on the basis of mean values for each sampling period, as discussed in Sec. 2.1. This effectively reduces the aliasing problem, and since the high frequency region is not emphasized in the present investigation, the detailed discussion is left out.

Some practical information concerning calculation of the turbulence characteristics may be mentioned at this point: Before application of the FFT-procedure, holes in the time series had to be taken care of. Holes were filled, or reduced to two smaller ones, by generating a value for a position in the middle as a sum of two contributions:

(1) A straight line interpolation between the values bordering the hole.
(2) A random term generated by assuming a Gaussian distribution, the width depending on the width of the hole and the standard deviation for the period in question.

This procedure was then repeated until the original hole was completely filled. Not more than 10% of the data in a single time series were replaced. The maximum tolerated length of one single hole was 127 points.

5.3 Turbulence spectra

5.3.1 Data input to the parameterization process

The spectral energy $M_i(f_k,z)$ for time series no. i corresponding to a height z and a frequency $f_k = k/T$ is obtained by averaging the sum of the squared Fourier coefficients defined in Eq.(3b).

$$R_n^2 = a_n^2 + b_n^2 \tag{1}$$

over a certain frequency range centered at f_k, i.e.

$$M_i(f_k,z) = \frac{T}{2}\frac{1}{2m+1}\sum_{n=k-m}^{k+m} R_n^2 \tag{2}$$

For large k, m was chosen to give intervals of constant length on a logarithmic scale with 3 intervals corresponding to a doubling of frequency. Smaller values of k were given special treatment. The detailed procedure adopted is that described in the final report from the Phase 1 project.

From the 26 frequency averaged spectral estimates $M_i(f_k,z)$ for each height z and 40 min period, appropriate ensemble averaging in narrow intervals of reference wind speed u_r (10 m, 40 min mean) and lapse rate γ provide our estimate for the spectral energy to be

$$M(f,u_r,\gamma,z) = \langle M_i(f_k,z)\rangle_{\Delta ur,\Delta\gamma} \tag{3}$$

For the reference wind speed u_r, 10 intervals are used in the range 10 - 22 m/s. The width of the intervals is taken to be equidistant in $\ln(u_r)$. Events with $u_r > 22$ m/s are included in the uppermost class.

For lapse rate, 10 intervals having the same width are defined in the range - 10 to 40 K/km.

For each interval in u_r the mean value of all events included in that interval is denoted the interval value, and used as input to the subsequent parameterization process. Lapse rate values are treated similarly.

Plots of the experimental values of f $M(f,u_r,\gamma,z)$ versus the frequency f for the various heights at the two stations are shown in Figs. 5.3.2 - 9 for 3 classes of wind speed and 3 classes of lapse rate.

5.3.2 The parameterization process

During the Phase 1 project theoretical 3 parameter spectral functions were fitted to the 26 frequency average spectral estimates M(f) for each 40 min period and each height level z. Next the 3 spectral parameters were related to the imposed variables u_r and γ for each 40 min period and each height level z.

The present analyses for the Phase 2 project has not adopted this procedure. The fit to a 3 parameter spectral function is now based on the ensemble averaged spectral estimates $M(f,u_r,\gamma,z)$. The dependence of these 3 parameters on u_r, γ and z is then further investigated from this basis. For this purpose a special minimalization program has been developed. The program can handle the strong correlations in the parameters usually found in this type of non linear fitting. Parameters entering linearly and non linearly are treated separately: For each set of non linear parameters, the linear parameters are calculated exactly.

Let $S(f,u_r,\gamma,z;\ p_1,\ \ldots,\ p_m)$ denote the theoretically expected smooth spectral function of u_r, γ and z, where $p_1,\ \ldots,\ p_m$ are coefficients or exponents, i.e. constants, to be determined to give the best fit to the ensemble averaged spectral estimates $M(f,u_r,\gamma,z)$. Then the objective is to determine the parameters so that

$$\sum_i W_i \cdot \left[M(f,u_r,\gamma,z) - S(f,u_r,\gamma,z;\ p_1,\ldots,p_m)\right]^2 = \text{minimum} \qquad (4)$$

where the sum runs over all intervals in f, u_r and γ and over all heights z. Note that an interval dependent weight function W_i has been introduced. The weight function W_i for each 4-D interval is from statistical theory expected to be

$$W_i = (\#\ \text{of events})/(\text{expectation value})^2$$

In the present context the expectation value is taken to be the ensemble averaged spectral estimate $M(f,u_r,\gamma,z)$. The "number of events" is the number of 40 min time series within the specified 2-D interval of u and γ times the number of frequencies within the specified frequency interval.

The weight function applied in the present study do, however, differ from the above theoretically justified one in several ways:

* In order to reduce fluctuations in the weight estimates, the weight adopted was the mean value over all lapse rate intervals. Thus, the weight assigned to an interval is independent of the lapse rate for the interval;
* In accordance with the discussion of Section 5.2 the weight for frequencies below (10 min) is set equal to zero:
* In order to avoid too strong high frequency influence on the spectral parameters and therefore on the spectral shape at low frequencies, the weight factor for frequencies higher than f_x = 0.065 Hz (15 sec) is reduced: The number of frequency values in an interval is proportional to the frequency (logarithmic spacing). Therefore the high frequencies will dominate the fit. This is avoided by freezing the frequency factor in the "number of events" for frequencies higher than f_x to that at f_x. In addition the weight is reduced by a factor of 0.5.

5.3.3 The parameterization scheme

In the final report for the Phase 1 project, turbulence spectra were well represented by the scheme

$$\begin{aligned} S(f) &= A \,/\, (B^n + f^n)^{5/3n} \\ A &= a\, u^{8/3}\, (z/z_r)^{-x} \\ B &= b\, u\, (z/z_r)^{-y} \\ y &= y_0\, g \end{aligned} \tag{5}$$

where a, b, n and g all showed lapse rate dependence of the type

$$a = a_0 + a_t \exp[\, (dT/dz) \,/\, \tau_a] \tag{6}$$

The attractive feature of this scheme is the exponent n which represent a generalization relative to the earlier schemes, n = 1 and n = 5/3 corresponding to the traditional Kaimal spectra and n = 2 to the Harris spectrum. By relating n to lapse rate it was hoped that this approach would explain the different values for the exponent found in the literature.

The overall fit obtained by (5) was quite good, but by part the scheme is not particularly elegant: To get a good fit versus z, the exponents x and y_0 had to be given z-dependence by "hand", indicating that the above power-law dependence was not very successful. This problem is primarily associated with the prescribed z-dependence of the turbulence length scale which for physical reasons is expected to depend on z for high frequencies and to be independent of z for low frequencies. For unstable conditions, n-values close to 0.5 were found, which is below the traditional range.

A major problem has also been to find a parameterization of atmospheric stability that is both simple and effective. The primary stability variable is of course the temperature gradient, or lapse rate $\gamma = -\, dT/dz$. But its impact on the spectra is modified both by wind speed and height - and as already discussed - varies with frequency. Traditionally, the situation has been simplified by imposing Monin-Obukov or mixed layer scaling, but it is well known that both approaches often fail over the ocean, as discussed by Panofsky and Dutton (1984). Basically, the problem is to parameterize a function depending on four variables.

The majority of suggested parameterization schemes for turbulence spectra are on the form of Eq.(5) or are for convenience written as

$$f\, S(f) = A\, f/(B^n + f^n)^{5/3n} \tag{7}$$

Because this essentially will be the working frame in the present description, the characteristic features will be briefly described below.

The high and low frequency asymptotes are, respectively,

$$A\, f^{-2/3} \qquad \text{and} \qquad A\, B^{-5/3}\, f$$

The peak frequency and corresponding maximum value of (7) are

$$\begin{aligned} f_x &= (3/2)^{1/n}\, B \\ f_x\, S(f_x) &= (0.3257)^{1/n}\, A\, B^{-2/3} \end{aligned} \tag{8}$$

and the total variance becomes

$$\sigma^2 = \int_0^\infty S(f)\, df = C(n)\, A\, B^{-2/3}$$

where C(n) is a function of the exponent n only, shown in Fig. 5.3.1a. Looking at Eq. (8), it follows that the variance can be conveniently expressed in terms of the maximum in the f S(f) spectrum.

$$\sigma^2 = \int_0^\infty S(f)\, df = Cx(n)\, f_x\, S(f_x)$$

where Cx(n) also is a function of the exponent n only, and is shown in Fig. 5.3.1a.

The high frequency asymptotic form obeys Kolmogorov scaling, and is in practice fixed by the high frequency data, which on a logarithmic frequency scale also carry most of the statistical weight. The low frequency asymptote together with peak frequency and maximum value will then determine B and n. Typical cases of f S(f) given by (7) are shown in Fig. 5.3.1b. For given values of A and B, the asymptotes are fixed, and n will determine the shape, increasing n meaning a sharper peak.

Because of the turbulence length scale problems experienced with the scheme Eq. (5), a revised scheme has been investigated. It was found that both B and n showed a dependence on lapse rate and wind speed very similar to that exhibited by the logaritmic height coefficient α discussed in Sec. 4.2.3, and the same ad hoc description was adopted. The following set of relations was used in the final minimalization:

$$\begin{aligned} S(f) &= A \,/\, (B^n + f^n)^{5/3n} \\ A &= a\, u^p\, (z/z_r)^{-q} \\ B &= b\, u_r\, (z/z_r)^{-y}\, [\, 1 - sig(\gamma, \gamma_{0b}, \gamma_{1b})\, sig(u_r, u_{0b}(z), u_{1b})] \\ u_{0b}(z) &= u_{z0} + u_{z1}\, \ln(z/z_r) \\ n &= n_0\, [\, 1 + n_1\, sig(\gamma, \gamma_{0n}, \gamma_{1n})\, sig(u_r, u_{0n}, -u_{1n})] \\ sig(x, x_0, x_1) &= 1 \,/\, \{\, 1 + \exp[-(x-x_0)/x_1]\} \end{aligned} \tag{9}$$

Here, a is a linear parameter and p, q, b, n_0, n_1, u_{z0}, u_{z1}, γ_{0b}, γ_{1b}, γ_{0n}, γ_{1n}, u_{0n} and u_{1n} are nonlinear parameters which are fitted (in practice, some were given "typical" values).

The 8 last parameters describe the lapse rate dependence. As in Sec. 4.2, the sigmoid function is used as a "soft" step function to characterize the lapse rate dependence, the accompanying sigmoid function in wind speed will essentially modify the amplitude of the variation, switching off the lapse rate dependence as wind speed increases.

The resulting fits, which can be obtained with the parameterization given by Eq. (9), are very similar to the ones shown in Figs. 5.3.2 - 9 below. Thus a good fit can be obtained with a single spectral function, as defined by Eq. (7), but the parameters B and n have to be defined as rather complicated functions of lapse rate and wind speed. Instead of pursuing this approach further, we shall switch to a description that uses a superposition of two spectral functions of the type given by Eq. (7).

Panofsky and Dutton (1984) recommend a scheme due to Høystrup which by part incorporates the above expected properties of the length scale:

$$\begin{aligned} f\,S(f) / u_*^2 &= 0.5\,\eta_i\,(-z_i/L)^{2/3}/(1 + 2.2\eta_i^{5/3}) + 105\,\eta/(1 + 33\eta)^{5/3} \\ \eta &= f\,z/u \qquad \eta_i = f\,z_i/u \end{aligned} \tag{10}$$

Here z_i is the thickness of the mixed layer or the height up to the lowest inversion. L is the Monin-Obukhov length. Whereas the first spectrum represents the convective part which is taken to be independent of z, the last part is the neutral spectrum for mechanical turbulence which is assumed to be scaled with z.

Attempts to describe the ensemble average of the observed spectra with Eq. (10) did not give the best results. The two heights z_i and L which are required as input, are not easily available, and were treated as free parameters during the fitting. This should be meaningful as far as L is concerned, as z/L is a measure for the atmospheric stability and related to the set of primary variables being used. This is not the case for the thickness z_i of the mixed layer, which depend on the history of the air mass. During this unsuccessful fitting, terms in (10) containing z_i were parameterized in analogy to the B term in the scheme (9).

In the final approach, the convective component in (10) was replaced with an expression on the form of Eq. (7), and A, B and n were considered as unknown functions of the primary variables u_r, γ and z. The complete scheme is essentially a combination of the Høystrup relation Eq. (10) and properties of the scheme Eq. (9). One goal was to isolate the effective stability dependence to a single variable. The starting point was a Richardson number type of variable on the form

$$\rho = (\gamma - \gamma_0)\,(u_r/10\ \mathrm{m/s})^{-\varepsilon}\,(z/z_r)^{\delta} \tag{11}$$

where γ_0, ε and δ were considered as free parameters. With $\varepsilon = \delta = 2$ and $\gamma_0 = 9.8$ K/km, it follows from Eq. (4.2.8) and (4.2.10) that $\rho/(\alpha^2\,T)$, where α is the logaritmic height coefficient and T is the absolute temperature, would be a true candidate for a Richardson number, apart from constant dimensional factors. Parameterizations of the potentially stability dependent terms A_1, A_2, B_1, B_2 and n on the form $c_0 + c_1 \exp(-c_2\,\rho)$

were found to fit the data quite well. After trial and error elimination of terms that did not give an essential improvement of the fit, only n and B_2 were found to have a significant dependence on lapse rate. The resulting formalism, which is further commented at the end of next section, can be written as

$$S(f) = u_r^p \{ a_1 (z/z_r)^{-q}/[B_1 + f]^{5/3} + a_2 /[B_2^n + f^n]^{5/3n} \}$$
$$B_1 = b_1 (u_r/z) \qquad B_2 = b_2 u_r \exp(-c_{b2} \rho) \qquad (12)$$
$$n = n_0 + n_1 \exp(-c_n \rho). \qquad \rho = \gamma / (u_r/10 \text{ m/s})^{\varepsilon}$$

Here, a_1 and a_2 are parameters entering linearly in the fitting process, whereas the 9 parameters ε p, q, b_1, b_2, c_{b2}, n_0, n_1 and c_n enter nonlinearly. With the chosen functional dependence, the best fit was statistically compatible with a simplified version of the stability variable ρ introduced in (11), with $\gamma_0 = 0$ ($\gamma_0 = 9.8$ K/km is ruled out) and no z-dependence. The nominator terms are mainly determined in the high frequency region, and additional u_r, z or ρ dependent terms were not found to improve the fit significantly.

5.3.4 Results from the experimental data

Resulting fits based on Eq. (12) are shown in Figs. 5.3.2 - 4 for Sletringen for the heights 42/46, 20 and 10 m. Corresponding plots for the restricted maritime sector [180°.240°] at Skipheia are shown in Figs. 5.3.5 - 9 for heights 100, 70, 40 20 and 10 m. The plots represent mean values for the sensors in the three masts at each height level.

When studying the spectra from 100 m height at Skipheia, it turned out that a lightning rod and a wind direction sensor mounted on the top of the mast (cmp. Fig. 2.1.7) did introduce significant turbulence over a wide angular sector. As a consequence, in the sector [180°.240°] all data from mast 2 at 100 m and 40% of the data from mast 4 at 100 m had to be rejected - as far as the spectra are concerned. At 75 m, there are sensors only in mast 2.

Each class in wind speed and lapse rate represented in the plots is defined as a weighted mean (according to the number of cases) over the corresponding three or four sub-classes used during the fitting process. The mean values of lapse rate corresponding to "stable", "neutral" and "unstable" conditions referred to in the plots, are 0, 10 and 20 K/km, respectively (the unstable class runs from γ = 15 K/km and up).

Note that the three lowest frequencies in each plot are less than $(10 \text{ min})^{-1}$. These frequencies were given zero weight in the fitting in agreement with the discussion in Sec 5.3.2. We shall argue below that the fit is otherwise quite good, although far from the statistical limit. The r.m.s. relative deviation in the full weight region is 1.5 times larger than the value expected statistically for a good fit for the Sletringen data, and 1.7 times larger for the Skipheia data.

We define a fit to be statistically good when the r.m.s. value of

$$(M_i - S_i)/\sigma_i$$

is one, when the mean of a large number of values is calculated. Here M_i - S_i is the difference between the experimental and theoretical values for variable cell no. i, and σ_i is the corresponding standard deviation. The key assumption is that each basic spectral estimate has a standard deviation equal to the expectation value (see e.g. Newland, 1984), and is normally distributed. The standard deviation of the mean of N estimates with the same expectation value m will then be $m/N^{1/2}$. In technical terms, the statistical indicator χ^2 is calculated. The fit to the total ensemble is defined to be good when the value of χ^2 is equal to the number of degrees of freedom.

The statistical criteria discussed are valid when a perfect theoretical description of the data is available, meaning deviations are caused only by purely statistical fluctuations inherent in the data. Additional deviations caused by an imperfect theoretical description are not accounted for. In our case, we are missing one of the primary variables in the description of the spectra, which is the height of the convective layer, as discussed in Sec. 5.3.3. We consider this fact to be the primary reason for the deviation from the statistical limit.

During the Phase 1 analysis, the individual spectra for each period were fitted to the representation defined by Eq. (7) (then called Model 4). The cumulative distribution of the χ^2 - values was shown in Fig. 4.2.1 in that report, and indicated that the fits were close to the statistical limit. However, when spectra within narrow classes in speed and stability were averaged, the r.m.s. deviation from the model curves was found to be a factor 1.5 larger than the limit imposed by the statistical fluctuations, which is the same experience as described above for the present analysis.

A striking feature of the data is that the turbulence spectra for stable and unstable conditions cross at a frequency near 0.01 Hz. For frequencies above this value, the turbulence is highest for stable conditions, whereas for lower frequencies the turbulence is generally highest for unstable conditions. The data for the maritime sector at Skipheia show this tendency most clearly in the high frequency end. The maritime data represent about 40 % of the total data from Skipheia, and it should be said that relatively few data are in the unstable class at this station. If all data for Skipheia are used (the corresponding plots are not shown), this "cross-over" feature disappears. In physical terms this can be understood as a "cleaning" effect: The low layer containing mechanical turbulence is simply swept away by the convective motion and replaced by air from higher levels with less high frequency turbulence. This phenomenon is often referred to as intermittency.

The experimental points for the very highest frequency values are somewhat higher than what is indicated by the trend from the neighbouring points below. This is due to the resolution noise, wind speed is registered as a certain number of counts in each period. The effect is most important for low wind speeds. Disregarding this effect, the experimental points for the highest elevations show a $f^{-2/3}$-behaviour for $f > 0.1$ Hz, in agreement with conventional theory. The fitted curves do not quite show this asymptotic slope, because the statistical weight of the high frequency region was reduced in the fitting process for reasons discussed earlier in this chapter.

Focussing again on the results for the higher elevations, the data for frequencies below 0.03 Hz are nearly compatible with a straight line fit in the log-log plots shown, i.e.

$$S(f) = C(u_r, z, \gamma)\, f^{-\alpha(ur,z,\gamma)} \qquad (13)$$

The "constants" C and α describing the height and slope of the line will of course be functions of u_r, z and γ, as indicated.

Comparing the experimental data in Figs. 5.3.2 - 9 to the idealized frequency functions in Fig. 5.3.1b, and keeping the low frequency straight line feature in mind, it is clear that a single Harris spectrum (n=2), which is recommended by NPD, is ruled out. Fit to a single spectral function of the type discussed, will require a rather low value for n. The results by Eidsvik (1985), also seem to rule out the Harris spectrum.

The parameter values corresponding to Eq. (12) and the fits shown in Figs. 5.3.2 - 10 are given i Table 5.3.1. Separate values are given for Sletringen and Skipheia, respectively. The value of the exponent p in the factor u_r^p multiplying the spectral functions, is found to be about 0.40 larger than the "conventional" scaling value of $p = 8/3$. Note also the high values of the exponent q in the term $(z/z_r)^{-q}$ in the nominator of the first spectral function in Eq. (12). From the traditional scaling, as given e.g. in the Høystrup formula, Eq. (10), $q = \frac{2}{3}$ is expected, whereas we find 1.5 and 1.64, respectively, for the two stations. This will effectively reduce the contribution from the first function for large values of z. The main contribution will then come from the second spectral function, which will have a rather low value for the n-parameter for both neutral and unstable conditions. Note also that the maxima of the two spectral functions are separated by a factor of 7 in frequency for stable conditions. This separation increases with increasing lapse rate (towards unstable conditions). The sum of the two contributions will approximately simulate a straight line in the region between the maxima. Thus, both spectral functions in Eq. (12) contribute significantly for all stability conditions. This is contrary to the Høystrup scheme, Eq. (10), where the convective part vanishes for neutral conditions, $L = \infty$. Also note that the Høystrup scheme is not valid for stable conditions.

In the Phase 1 project, the fitting was based on a model corresponding to Eq. (7). A variation of n from 1.0 to 0.4 was then found for the lapse rate range 0 to 40 K/km (from stable to unstable conditions). In the present work, we are fitting to a sum of two spectral functions, the first with $n = n_1 = 1$ being kept fixed, the second with a lapse rate dependence. The range of n_2 values was found to be from 0.71 to 0.28 for the Sletringen data, and from 0.73 to 0.18 for the Skipheia data. Thus, the results are not directly comparable for several reasons:

(1) The models are different. The fact that the value of n for the first spectral function is kept fixed (1.0) will tend to reduce the value of n for the second one for unstable conditions, whereas the separate maximum point of the two functions, should tend to give a larger value for the free n for all conditions.

(2) During the Phase 1 analysis, a purely statistical weighting was applied, which meant that the high frequency data were given much more weight than during Phase 2. Inspection of Fig. 5.3.2 - 9, and comparison to Fig 5.3.1a indicate that full weight to the high frequency data would most probably have increased the value of n.

(3) The difference between the Phase 1 and 2 stable spectra are harder to explain- During Phase 1 there were relatively few spectra for stable conditions, where the difference is hardest to explain, during Phase 1. The single spectra fits showed a large scatter for the resulting n (cmp. Fig. 4.4.3 in the Phase 1 report, a lower limit of n = 0.25 was imposed for technical reasons). Since the lapse rate parameterization was different in the two cases, the more numerous neutral range data might easily "force" an end range value of limited significance.

As a conclusion, we do not think that the Phase 2 results contradict the Phase 1 results, but simply reflect differences in parameterization, fitting and raw data material.

Table 5.3.1 Parameter values for the model described by Eq. (12) for a least square fit to the data.
Units assumed for z, u_r and γ are m, m/s and K/km, respectively.

Parameter	Sletringen	Skipheia
a_1	$2.03\ 10^{-5}$	$2.35\ 10^{-5}$
a_2	$1.18\ 10^{-5}$	$1.15\ 10^{-5}$
ε	1.40	0.30
p	3.07	3.05
q	1.50	1.64
b_1	$1.82\ 10^{-2}$	$1.50\ 10^{-2}$
b_2	$3.56\ 10^{-4}$	$3.35\ 10^{-4}$
c_{b2}	0.293	0.146
n_0	0.281	0.176
n_1	0.428	0.558
c_n	0.183	0.074

5.4 Cross spectra

5.4.1 Definition of coherence and phase difference

Let the time series for the two variables x and y be defined by the Fourier coefficients (a_{xn}, b_{xn}) and (a_{yn}, b_{yn}), respectively. In analogy with the case for one-point spectra, the cospectrum C and quadrature spectrum Q are defined as the interval mean values

$$C\,(f, u_r, \gamma, d) = < a_{xn}a_{yn} + b_{xn}b_{yn} > \tag{1}$$

$$Q\,(f, u_r, \gamma, d) = < a_{xn}b_{yn} - b_{xn}a_{yn} > \tag{2}$$

Here, d is a representation of the (vector) distance between the two sensors. The brackets $< >$ denote that an ensemble average of the coefficient combinations is taken over some cell in the f, u_r, γ and d variable space. The cross spectra for two sensors with a horizontal separation will in general depend on wind direction, which will enter as a fifth variable when comparing to the case of one-point spectra. Consequently, sensor positions will have to be defined in 3 dimensions. For each spectrum, sensor separations can then be calculated in the vertical direction, in the transversal direction and in the along-wind direction.

Rather than studying the co- and quadrature spectra directly, we shall discuss spectra of coherence and phase difference.

Coherence is a measure of the correlation (independent of a phase) between the individual frequency components of two time series in the interval, and is defined by

$$Coh(f, u_r, \gamma, d) = [C^2 + Q^2]/(M_x\, M_y) \tag{3}$$

where M_x and M_y are the spectral densities for each of the two time series (in the literature, the quantity defined in Eq. (3) is also referred to as coherence squared). To obtain stable estimates, all the spectral quantities involved have to be defined as mean values for the same variable cell, with M_x and M_y evaluated for the same set of simultaneous time series as used to calculate C and Q.

The coherence is limited by $0 \leq Coh \leq 1$, the upper limit corresponds to complete correlation between the frequency components, the lower to no correlation.

The phase difference ϕ representative for the group of Fourier-components involved in one cell average, can be determined from the C- and Q spectra (Eqs. (1) and (2)), as

$$\sin\phi = -Q / (C^2 + Q^2)^{1/2}$$
$$\cos\phi = C / (C^2 + Q^2)^{1/2} \tag{4}$$

To illustrate the physical meaning of these quantities, and some computational problems, we will discuss these concepts somewhat further. Let the two time series in question be

$$x(t) = \sum_{n=1}^{N} X_n \cos(2\pi f_n t + \alpha_n) \qquad f_n = n / T$$

$$y(t) = \sum_{n=1}^{N} Y_n \cos(2\pi f_n t + \beta_n) \qquad f_n = n / T \tag{5}$$

The Fourier coefficients entering in Eqs. (1) and (2) are then given by

$$\begin{aligned} a_{xn} &= X_n \cos(\alpha_n) \qquad b_{xn} = - X_n \sin(\alpha_n) \\ a_{yn} &= Y_n \cos(\beta_n) \qquad b_{yn} = - Y_n \sin(\beta_n) \end{aligned} \tag{6}$$

A small exercise with standard trigonometric formulae gives the co- and quadrature spectra as

$$\begin{aligned} C &= < X_n Y_n \cos(\alpha_n - \beta_n) > \qquad & Q &= - < X_n Y_n \sin(\alpha_n - \beta_n) > \\ M_x &= < X_n^2 > & M_y &= < Y_n^2 > \end{aligned} \tag{7}$$

If the phase difference $\alpha_n - \beta_n = \Theta$ is constant within a particular averaging cell, then it follows from Eq. (3) that

$$Coh = <X_n Y_n>^2 / [<X_n^2> <Y_n^2>]$$

which is simply the square of the correlation coefficient between the energy densities of the two variables. Further, it follows from Eq. (4) that the phase estimate is $\phi = \Theta$. If in addition $X_n = c\, Y_n$, c = constant, then Coh = 1. This is also the result if only one realization of the time series pair and one single frequency is involved in the averaging process in Eq. (7). Thus a faithful estimate of the coherence requires an average over several frequency values and/or several realizations. If the phase difference varies randomly in the averaging cell, both the C- and Q spectra will vanish provided the total number of coefficient pairs involved in the averaging process indicated by Eq. (7) is large enough. Of course, the phase ϕ is not defined in that case.

In the present case with time series of wind speed data, phase differences will typically represent time lags due to the transit time for a particular disturbance from an upwind to a downwind sensor. If the above x-series represents an upwind sensor, and the y-series a sensor a distance d_l downwind (in general d_l is the projection of the intersensor distance on the wind direction), then we expect the total harmonic phases of the x- and y sensors to be related as

$$2\pi f_n t + \alpha_n \simeq 2\pi f_n (t + d_l/v) + \beta_n$$

where d_l/v is the typical flight time of the dominating turbulence features between the two sensors, v being the corresponding speed. The characteristic difference between the phase constants is then

$$\theta_n = \beta_n - \alpha_n = - 2\pi f_n d_l/v \tag{8}$$

During the averaging process, the value of θ_n should not vary too much due to variation in the variables f_n, d_l and v, because otherwise the coherence estimate is affected.

5.4.2 Data input to the parameterization process

The averaging and parameterization of the bivariate spectra are done in much the same way as for the one-point spectra. However, the inter sensor distance representation must now reflect two horizontal components referenced to the wind direction, in addition to vertical separation.

To represent the transversal and along wind components of the separation, the data must now be sorted in wind direction classes in addition to the classes in the other variables discussed in Sec. 5.3. Thus, each event will be referenced to a 5 - dimensional set of variables, frequency, reference wind speed, lapse rate, height and wind direction, and the cross spectra must in general be parameterized with respect to this space. However, as sensors within one mast have vertical separation only (or very small separations in the horizontal directions), their cross spectra can be discussed within the four-dimensional space used to discuss single spectra.

Only the maritime sector is of interest in the present investigation. As discussed in the final report for the Phase 1 project, this sector will be from 160° to 40° through north, or from south - south-east to north-east for the Sletringen station. For the Skipheia station, the sector 180° - 240° is reasonably "maritime", as discussed in Sec. 4.2.2.

In order to be able to run the minimalization on our computer in a reasonable time, not more than 8 direction classes can be accommodated. This means a bin width of 30° for the full maritime sector, and 7.5° for the restricted Skipheia sector, which should be sufficient. For wind speed and lapse rate, 10 classes are chosen as discussed in Sec. 5.3. Frequency classes have been chosen "logarithmically" as for the single spectra, with 3 per factor two, or about 10 classes per factor ten in frequency, meaning a total of 26. As discussed in Sec. 5.4.1, the cell size should be so small that systematic phase differences do not arise due to the variable range, cmp. Eq. (19). We will return to this problem below, when the experimental data are discussed. For each cross spectrum we will in general have $8 \cdot 10 \cdot 10 \cdot 26 = 20800$ variable cells. A sufficient number of cross spectra based on the set of time series for the sensors involved can be treated simultaneously.

5.4.3 Parameterization schemes for coherence. Experimental results

5.4.3.1 Vertical separation

For time series of wind speed at two heights z_1 and z_2 (no horizontal separation), a modified Davenport model for the coherence is adopted. The original Davenport formulation was

$$\text{Coh} = \exp[\, -a\, f\, |\Delta z|/u] \tag{9}$$

Various investigations have shown that the coefficient a depends on Δz and z (see e.g. Panofsky and Dutton (1984) for a survey), a dependence on lapse rate is of course also expected. The present data set indicates that the total dependence on Δz can be separated and written as

$$\begin{aligned} \text{Coh} &= \exp[\, -(\, |\Delta z|/\lambda_z\,)^q] \\ \lambda_z &= (\, u_r / f\, a_z\,)^{1/q} \end{aligned} \tag{10}$$

where a_z no longer depends on Δz, and λ_z may be called the coherence length for the z-direction.

The following rather compact parameterization has been found to give a good fit to the observed coherence spectra for sensors within a single mast:

$$\begin{aligned} \text{Coh}(f, u_r, \gamma, \Delta z) &= \exp[\, -a_z(\gamma, f)\, |\Delta z|^q\, f / u_r)] \\ a_z(\gamma, f) &= z_g^{-p}\, [a_0 + a_1 \exp(-b_1 f)\, \text{sig}(\gamma, \gamma_0, -\gamma_1)] \\ z_g &= (z_1\, z_2)^{1/2} / z_r \end{aligned} \tag{11}$$

The sig-function is defined in Eq.(5.3.9), and a_0, a_1, p, q b_1 and γ_1 are coefficients to be determined. z_g is the geometric mean height relative to the reference height of the two sensors being compared. The median value (0.5) of the lapse rate function has been fixed to the adiabatic lapse rate value, γ_0 = 9.8 K/km. Leaving this as a free parameter does not improve the fit. A wind speed dependence in the lapse rate parameterization did not improve the fit in the present case.

The fitting has been done in the same way as described in Sec. 5.3. except that the weight factor has been taken as the number of observations in the class. The resulting coefficients are shown in Table 5.4.1, with separate values for Sletringen and Skipheia. The Skipheia numbers represent mean values for the three masts. Data from the full maritime sector are used. The agreement between the results for the two stations is very good. The only main disagreement is in the stability coefficient γ_1. This should not be too surprising, bearing in mind the somewhat poor correlation between the lapse rate measurements at the two stations as discussed in Sec. 4.2.2.

Table 5.4.1 Values of the coefficients in the parameterization of vertical coherence, as defined by Eq. (11).

Station	a_0	a_1	p	q	b_1/Hz^{-1}	γ_1/K/km
Sletringen	19.6	30.3	0.51	1.24	88.1	5.0
Skipheia	20.9	33.8	0.50	1.26	90.6	9.8

Averaged plots of coherence versus frequency for 3 speed classes and 3 lapse rate classes are shown in Figs. 5.4.1 - 5 for the height pairs 46/42, 46/20, 46/10, 42/20 and 20/10 at Sletringen. The sensor at 46 m is displaced 1 m to the east of the vertical line through the lower sensors, but it can be shown on the basis of the lateral results given below, that this will not matter. As for the single spectra, both experimental and fitted values for the three classes in speed and lapse rate are calculated as a weighted mean over three or four of the 10 classes used in the fitting process. The weight factor is again the number of observations in the sub-class.

Corresponding average results for the masts at Skipheia are shown in Figs. 5.4.6 - 10 for the heights 100/40, 70/40, 40/10, 40/20 and 20/10 m. As mentioned in Sec. 5.3.4, a large part of the data from the sensors at 100 m had to be excluded from the spectral analysis due to disturbances from the lightning rod and the wind direction sensor. This explains the large scatter in Fig. 5.4.6. The data represent the full maritime sector 140° - 400°. Data from the restricted sector, 180° - 240° do not show much difference.

As is apparent from Table 5.4.1 and the plots, there is not much difference between the Skipheia and Sletringen results, even when the full maritime sector is used. This is somewhat remarkable, due to the problems discussed in Sec. 4.2.

A special feature of the chosen parameterization, is that the lapse rate dependence is damped by a factor depending on the frequency. The dependence on atmospheric stability is important in the low frequency region, f < 0.02 Hz, only. Based on Eq. (10) and (11) and Sletringen "rounded" values from Table 5.4.1, the vertical coherence length λ_z can be written

$$\lambda_z = \{(u_r/f) z_g^{0.5} [20 + 30 \exp(-90 f) \, \mathrm{sig}(\gamma, 9.8, -5.0)]^{-1} \}^{0.8} \qquad (12)$$

where the units for f and γ are Hz and K/km respectively. Some values of this coherence length are given in Table 5.4.2.

Table 5.4.2 Vertical coherence length λ_z (in meters) as defined by Eq. (12). u_r = 20 m/s, $z_g = (z_1 z_2)^{1/2}/z_r = 1$.

Atmospheric stability (γ/K/km)	Frequency/Hz						
	0.001	0.002	0.005	0.01	0.02	0.05	0.1
Stable (0)	134	80	43	28	20	10.9	6.3
Neutral (10)	166	98	51	32	21	10.9	6.3
Unstable (20)	224	130	64	38	22	11.0	6.3

Diagrams showing a_z and λ_z versus f for the three lapse rate classes are given in Figs. 5.4.22 - 23. The curves correspond to the values u_r = 20 m/s and z_g = 4 (z_g = 1 is used in Table 5.4.2) and the parameterization defined by Eqs. (10-12) is used to calculate the frequency dependence.

The coherence is strongest for unstable conditions and low frequencies, as one might expect. Thermal convection increases the correlation between the fluctuations at various heights. In the high frequency region, mechanical turbulence dominates, and the stability dependence vanishes. Another noticeable feature is that the coherence length increases proportionally to the square root of the geometric mean height.

5.4.3.2 3-dimensional separation

Transversal and longitudinal coherence is usually represented similarly to that in the vertical direction. A candidate for a general expression for the coherence is

$$\mathrm{Coh}(f,u_r,\gamma,\Delta r) = \exp\{-(f/u_r)\,[a_x^2\,\Delta x^2 + a_y^2\,\Delta y^2 + a_z^2\,\Delta z^{2q}]^{1/2}\} \qquad (13)$$

where the parameters a_x, a_y, a_z generally will have lapse rate and z dependence. The x-direction is the mean wind direction, and a_x is usually assumed to be smaller than the transversal damping coefficients a_y and a_z. For a separation along one of the coordinate axis, Eq. (13) gives the same result as Eq. (9) and the equivalents for the x- or y-direction. For a general separation, the coherence is assumed to be constant on a generalized ellipsoid which gives the single axis values. In other words, this description implies that the coherence falls off with increasing distance between the two points in question, with an effective decay coefficient depending smoothly on direction.

Three dimensional coherence can be determined from the Skipheia data only. From a total of 12 different wind speed time series, a total of 78 cross spectra may be calculated. So far only cross spectra between sensors at different heights but in the same mast (see above), and cross spectra between sensors at the same height, but in different masts (see

below), have been examined. Thus the three dimensional structure of Eq. (13) has been compared to experimental data only for one or two dimensional situations.

The damping constants a_x and a_y have been parameterized in a way analogous to a_z, viz.

$$a_x = (z/z_r)^{-p} [a_0 + a_1 \exp(-b_1 f) \, sig(\gamma - \gamma_0, -\gamma_1)] \qquad (14)$$

and similarly for a_y, but with different sets of values for the coefficients p, a_0, a_1, b_1 and γ_1. The remaining symbols have the same meaning as in Eq. (11) above. Extra exponents on the separations Δx and Δy do not improve the fit significantly, and the coherence length in the x direction is consequently given as

$$\lambda_x = u_r / f a_x \qquad (15)$$

and analogously for the y direction.

Results from least square fits to the total of 9 cross spectra which can be calculated for the heights 40, 20 and 10 m in the three masts are shown in Table 5.4.3. Results for both the full oceanic range 160° - 400° and the restricted maritime range 180° - 240° are shown. The latter contains about 40% of the observations, and although the parameters are not very different for the two direction sectors, the fit is significantly better for the restricted range.

Table 5.4.3 Values of the coefficients in the parameterization of longitudinal ("x-direction") and lateral ("y-direction") coherence defined by Eq. (14) for two direction sectors.

Coherence	Sector	a_0	a_1	p	b_1/Hz^{-1}	γ_1/K/km
Longitu-dinal	180° - 240°	3.45	3.19	0.42	78.9	- 2.98
	160° - 400°	2.93	8.68	0.45	78.9	- 3.03
Lateral	180° - 240°	18.4	131	0.38	34.1	25.8
	160° - 400°	16.6	141	0.37	22.0	20.8

It is remarkable that the coherence for longitudinal separations decreases with increasing lapse rate (decreasing stability), whereas coherence both for vertical and lateral separations increases. The large absolute value of a_1 and γ_1 makes the frequency dependence the dominating feature of the lateral coherence. This is exemplified in Table 5.4.4 for 40 m height for three values of the lapse rate. Values of a_x and a_y calculated from Eq. (14) with coefficients from the fit for the restricted maritime sector are shown for

a set of frequencies, together with corresponding coherence lengths for reference wind speed u_r = 20 m/s.

Table 5.4.4 Damping coefficients a_x and a_y for longitudinal and lateral separation for selected frequencies and 3 lapse rate classes for $z_1 = z_2 = z = 40$ m .
Eq. (14), u_r = 20 m/s, restricted maritime sector.

Atmospheric stability (γ/K/km)	a_i/m^{-1} or λ_i/m	Frequency/Hz						
		0.001	0.002	0.005	0.01	0.02	0.05	0.1
Stable (0)	a_x	2.0	2.0	2.0	2.0	1.9	1.9	1.9
	a_y	55.5	54.0	49.8	43.7	34.2	19.2	12.4
	λ_x	10088	5055	2033	1023	516	207	104
	λ_y	361	185	80	46	29	21	16
Neutral (10)	a_x	2.8	2.7	2.5	2.3	2.1	1.9	1.9
	a_y	48.3	47.0	43.5	38.4	30.4	17.9	12.1
	λ_x	7271	3720	1582	858	474	206	104
	λ_y	414	213	92	52	33	22	17
Unstable (20)	a_x	3.5	3.4	3.1	2.7	2.3	2.0	1.9
	a_y	41.1	40.1	37.2	33.1	26.7	16.5	11.9
	λ_x	5683	2943	1295	738	438	204	104
	λ_y	468	249	107	60	37	24	17

Diagrams of the coherence length and damping coefficients versus frequency are shown in Figs. 5.4.22 - 23 for the same values of the variables and parameters as for Table 5.4.4.

The ratio of the longitudinal coherence length to the lateral one is seen to be about 6 for 0.1 Hz . For decreasing frequencies, the ratio is seen to increase to about 12 for stable conditions, to 17 for neutral, and to 25 or more for unstable conditions. The order of magnitude for this ratio agrees well with Taylor's hypothesis of frozen turbulence. However, the ratios are somewhat larger than expected (cmp. e.g. Frost et al. (1978) where a_x = 4.5 and $a_y = a_z$ = 7.5 are proposed as the result of a review of the then available literature). We have no particular reason to believe our results are erroneous, but feel more data should be collected with great attention being paid to the measurement of wind direction and temperature gradient. The low frequency values of the longitudinal

coherence length and damping coefficients are really an extrapolation from a region with much less reduction than 1/e, which is the traditional damping value for a definition.

If the wind direction deviates an angle θ from the line intersecting two sensors, it follows from Eq. (13) that the contributions from lateral and longitudinal terms are equal for

$$\tan \theta = a_x / a_y$$

A typical value for this ratio is 0.1, corresponding to an angle of 6°, which is on the limit of the practical accuracy of the present wind direction measurements. But with care, an accuracy of about 1° can probably be obtained. One would then also have to worry about Ekman effects, i.e. a systematic variation of wind direction with height. Also fluctuations in wind direction with periods longer than the transit time between the two masts would have to be considered. Over the 40 min period, the standard deviation for the 0.85 Hz wind direction measurements is typically 6° for u_r = 10 m/s, decreasing to 4° for $u_r \geq 13$ m/s. The standard deviation corresponding to the transit time will be less, but has so far not been evaluated. For practical purposes, however, longitudinal coherence will have to be defined to include the transversal effects due to the fluctuations of the wind direction around the mean value.

A comparison of the observed coherence and the parameterization is shown versus frequency for three wind speed classes and three lapse rate classes in Figs. 5.4.11 - 13 for the heights 40, 20 and 10 m. The plots represent mean values for the three masts for the restricted direction sector 180° - 240°, and for subclasses in lapse rate and wind speed as explained for the plots of vertical coherence. The fit is reasonable, although some systematic deviations are apparent, especially for 10 m height and high frequencies. Because $a_y \gg a_x$, it follows from Eq. (13) that the lateral terms in general will dominate, making the coherence largest for unstable conditions.

In order to try to demonstrate the large ratio of longitudinal to lateral coherence directly, observations in sectors of width 30° symmetric around directions parallel and sidewise orthogonal to the sensor - sensor distances for masts 2 - 3 and 2 - 4 have been treated separately. In the parallel case one would expect longitudinal coherence to dominate. When the inter sensor direction is normal to the wind direction, lateral coherence will dominate. The positions of the masts and sensors are discussed in Sec. 2.1. The distance between mast 2 and 3 is 170 m, between mast 2 and 4, 79 m. However, because of the large value of a_y compared to a_x, it is really not possible to get a clean sample determining a_x separately. IF D is the inter sensor distance, the square root in Eq. (25) will for a small angle θ be approximately equal to

$$D [a_x^2 + (a_y^2 - a_x^2) \theta^2]^{1/2} \simeq D [a_x^2 + a_y^2 \theta^2]^{1/2} \quad \text{when } a_y \gg a_x$$

The maximum angle in the parallel set is ± 15° corresponding to $\theta = \pm 0.26$. Thus,

θ $a_y > a_x$ in the outer part of the sector, and the lateral decay length may also have a substantial influence in the along-wind case supposed to isolate the longitudinal term. Reducing the angular range further leaves too few observations to give meaningful distributions.

Coherence data between mast 2 and 4 for the direction sector 198 - 228° for three wind speed and three lapse rate classes are shown in Figs. 5.4.14 - 16 for the heights 40, 20 and 10 m. These data are dominated by lateral coherence. The curves shown correspond to the fit specified in Tables 5.4.3 and 5.4.4 and were discussed above. The sensor distance is 79 m, and for $f > 0.01$ Hz, there is very little coherence left, in agreement with the results in Table 5.4.4. Coherence data for the same masts in the sector 288° - 318° for three lapse rate classes and three heights are shown in Fig. 5.4.17. Only the lowest wind speed class (mean 12 m/s) is represented in this sector. The curves represent the same parameterization as for the set above (this sector is outside the restricted maritime sector). Although influenced by the lateral decay constant (which actually dominates the lapse rate behaviour) as discussed above, this is as close as we can presently get to a demonstration of pure longitudinal coherence. Comparing the plots in Fig. 5.4.17 to the bottom plots in Figs. 5.4.14 - 16 (lowest wind speed class), one will observe that the first sets typically decay for frequencies one decade above the corresponding sets of lateral coherence, in rough agreement with the results presented in Table 5.4.4.

In Fig. 5.4.18, plots of lateral coherence for masts 2 and 3 (sector 277° - 307°) are shown for three lapse rate classes and three heights. The lowest wind speed class (mean 12 m/s) only is represented. Coherence data for the same two masts in the sector 187° - 217°, symmetric around the sensor - sensor direction, and for the two lower classes of wind speed and lapse rate (stable and neutral conditions) are presented in Figs. 5.4.19 - 21 for the heights 40, 20 and 10 m. The curves presented in Figs. 5.4.18 - 21 represent the same parameterization as those presented in Figs. 5.4.14 - 17, and the same type of comments apply. In the lowest wind speed class, the lapse rate dependence of the longitudinal coherence is seen to dominate.

Other pairs of narrow sectors parallel and orthogonal to the sensor - sensor directions do not have enough strong wind data to contribute significantly to the present discussion.

The eight plots presented for the narrow direction sectors confirm the main features of our parameterization: The decay-lengths in the longitudinal and lateral directions are different by an order of magnitude in the region around 0.01 Hz. However, our data are not very sensitive to the very low frequency region, $f < 0.003$ Hz.

5.4.4 Parameterization schemes for phase differences. Experimental results

The general principles for an experimental determination of the phase differences between two sensors were discussed in Sec. 5.4.1. An estimate is meaningful only if the signals are correlated, i.e. the coherence must be above the noise level. In the actual parameterization procedure, the same general principles as discussed in Sec. 5.4.3, are

followed, except that the experimental estimate of coherence is included as a factor determining the weight of a given variable cell.

The experimental estimate of the phase angle, ϕ, is calculated from the co- and quadrature spectra, as defined by Eqs. (1), (2) and (4). This defines ϕ in an interval $[-\pi, \pi]$. The natural "physical" value, as defined e.g. by Eq. (8), may be outside this range by a multiple of 2π.

The phase difference is believed to be a continuous function of the frequency f, going to zero as $f \rightarrow 0$. Thus, below a certain frequency, there is no phase ambiguity. Starting from the low frequency side, the 2π problem can be resolved by comparing the estimate from the spectra to an extrapolated value for the same frequency. This is not a very critical procedure in practice, as the coherence usually goes to zero when the phase difference approaches 2π, meaning that a determination is meaningless in any case.

5.4.4.1 Phase differences in the horizontal plane

In Sec. 5.4.1, it was argued that a sensor a distance d_l downwind from a reference sensor would be expected to show a phase difference $- 2\pi f d_l / v$, where f is the frequency and v some typical transport speed. A lateral component in the separation is not expected to give a mean contribution to the phase difference which is different from zero.

To resolve the phase difference at a given frequency, the correlation between the signals from the two sensors must be above the noise level, as discussed in Sec 5.4.1. In Sec. 5.4.3, coherence was found to decrease rapidly with lateral separation. Therefore, phase differences in the wind direction have been studied in the direction sectors within $\pm 15^{\circ}$ to the mast intersections, the same sectors as used in Sec. 5.4.3 to demonstrate longitudinal coherence. This selection is made in order to keep lateral separation small. This gives a relatively high coherence, enabling experimental phase resolution to the highest frequencies possible.

It turns out that a lapse rate dependence in the parameterization scheme does not improve significantly the fit to the longitudinal phase lag data. The straight forward generalization of Eq. (8) used to fit the data is

$$\theta = 2\pi A f d_l / (z_g^{\alpha} u_r) \qquad (16)$$

where A is a factor and α an exponent to be determined. d_l is the projection of the sensor distance on the mean wind direction. Since the pair of sensors is at the same height, $z_g = z/z_r$, meaning a power law assumption has been made concerning the height dependence of the effective transport wind speed. As described above, the parameters A and α are obtained by minimalizing

$$\sum_n (\phi_n - \theta_n)^2$$

where the sum is over all variable cells with an appreciable coherence, ϕ_n being the experimental estimate and θ_n the theoretical cell value.

Fit to the data in the $\pm$ 15° sector centered at the line between the masts 2 and 4 at Skipheia (101 observations, mast separation 79 m) for 3 lapse rate classes and the heights 40, 20 and 10 m is shown in Fig. 5.4.24. Only one speed class (mean speed approx. 12 m/s) is represented in this sample. Fits to the data for the corresponding sector for masts 2 and 3 (96 observations, mast separation 170 m) are shown for the 2 lower wind speed classes and 2 lapse rate classes (stable and normal conditions) in Figs 5.4.25 - 27 for the heights 40, 20 and 10 m, respectively. As already noted, no significant lapse rate dependence is apparent in the data. Fitted curves for two lapse rate classes may however show small deviations due to differences in the population of sub classes in speed and direction, even if no explicit lapse rate dependence is included in the parameterization.

The parameters resulting from fit to the two data sets are

$$\begin{array}{lll} A = 0.87 & \alpha = 0.073 & \text{Masts 2 - 4} \\ A = 1.05 & \alpha = 0.040 & \text{Masts 2 - 3} \end{array} \qquad (17)$$

The difference in A-values is somewhat puzzling, but is statistically of marginal significance, only. But within 13 %, turbulence structures seem to be transported with the mean wind speed. The value of the exponent α reflects the increase of wind speed with height.

5.4.4.2 Phase differences for vertical separation

Wind structures at higher levels usually precede those at lower levels. For vertical separation only, the phase difference is according to Panofsky and Dutton (1989), well represented by the simple formula

$$\theta(f) = s_z \, 2\pi f \, \Delta z/u \qquad (18)$$

with $s_z \simeq 1.3$. The physical significance of this can be found by comparison to Eq. (8), and keeping in mind (Eq. (17)) that the effective transport speed for turbulent eddies is the local mean wind speed. The line through points with constant phase is "leaning forward" with an angle ζ given by

$$\tan \zeta = d_l/\Delta z = s_z \qquad (19)$$

or $\zeta = 52°$ for the given s_z value.

However, there are no clear-cut physical arguments for a simple formula like Eq. (18), and the effective value of s_z may well depend on the other variables.

Our data deviate significantly from the description implied by Eq. (18) if s_z is understood to be a constant. In addition to a rather weak dependence on lapse rate, a

dependence on the relative geometrical mean height, $z_g = (z_1 z_2)^{1/2}/z_r$, and rather strong nonlinear dependence on f and u seem to be present. The following formula was found to give a reasonable fit

$$\theta(f) = 2\pi [A_1 + A_2 \, sig(\gamma,\gamma_0,\gamma_1) \, sig(u_r,u_s,-0.2\, u_s)] \, \Delta z \, z_g^{\,p} \, [1-\exp(-c_f f)] \, (f/u_r)^q$$
$$u_s = u_s(z_g) = u_{z0} + u_{z1} \ln(z_g) \qquad \gamma_0 = 9.8 \text{ K/km}, \; \gamma_1 = 5 \text{ K/km} \tag{20}$$
$$sig(x,x_s,d) = 1/\{1 + \exp[-(x-x_s)/d]\}$$

The lapse rate dependence is similar to that found in the discussion of the wind speed profiles in Sec. 4.2. The parameters A_1, A_2, p, q, c_f, u_{z0}, u_{z1} have been determined by a minimalization as described above, while γ_0 and γ_1 have been held fixed at the "typical" values.

The data and resulting fits for 3 speed classes and 3 lapse rate classes are shown in Figs. 5.4.28 - 30 for the 42/20, 42/10 and 20/10 m wind speed sensors at Sletringen. These sensors are located in a vertical line.

Corresponding plots for the heights 70/40, 40/20, 40/10 and 20/10 m at Skipheia are shown in Figs. 5.4.31 - 34.

The parameter values are shown in Table 5.4.5. Also shown are "reference" values s_{zr} of s_z in the simplified representation defined by Eq. (18) valid for $z_g = 1$, $u_r = 20$ m/s and f = 0.01 Hz.

As is evident both from the Eq. (20) and the plots, lapse rate dependence is not very important at high wind speeds. With the parameter values of Table 5.4.5, the wind speed dependent factor in the lapse rate term in Eq. (20) vanishes rapidly when u_r increases in the range of interest here. A simplified representation in terms of reference wind speed can then be written

$$\theta(f) = s_z(z,f/u_r) \, [1-\exp(-c_f f)] \, 2\pi f \, \Delta z/u_r \qquad u_r \geq 15 \text{ m/s}$$
$$s_z(z,f/u_r) = s_{zr} \, z_g^{\,p} \, (L_r \, f/u_r)^{q-1}, \quad L_r = 2000 \text{ m} \tag{21}$$

where the parameter s_{zr} and the exponents p and q are given in Table 5.4.5. By construction, $s_z(z_r,f/u_r) = s_{zr}$ at the "reference point" $z_g = 1.0$, f = 0.01 Hz and $u_r = 20$ m/s.

For $f \geq 0.01$ Hz, the frequency dependence in the square bracket term may be neglected. Comparing the value in Table 5.4.5 of $s_{zr} \simeq 7$ with the value of $s_z = 1.3$ recommended in combination with Eq. (18), it is quite clear that our description gives a somewhat different picture. Rather than a constant value of s_z, corresponding to constant phase angle (Eq. (19)) of 38° with the horizontal plane, it is found that these quantities depend on the basic variables. At the chosen reference point, we find the effective value of s_z in Eq. (18) to be about a factor 5 larger than the value given by Panofsky and Dutton, otherwise it increases roughly with the square root of (u_r/f) and decreases with the square root of the geometrical mean height. Thus for a mean height of e.g. 50 m, $u_r = 10$ m/s

and f = 0.025 Hz, the "normal" s_z = 1.3 is found. For f << 0.01, there is an extra reduction of the phase shift as given by the square bracket term in Eq. (21). The physical meaning of these results is e.g. that for u_r = 20 m/s and f = 0.01 Hz, variations at 10 m height will be in phase with variations at 20 m at a point 50 m down wind, meaning the line of constant phase discussed above has an angle of only 12° to the horizontal plane.

Table 5.4.5 Values of the parameters in Eq. (20) resulting from a least square fit to the experimental phase shift data for wind speed sensors with only vertical separation.
Effective values of the "constant" s_z in Eq. (18) for 10 m height (z_g = 1), u_r = 20 m/s and f = 0.01 Hz are also given.

Station	A_1	A_2	p	q	u_{z0}/m/s	u_{z1}/m/s	c_f/s	s_{zr}
Sletringen	0.150	-0.114	-0.61	0.49	6.2	5.7	241	7.2
Skipheia	0.078	-0.036	-0.50	0.42	2.8	4.8	253	6.4

USER's GUIDE

USER's GUIDE

The main purpose for working out this User's Guide is to help the reader to easily find the recommended schemes (Sections, equations, tables) and to show by some practical examples how the calculations shall be made. It is not the purpose to provide discussions of the properties/limitations of the schemes with respect to extrapolation or other particular subjects.

1. The 1h mean wind speed profile

Section: 4.2
Scheme: Eqs. 3, 17, 18 and 19 (or 20 and 21)
Input data: Height z = 75m;
Reference wind speed 25 m/s:
Lapse rate 0 (stable), 10 (neutral) and 20 K/km (unstable);
Air-sea temperature difference 4 K (stable), 0 K (neutral) and - 4 K (unstable).

From Eq. 19 we first calculate U_{rs} og U_{rd} to be

$$16.26 \text{ m/s and } -3.25 \text{ m/s}$$

The sigmoid function Eq. 18 depending on wind speed now becomes

$$sig(U_r, U_{rs}, U_{rd}) = 0.0636$$

and from Eqs. 17 and 19 the logaritmic coefficient becomes

$$\alpha = 0.10 + 0.025 - 2 \cdot 10^{-4} \cdot \gamma - 0.06 \cdot sig(\gamma, 6, 3) \cdot 0.0636$$

Thus, for the 3 lapse rate conditions we find

Lapse rate (K/km)	Log. coefficient	U(75m) (m/s)
0	0.1245	31.27
10	0.1200	31.04
20	0.1172	30.90

If instead data for air-sea temperature differences Δ are available, we have to use Eqs. 20 and 21. In that case the logaritmic coefficient becomes

$$\alpha = 0.10 + 0.025 + 10^{-3} \cdot \Delta - 0.06 \cdot sig(\Delta, -0.25, -1.0) \cdot 0.0636$$

Thus. for the 3 air-sea temperature difference conditions we find

Air-sea temp.diff. (°K)	Log.coefficient	U(75m) (m/s)
4	0.1289	31.50
0	0.1233	31.21
-4	0.1173	30.91

2. The reference gust profile

Section: 4.4.2
Scheme: Eq. 7
Input data: Height z = 75m;
Reference wind speed 25 m/s;
Lapse rate 0 (stable), 10 (neutral) and 20 K/km (unstable);
Gust duration T_i = 1s and 60s

We want to calculate the most likely maximum wind speed corresponding to the above input data. From Eq. 7 and the definition of the sigmoid function we find

$$U_{MAX}(T_i,\gamma,25m/s,75m) = 25\cdot[(0.97+0.2015 - 0.0389\cdot\ln(T_i/3600))\cdot 1.06 + 0.0095\ sig(\gamma,10,3)]$$

from which it follows that

T_i(s)	γ(K/km)	U_{MAX} (m/s)
1	0	39.49
1	10	39.61
1	20	39.72
60	0	35.27
60	10	35.38
60	20	35.50

3. The gust distribution

Section: 4.4.1 and 4.4.2
Scheme: Eq. 3 with parameters given by Eq. 8 subject to Eq. 9 or 10.
Recommended for neutral conditions.
Input data: Height z = 75m;
Reference wind speed 25 m/s;
Gust duration T_i = 10s

Conservatively, the parameters defined by Eq. 10 are assumed to be valid for $u_r > 18$ m/s. It then follows that the parameter α becomes

$$\alpha = 0.956 + 0.2619 + 0.3014 - 0.1056 = 1.4137$$

Then, from Eq. 8 together with the parameter values of Eq. 10 we find

$$\sigma = 1.0 \cdot (1.4137 - 0.80 - 0.2720) \cdot (0.066 + 0.04634) = 0.03839$$
$$\delta = 1.0 \cdot (1.4137 - 0.80 - 0.3405) \cdot (0.18 + 0.2055) = 0.1053$$

The gust value for the intersection between the Gaussian and the exponential distribution now becomes

$$G_C = \alpha + (\sigma^2/\delta) = 1.4137 + 0.0140 = 1.4277$$

and the distribution function becomes

$$f(G) = \begin{cases} N \exp\left(-\left(\frac{G - 1.4137}{0.0543}\right)^2\right) & \text{for } G < 1.4277 \\ N \exp\left(-\frac{G - 1.4207}{0.1053}\right) & \text{for } G > 1.4277 \end{cases}$$

The normalization constant N is given by Eq. 4. and we find

$$N = 6.237$$

For small exceedance probabilities p the gust factor can be determined from Eq. 12. For p = 0.001 we find

$$G = 1.4137 + 0.007 + 0.1053 \cdot \ln(N \cdot 105.3)$$

Because G is defined relative to the reference wind speed, it follows that the 10s maximum wind gust with exceedance probability 0.001 at the level 75m becomes

$$U_{MAX} = G \cdot U(10m) = 2.104 \cdot 25.0 = 52.6 \text{ m/s}$$

This result for the limiting gust factor may also be confirmed by interpolation from Fig. 4.4.21.

4. Turbulence intensity

Section: 4.5
Scheme: Eq. 1 and 2
Input data: Height z = 75m;
Reference wind speed 25 m/s:
Lapse rate 0 (stable), 10 (neutral) and 20 K/km (unstable).

We want to calculate turbulence intensity and the r.m.s. value σ_u of the wind speed fluctuations for these conditions.

From Eq. 2 we find

$$I = 0.05456 + 0.0475 + 1.8 \cdot 10^{-4} \cdot sig(\gamma, 15, 3)$$

and from Eq. 1 we find

$$\sigma_u = I \cdot U(z)$$

where U(z) is the mean wind speed calculated in Section 1. Thus, we find

Lapse rate (K/km)	Turbulence intensity	R.m.s.fluct. (m/s)
0	0.1021	3.19
10	0.1021	3.17
20	0.1022	3.16

5. The distribution of turbulence intensity

Section: 4.5
Scheme: Eqs. 3,4.5 together with Table 4.5.1
Input data: Height z = 75m;
Reference wind speed 20 m/s;
Lapse rate: Near neutral

From Table 4.5.1b and Eqs. 4 and 5 we find

$$I_0 = 0.070 + 0.0500 \cdot 0.3651 = 0.08826$$
$$\sigma_1 = 0.009 + 0.0000 \cdot 2.015 = 0.009$$
$$\sigma_2 = 0.023 + 0.0015 \cdot 2.015 = 0.026$$

The variables d_1 and d_2 in Eq. 3 become

$$d_1 = (I - 0.08826) \cdot 111.11 = 2.889 \cdot I'$$
$$d_2 = (I - 0.08826) \cdot 38.46 = I'$$

The relative distribution is now determined for all values of I. However, the normalization factor N should have been determined in order to obtain a correct distribution. This must be done by numerical integration methods. Rather than going into that, we will finish by simply writing the distribution function

$$f(I') = N \cdot \frac{111.11 \cdot \exp(-4.173 \cdot I'^2 - 2.889 \cdot I') + 38.46 \cdot \exp(-0.5 \cdot I'^2 + I')}{\exp(-2.889 \cdot I') + \exp(I')}$$

$$I' \geq -3.3945$$

Fig. 4.5.4 gives the connection between exceedance probability p and the corresponding limit on the turbulence intensity I for the set of heights at Sletringen (10 to 46 m). Although 75 m is not covered, the smooth variation allows us to estimate:

Exceedance probability	Turbulence intensity
0.01	0.147
0.001	0.17

6. Wind direction fluctuations

Section: 4.6.2 and 4.6.3
Scheme: Eq. 4 together with list of parameter values in Sections 4.6.2 or 4.6.3
Input data: Gust duration 30s
Reference wind speed 25 m/s:
Lapse rate: Near neutral

It is first observed that the distribution function Eq. 14 is specified without reference to lapse rate and wind speed when applied to wind direction gusts. Thus, the distribution depends on averaging time interval T_i only. Note, however, that the validity is more or less restricted to strong wind and therefore near neutral conditions.

Logarithmic interpolation between the given D_{0i} values then give

$$\frac{D_{0i} - 8.0}{\ln 30 - \ln 15} = \frac{6.0 - 8.0}{\ln 60 - \ln 15}$$

and $D_{0i} = 7.0^{\circ}$. The most likely wind direction gust of duration 30s is then slightly below 7.0°.

The distribution function for wind direction gusts with duration 30s now becomes

$$f(D) = N \cdot \frac{0.67 \cdot \exp(-0.5 \cdot d_1^2 - d_1) + 0.11 \cdot \exp(-0.5 \cdot d_2^2 + d_2)}{\exp(-d_1) + \exp(d_2)}$$

with

$$d_1 = 0.67 \cdot (D - 7.0)$$
$$d_2 = 0.11 \cdot (D - 7.0)$$

Although determination of the normalization factor N requires numerical integration from $D = 0$ to $D = \infty$, we can determine directly the maximum point more precisely. The result is

$$D_{MAX} = 6.5^{\circ}$$

From Fig. 4.6.4, the limit of extreme wind direction fluctuations corresponding to a given exceedance probability p can be estimated. For an averaging interval of 30 s we find as an example

Exceedance probability	θ_{max} (°)
0.01	31
0.001	35

The distribution of the standard deviation of the wind direction fluctuations is described by Eq. 14 together with the parameters of Section 4.6.3 which essentially are referred to the strong wind case but with dependency on lapse rate. Thus, the most likely standard deviation for the present situation becomes slightly below 4.0°. A more precise determination can be made from Eq. 4 with parameter values

$$D_0 = 4.0^\circ, \quad \sigma_1 = 1.0^\circ, \quad \sigma_2 = 4.0^\circ$$

From Fig. 4.6.5. the limit of extreme values of the standard deviation of wind direction fluctuations corresponding to a given exceedance probability p can be estimated. As an example, we find

Exceedance probability	σ (°)
0.01	14
0.001	17

7. One point turbulence spectra

Section: 5.3.3
Scheme: Eq. 12 together with parameter values in Table 5.3.1 (Sletringen)
Input data: Height 75m
Reference wind speed 25 m/s;
Lapse rate: 0 (stable), 10 (neutral) and 20 K/km (unstable).
Frequencies: $(5\ \text{min})^{-1}$, $(1\ \text{min})^{-1}$, $(10\ \text{s})^{-1}$

From the relationships of Eq. 12 we find

$$\rho = \gamma \cdot 0.2773$$
$$n = 0.281 + 0.428 \cdot \exp(-0.05075 \cdot \gamma)$$
$$B_2 = 0.0089 \cdot \exp(-0.08125 \cdot \gamma)$$
$$B_1 = 6.07 \cdot 10^{-3}$$

and the spectral function becomes

$$S(f) = \frac{1.93 \cdot 10^{-2}}{(6.07 \cdot 10^{-3} + f)^{5/3}} + \frac{0.2310}{(B_2{}^n + f^n)^{5/3n}}$$

For the given frequencies and lapse rate conditions we calculate each of the contributing terms and their sum. Using Eq. (5.3.8) and Fig. 5.3.1a, the total variance may also be calculated. The results are:

	Lapse rate (K/km)	Frequency (Hz) $3.33 \cdot 10^{-3}$	$1.67 \cdot 10^{-2}$	0.1	σ^2 $(\text{m/s})^2$
Term 1	0	46.1	10.6	0.8	0.87
Term 2	0	233.7	66.2	7.3	5.80
Sum		279.8	76.8	8.1	6.67
Term 1	10	46.1	10.6	0.8	0.87
Term 2	10	315.0	65.7	6.5	6.77
Sum		361.1	76.3	7.3	7.64
Term 1	20	46.1	10.6	0.8	0.87
Term 2	20	361.8	62.8	5.9	7.79
Sum		407.9	73.4	6.7	8.66

Using Eq. 8a and Fig. 5.3.1a to calculate the total variance, we find for the stable case

$\sigma^2 = 9.95$

Using the result found in Sec.1 above for U (75m), the corresponding value for turbulence intensity becomes

$I = \sigma/u(75m) = 0.1009$

which corresponds well to the Sec. 4 result of 0.1021.

When discussing the turbulence intensity in Sec. 4 above for the same set of conditions, we found values indicating that the total variance is close to 10 $(m/s)^2$ for all three lapse rate cases. The values of σ^2 for stable and normal conditions found here are somewhat less. The discrepancy is probably due to the very low frequency region around 10^{-3} Hz which was excluded when fitting the spectra, but effectively included when calculating the turbulence intensity. This region contributes significantly to the variance when estimated by the integral Eq. (5.3.8), and glancing at Fig. 5.3.2, it appears that the spectral fits may indeed underestimate the turbulence in this region, especially for stable conditions. Note that the frequency region from zero to infinity is included in the integral formulation, whereas the experimental evaluation excludes both the very high ond very low (through trend subtraction) frequency region. However, the practical implications of this are minor.

8. Coherence for vertical separation

Section: 5.4.3.1
Scheme: Eqs. 11 and 12 together with parameter values in Table 5.4.1 (Sletringen)
Input data: Mean height 75m
Vertical separation 20m
Reference wind speed 25 m/s;
Lapse rate: Neutral
Frequencies: $(5\ \text{min})^{-1}$. $(1\ \text{min})^{-1}$. $(10\ \text{s})^{-1}$

From Eq. 11 the non-dimensional height becomes

$$z_g = 7.433$$

and the exponential decay "constant" becomes

$$a_z = 7.433^{-0.51}\cdot(19.6 + 30.3\ \exp(-\ 88.1\cdot f)\cdot \text{sig}(9.8,9.8,-5.0)) = 0.3595\cdot(19.6 + 15.15\cdot\exp(-88.1\cdot f))$$

The coherence function now becomes

$$\text{Coh} = \exp(-a_z\cdot(20^{1.24}/25)\cdot f)$$

and from Eq. 12 the coherence length becomes

$$\lambda_z = f^{-0.8}\cdot 29.3\cdot(20 + 15\cdot\exp(-90\cdot f))^{-0.8}$$

For the given set of frequencies and the given synoptic situation we find

	Frequency (Hz)		
	$3.33\cdot10^{-3}$	$1.67\cdot10^{-2}$	0.1
a_z	11.11	8.30	7.05
Coh	0.941	0.797	0.314
λ_z(m)	179.7	62.3	16.8

9. Coherence for horizontal separation

Section: 5.4.3.2

Scheme: Eqs. 13 and 14 together with parameter values in Table 5.4.3 (restricted maritime sector)

Input data: Height 75m
Horizontal separation Δx = 500m, Δy = 50m
Reference wind speed 25 m/s;
Lapse rate: Stable (0 K/km)
Frequencies: $(5\ \text{min})^{-1}$, $(1\ \text{min})^{-1}$, $(10\ \text{s})^{-1}$

In addition to the coherence between the 2 points, we will also calculate the 2 coherence lengths corresponding to the given situation. The exponential decay "constants" for the along- and across wind directions now become

$$a_x = 0.429\cdot(3.45 + 3.19\cdot\exp(-78.9\cdot f)\cdot\mathrm{sig}(\gamma,9.8,2.98))$$
$$a_y = 0.465\cdot(18.4 + 131\cdot\exp(-34.1\cdot f)\cdot\mathrm{sig}(\gamma,9.8,-25.8))$$

and from Eq. 15 we find

$$\lambda_x = 25/(f\cdot a_x)$$
$$\lambda_y = 25/(f\cdot a_y)$$

The results are found to be

	Frequency (Hz)		
	$3.33\cdot10^{-3}$	$1.67\cdot10^{-2}$	0.1
a_x	1.52	1.49	1.48
a_y	40.84	29.03	9.75
Coh	0.748	0.328	0.029
λ_x(m)	4939.1	1004.7	168.9
λ_y(m)	183.8	51.6	25.6

10. Phase differences for horizontal separation

Section: 5.4.4.1
Scheme: Eqs. 16 and 17 (Masts 2-4)
Input data: Height 75m
Along wind separation 500m
Reference wind speed 25 m/s;
Frequencies: $(5\ \text{min})^{-1}$, $(1\ \text{min})^{-1}$, $(10\ \text{s})^{-1}$

The phase difference now becomes

$$\theta = 2\pi \cdot 0.87 \cdot f \cdot 500/(7.5^{0.073} \cdot 25) = f \cdot 94.6$$

and for the given frequencies we find

	Frequency (Hz)		
	$3.33 \cdot 10^{-3}$	$1.67 \cdot 10^{-2}$	0.1
Phase (rad/ °)	0.315 (18.0)	1.580 (90.5)	9.46 (543.0)

The phase value 543° for f = 0.1 Hz is rather theoretical, considering the low value 0.03 of the corresponding coherence.

11. Phase differences for vertical separation

Section: 5.4.4.2
Scheme: Eqs. 20 and 18 and Table 5.4.5 (Sletringen)
Input data: Heights 10 and 75m
Vertical separation 10m
Reference wind speed 25 m/s:
Frequencies: $(5\ \text{min})^{-1}$, $(1\ \text{min})^{-1}$, $(10\ \text{s})^{-1}$
Lapse rate: 0 K/km

From Eq. 20 and Table 5.4.5 we find

$$U_S = 6.2 + 5.7 \cdot \ln(z/z_r)$$

and

$$\begin{aligned}\theta(f) &= 2\pi \cdot (0.150 - 0.114 \cdot \text{sig}(0,9.8,5) \cdot \text{sig}(25,U_S,-0.2 \cdot U_S)) \\ &\quad \cdot 10 \cdot (z/z_r)^{-0.61} \cdot (1-\exp(-241 \cdot f)) \cdot (f/25)^{0.49} \\ &= 62.83 \cdot (0.15 - 0.0141 \cdot \text{sig}(25,U_S,-0.2 \cdot U_S)) \cdot (z/z_r)^{-0.61} \\ &\quad (1 - \exp(-241 \cdot f)) \cdot (f/25)^{0.49}\end{aligned}$$

The angle α between the line of constant phase and the horizontal plane can be found from Eq. 18 to be

$$\alpha(f) = 90^{\circ} - \text{arctg}\left(\frac{\theta(f) \cdot U(z)}{2\pi \cdot f \cdot \Delta z}\right)$$

where U(z) for z = 75m is given in Section 1.

For the given heights and frequencies we now find

Height		Frequency (Hz) $3.33 \cdot 10^{-3}$	$1.67 \cdot 10^{-2}$	0.1
10 m	Phase (rad/ °)	0.066 (3.8)	0.257 (14.7)	0.630 (36.1)
	α (°)	7.3	9.3	21.8
75 m	Phase (rad/ °)	0.019 (3.8)	0.257 (14.7)	0.630 (36.1)
	α (°)	19.4	24.2	47.8

ACKNOWLEDGEMENTS

The authors wish to thank Mr. Sverre Haver, Statoil, R&D Division, and Mr. John C. Heidemann, Exxon Production Research Company, for numerous discussions and valuable suggestions. We are in particular indebted to Mr. Haver for a critical reading of the draft reports.

REFERENCES

Aasen,S.E., 1989. The maritime turbulent wind field, Measurements and models, Appendix report No. 1.

Chatfield,C., 1984. The analysis of time series, third ed., Chapman and Hall, London.

Eidsvik,K.J., 1985. Boundary Layer Met. **32**, 103-132.

Heggem,T., J.Loevseth, K.Mollestad and O.J.Andersen, 1989. Turbulence structure in the maritime wind field, Final report of Phase 1 of this project.

Høistrup,J., 1982. J.Atmos. Sci. **39**, 2239-2248.

Frost,W., B.H.Long and R.E.Turner, 1978. Engineering handbook on the atmospheric environmental guidelines for use in wind turbine generator development, NASA Technical Paper 1359.

Newland,D.E., 1987. An introduction to random vibrations and spectral analysis, 2nd ed., Longman Scientific & Technical.

Panofsky,H.A. and J.A. Dutton, 1984. Atmospheric turbulence, John Wiley & Sons, New York.

FIGURES FOR SECTION 2

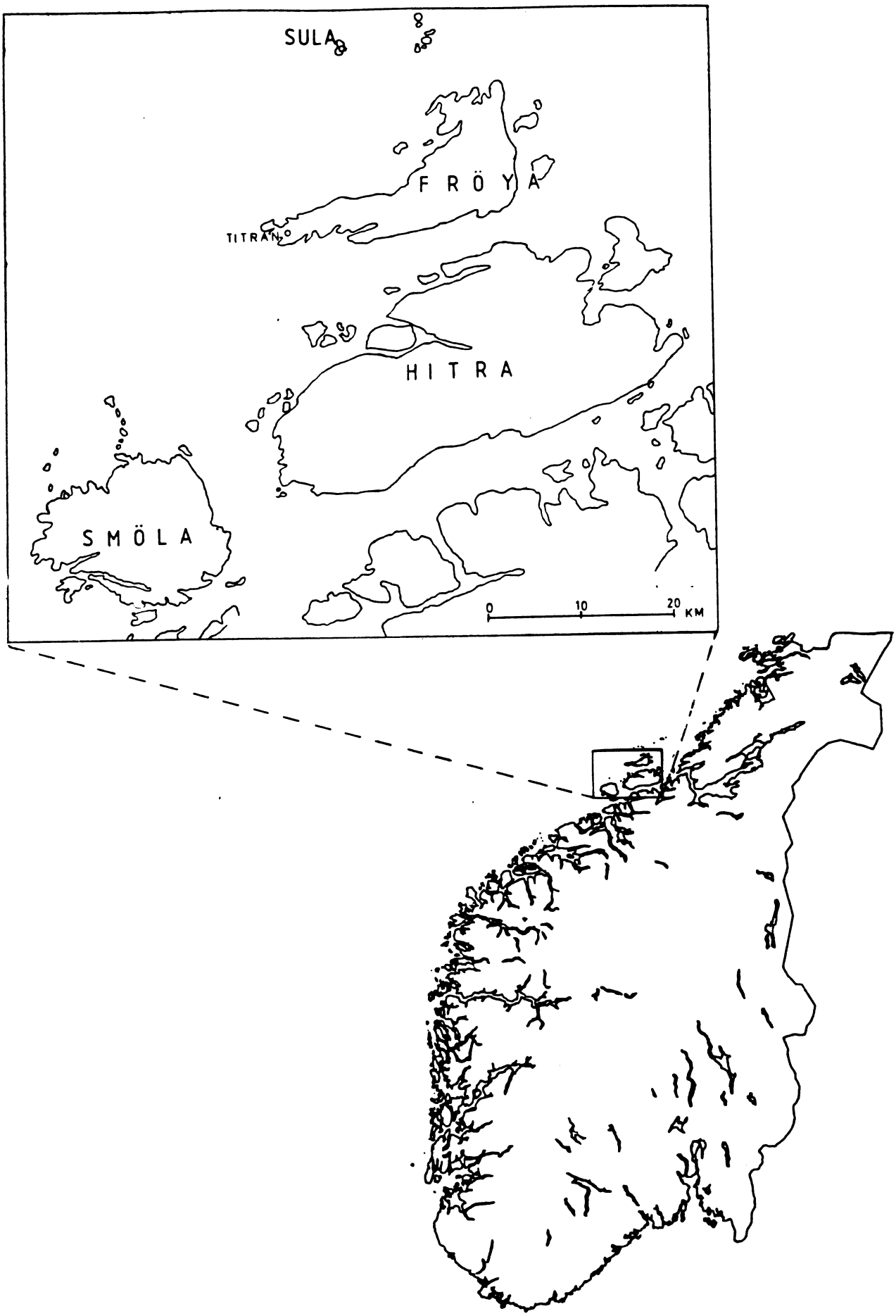

Fig. 2.1 Map showing the location of the wind measurement stations at the coast outside Trondheim.

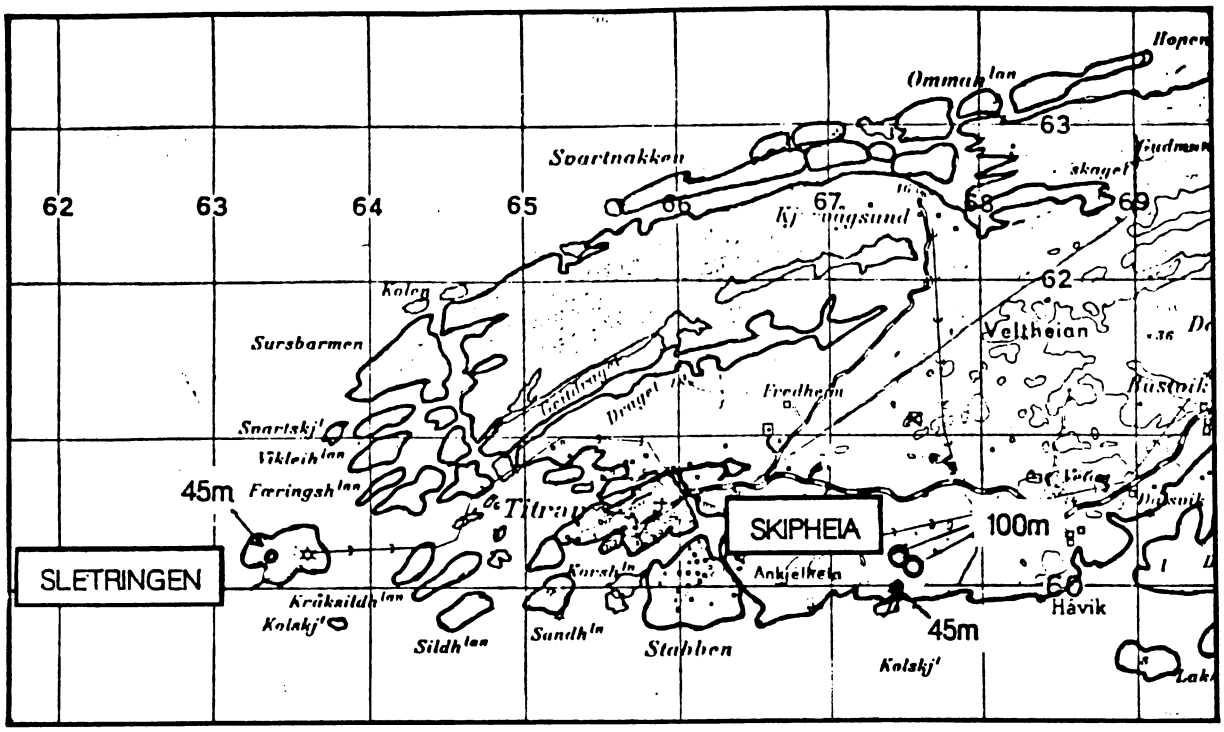

Fig. 2.2 Map of the western part of Frøya showing the location of the wind measurement stations.

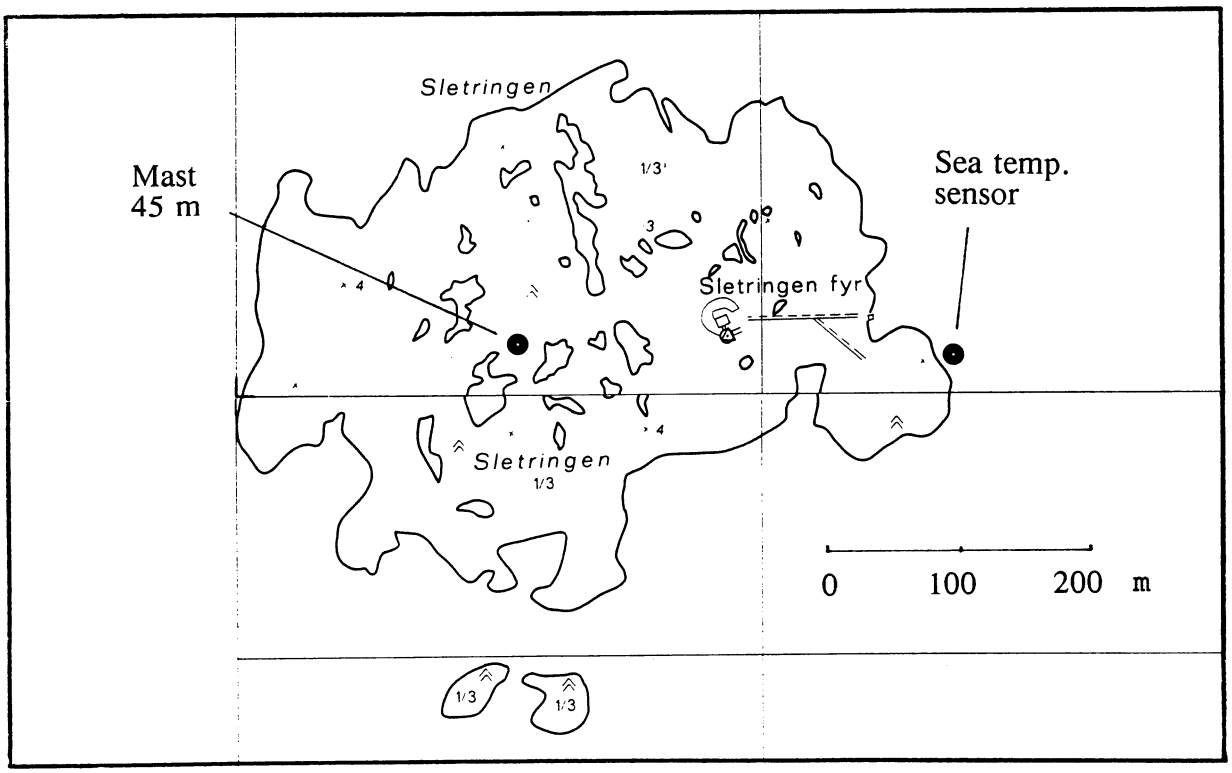

Fig. 2.3 Map showing the location of the mast at Sletringen.

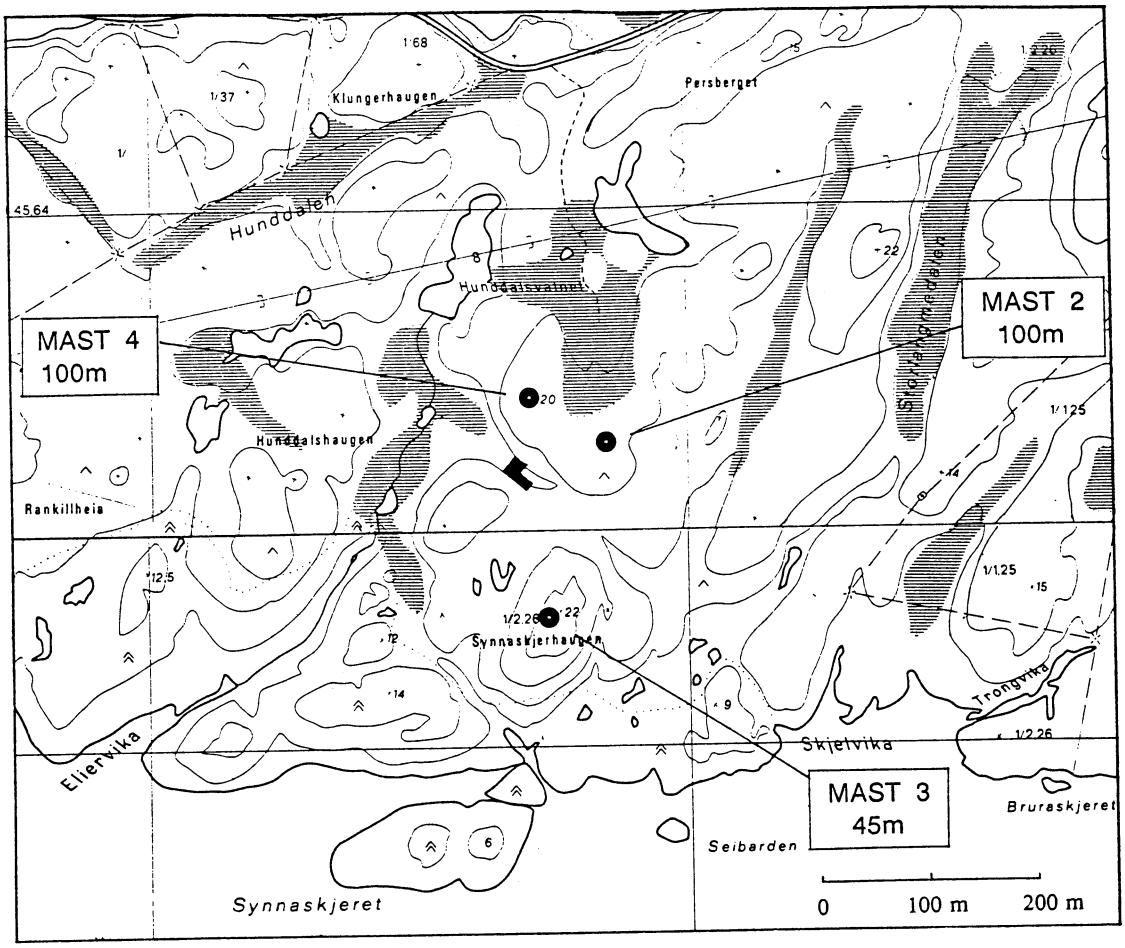

Fig. 2.4 Map showing the location of the masts at Skipheia.

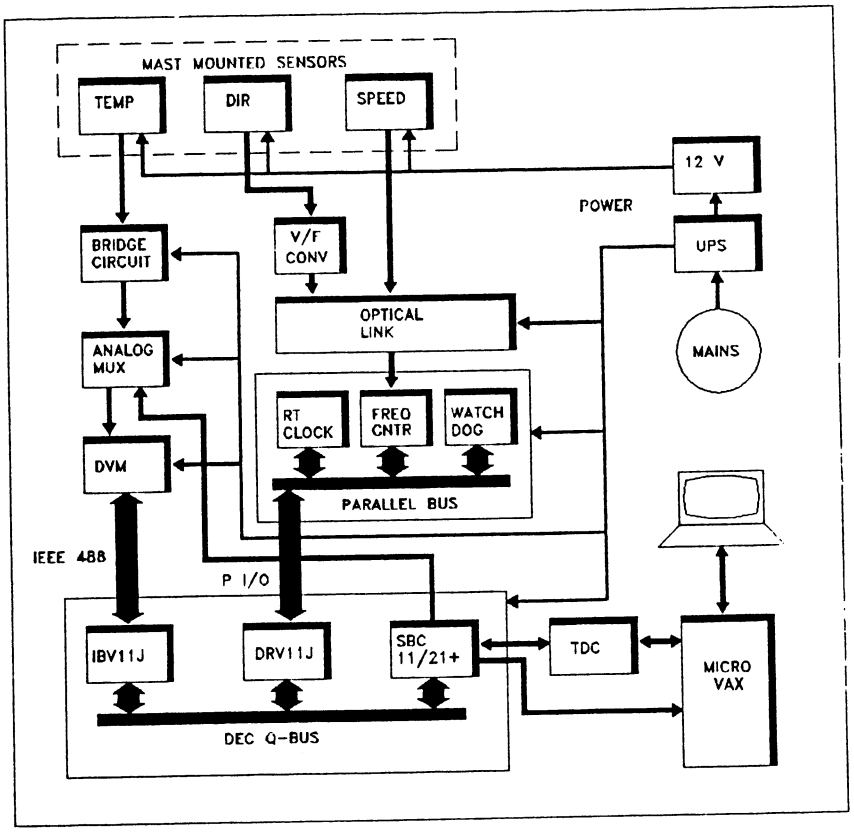

Fig. 2.5 The data acquisition system.

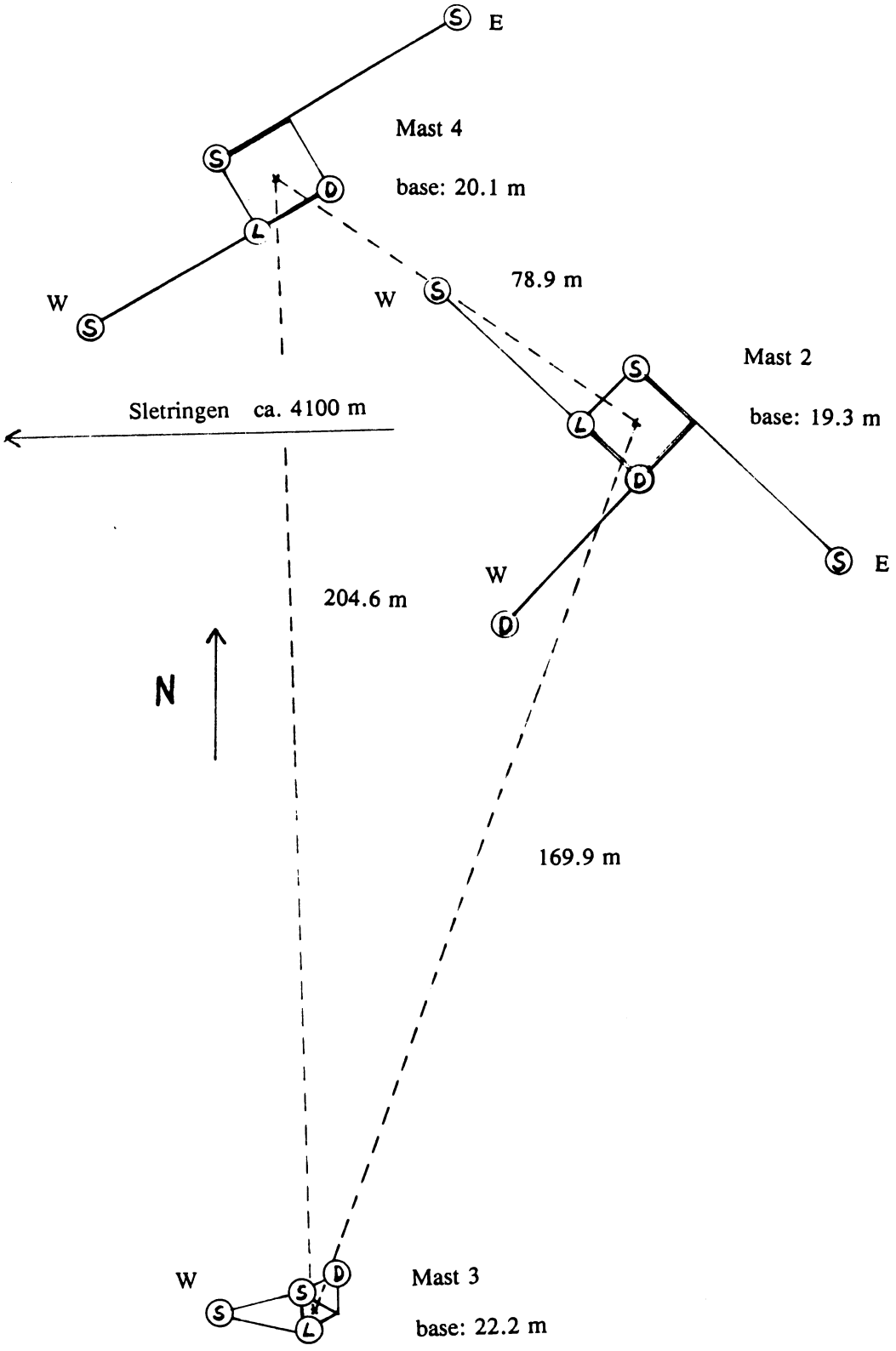

S - wind speed sensor.
D - wind direction sensor
L - lightning-bar
W - West
E - East

Fig. 2.6 Orientations of the masts and distances between the masts at Skipheia. The orientations of the sensors, and the coordinates of the base points are given in Table 2.1.

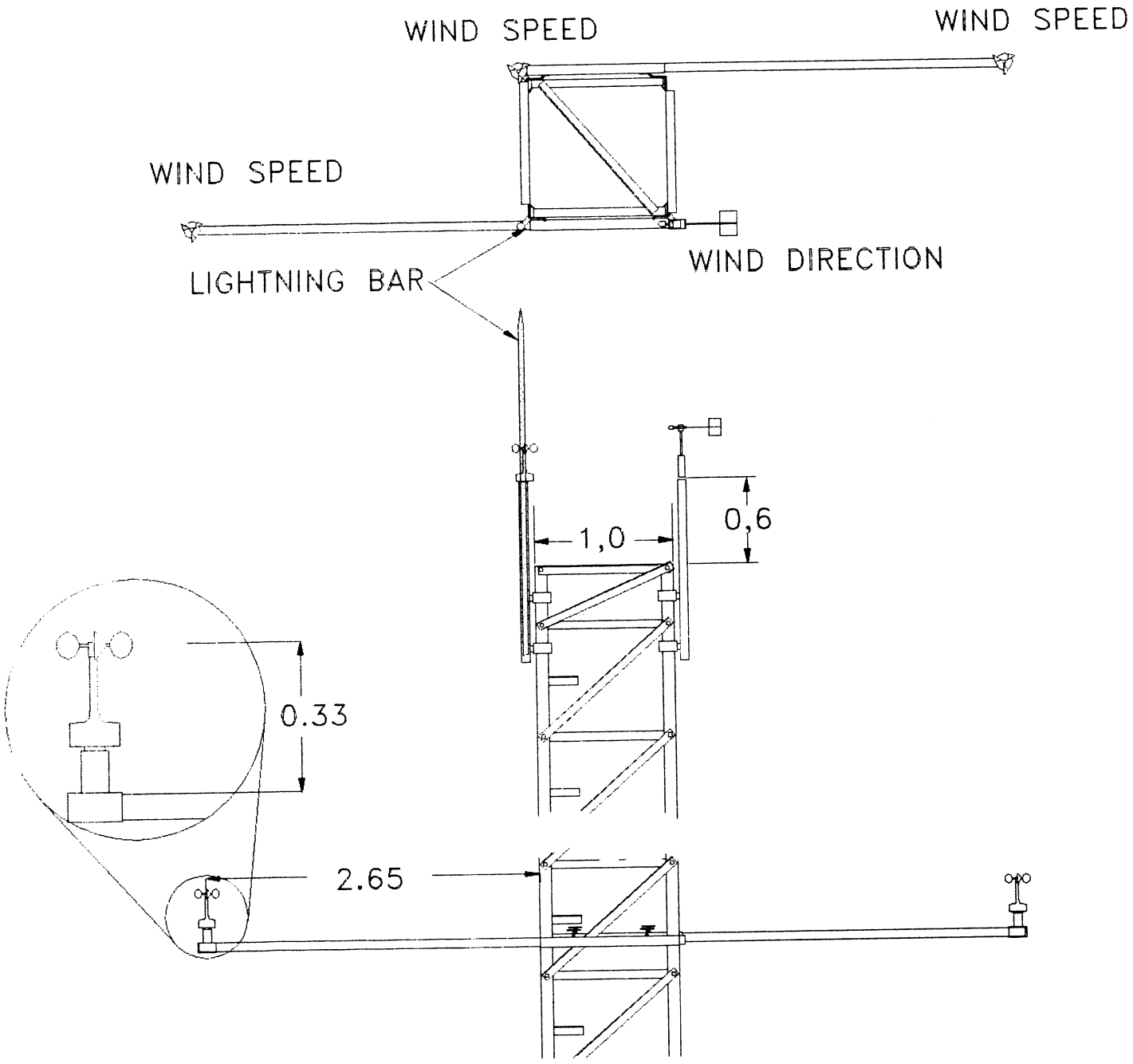

Fig. 2.7 Mounting of the sensors in the 100 m masts.

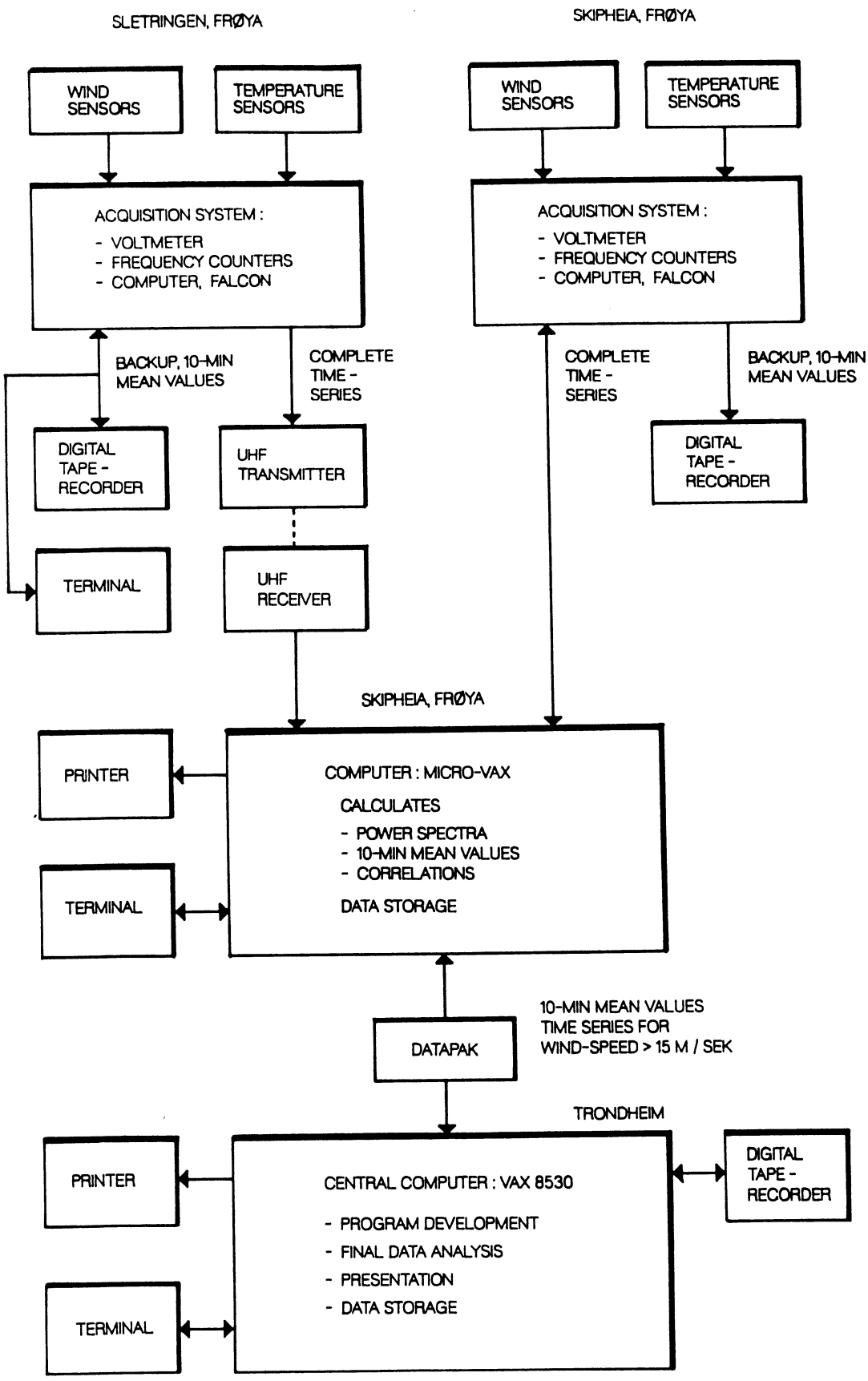

Fig. 2.8 Data flow chart.

FIGURES FOR SECTION 3

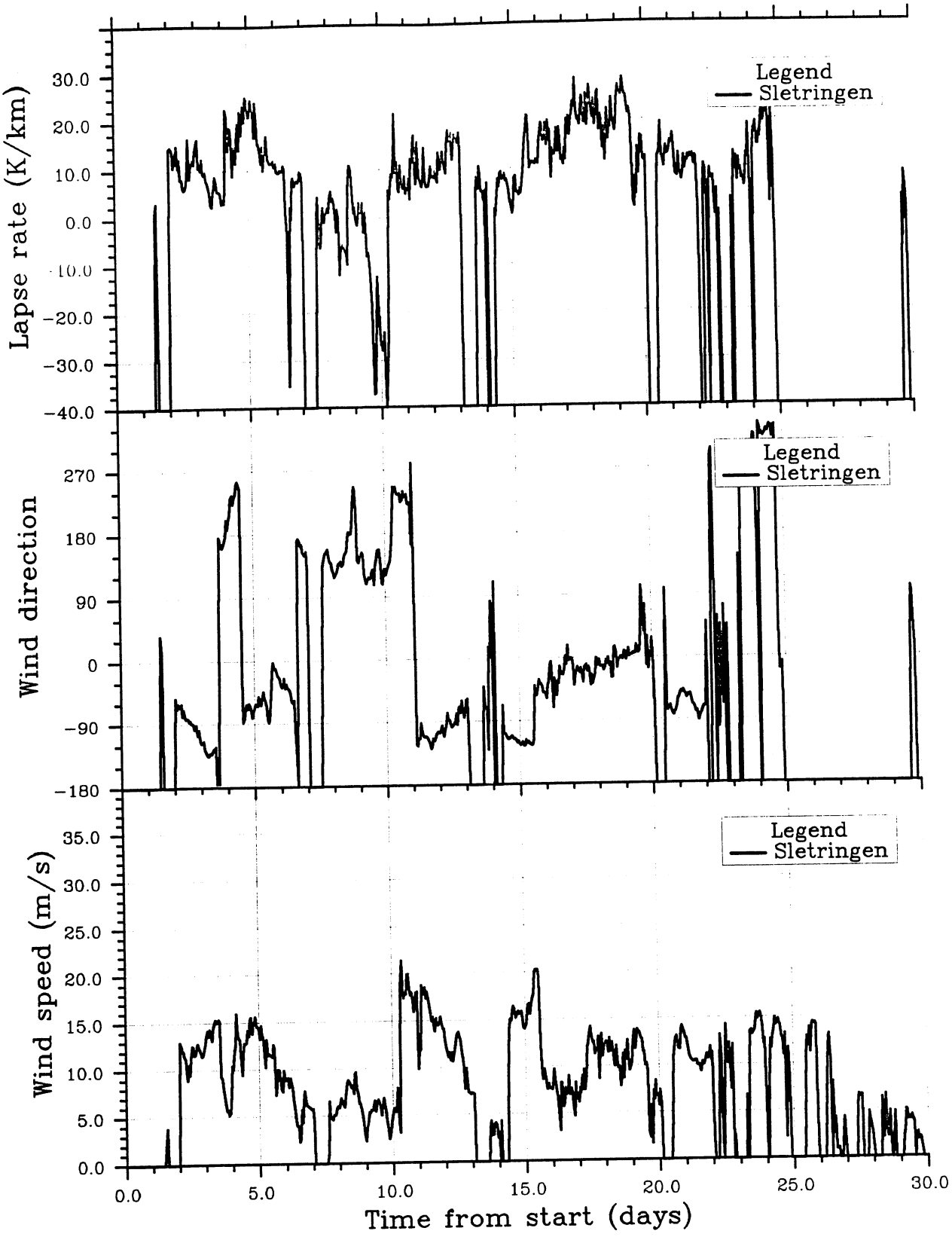

Fig. 3.1.1 Mean value (1-h period) of lapse rate (top), wind direction (middle) and wind speed at 10 m height (bottom) for November 1988 at Sletringen.

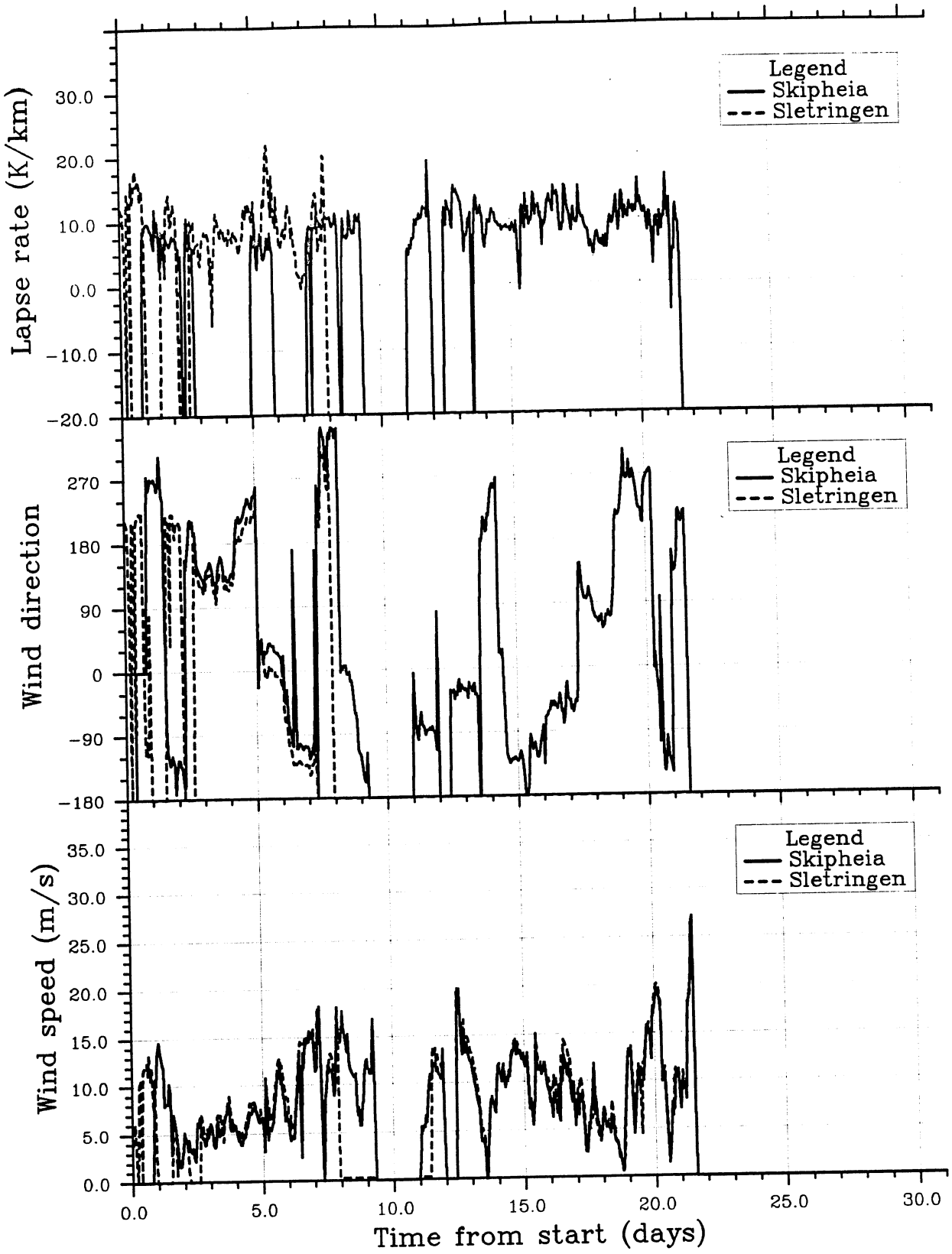

Fig. 3.1.2 Mean value (1-h period) of lapse rate (top), wind direction (middle) and wind speed at 10 m height (bottom) for December 1988 at Sletringen and Skipheia.

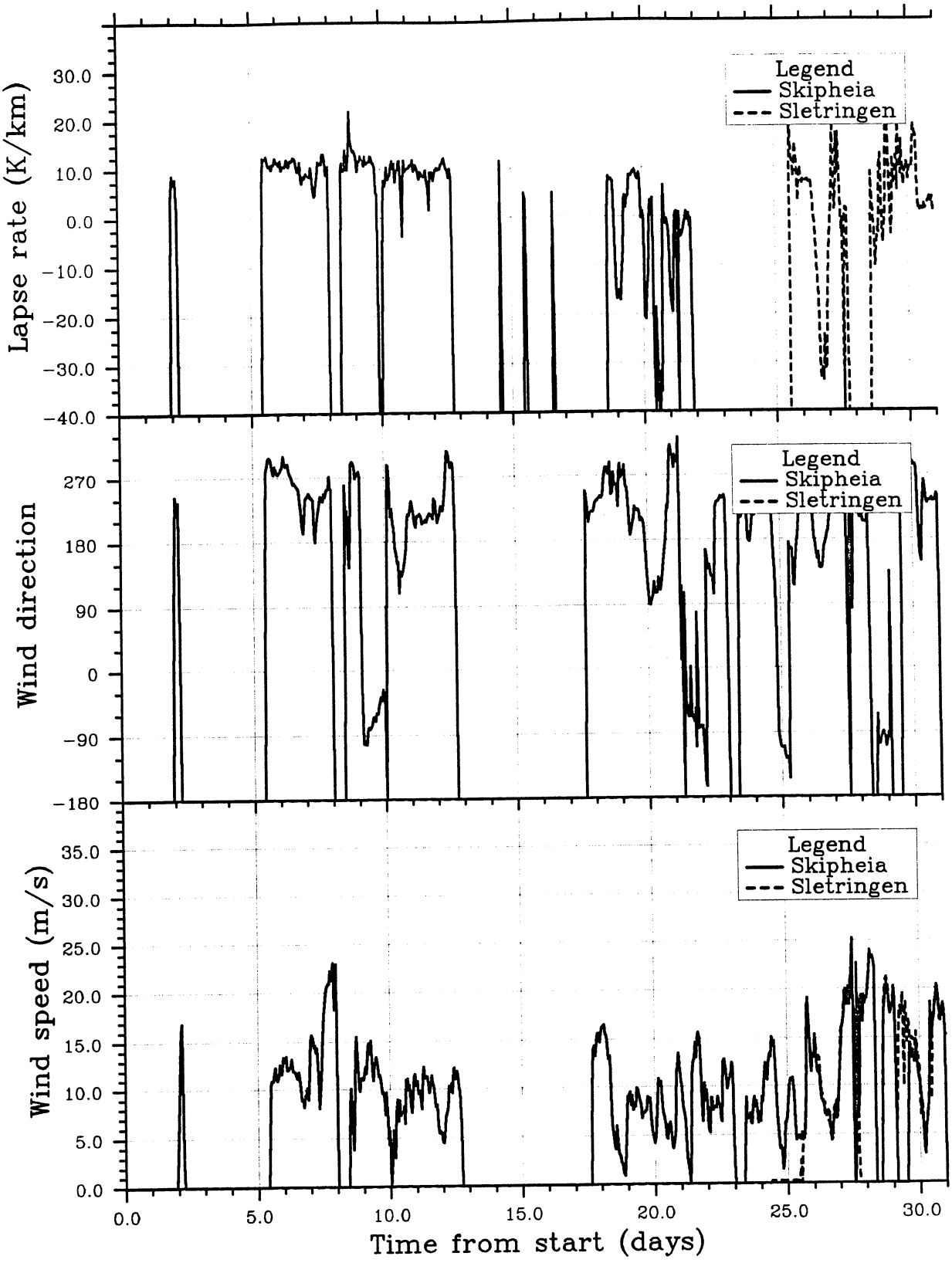

Fig. 3.1.3 Mean value (1-h period) of lapse rate (top), wind direction (middle) and wind speed at 10 m height (bottom) for January 1989 at Sletringen and Skipheia.

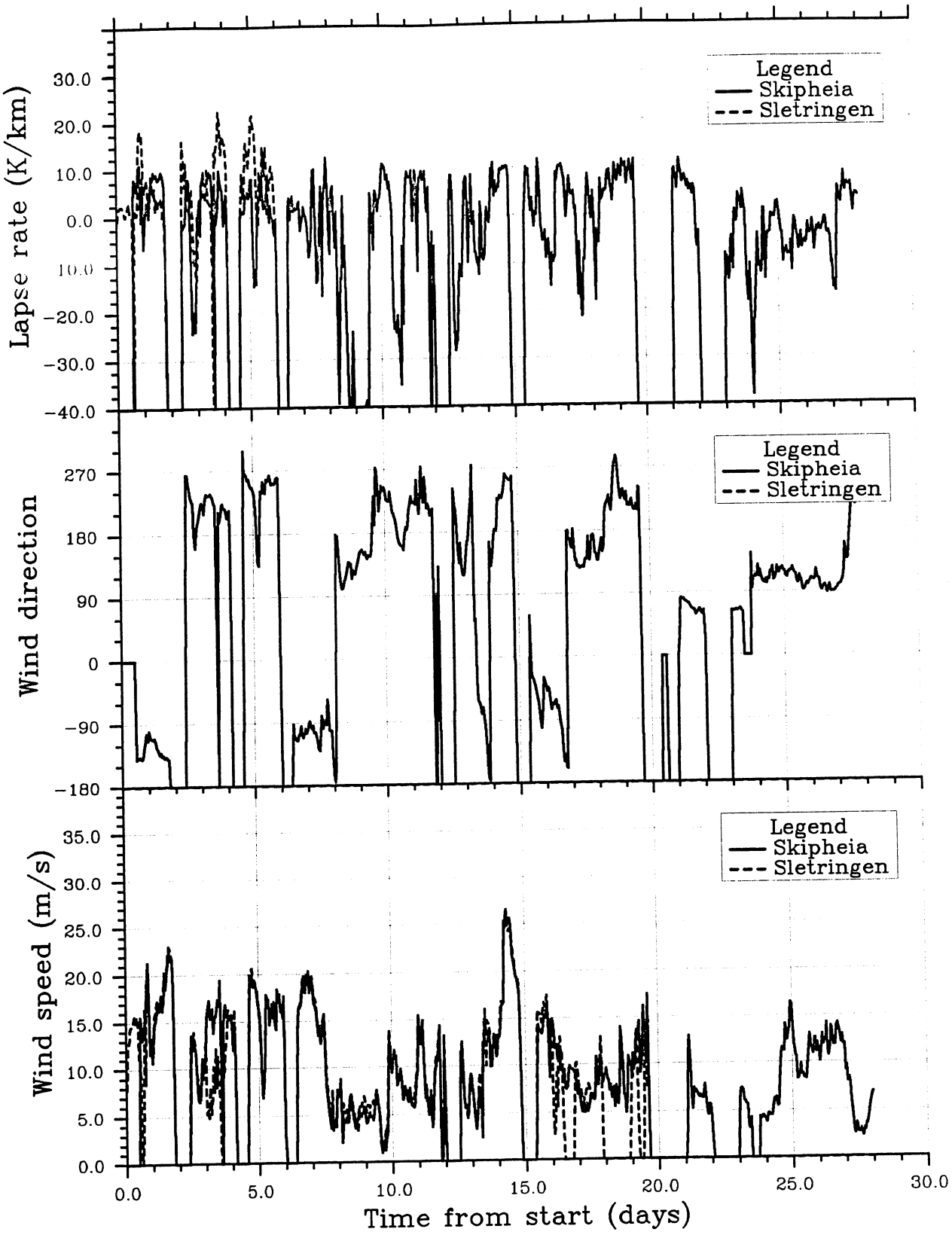

Fig. 3.1.4 Mean value (1-h period) of lapse rate (top), wind direction (middle) and wind speed at 10 m height (bottom) for February 1989 at Sletringen and Skipheia.

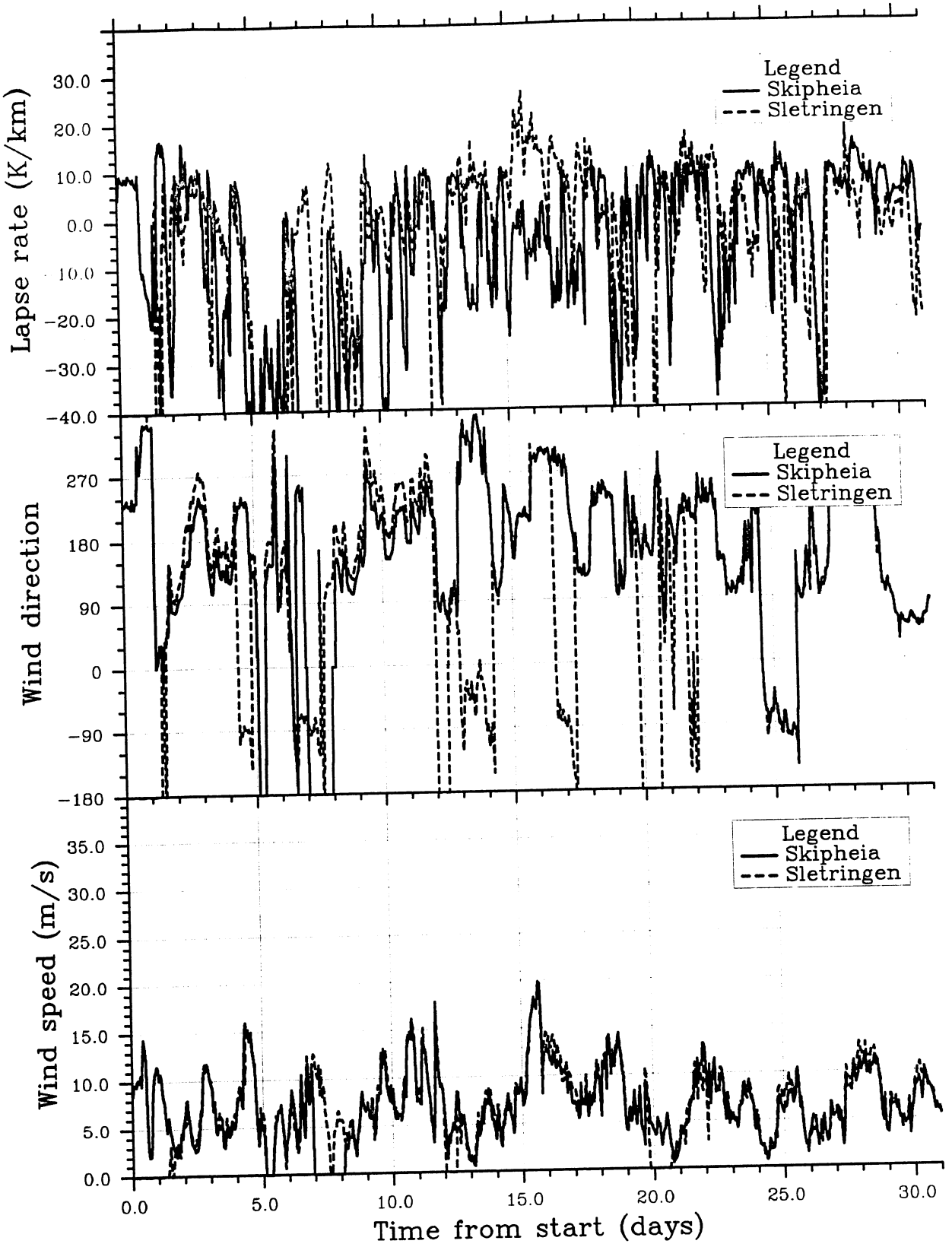

Fig. 3.1.5 Mean value (1-h period) of lapse rate (top), wind direction (middle) and wind speed at 10 m height (bottom) for March 1989 at Sletringen and Skipheia.

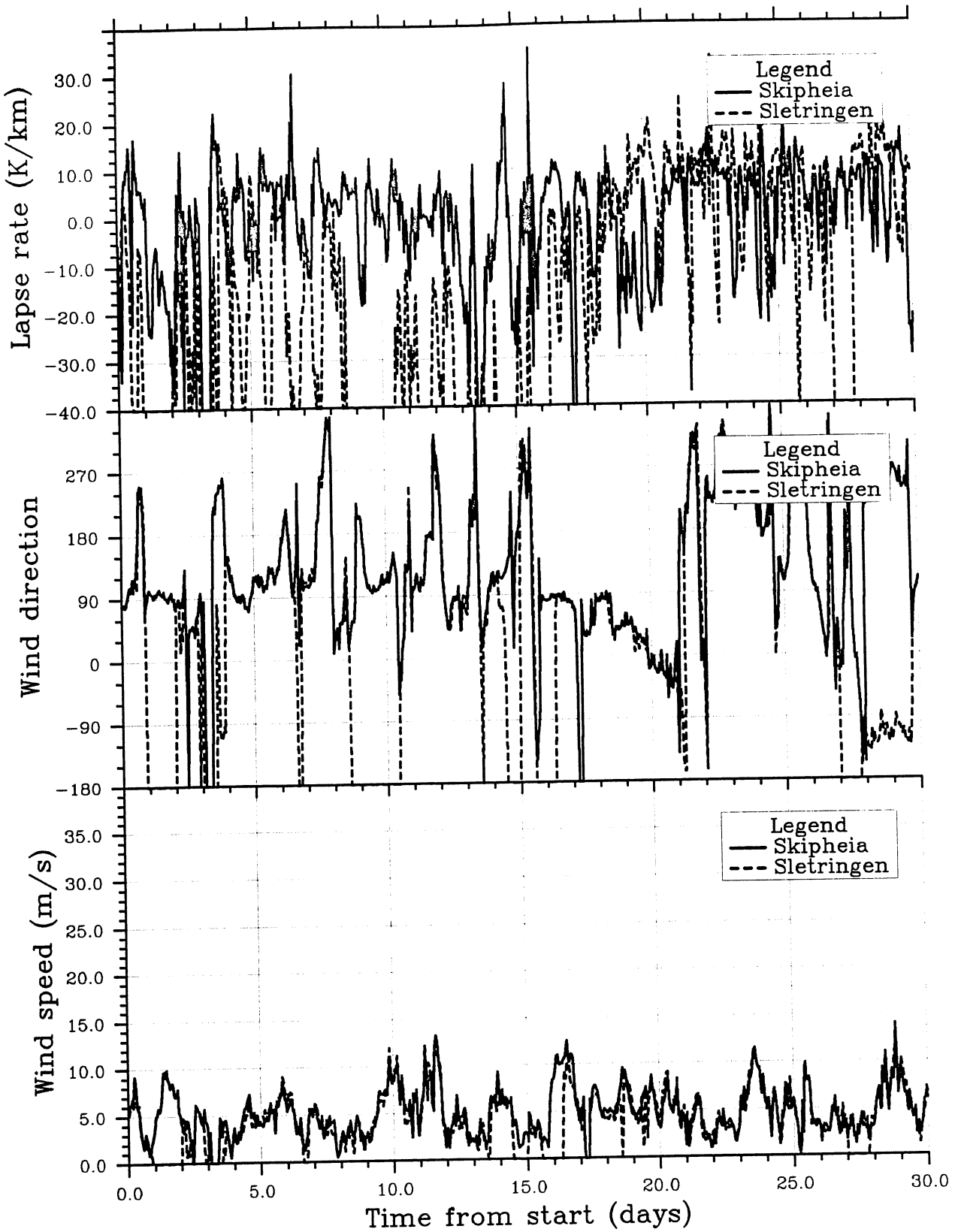

Fig. 3.1.6 Mean value (1-h period) of lapse rate (top), wind direction (middle) and wind speed at 10 m height (bottom) for April 1989 at Sletringen and Skipheia.

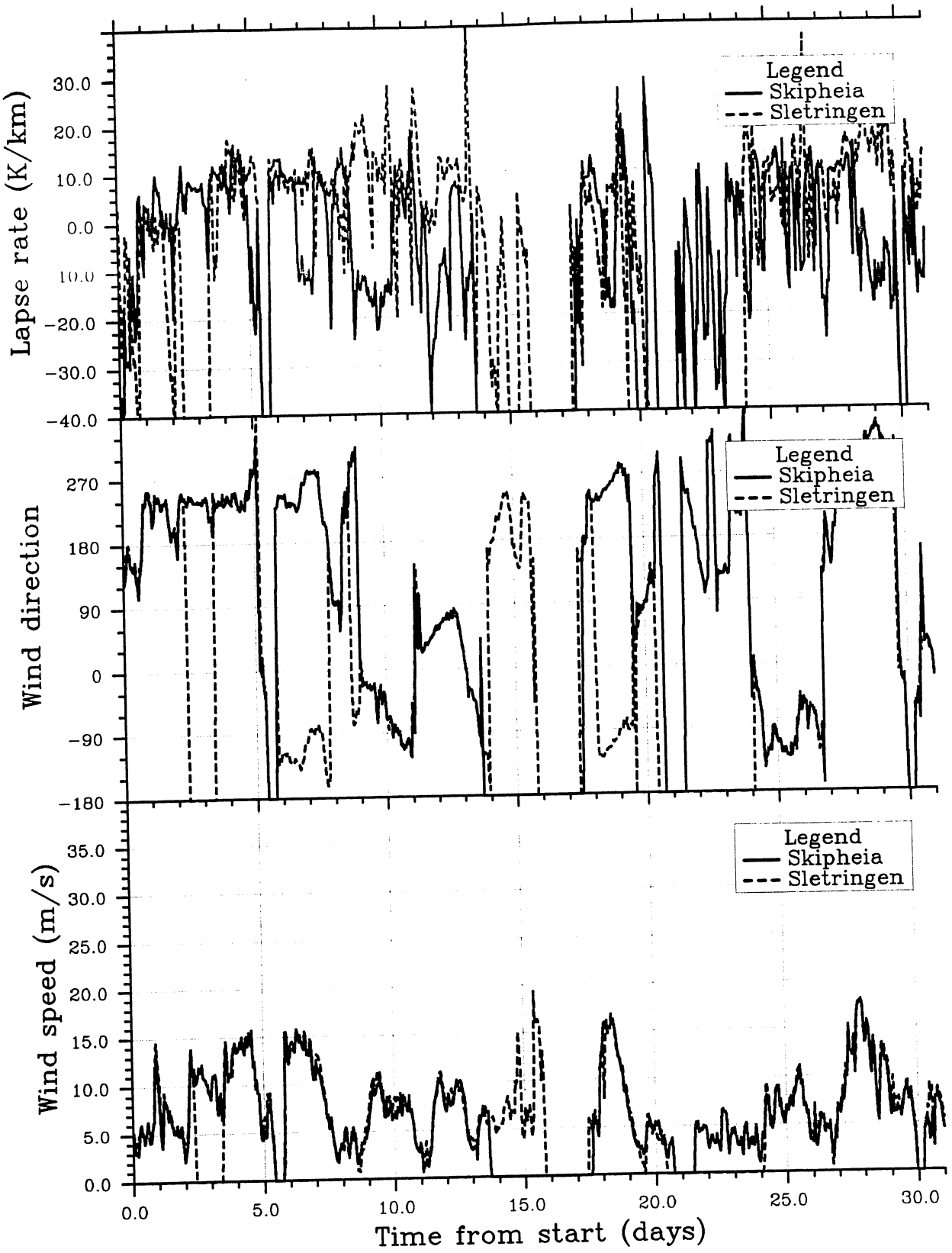

Fig. 3.1.7 Mean value (1-h period) of lapse rate (top), wind direction (middle) and wind speed at 10 m height (bottom) for May 1989 at Sletringen and Skipheia.

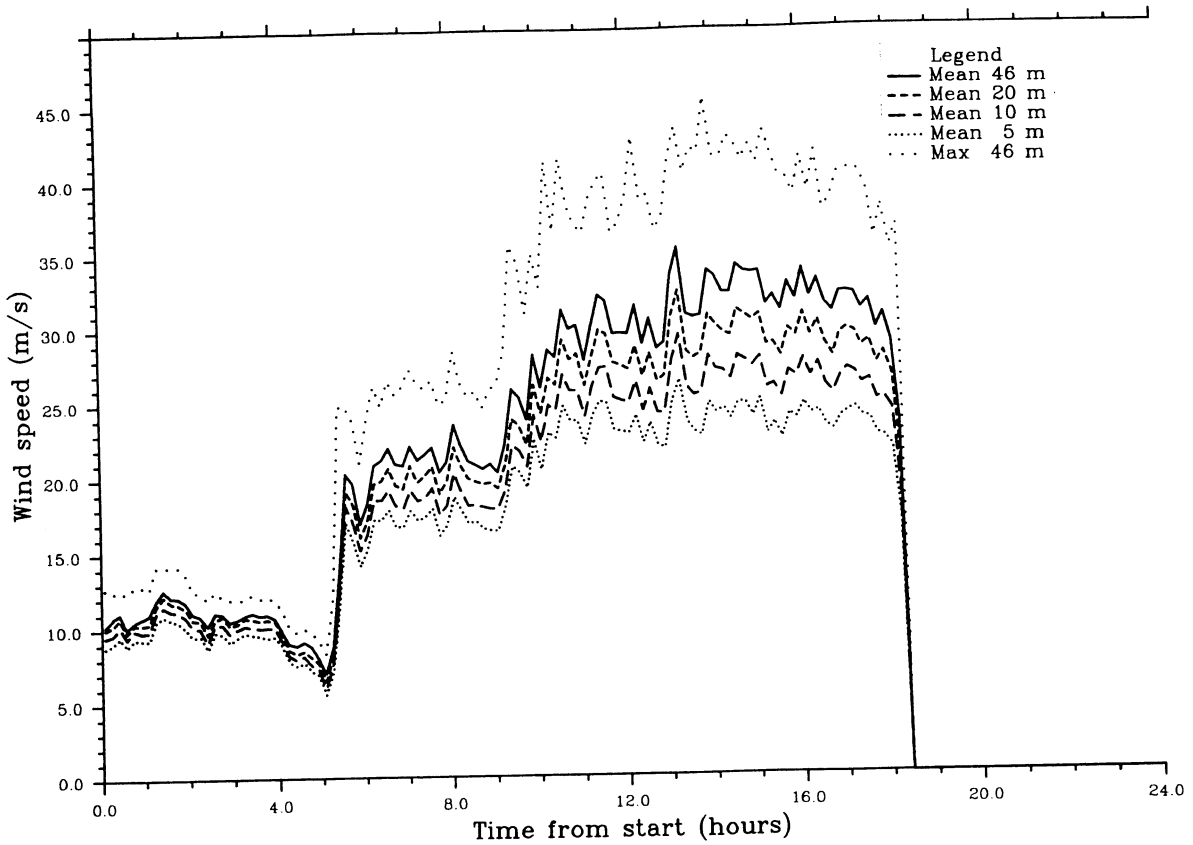

Fig. 3.1.8 Selected time series of 10-min. values observed at Sletringen on December 22, 1988.

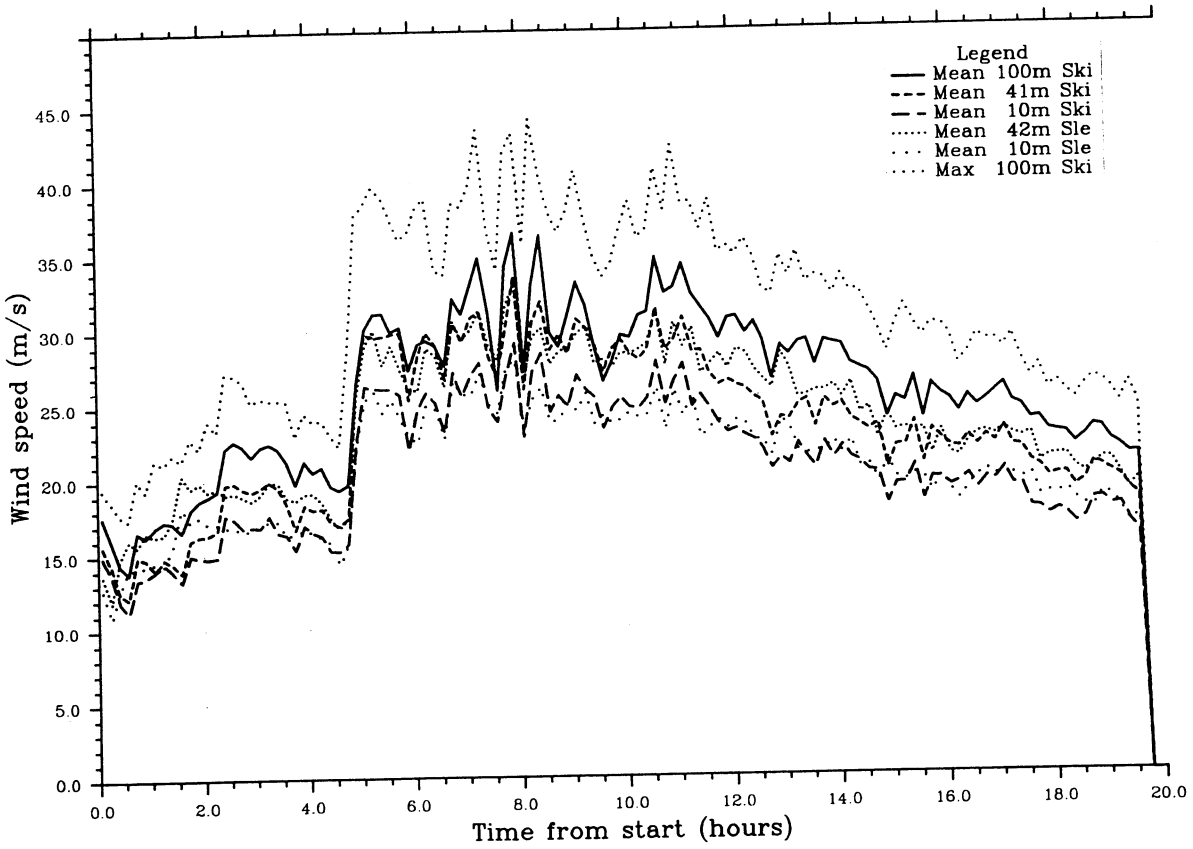

Fig. 3.1.9 Selected time series of 10-min. values observed at Sletringen and Skipheia on February 15, 1989.

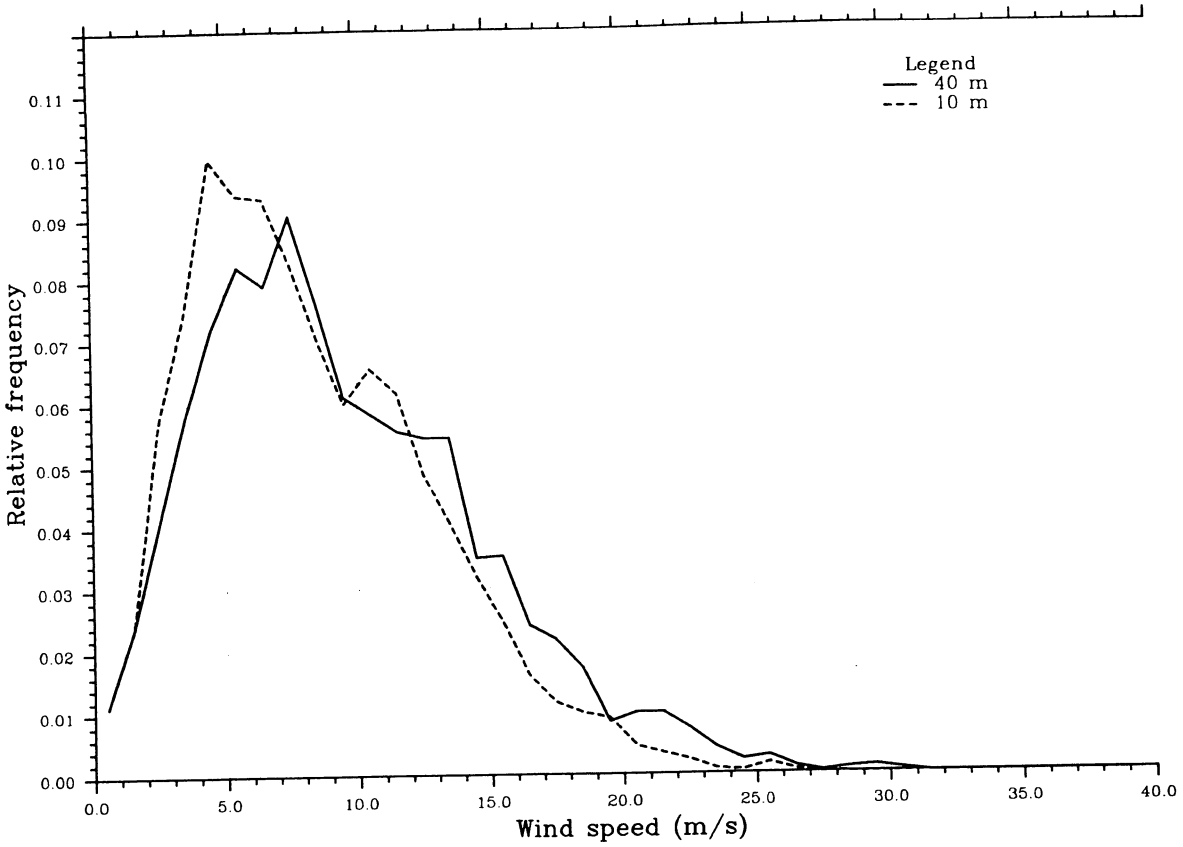

Fig. 3.2.1 The relative frequency distribution of 1 h mean wind speed values (bin width 1 m/s) at heights 40 and 10 m (see text).

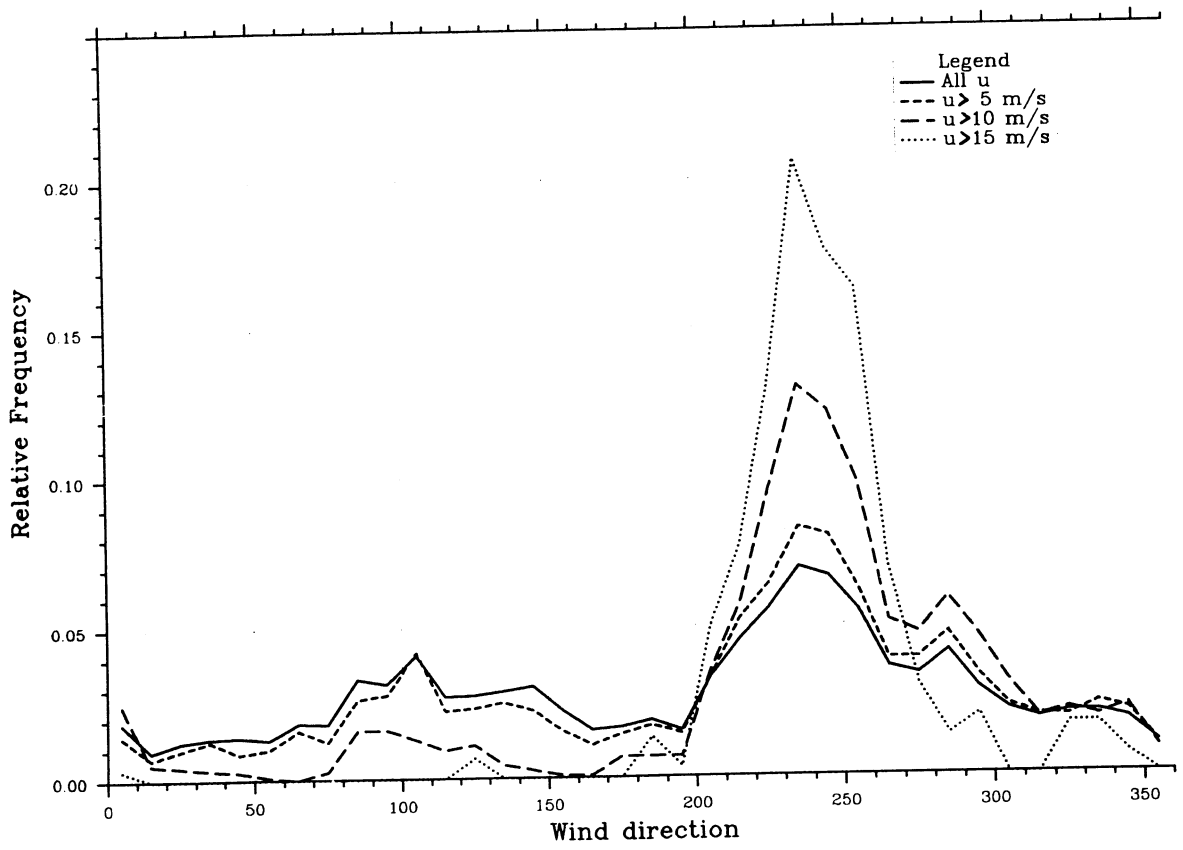

Fig. 3.2.2 The relative frequency distribution of wind direction (bin width 10°) for lower limits of wind speed of 0, 5, 10 and 15 m/s.

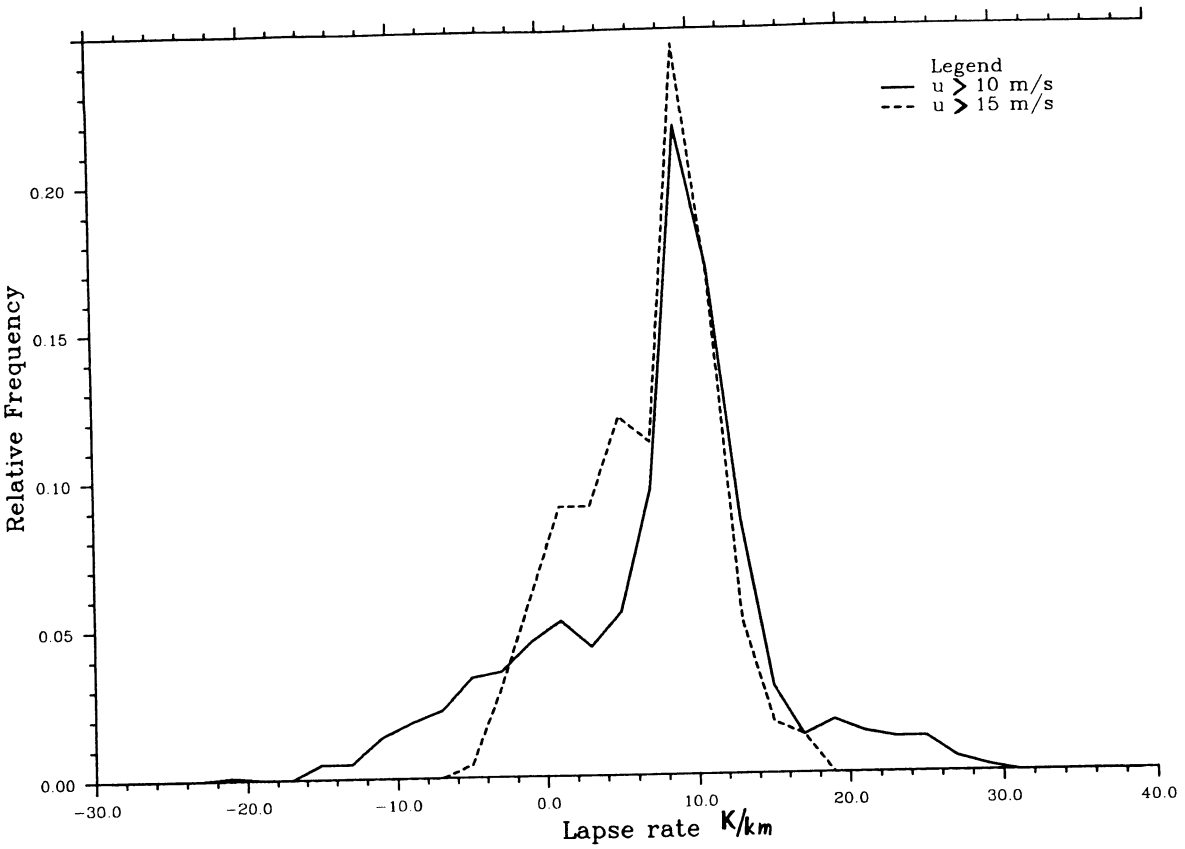

Fig. 3.2.3 The relative frequency distribution of 1 h mean lapse rate values (bin width 2 K/km). See text.

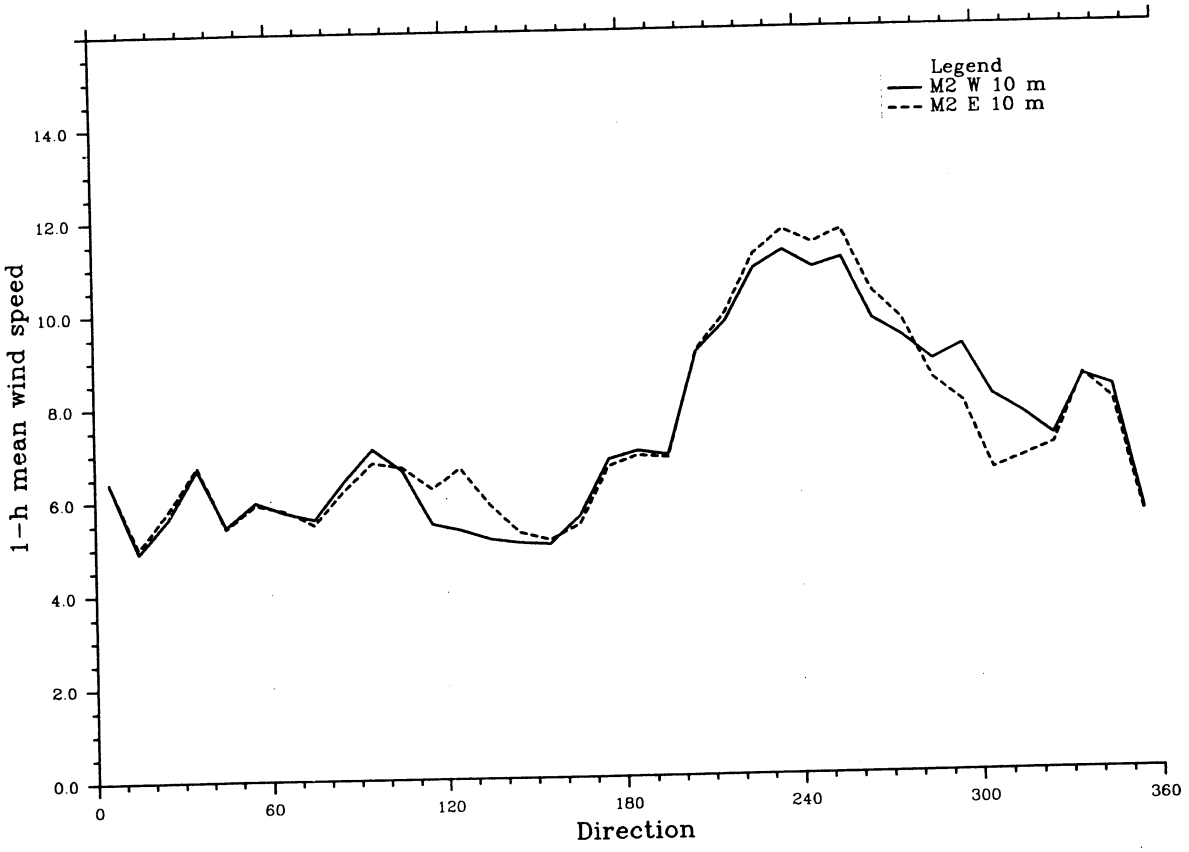

Fig. 3.2.4 The period average of the observed wind speed versus wind direction at 10 m height, Skipheia, for the west and east sensor in mast 2.

FIGURES FOR SECTION 4

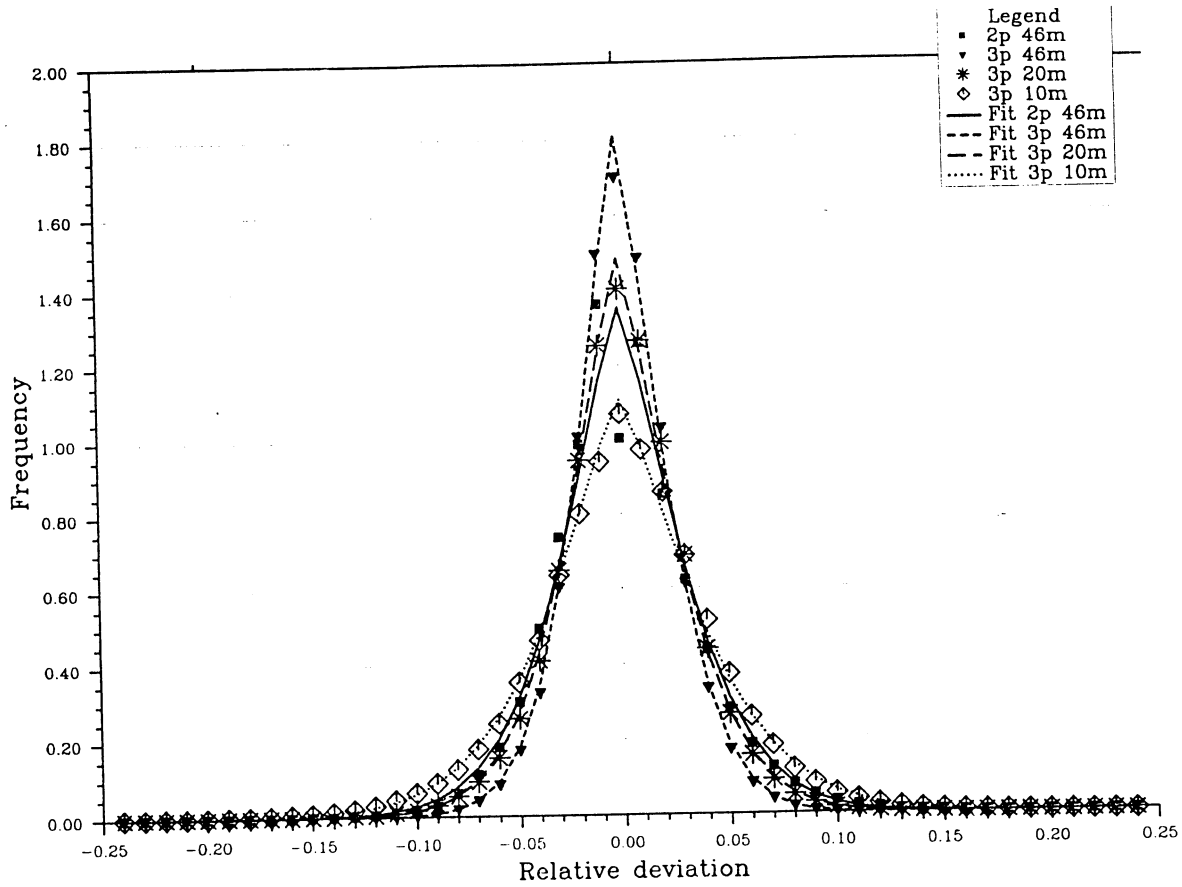

Fig. 4.1.1 Examples of distributions of the quantities g_2 and g_3 for Sletringen and fits defined by Eq. (3) and Table 4.1.1.

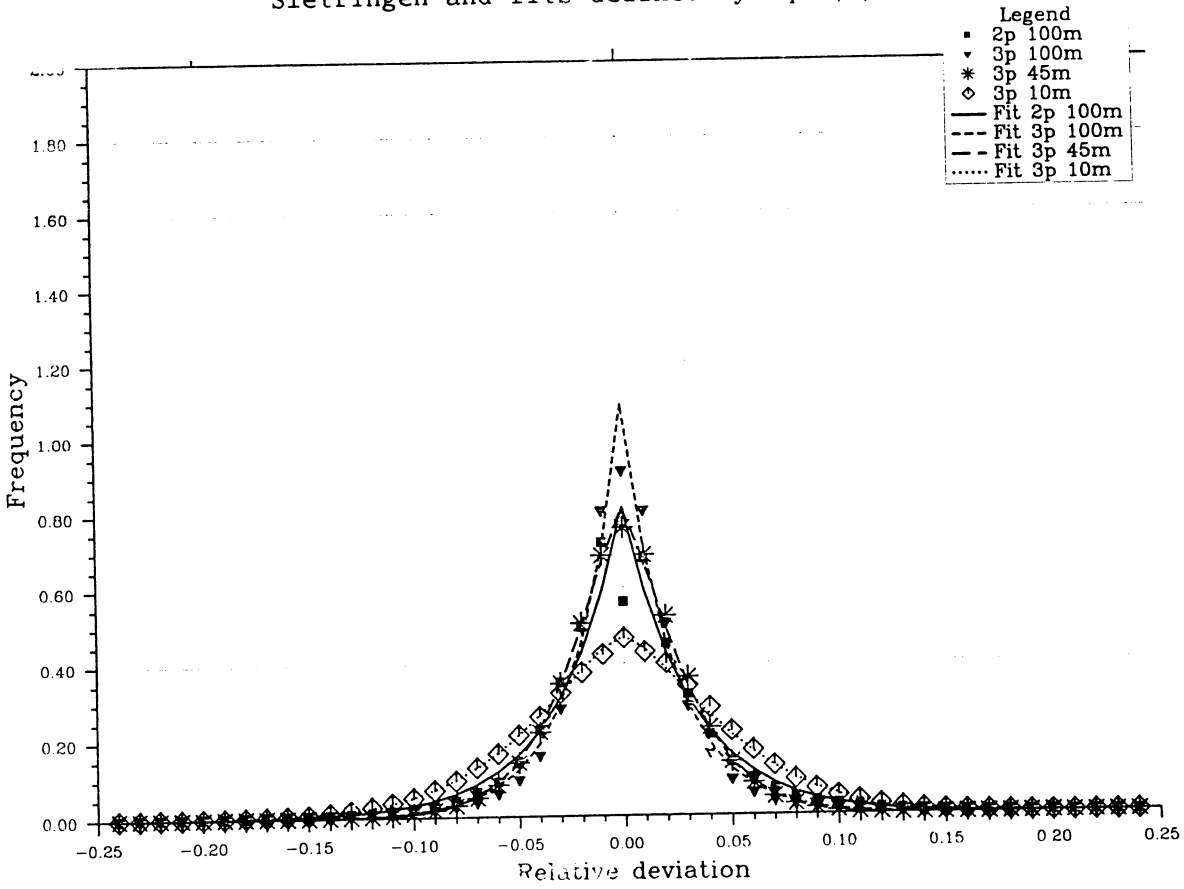

Fig. 4.1.2 Same as Fig. 4.1.1 for Skipheia.

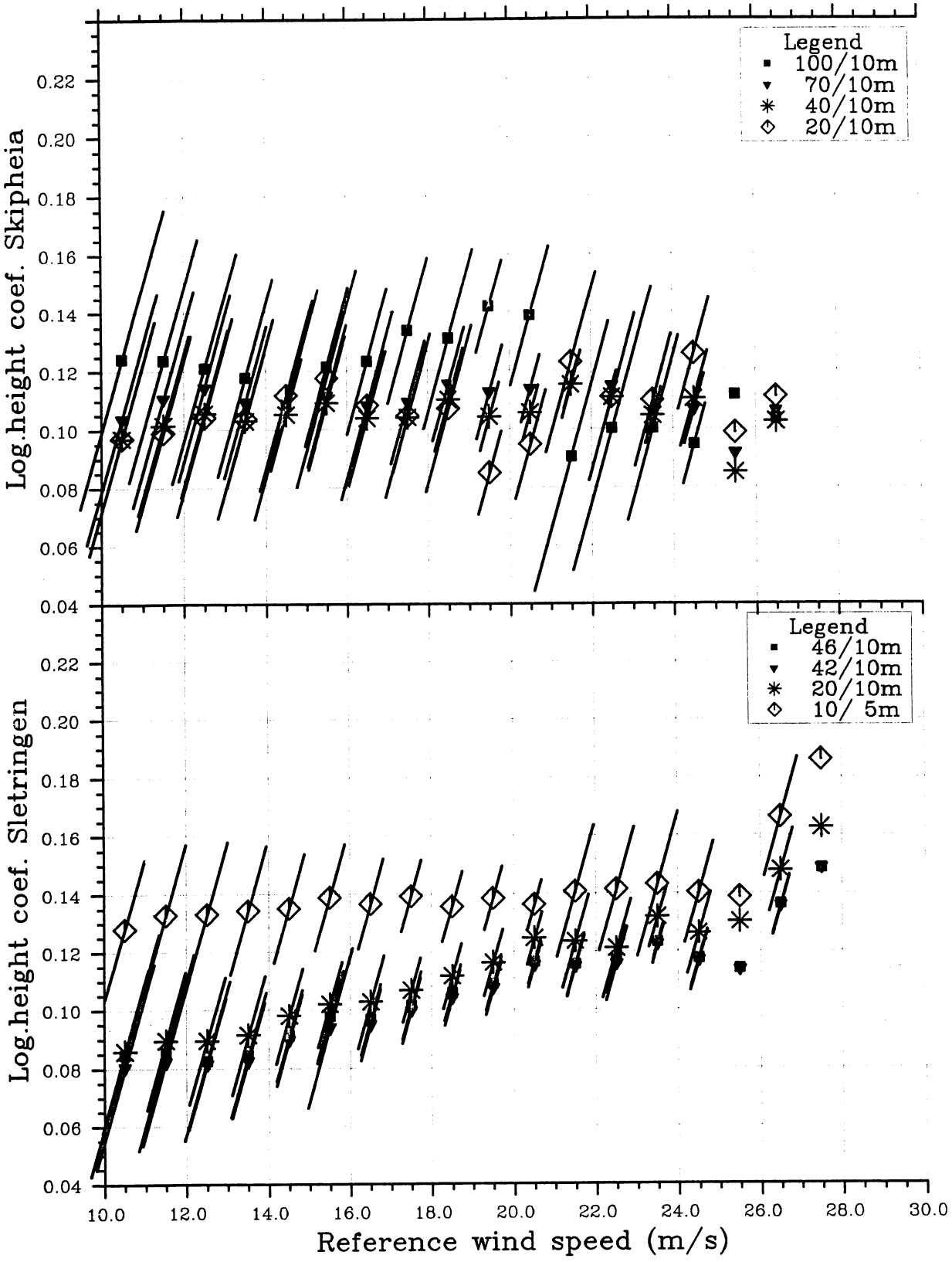

Fig. 4.2.1 Logarithmic height coefficient α versus reference wind speed. Top: Skipheia mast M2. Bottom: Sletringen. All data are included.

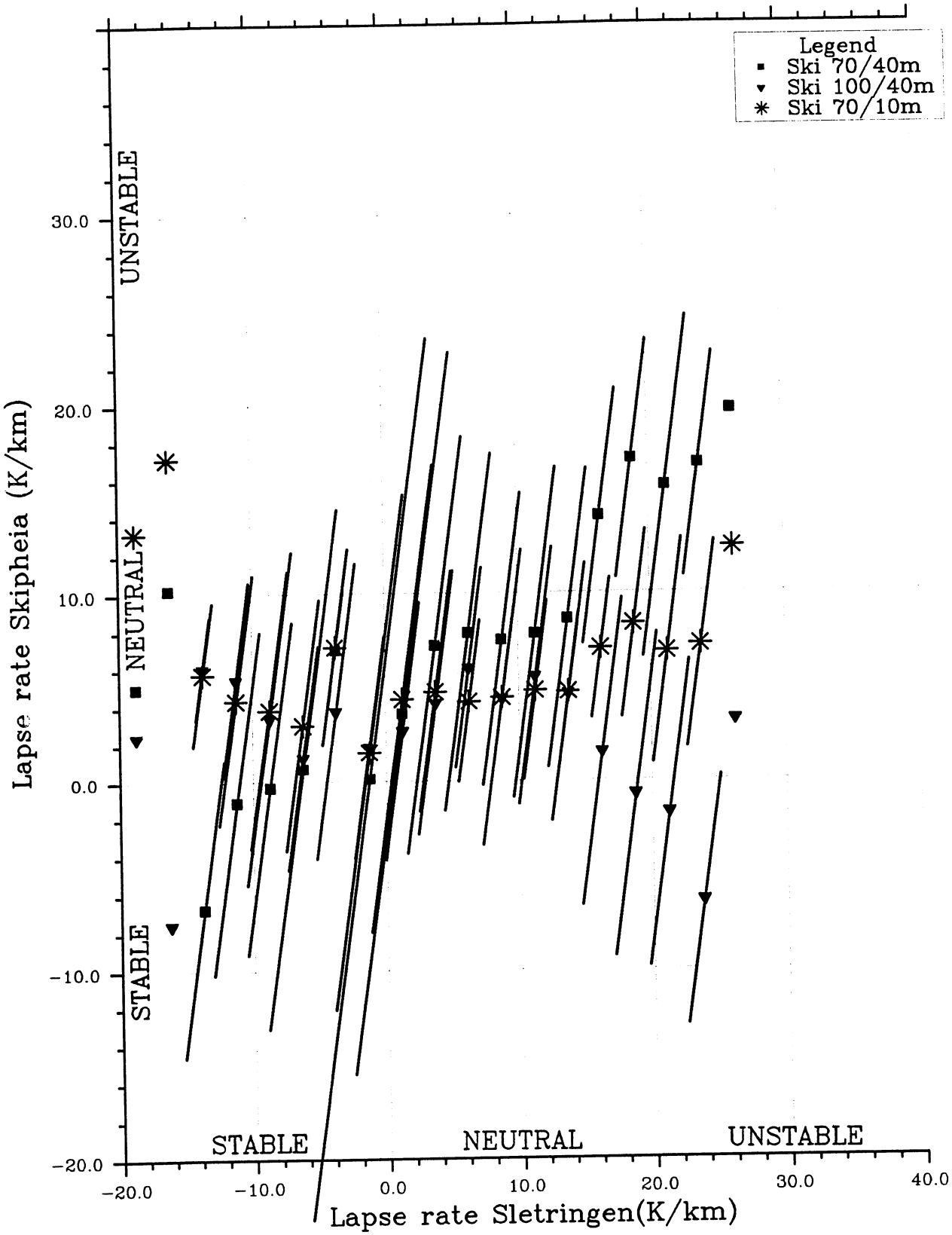

Fig. 4.2.2 Lapse rate at Skipheia versus lapse rate at Sletringen.

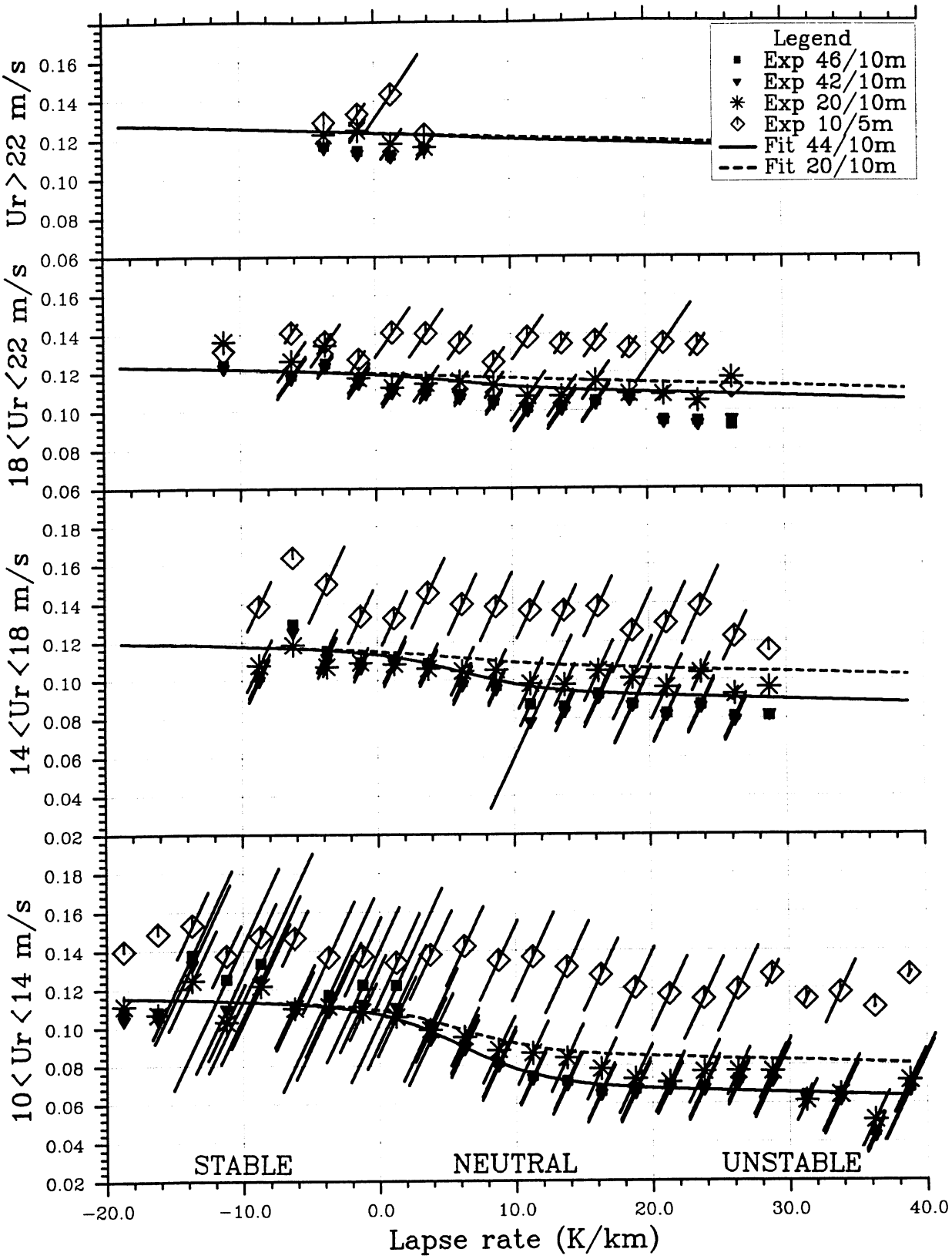

Fig. 4.2.3 Logarithmic height coefficient α versus lapse rate at Sletringen for four classes of reference wind speed. The full set of data is used. The curves represent the proposed parameterization for height ratioes 20/10 and 44/10. See Sections 4.2.2 and 4.2.3 for discussions.

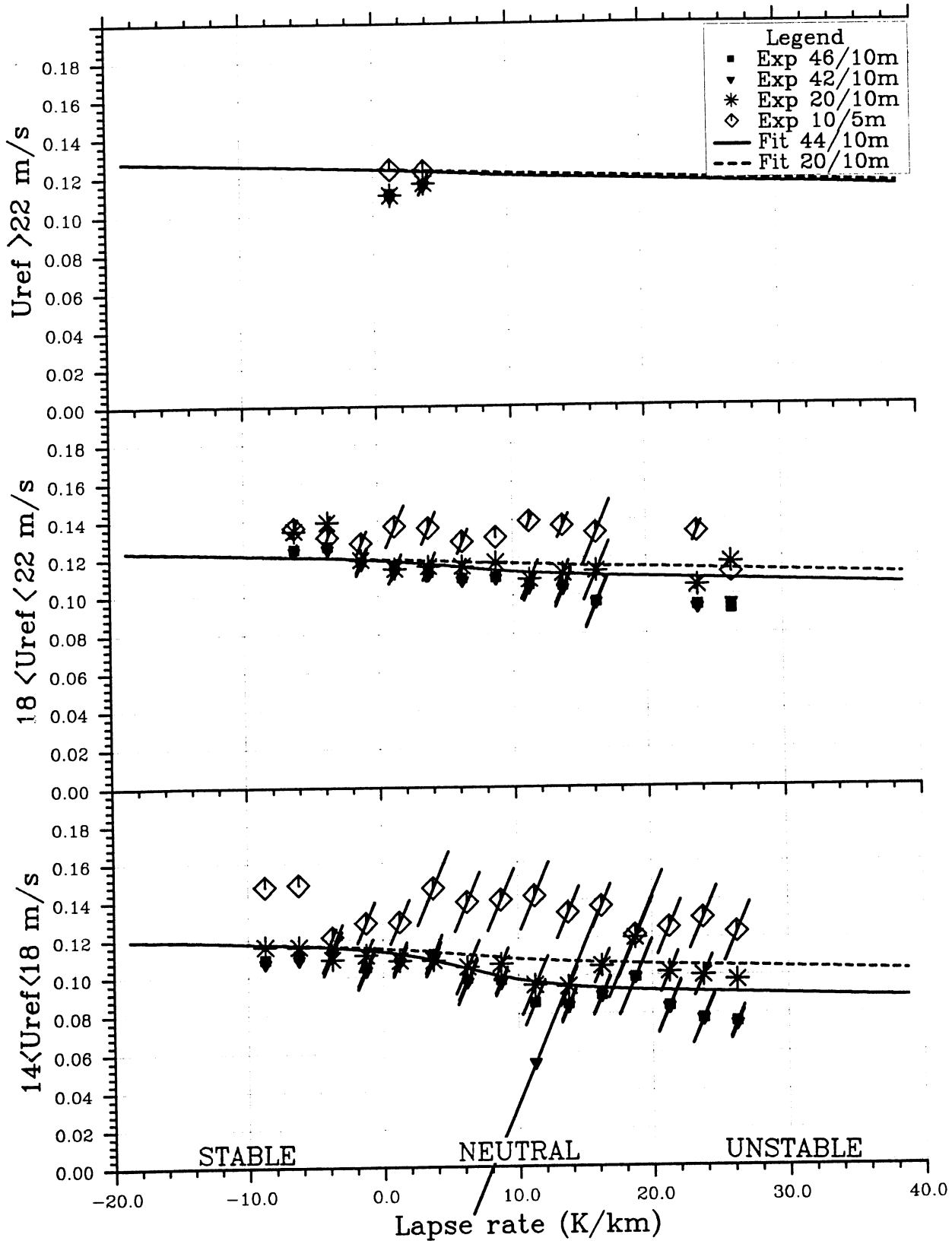

Fig. 4.2.4 As Fig. 4.2.3, but with QS-data.

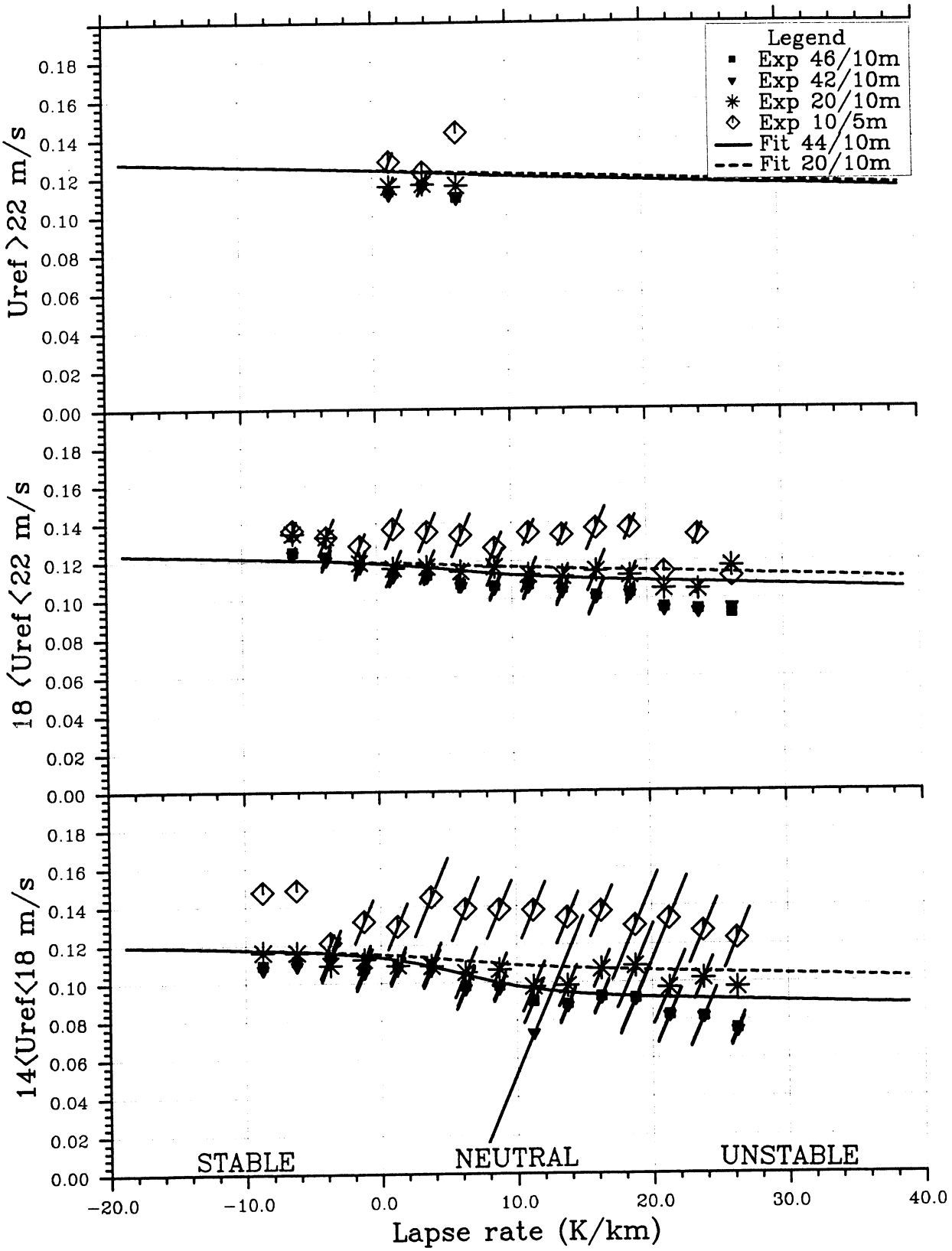

Fig. 4.2.5 As Fig. 4.2.3, but with PQS data.

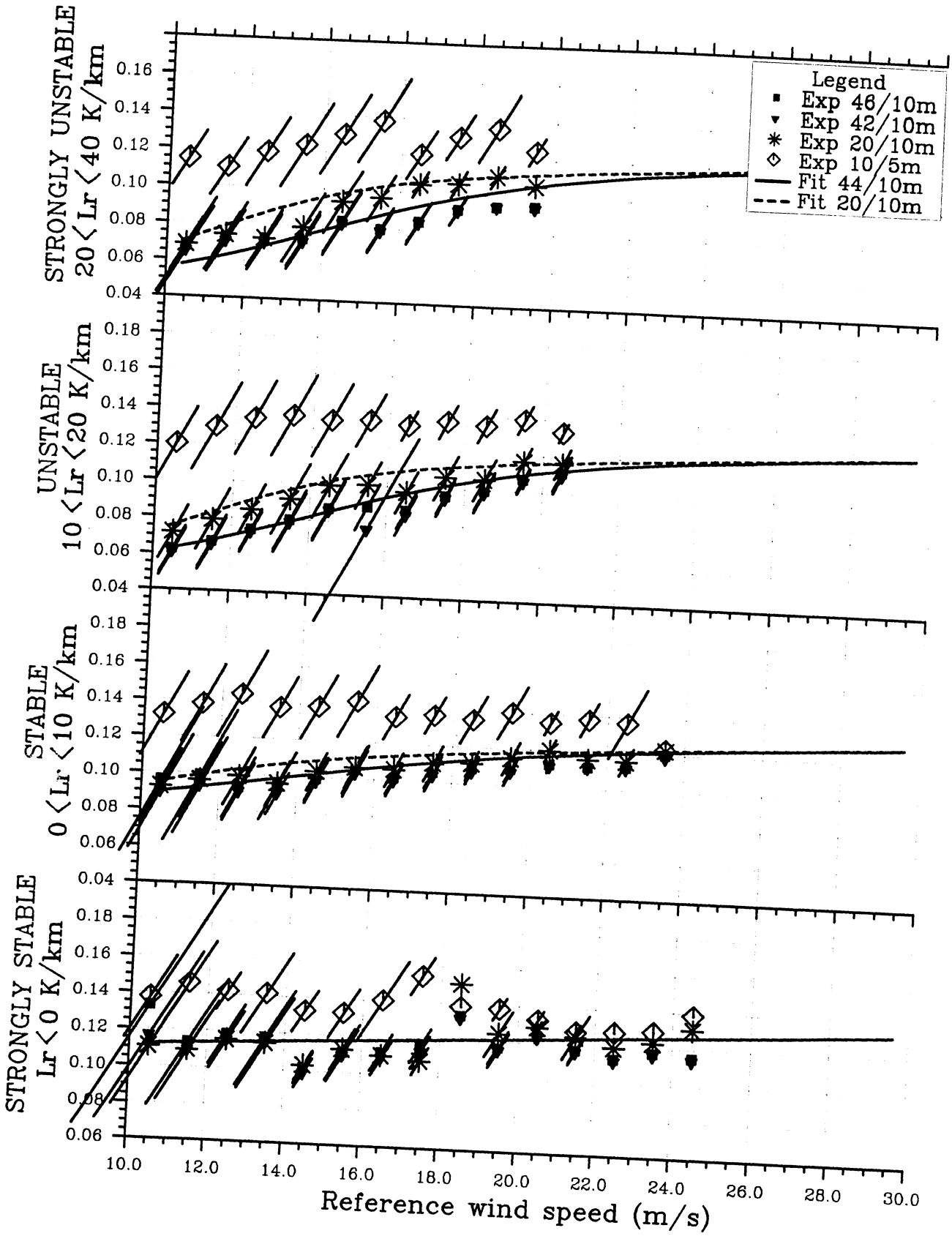

Fig. 4.2.6 Logarithmic height coefficient α versus reference wind speed at Sletringen for four classes of lapse rate. The full set of data is used. The curves represent the proposed parameterization for height ratioes 20/10 and 44/10. See Sections 4.2.2 and 4.2.3 for discussions.

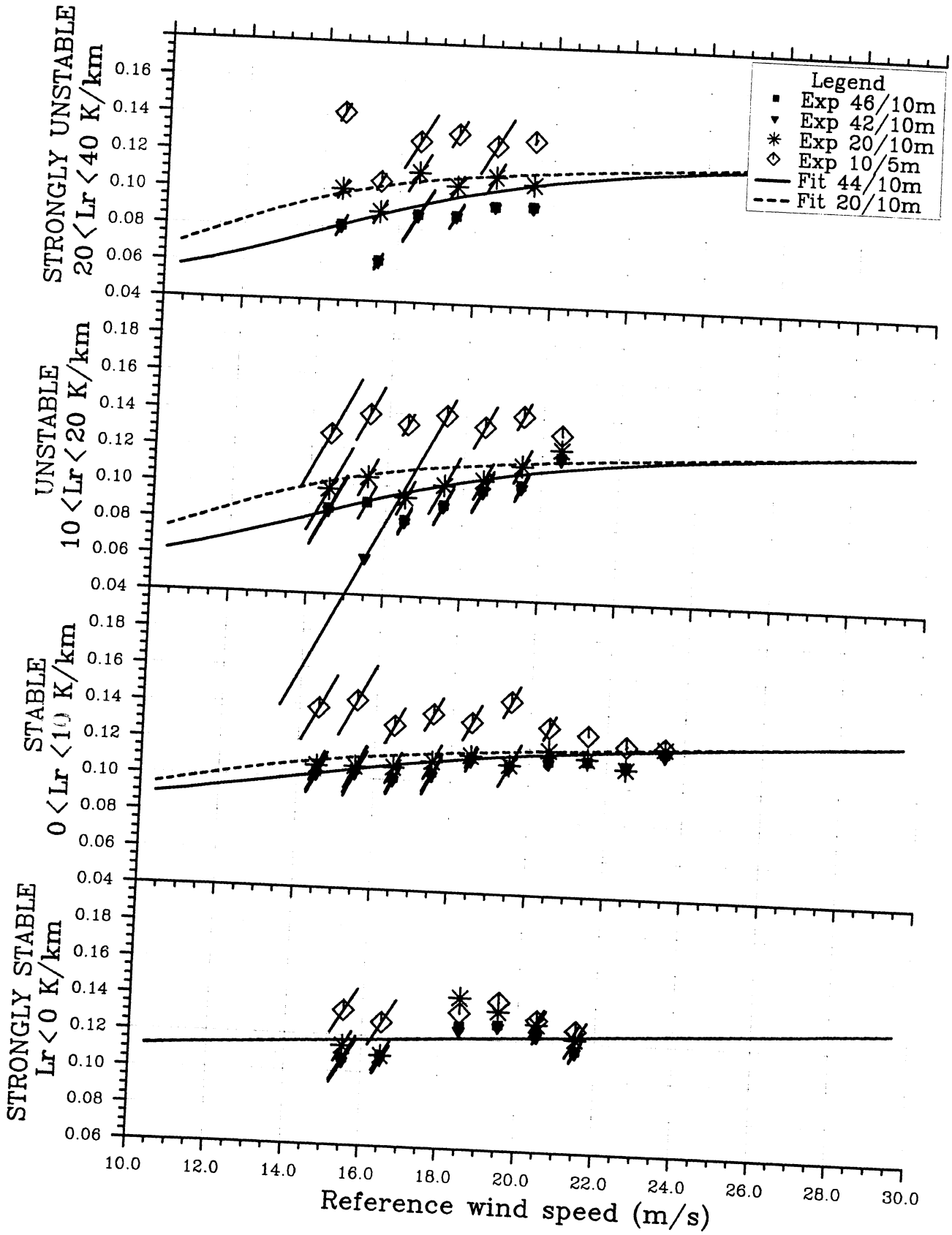

Fig. 4.2.7 As Fig. 4.2.6, but with QS-data.

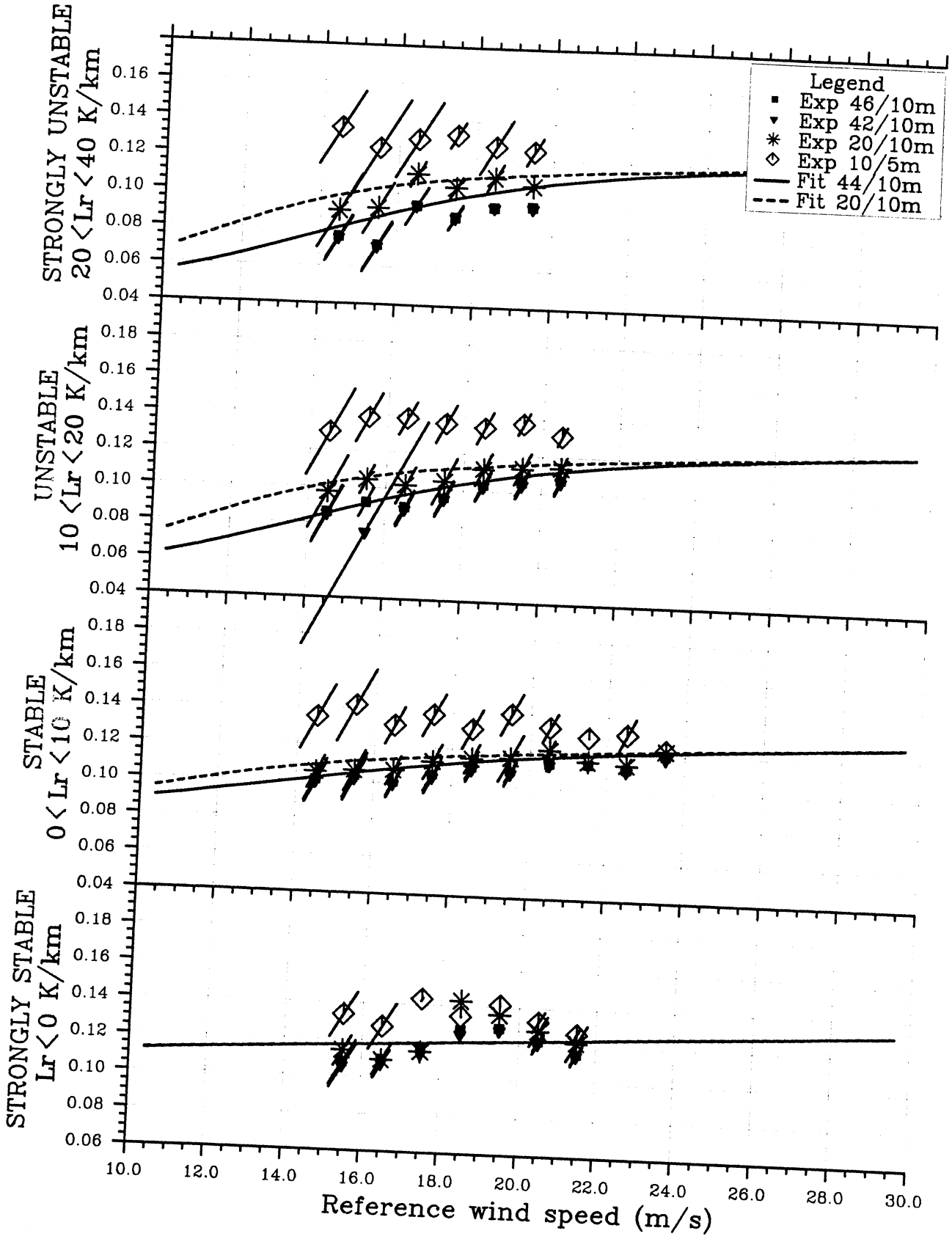

Fig. 4.2.8 As Fig. 4.2.6, but with PQS data.

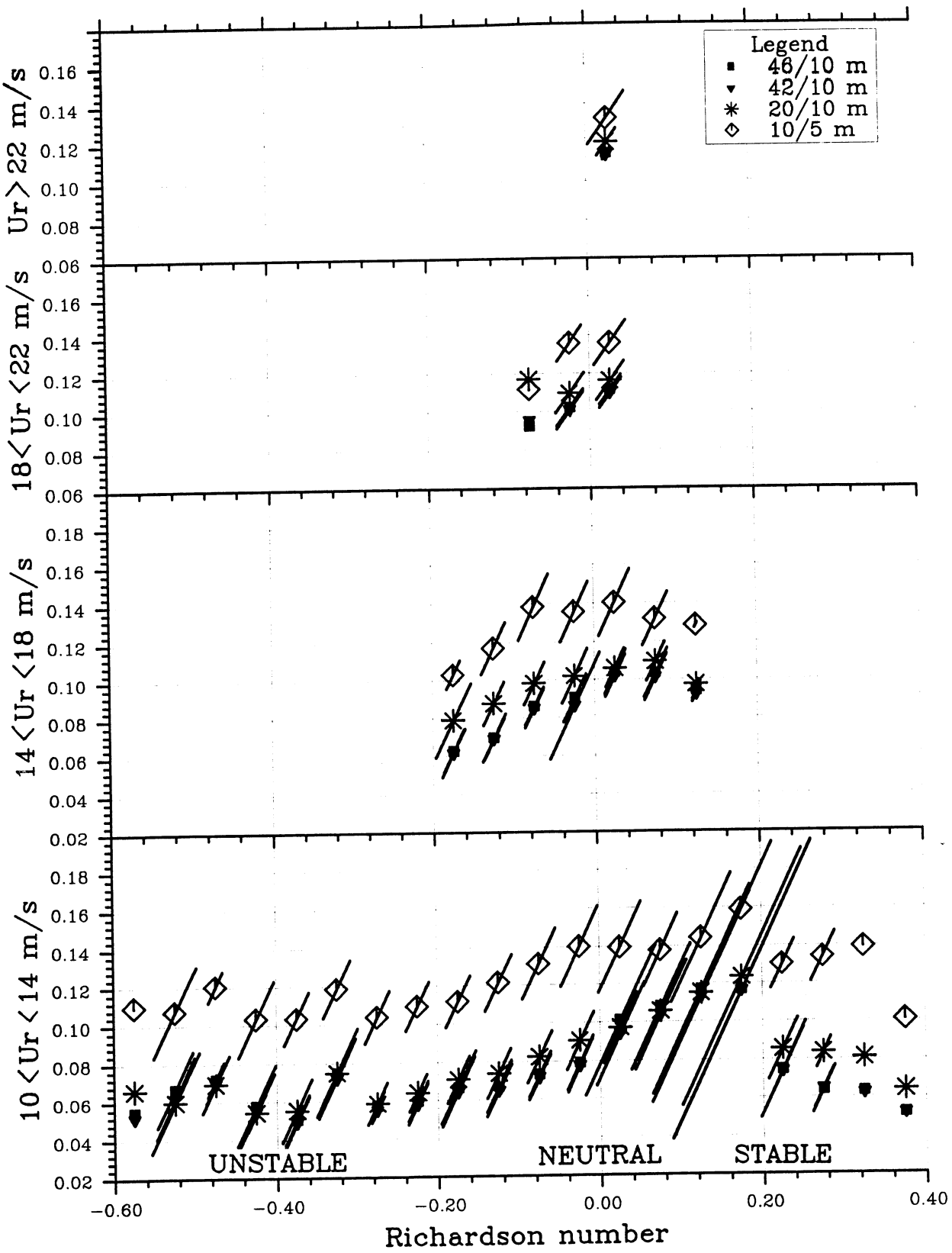

Fig. 4.2.9 Logarithmic height coefficient α at Sletringen versus bulk Richardson number Ri_b (defined by Eq. (11)) for four classes of reference wind speed. The full set of data is used. See text for discussion.

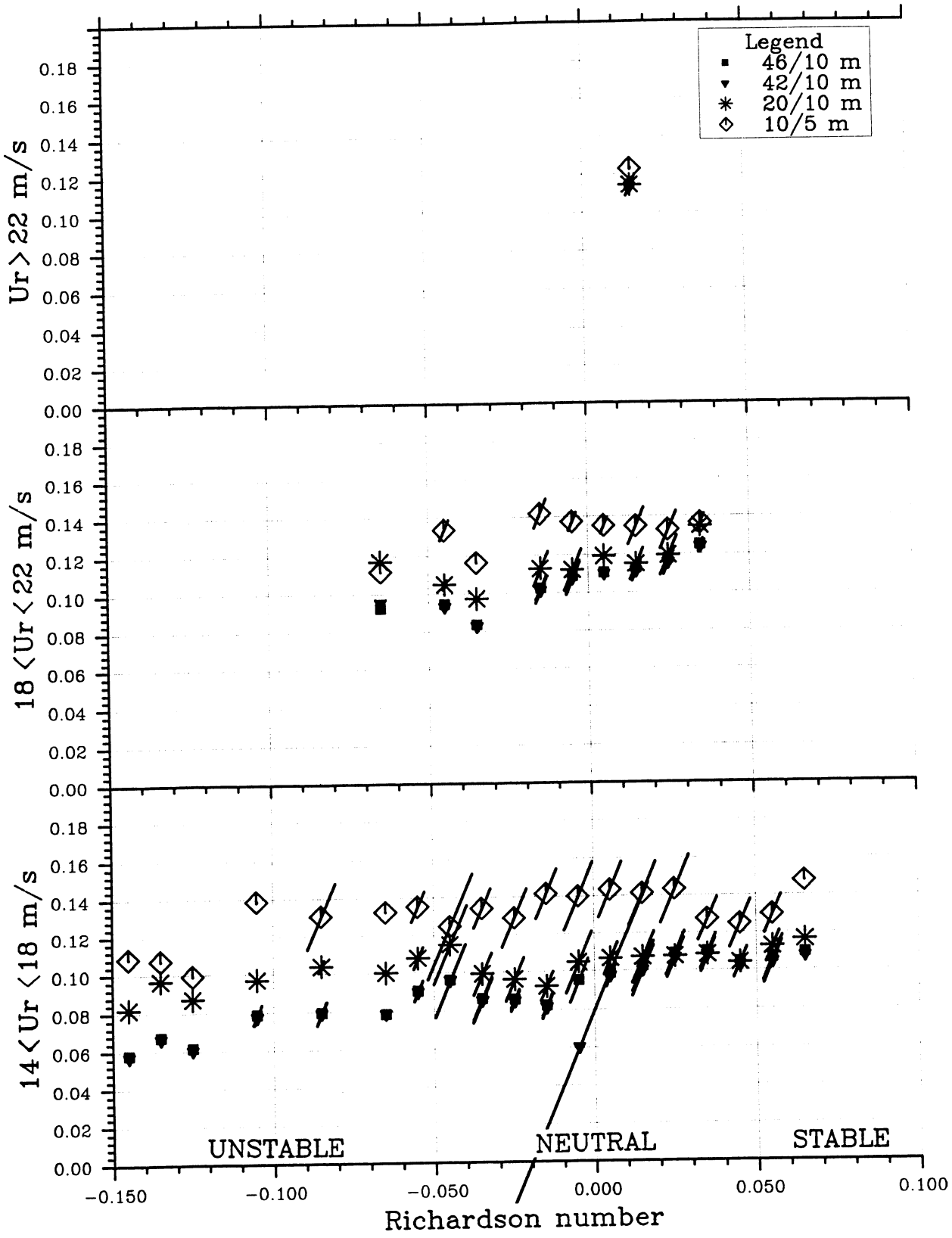

Fig. 4.2.10 As Fig. 4.2.9, but with QS-data.

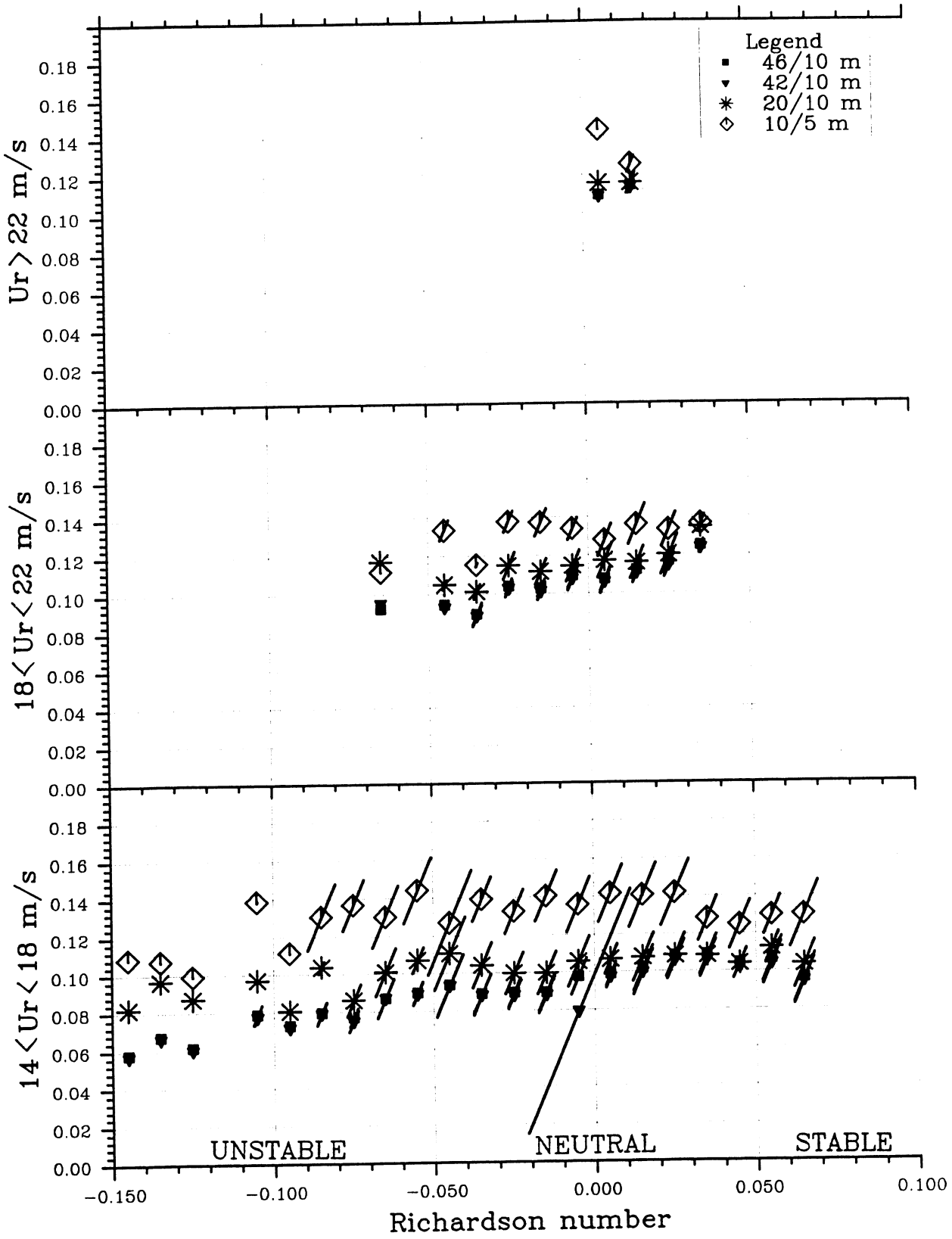

Fig. 4.2.11 As Fig. 4.2.9, but with PQS data.

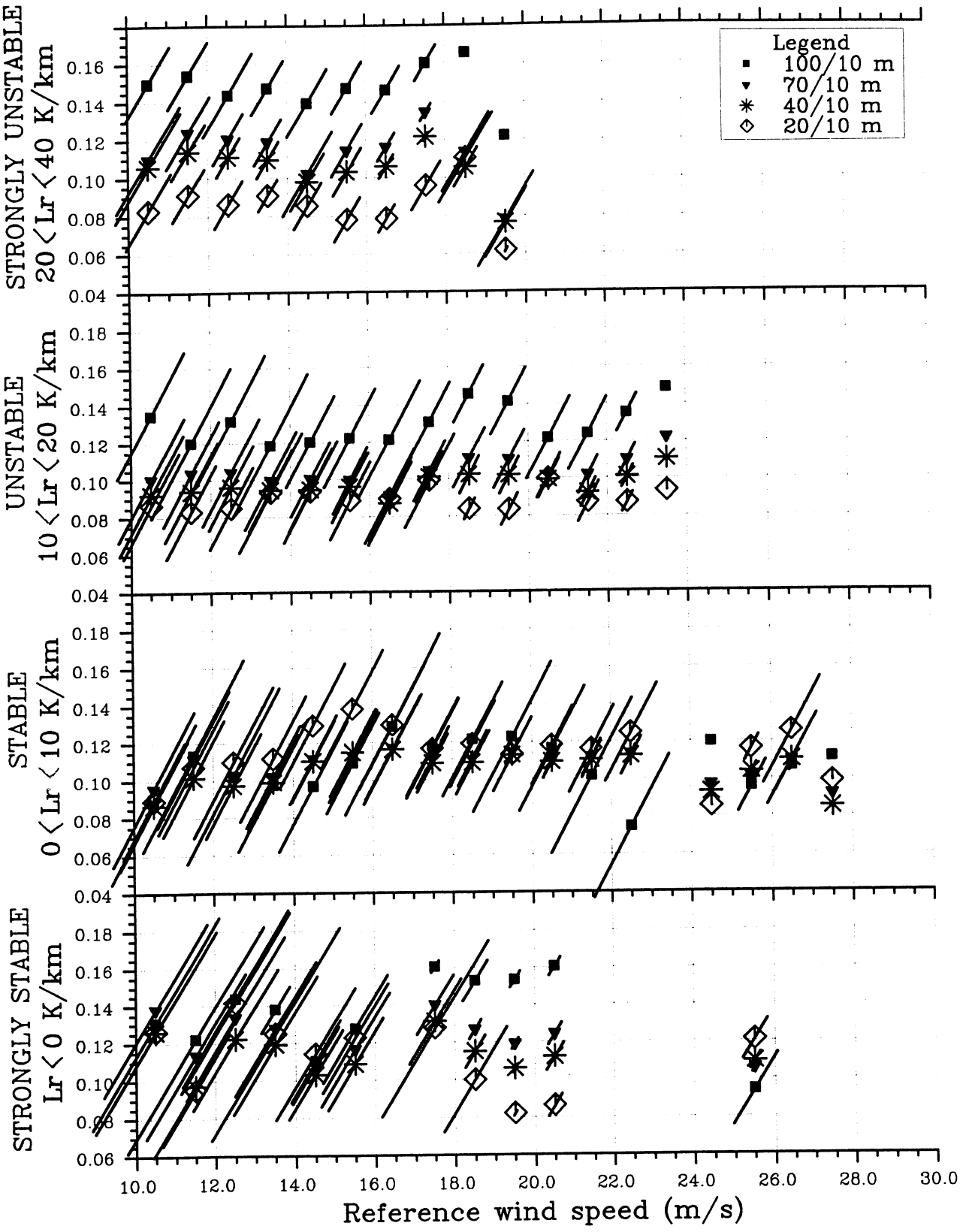

Fig. 4.2.12 Logarithmic height coefficient α versus reference wind speed at Skipheia for four classes of lapse rate. The full set of data is used. The curves represent the proposed parameterization for height ratioes 20/10 and 44/10. See Sections 4.2.2 and 4.2.3 for discussions.

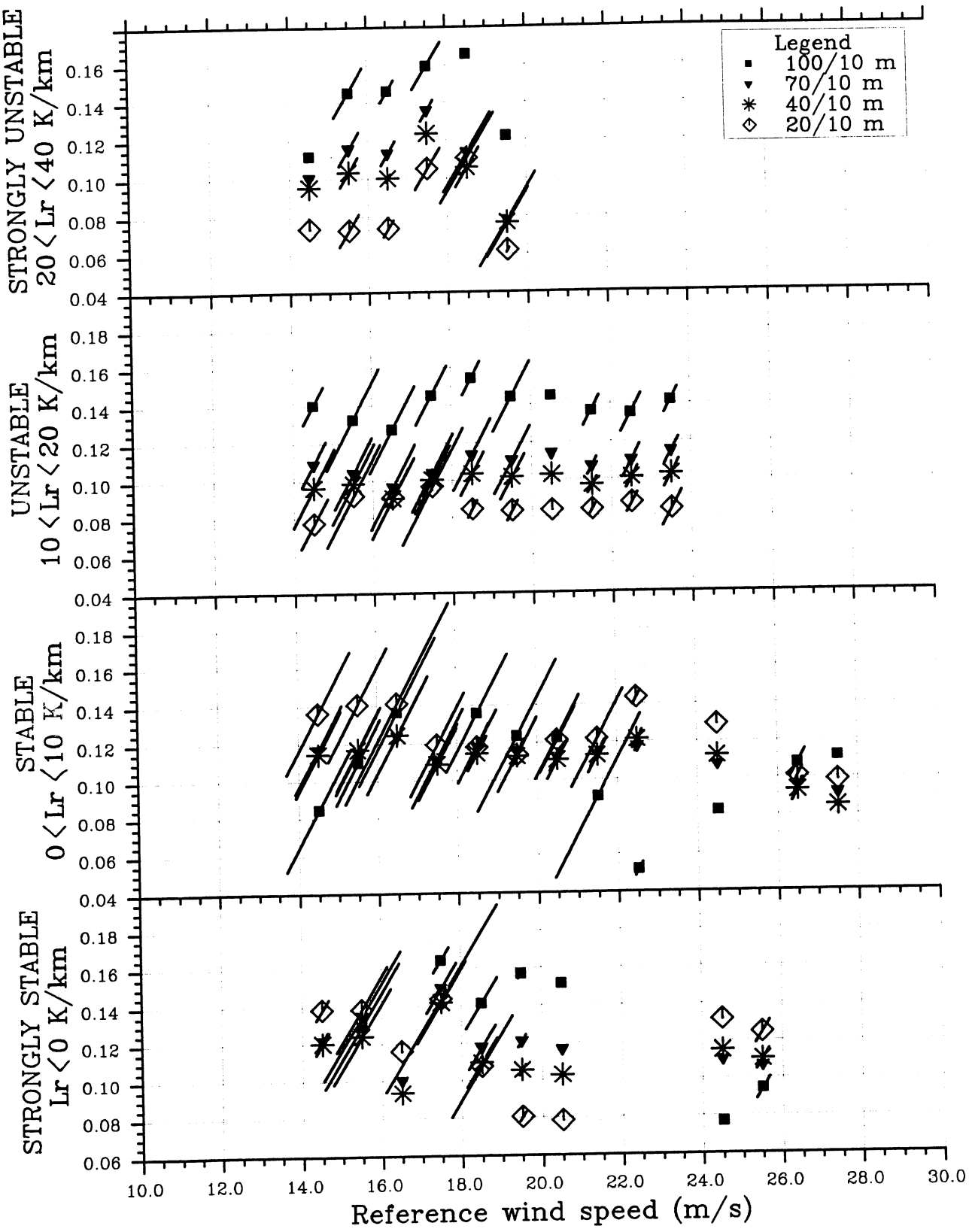

Fig. 4.2.13 As Fig. 4.2.12, but with QS-data.

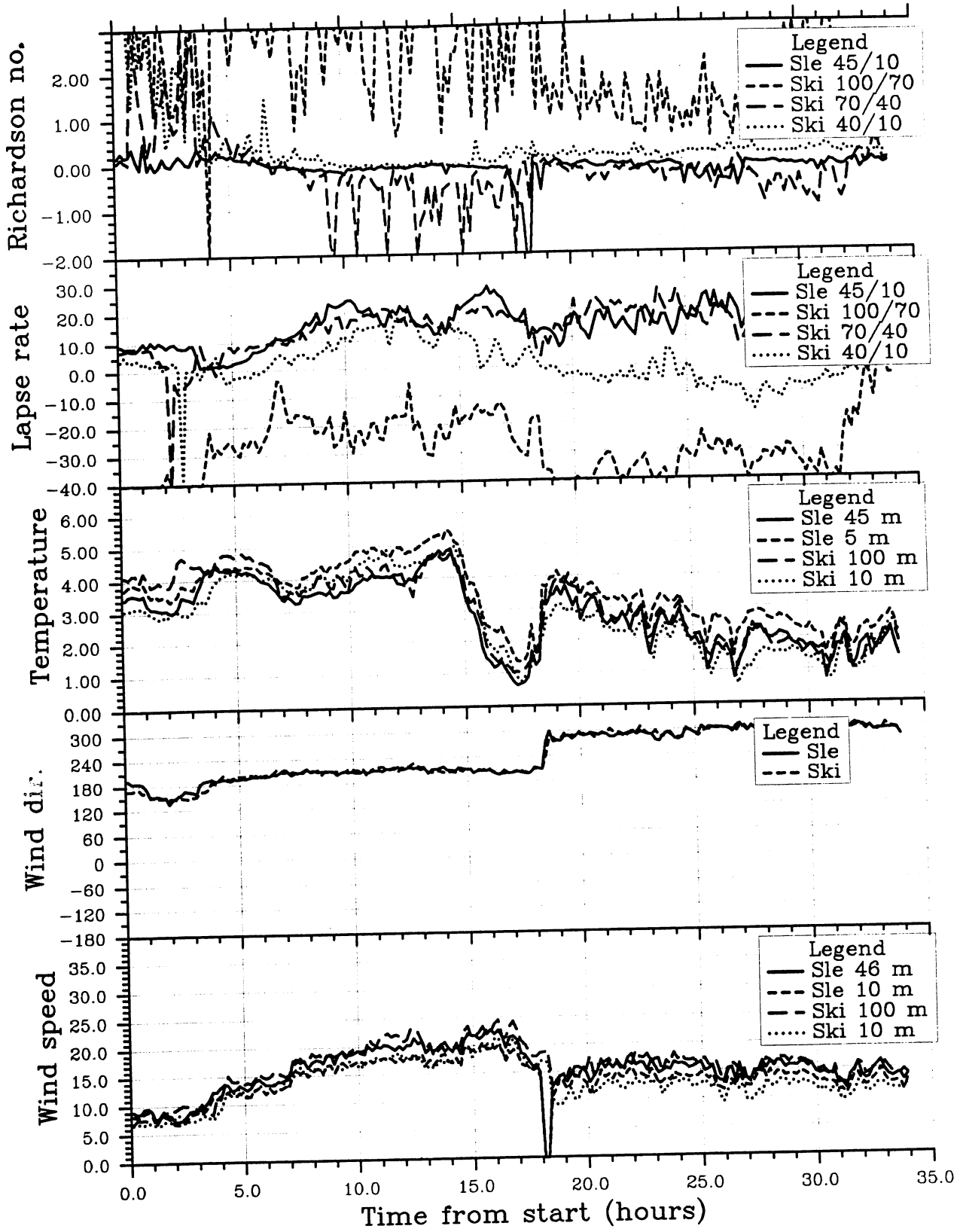

Fig. 4.2.14 Time series for Richardson number, lapse rate, air temperature, wind direction and wind speed from various heights at Sletringen and Skipheia. All quantities are based on 10 min mean values. Starting time: March-16-1989 00:00. Duration: 34 hours.

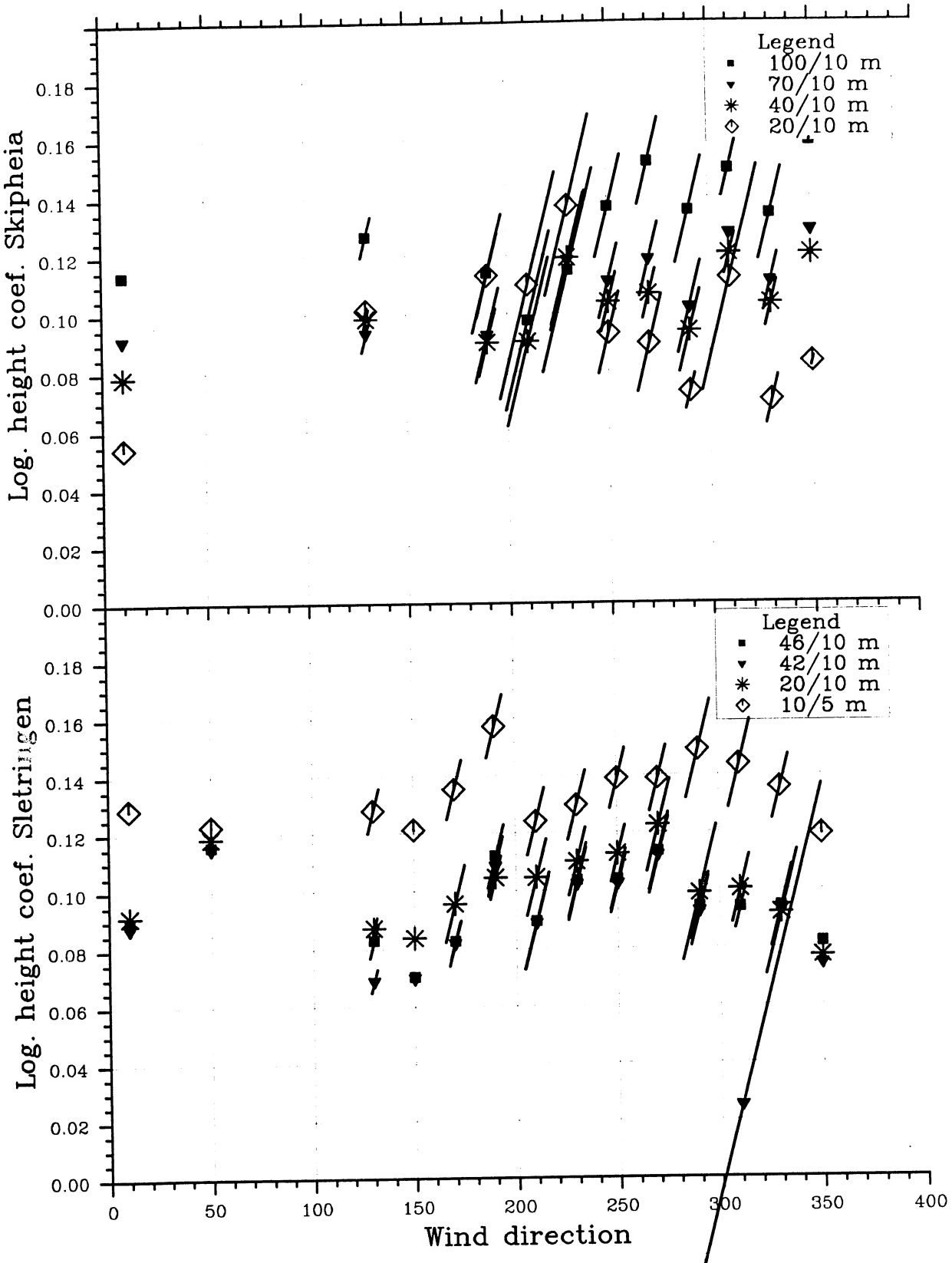

Fig. 4.2.15 Logarithmic height coefficient α versus wind direction for Skipheia (top) and Sletringen (bottom). Reference wind speed u_r > 15 m/s.

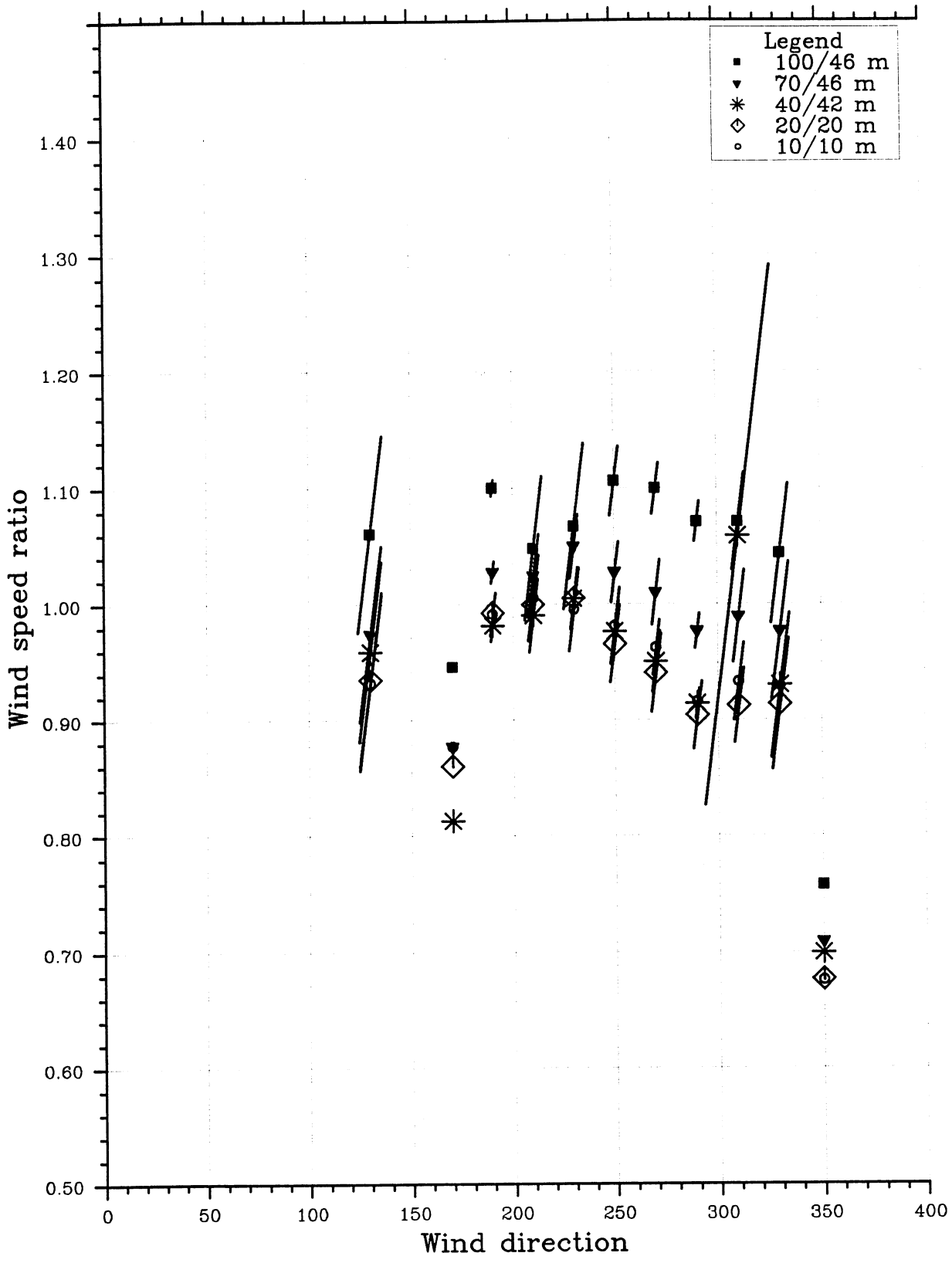

Fig. 4.2.16 Ratio of wind speed at Skipheia to wind speed at Sletringen for selected sensors versus wind direction. Reference wind speed u_r > 15 m/s.

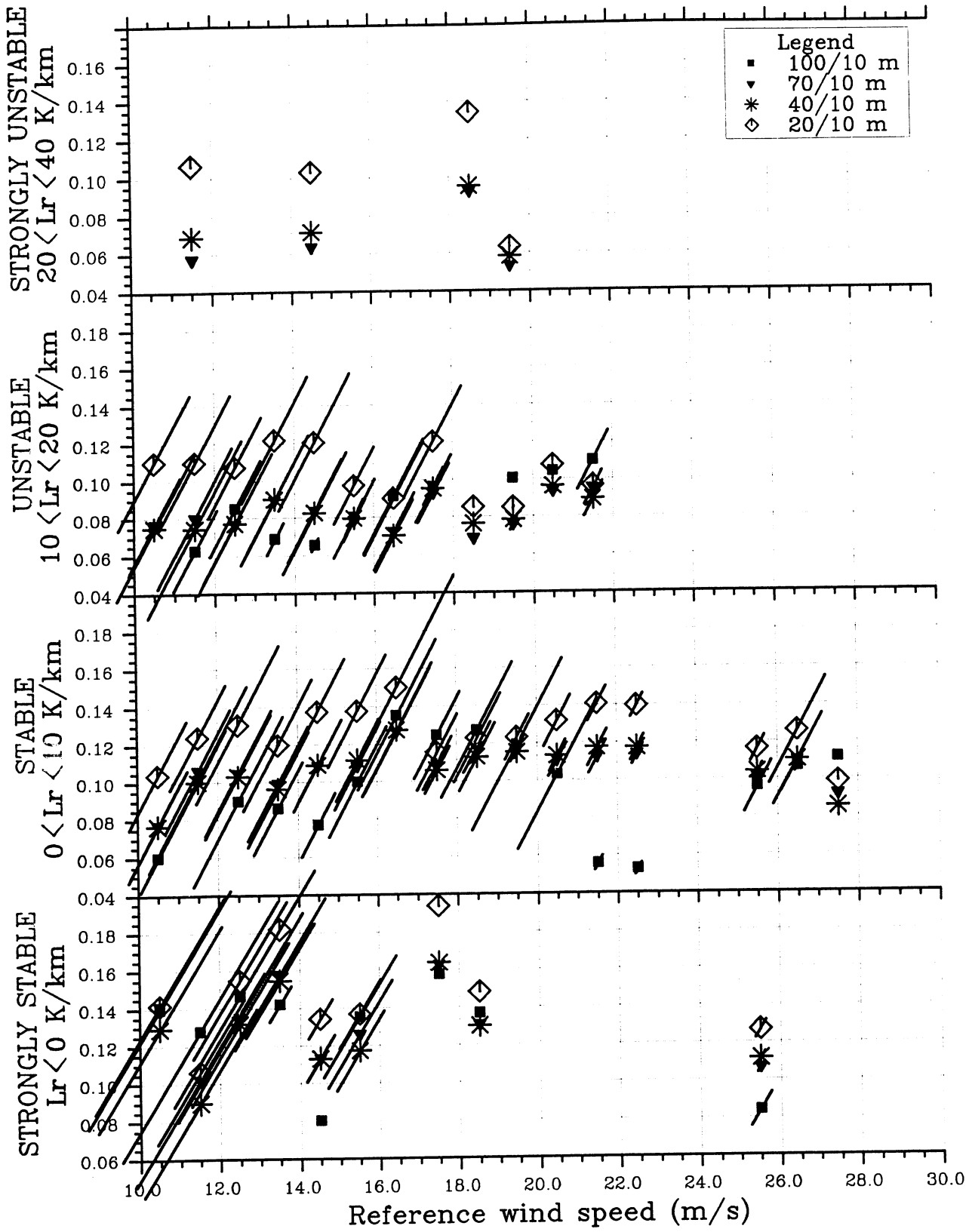

Fig. 4.2.17 Logarithmic height coefficient α versus reference wind speed at Skipheia for four classes of lapse rate in the direction sector 180-240°. Missing lapse rate data at Skipheia are replaced by lapse rate data from Sletringen.

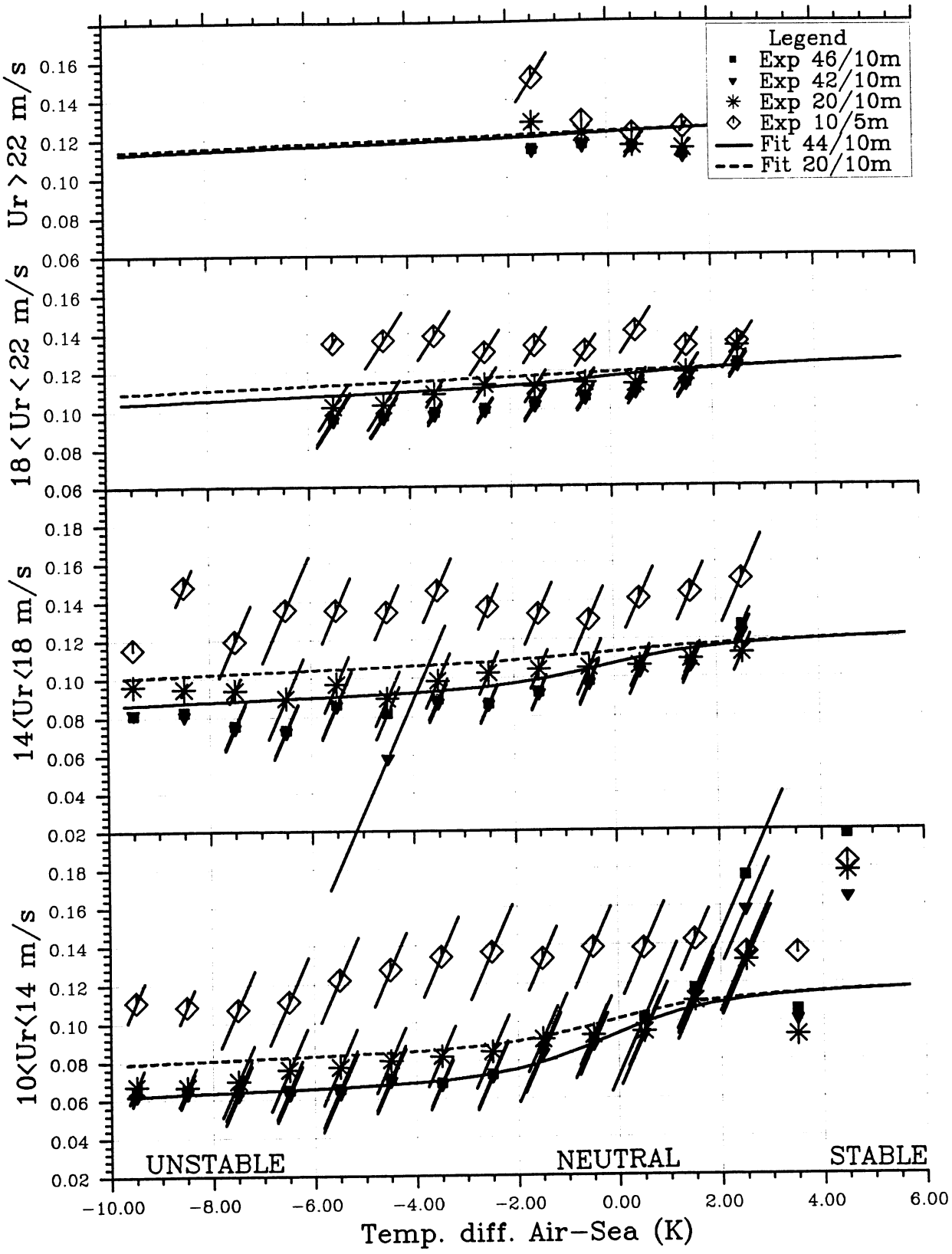

Fig. 4.2.18 Logarithmic height coefficient α versus temperature difference air (45 m) - sea at Sletringen for four classes of reference wind speed. The full set of data is used. The curves represent the proposed parameterization for height ratioes 20/10 and 44/10. See Sections 4.2.2 and 4.2.3 for discussions.

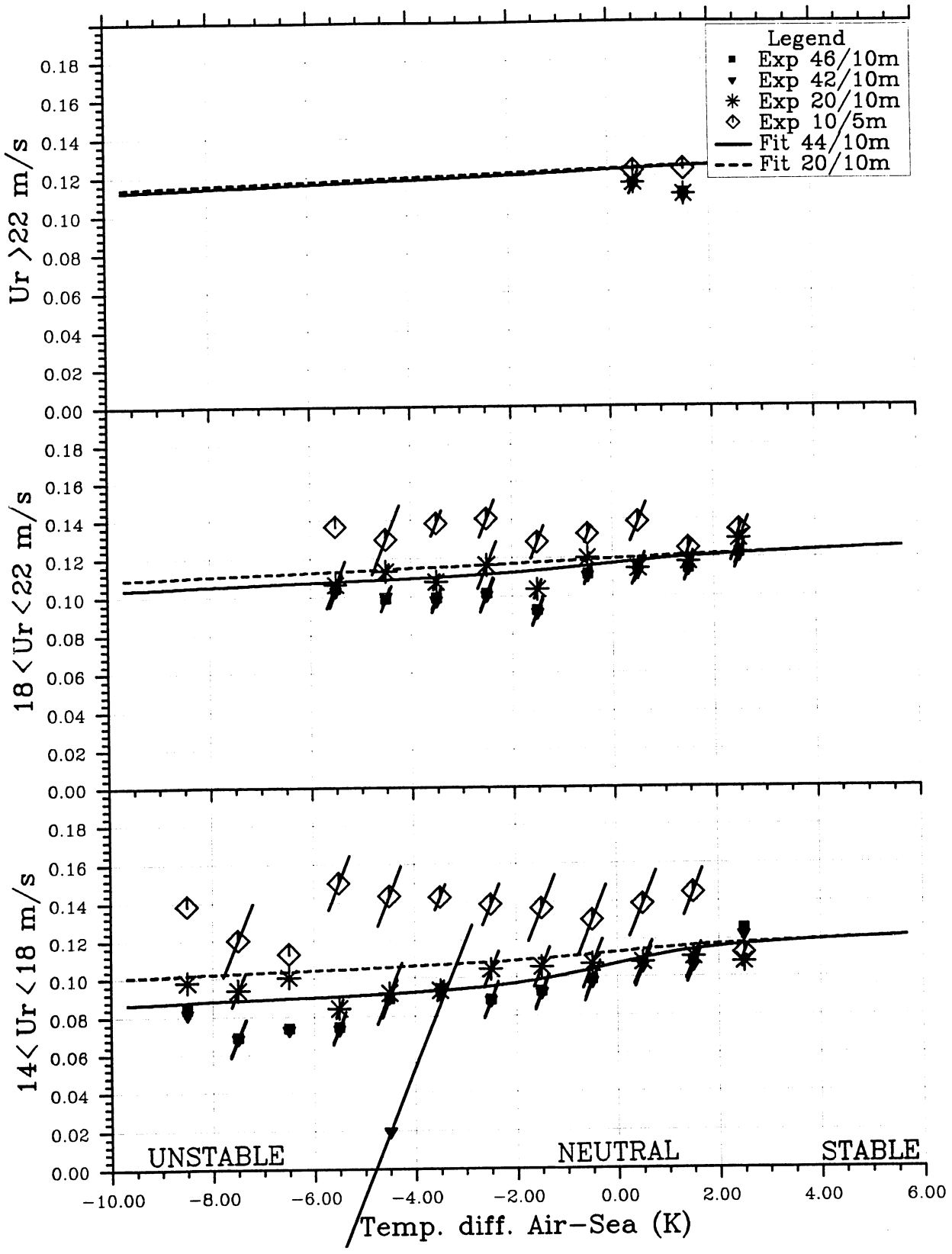

Fig. 4.2.19 As Fig. 4.2.18, but with QS-data.

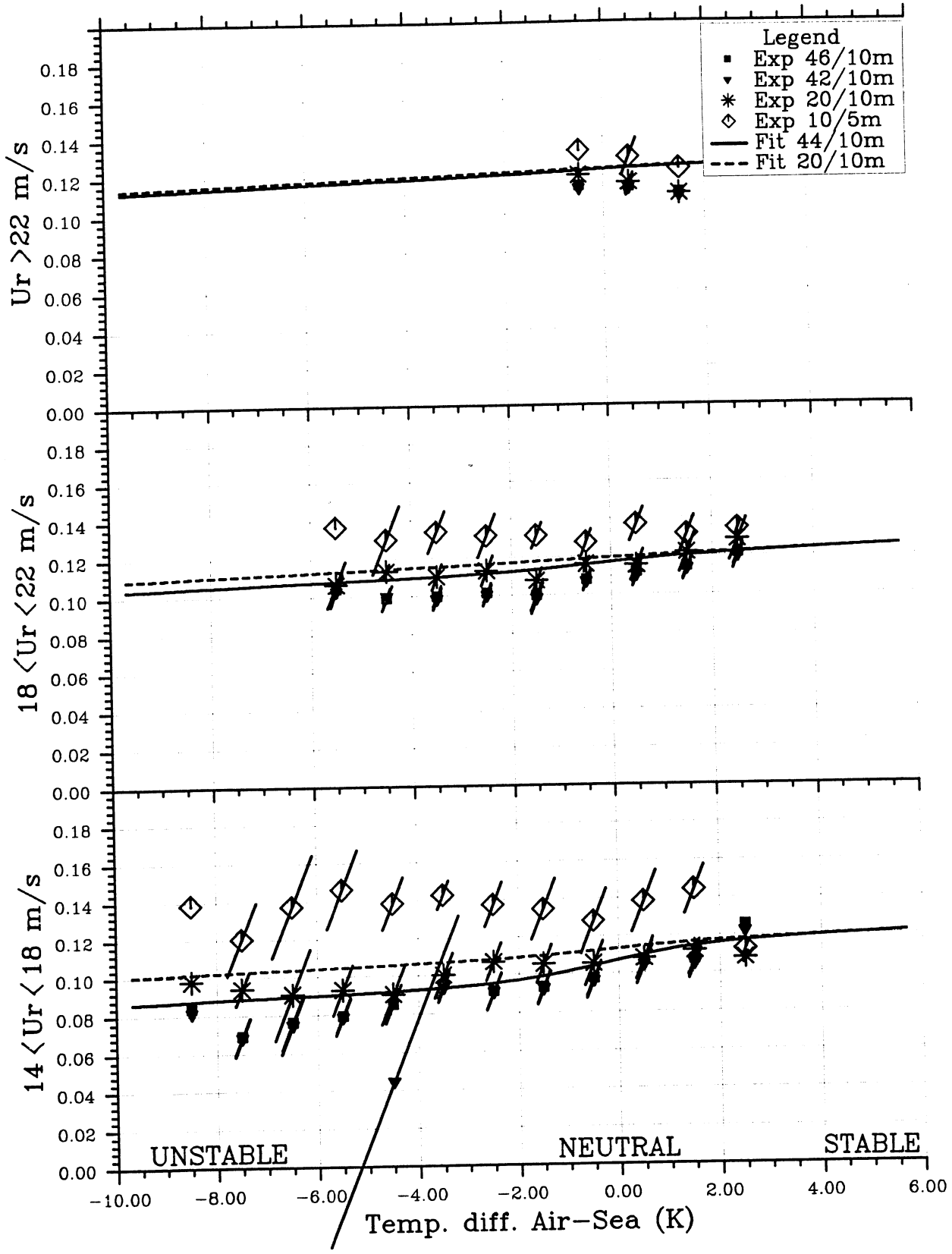

Fig. 4.2.20 As Fig. 4.2.18, but with PQS-data.

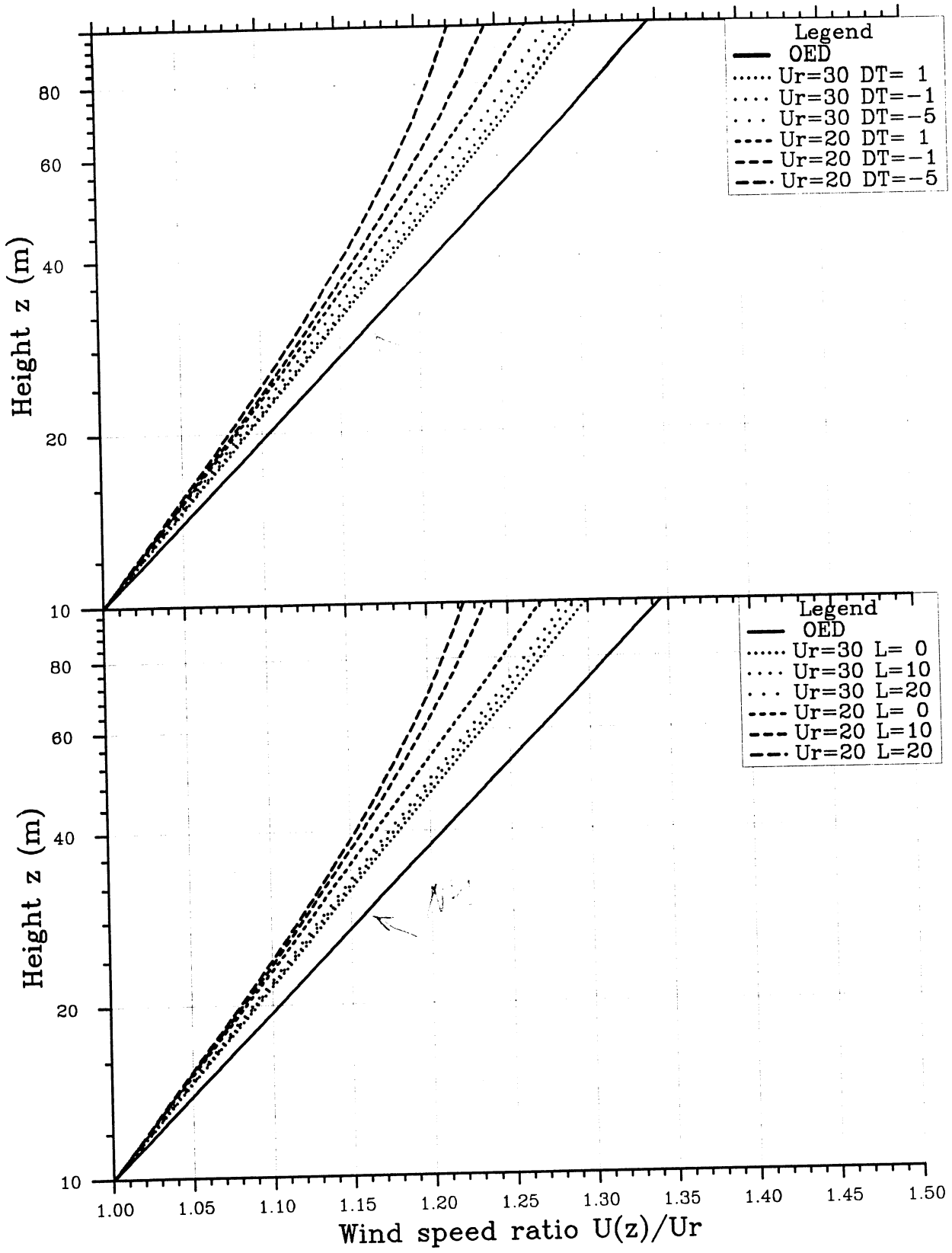

Fig. 4.2.21 Ratio of 1h mean wind speed at height z to the reference wind speed u_r. Top: Curves for temp. diff. air-sea of 1, -1 and -5 K for u_r = 20 m/s (dotted lines) and u_r = 30 m/s (dashed lines). Full line corresponds to α = 0.15. Bottom: Curves for 3 values of lapse rate - 0, 10 and 20 K/km - for u_r = 20 m/s (dotted lines) and u_r = 30 m/s (dashed lines).

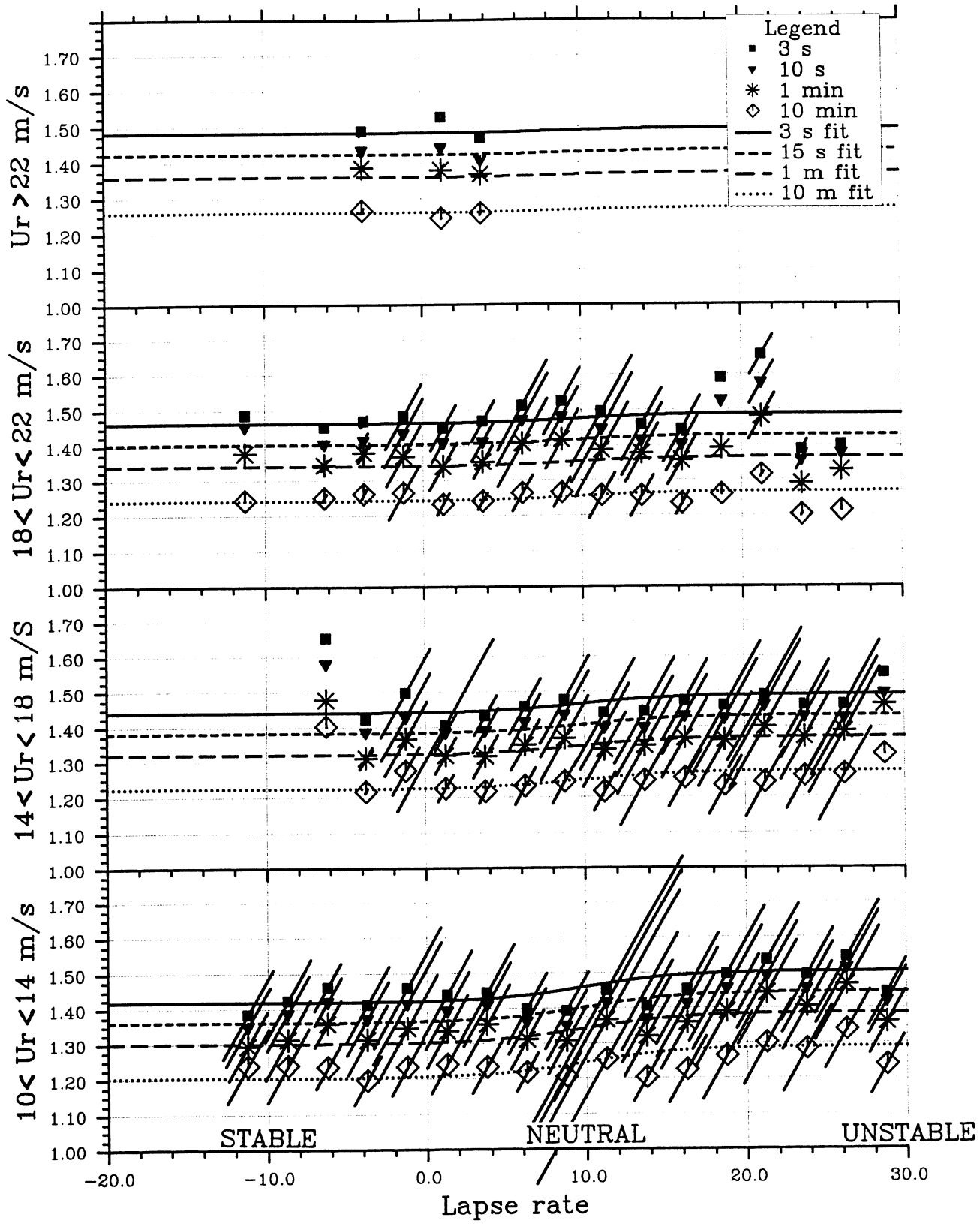

Fig. 4.4.1 Mean value and standard deviation of the the reference gust factor at 46 m height at Sletringen versus lapse rate for 4 classes of reference wind speed u_r. See text for discussion.

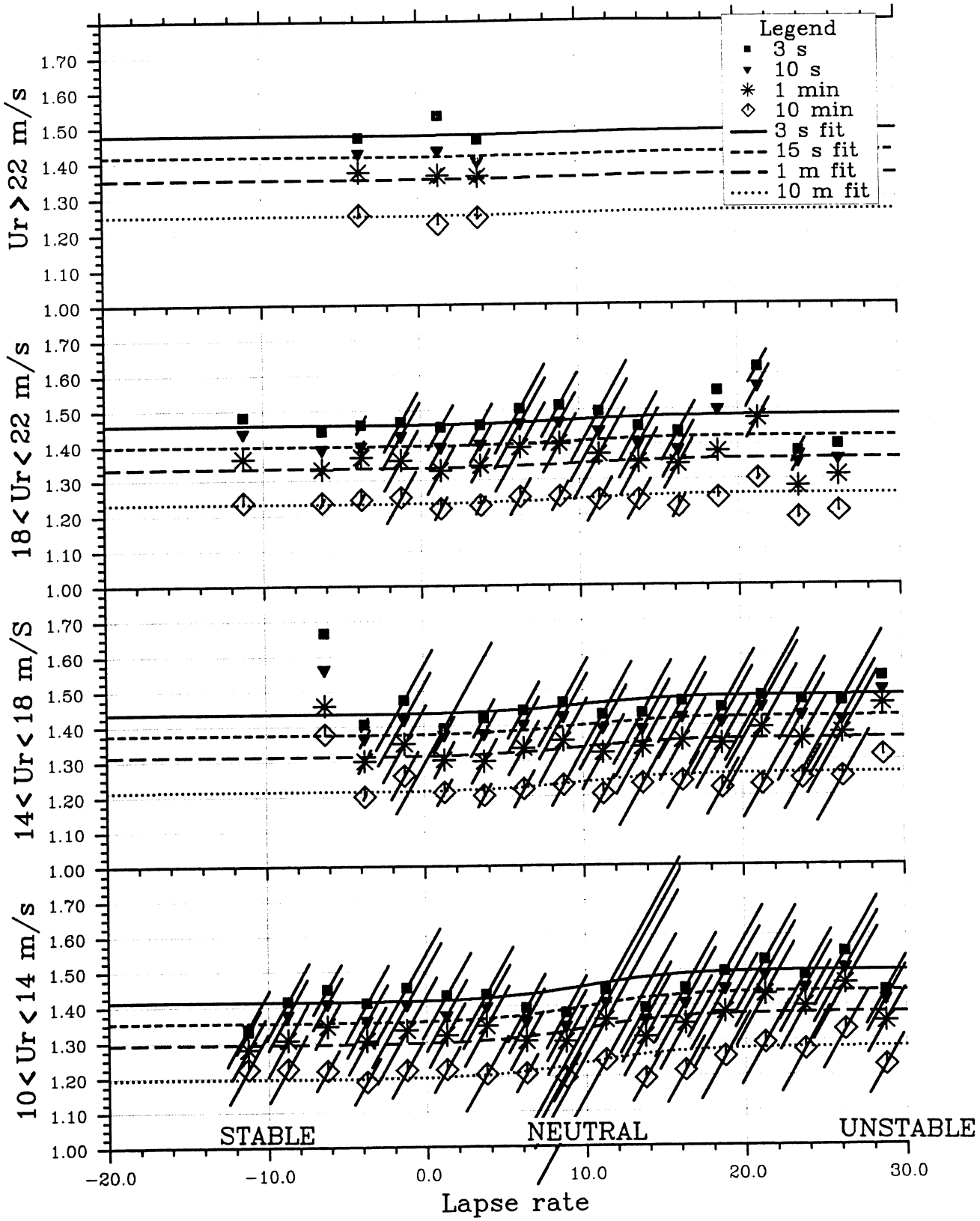

Fig. 4.4.2 As Fig. 4.4.1, but for 42 m height at Sletringen.

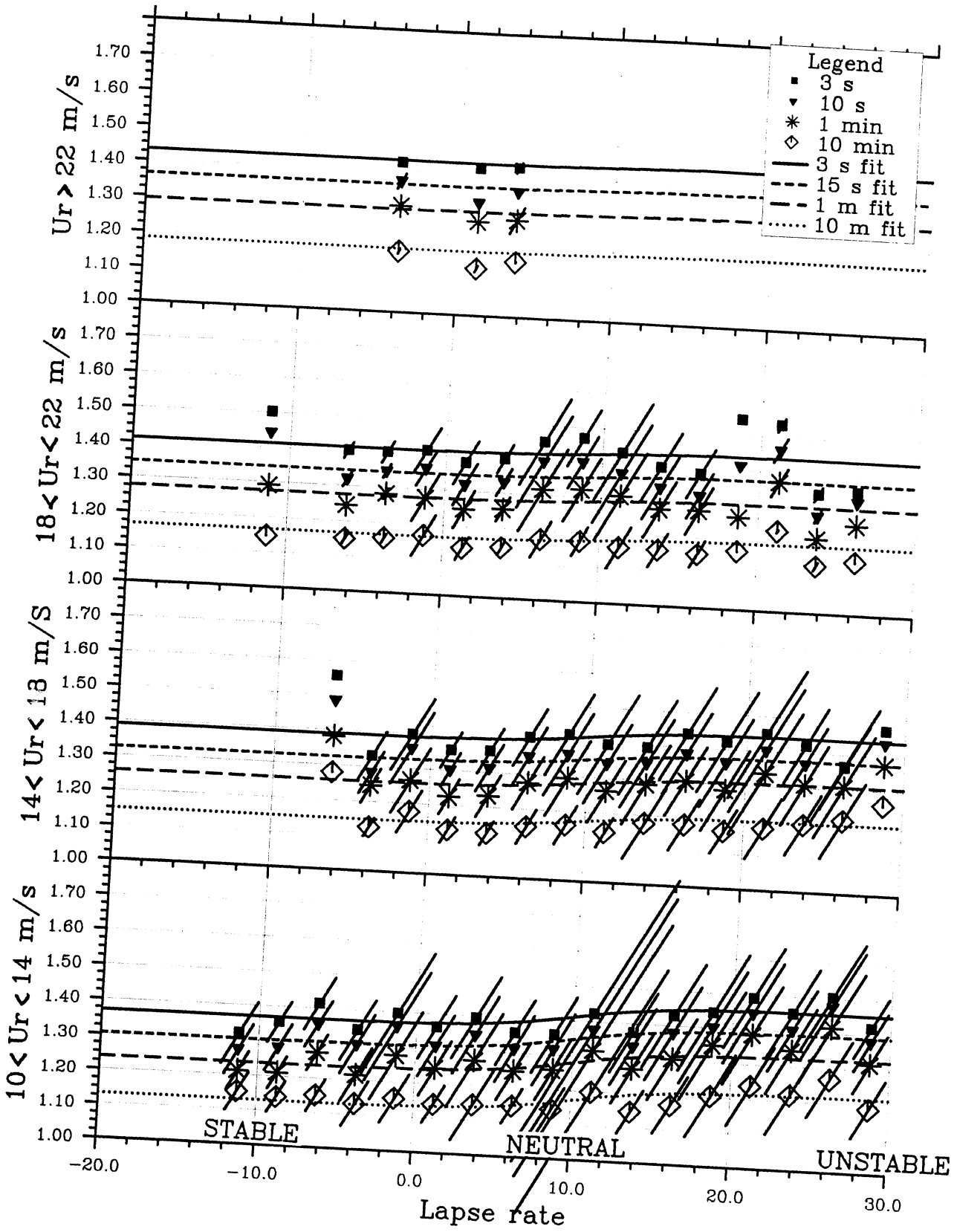

Fig. 4.4.3 As Fig. 4.4.1, but for 20 m height at Sletringen.

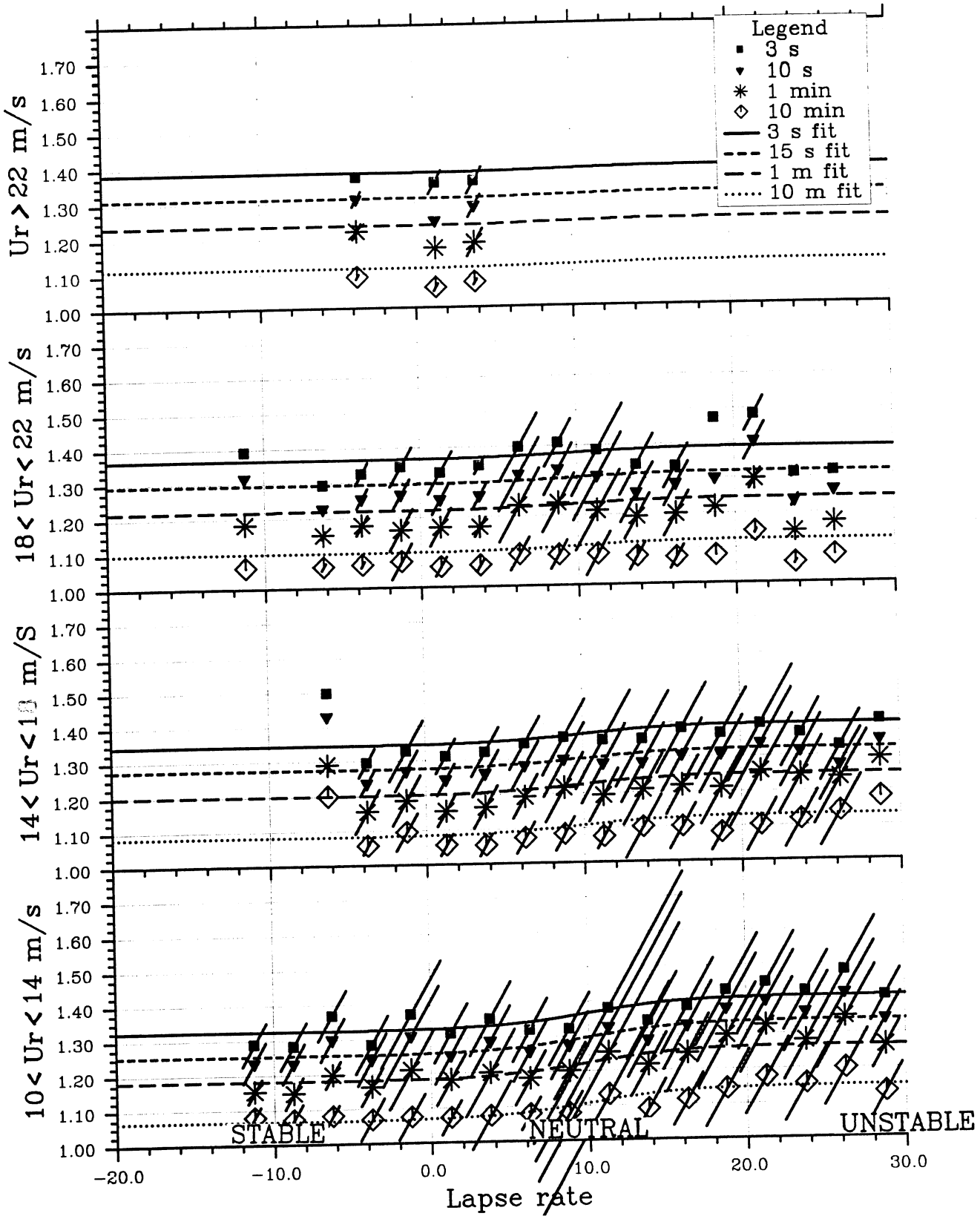

Fig. 4.4.4 As Fig. 4.4.1, but for 10 m height at Sletringen.

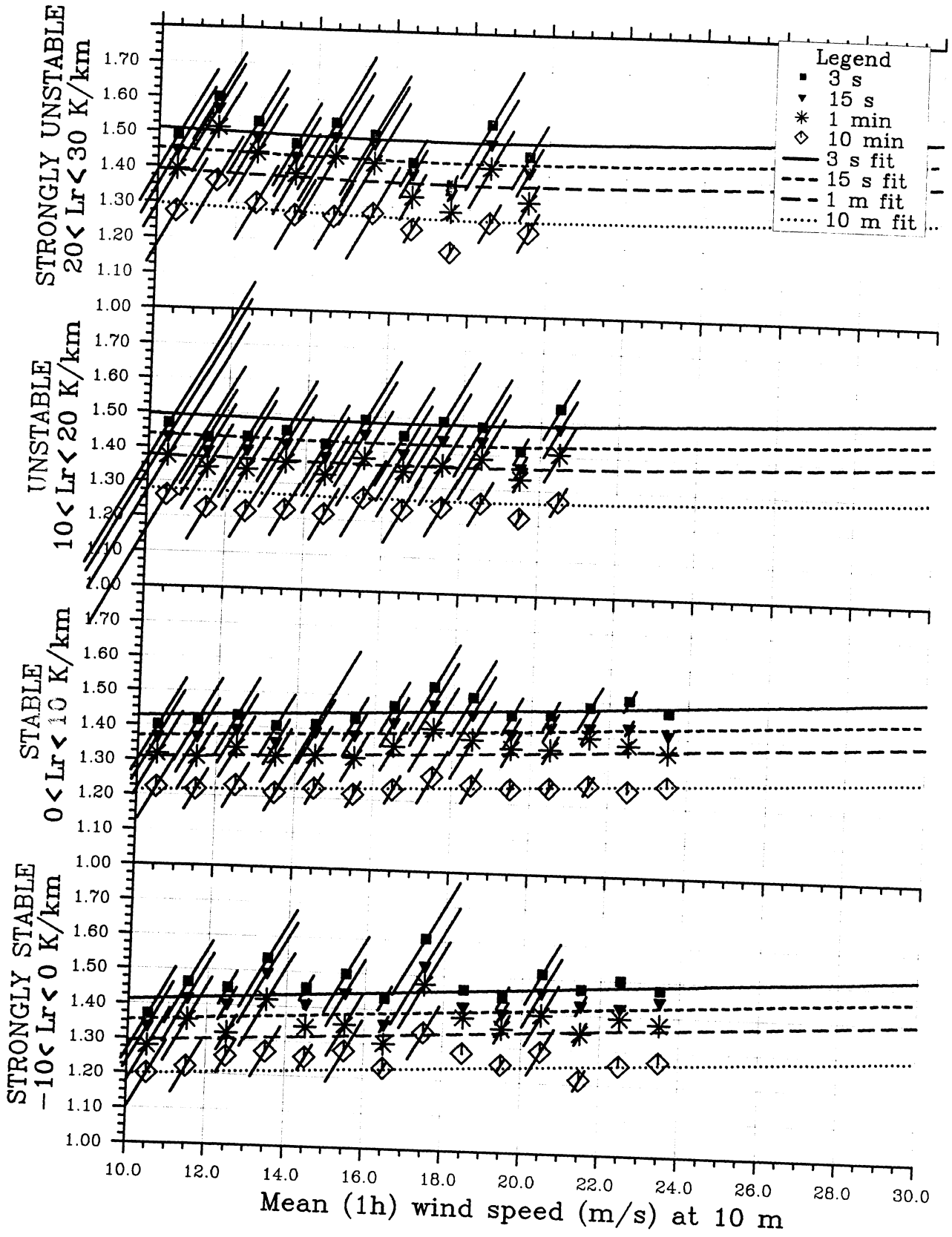

Fig. 4.4.5 Mean value of the reference gust factor at 46 m height at Sletringen versus wind speed for 4 lapse rate classes. See text for discussion.

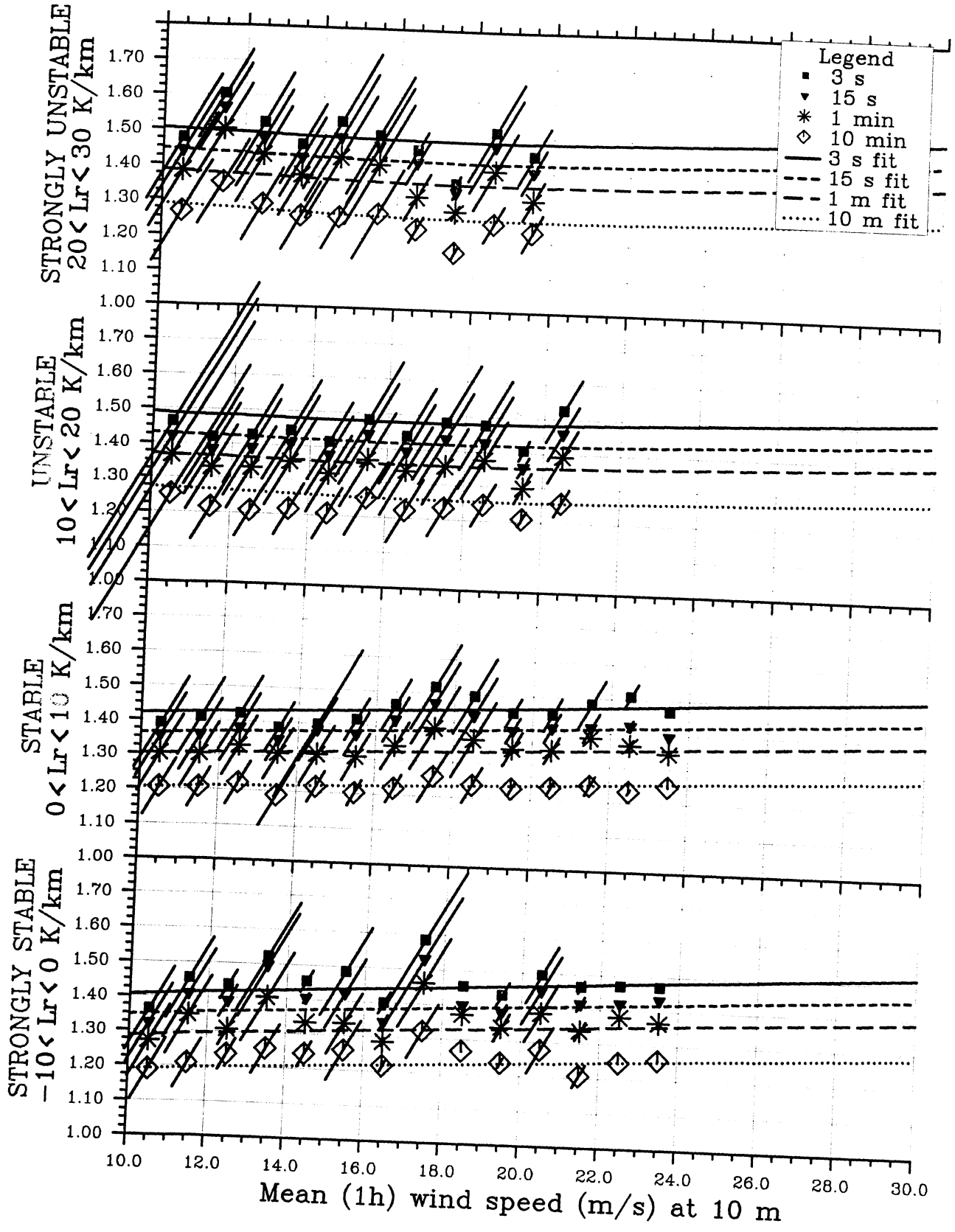

Fig. 4.4.6 As Fig. 4.4.5, but for 42 m height at Sletringen.

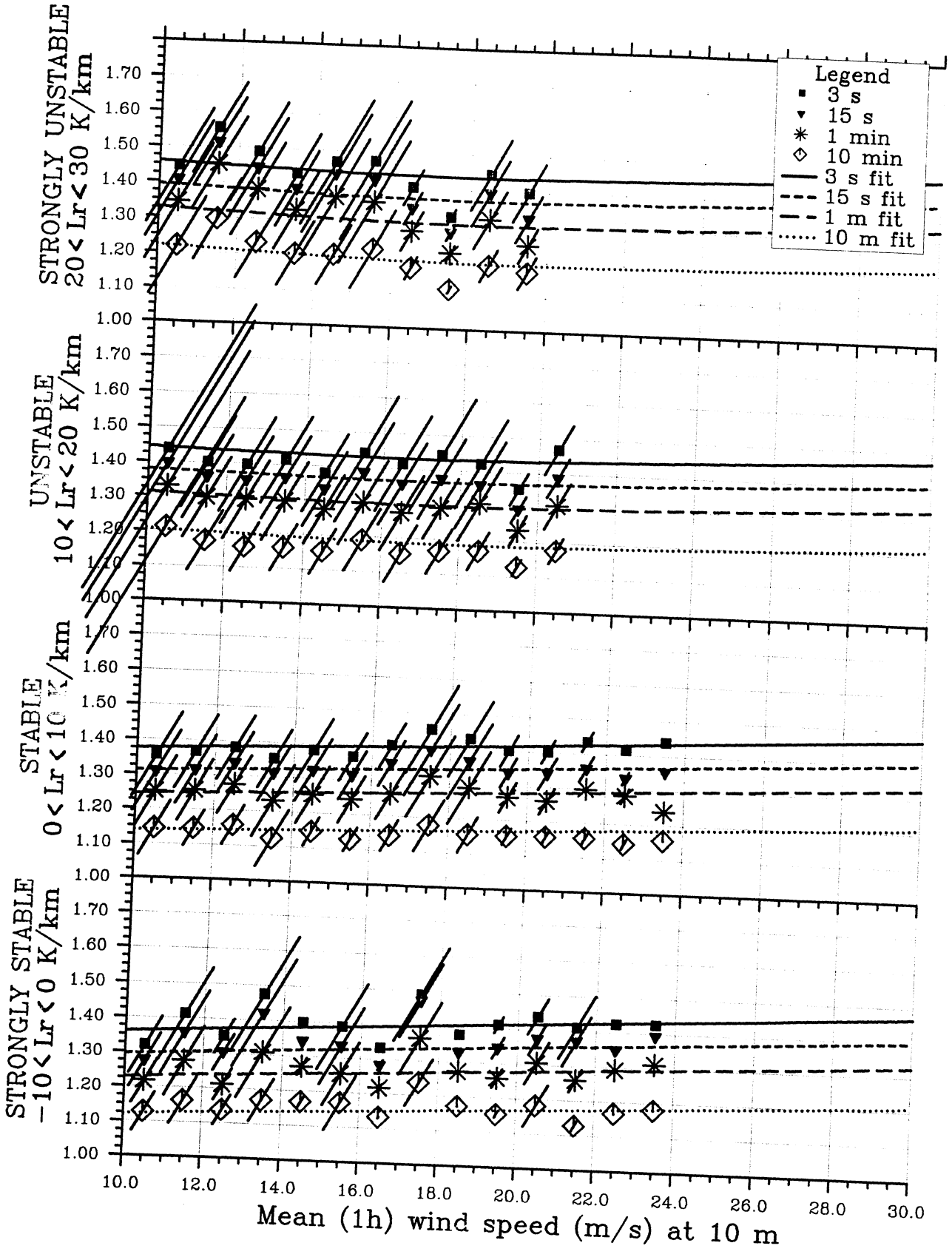

Fig. 4.4.7 As Fig. 4.4.5, but for 20 m height at Sletringen.

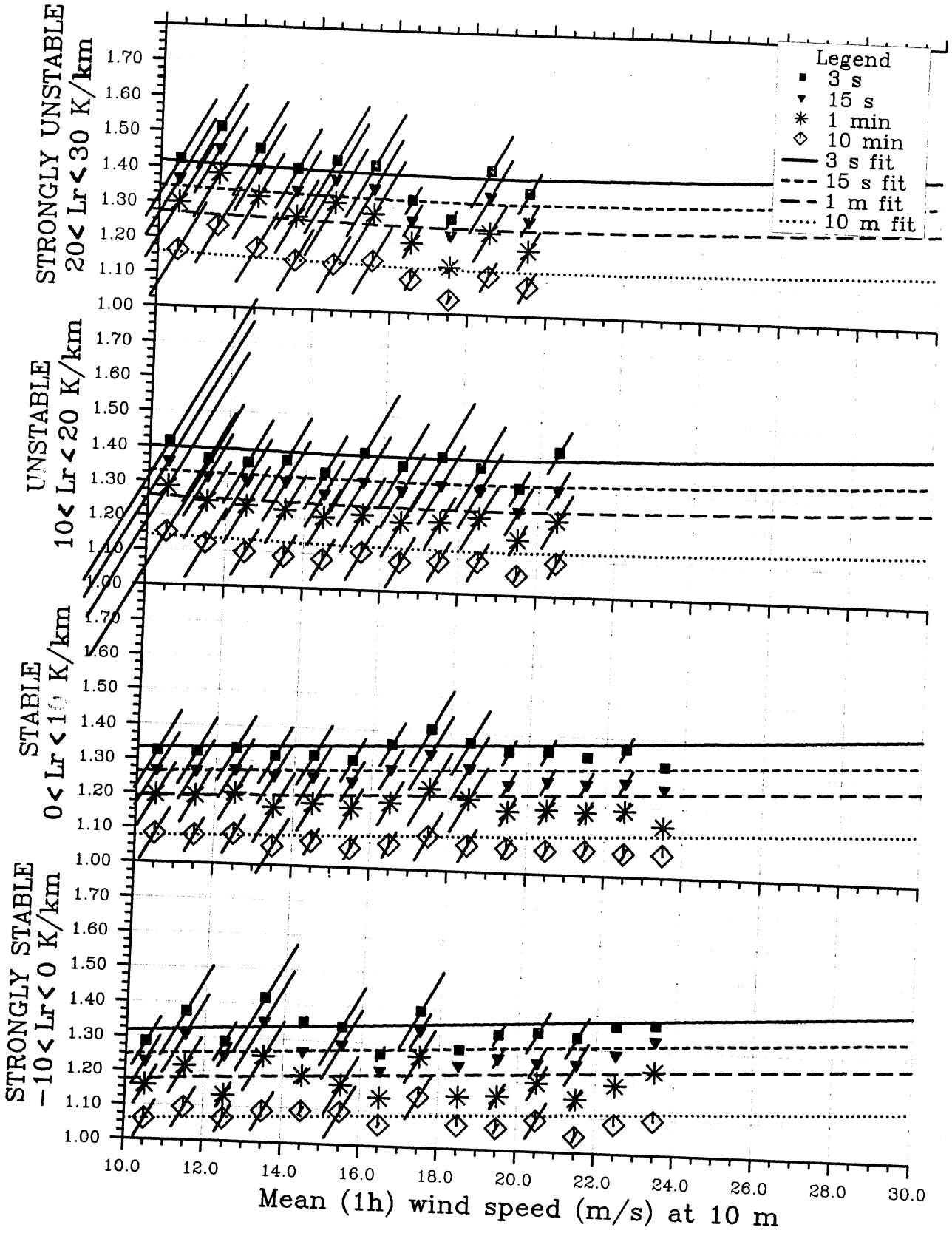

Fig. 4.4.8 As Fig. 4.4.5, but for 10 m height at Sletringen.

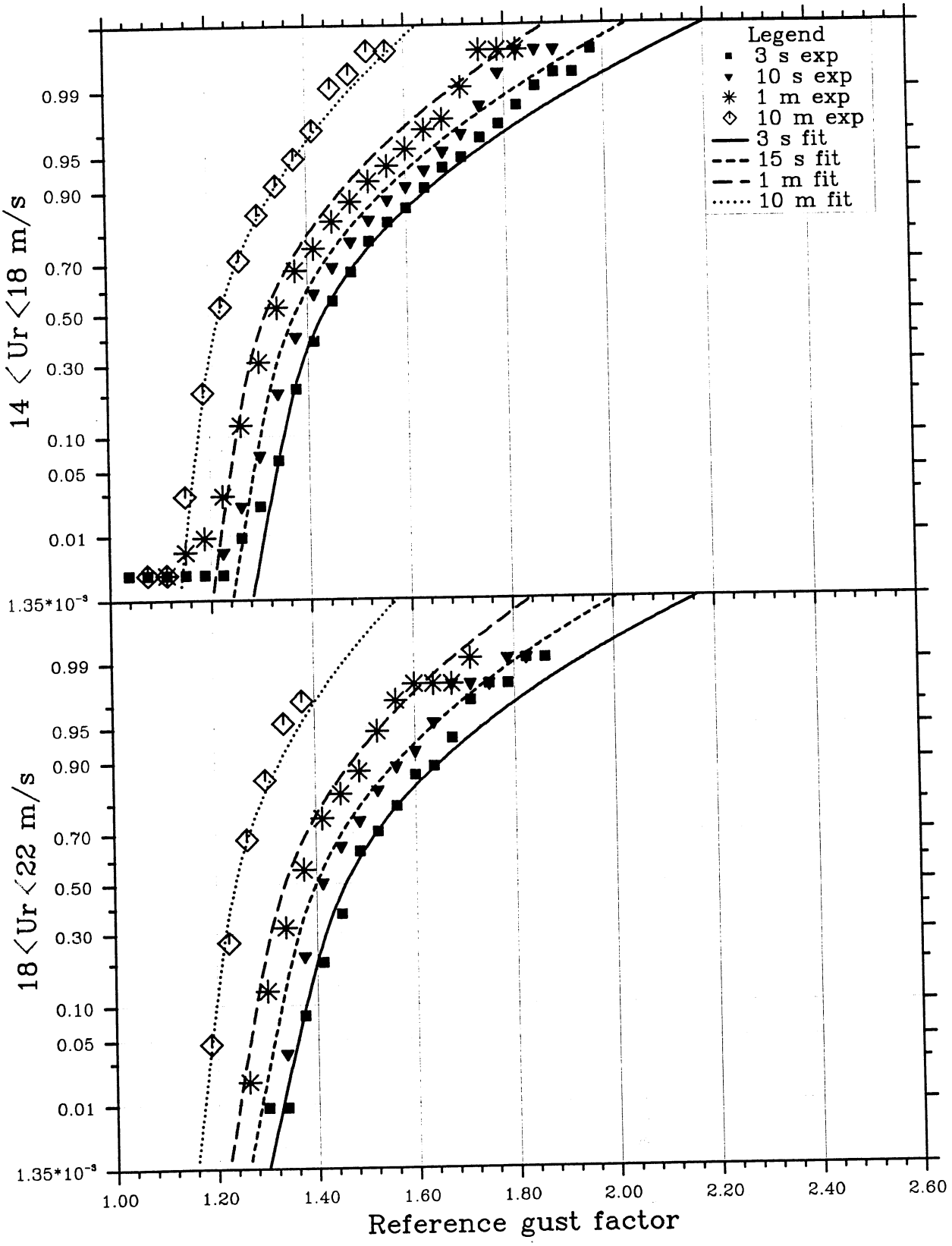

Fig. 4.4.9 Cumulative distributions of the reference gust factor at 46 m height at Sletringen for 2 classes of reference wind speed. See text for discussion.

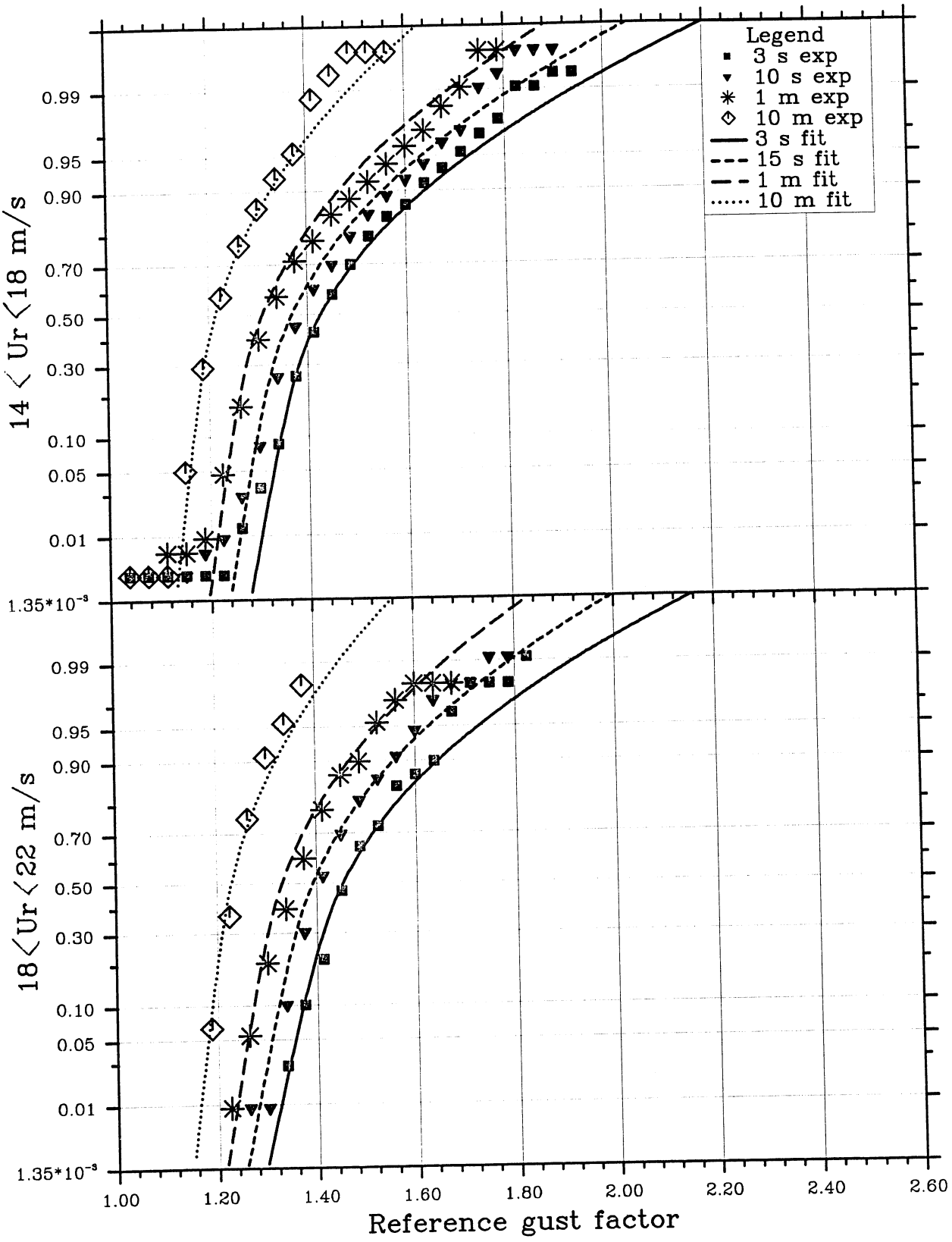

Fig. 4.4.10 As Fig. 4.4.9, but for 42 m height at Sletringen.

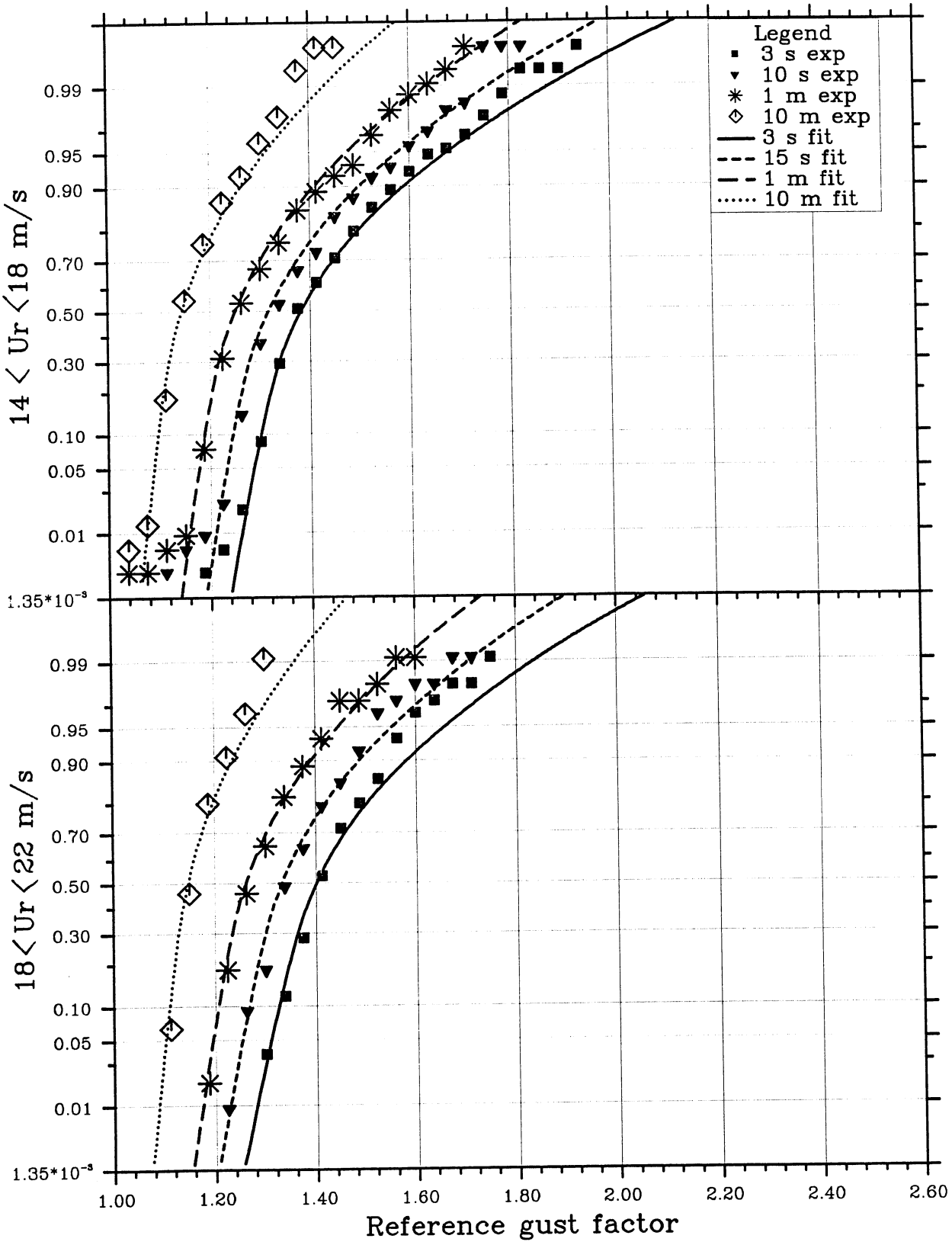

Fig. 4.4.11 As Fig. 4.4.9, but for 20 m height at Sletringen.

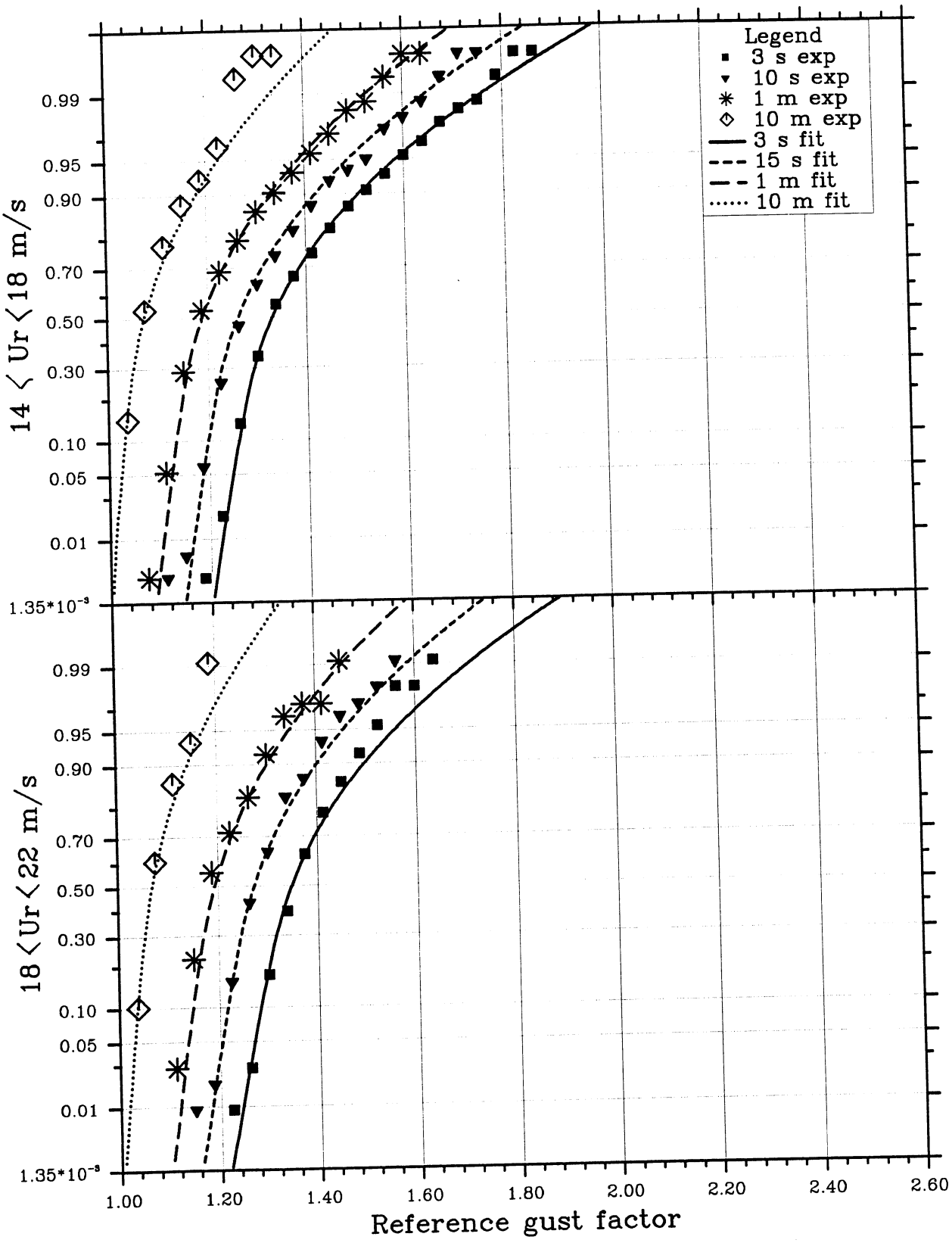

Fig. 4.4.12 As Fig. 4.4.9, but for 10 m height at Sletringen.

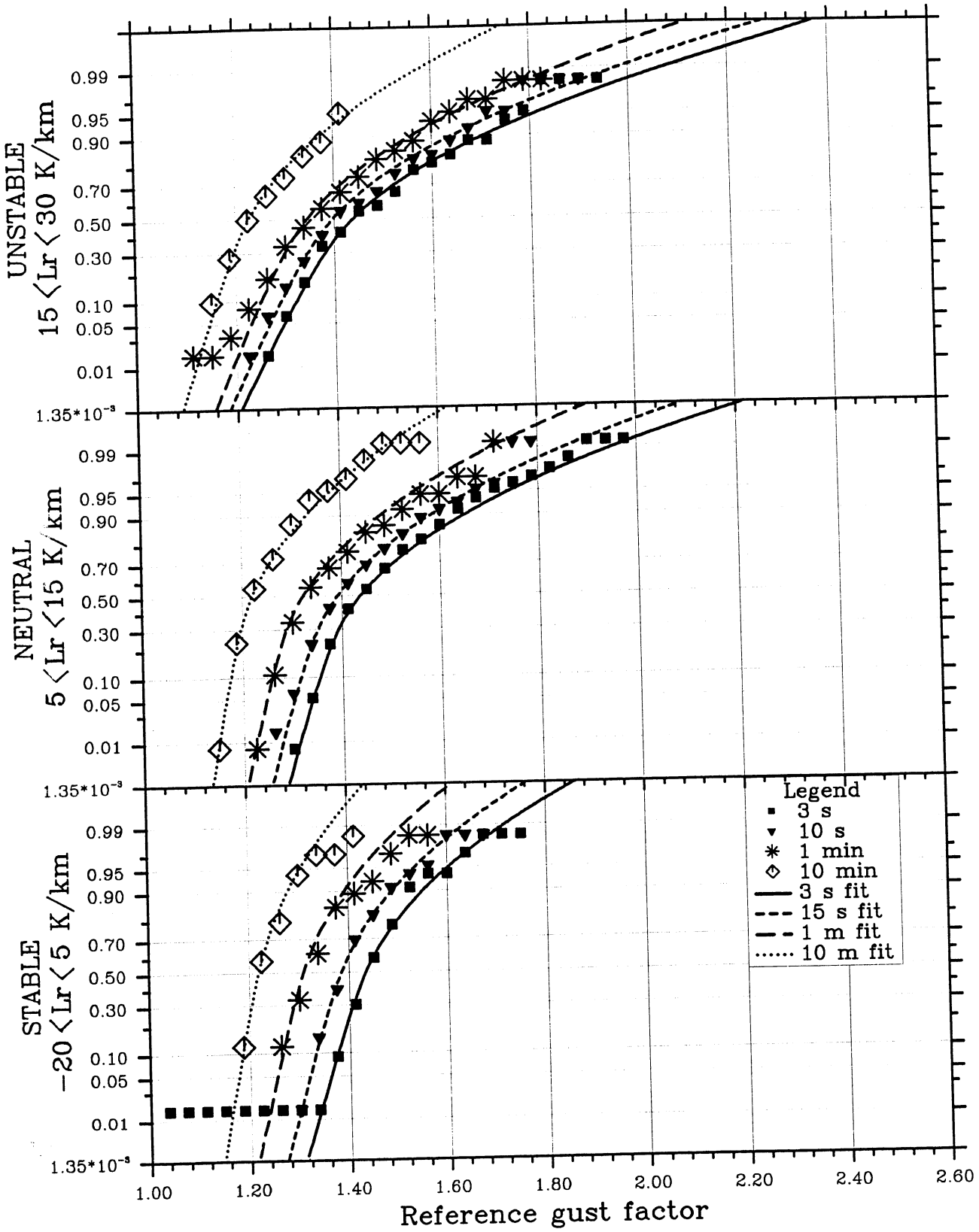

Fig. 4.4.13 Cumulative distributions of the reference gust factor at 46 m height at Sletringen for the reference wind speed range 14 -18 m/s and three classes of lapse rate. See text for discussion.

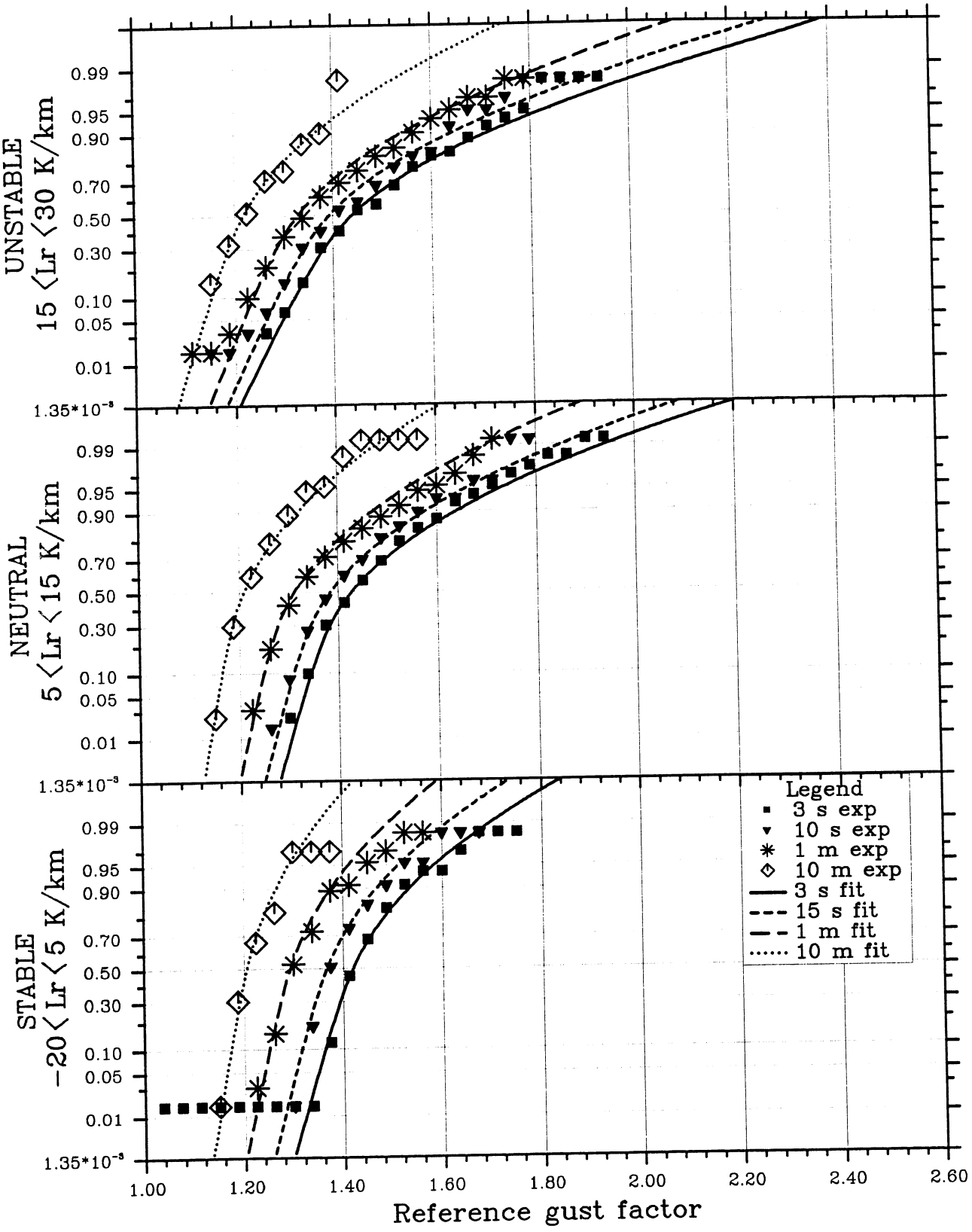

Fig. 4.4.14 As Fig. 4.4.13, but for 42 m height at Sletringen.

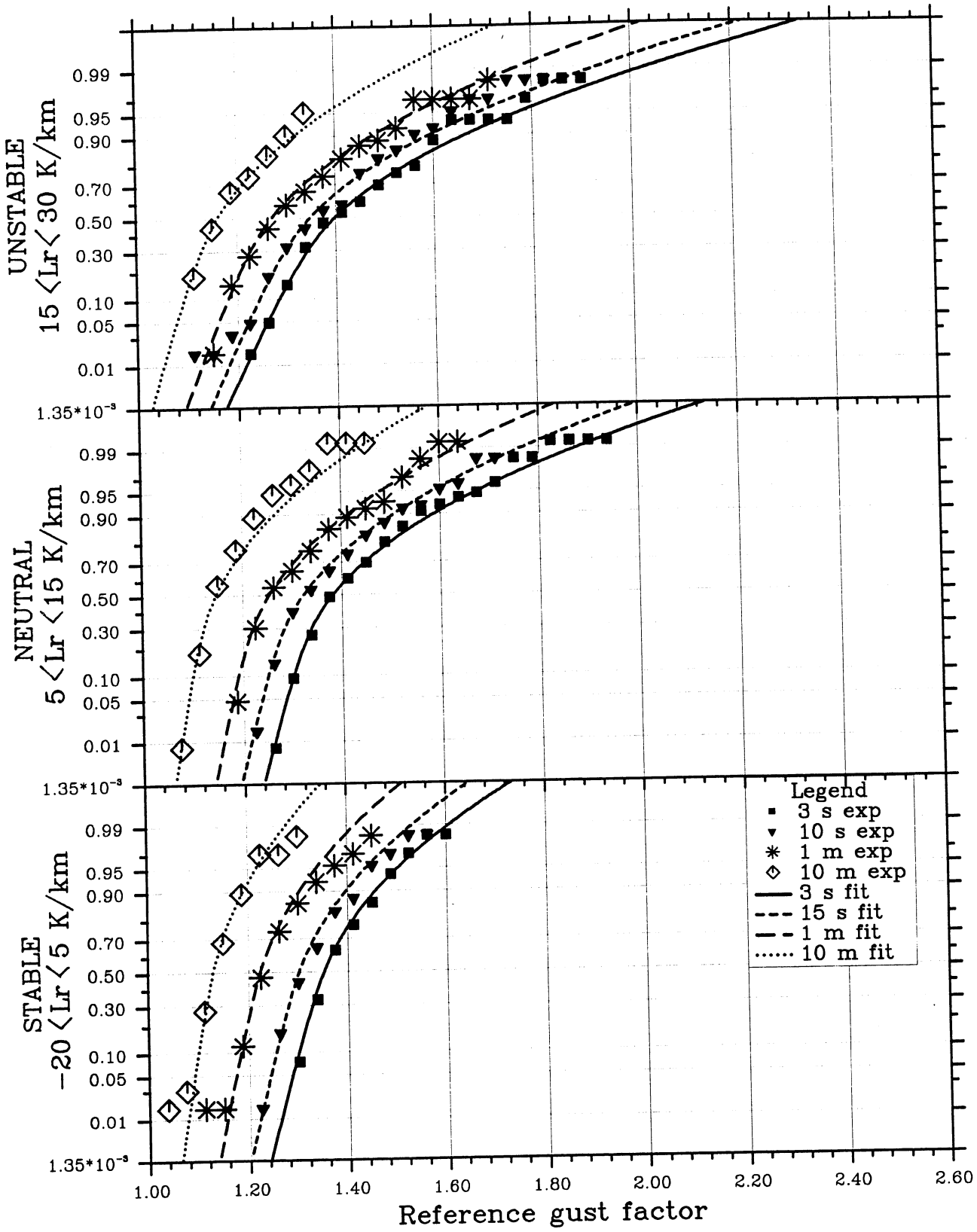

Fig. 4.4.15 As Fig. 4.4.13, but for 20 m height at Sletringen.

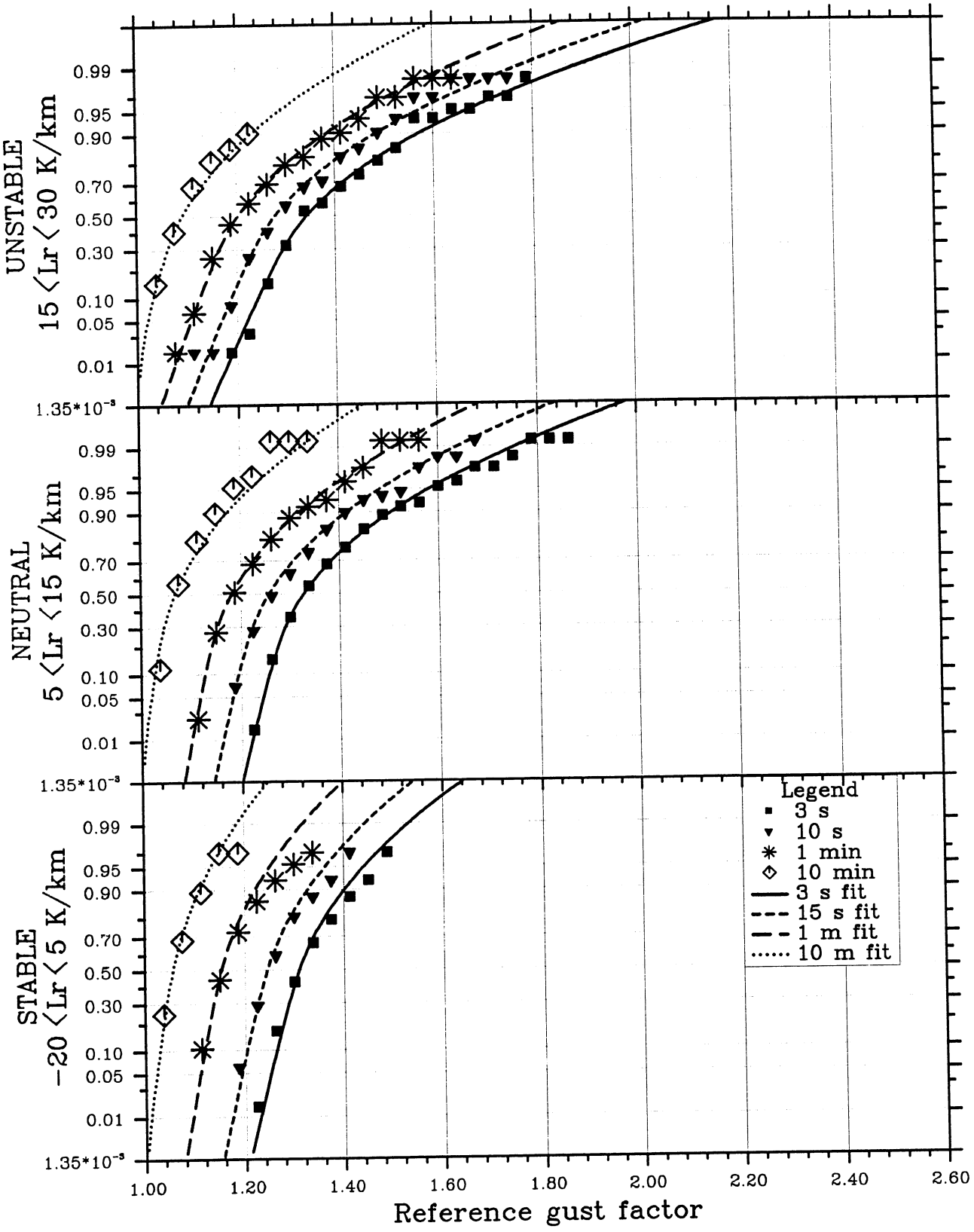

Fig. 4.4.16 As Fig. 4.4.13, but for 10 m height at Sletringen.

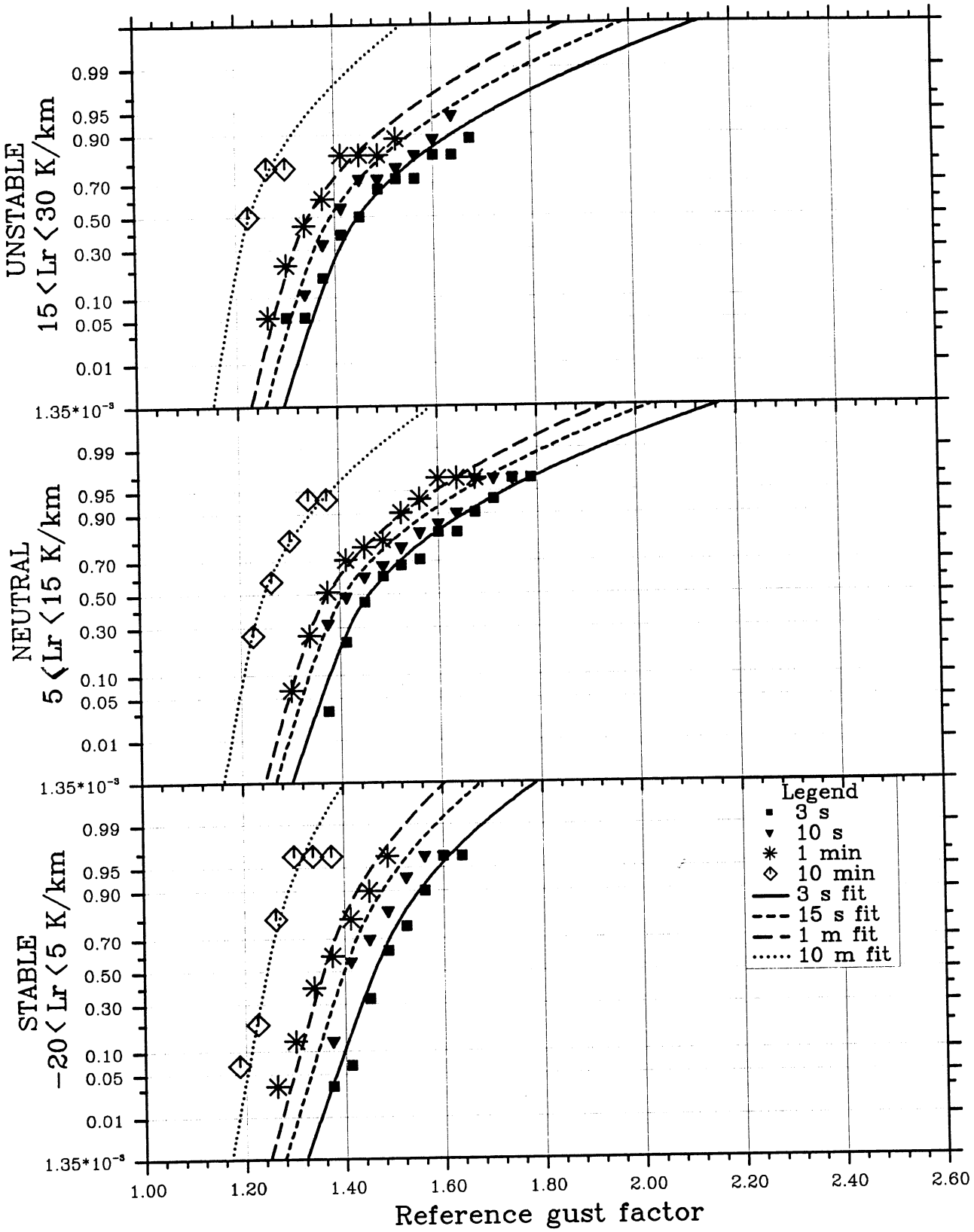

Fig. 4.4.17 Cumulative distributions of the reference gust factor at 46 m height at Sletringen for the reference wind speed range 18 - 22 m/s and three classes of lapse rate. See text for discussion.

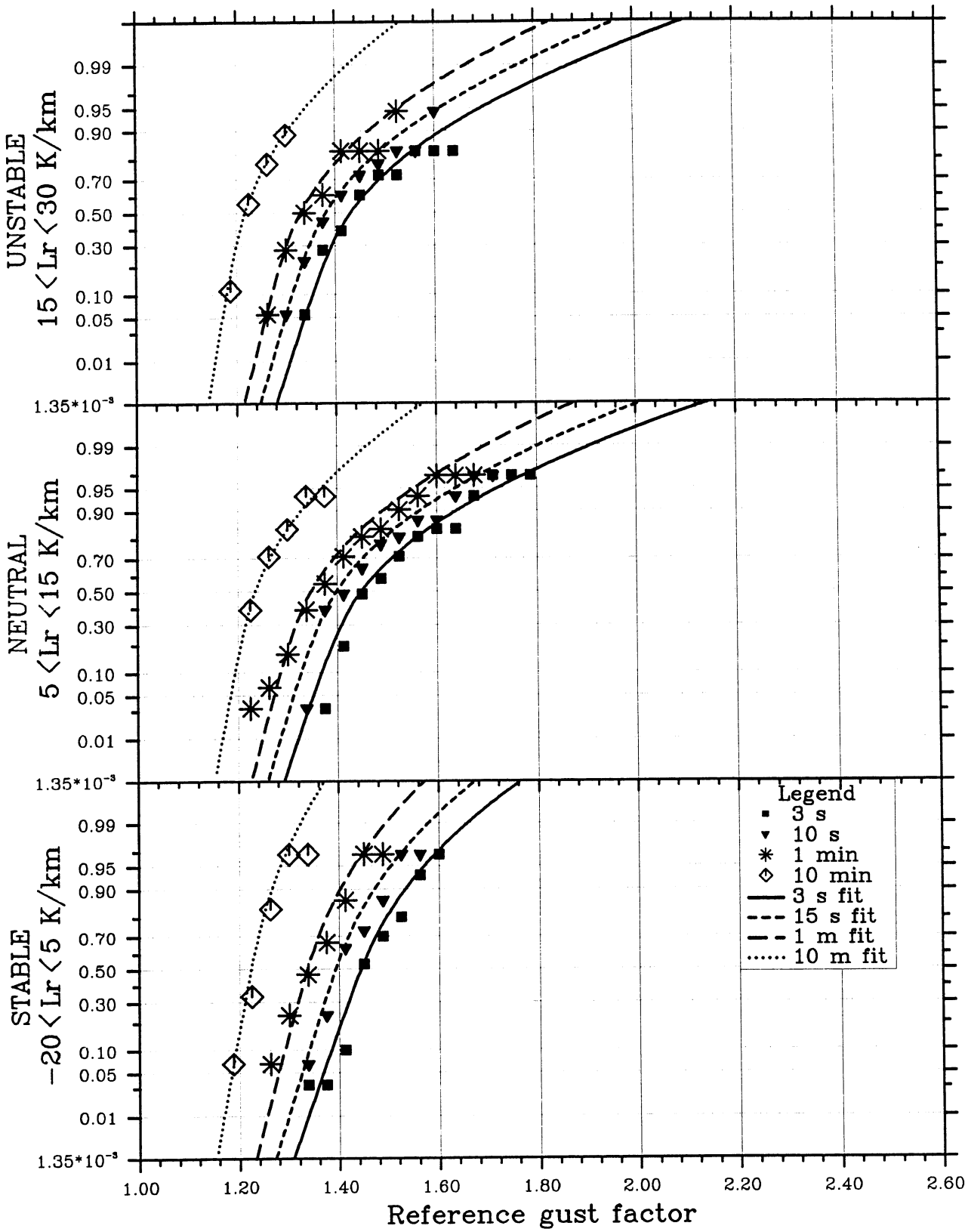

Fig. 4.4.18 As Fig. 4.4.17, but for 42 m height at Sletringen.

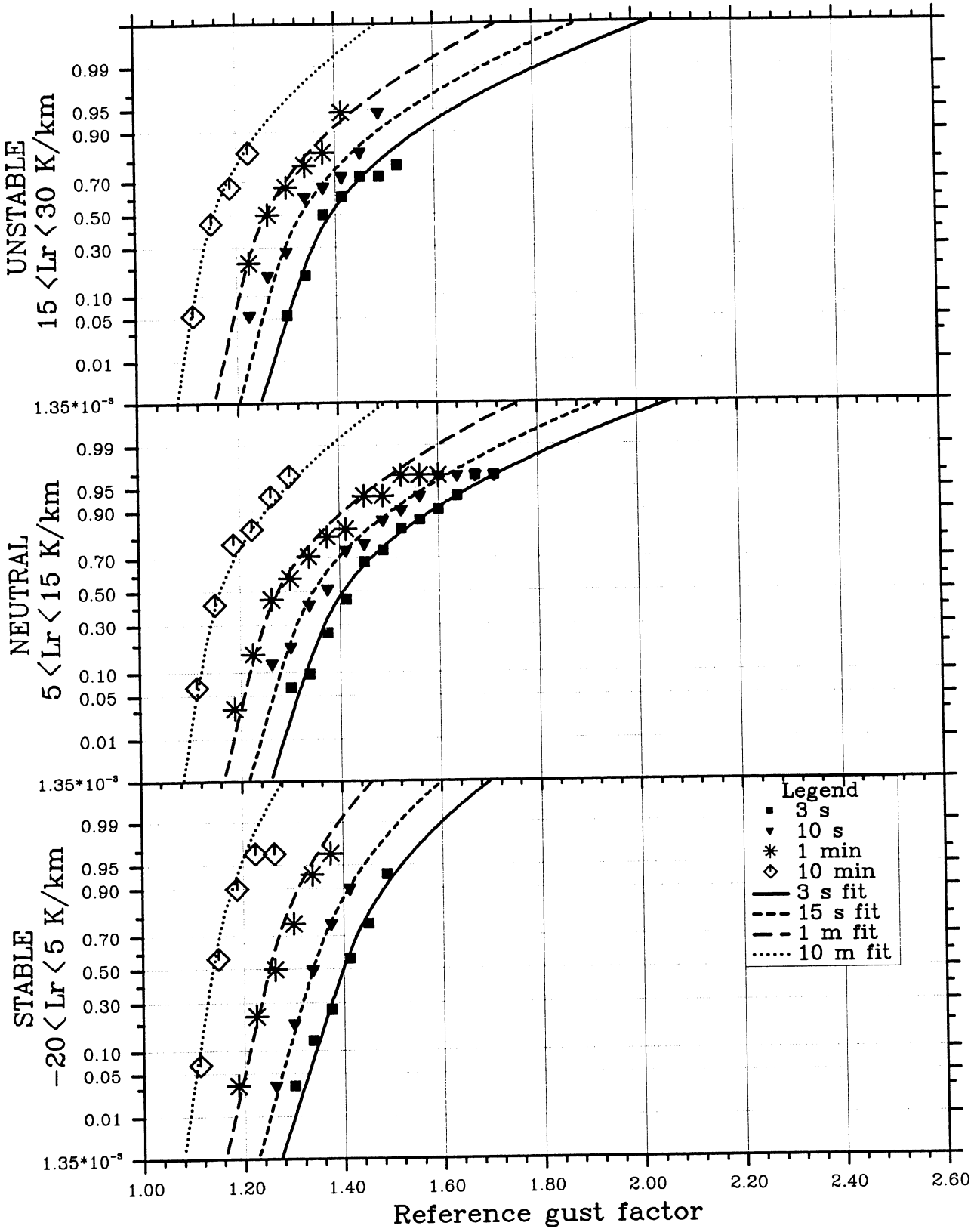

Fig. 4.4.19 As Fig. 4.4.17, but for 20 m height at Sletringen.

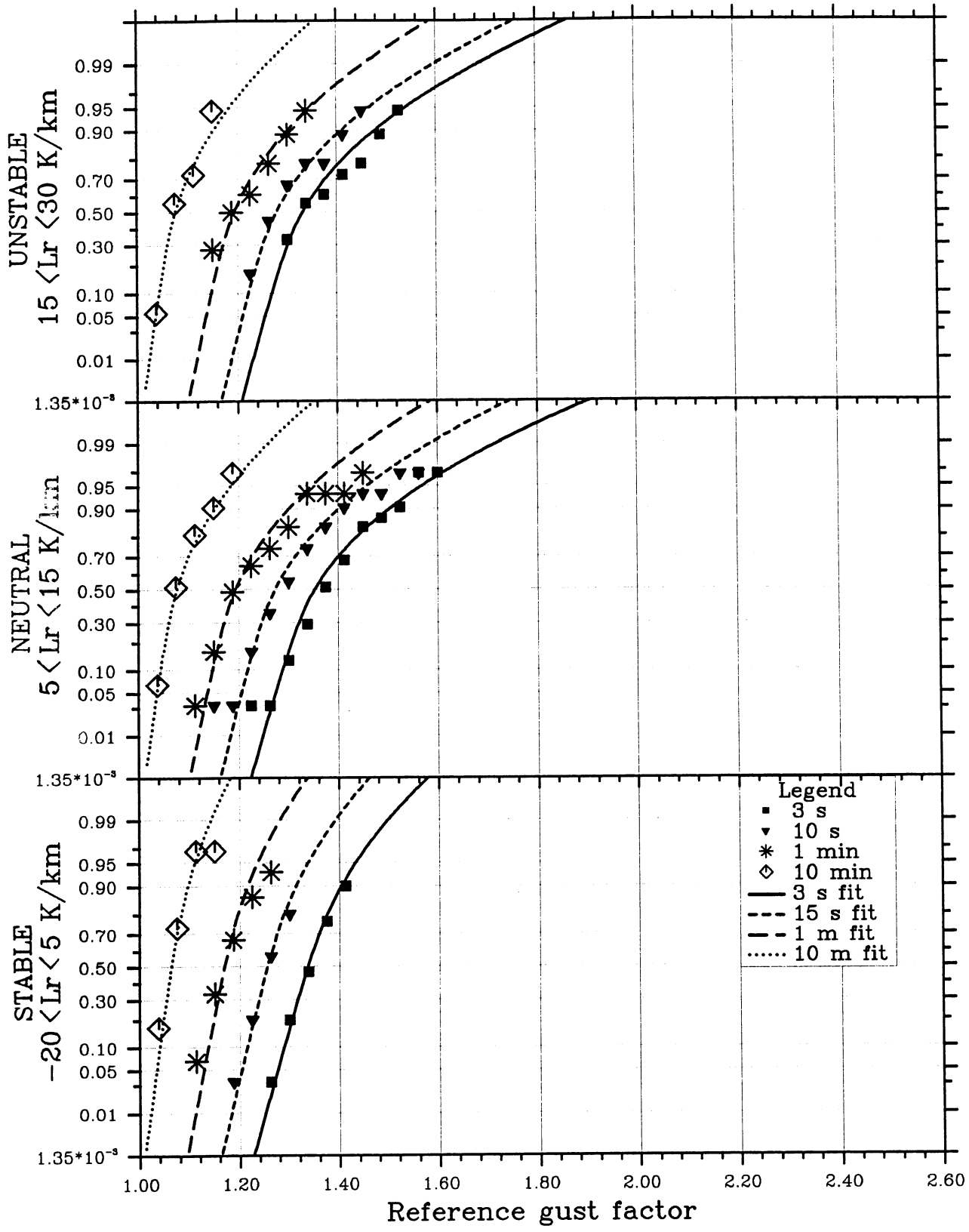

Fig. 4.4.20 As Fig. 4.4.17, but for 10 m height at Sletringen.

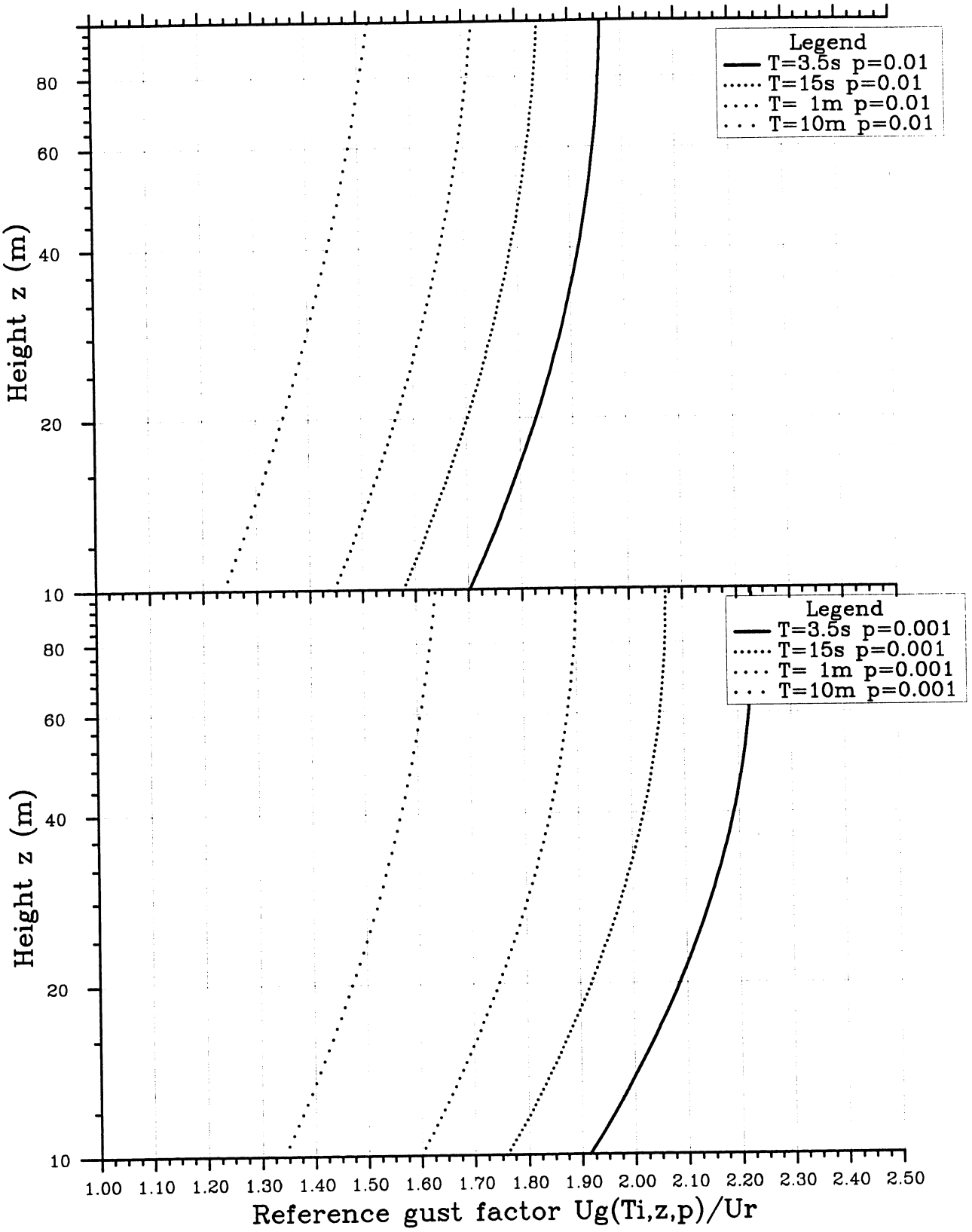

Fig. 4.4.21 Limiting reference gust factor which is exceeded with a probability of 1 per cent (top) and 1 per mille (bottom). Reference wind speed u_r = 20 m/s. See text for discussion.

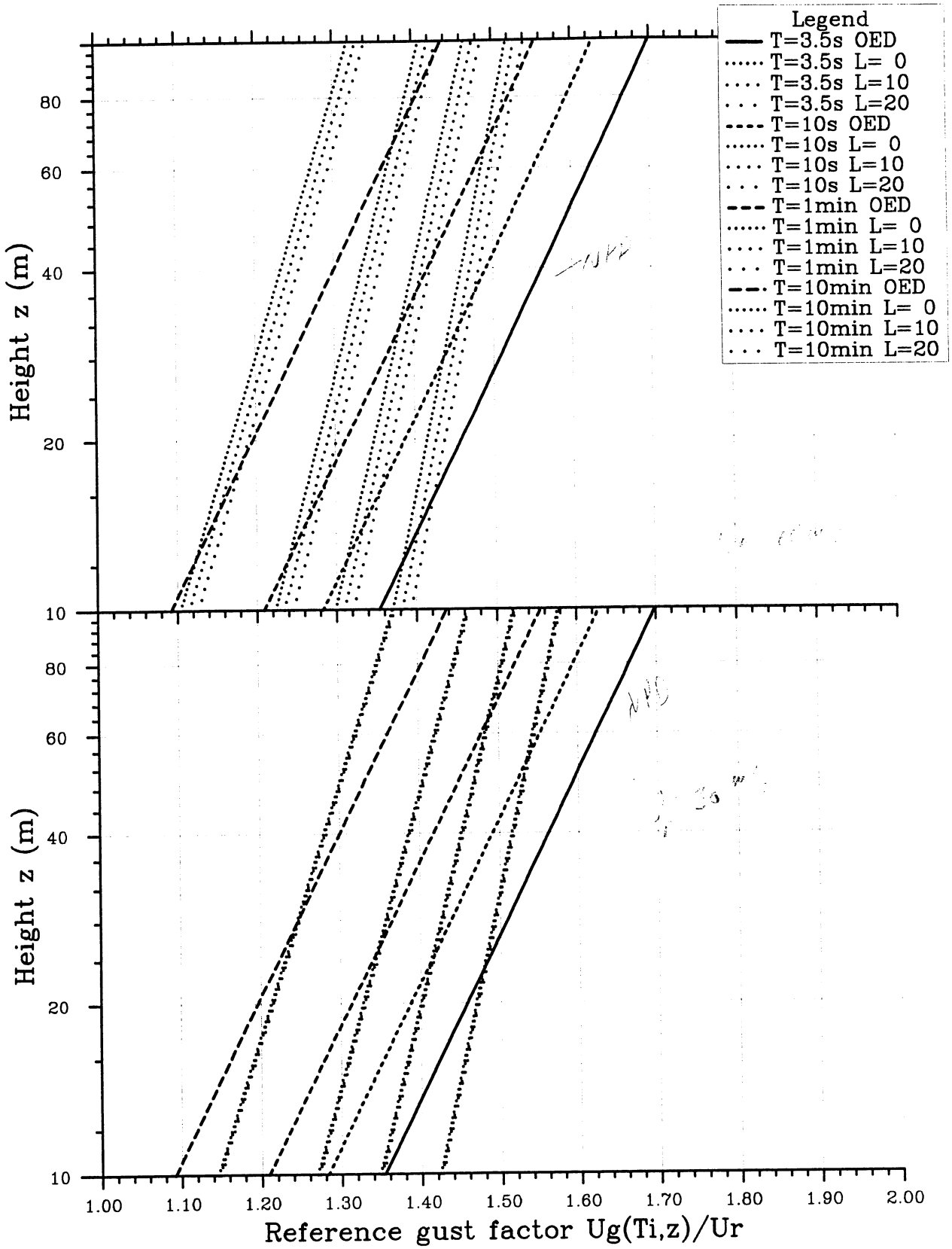

Fig. 4.4.22 Mean reference gust factor versus height z. Comparison between NPD formula for 4 selected gust durations to our parameterization Eq.(7). Top: Reference wind speed u_r = 20 m/s. Bottom: u_r = 30 m/s. See text for discussion.

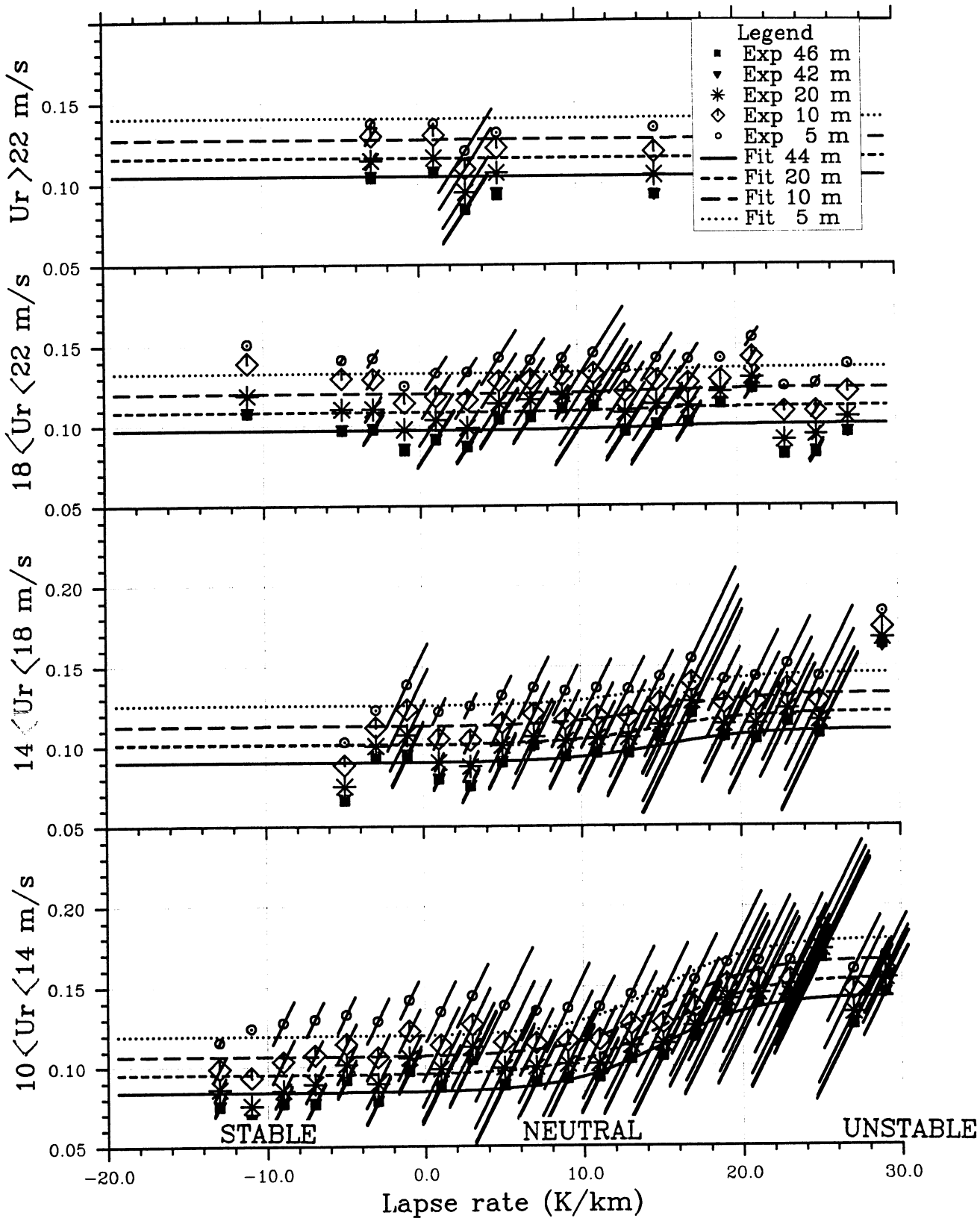

Fig. 4.5.1 Mean value and standard deviation of the turbulence intensity at 46, 42, 20, 10 and 5 m height at Sletringen versus lapse rate for 4 classes of reference wind speed u_r. See text for discussion.

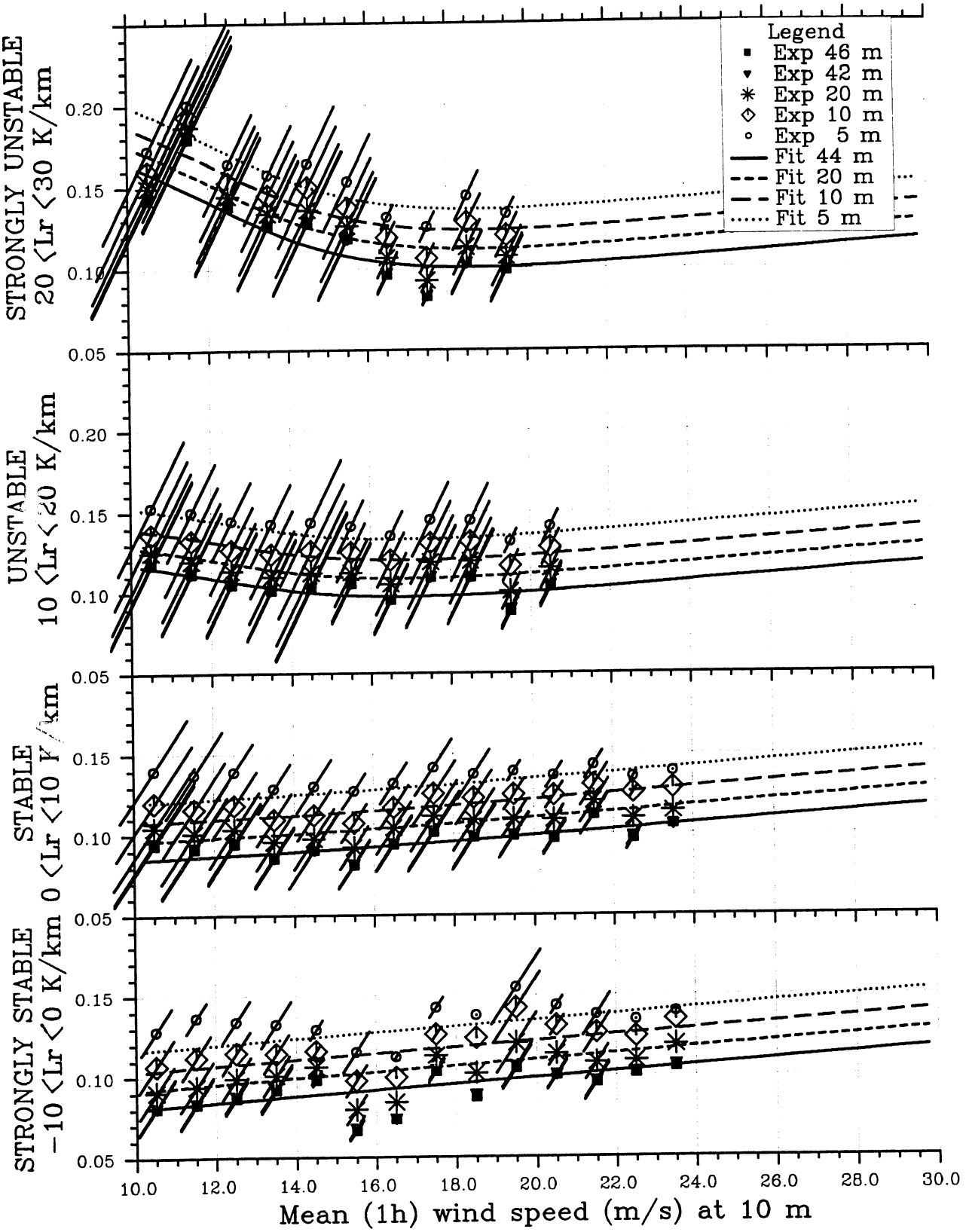

Fig. 4.5.2 Mean value and standard deviation of the turbulence intensity at 46, 42, 20, 10 and 5 m height at Sletringen versus reference wind speed for 4 classes of lapse rate. See text for discussion.

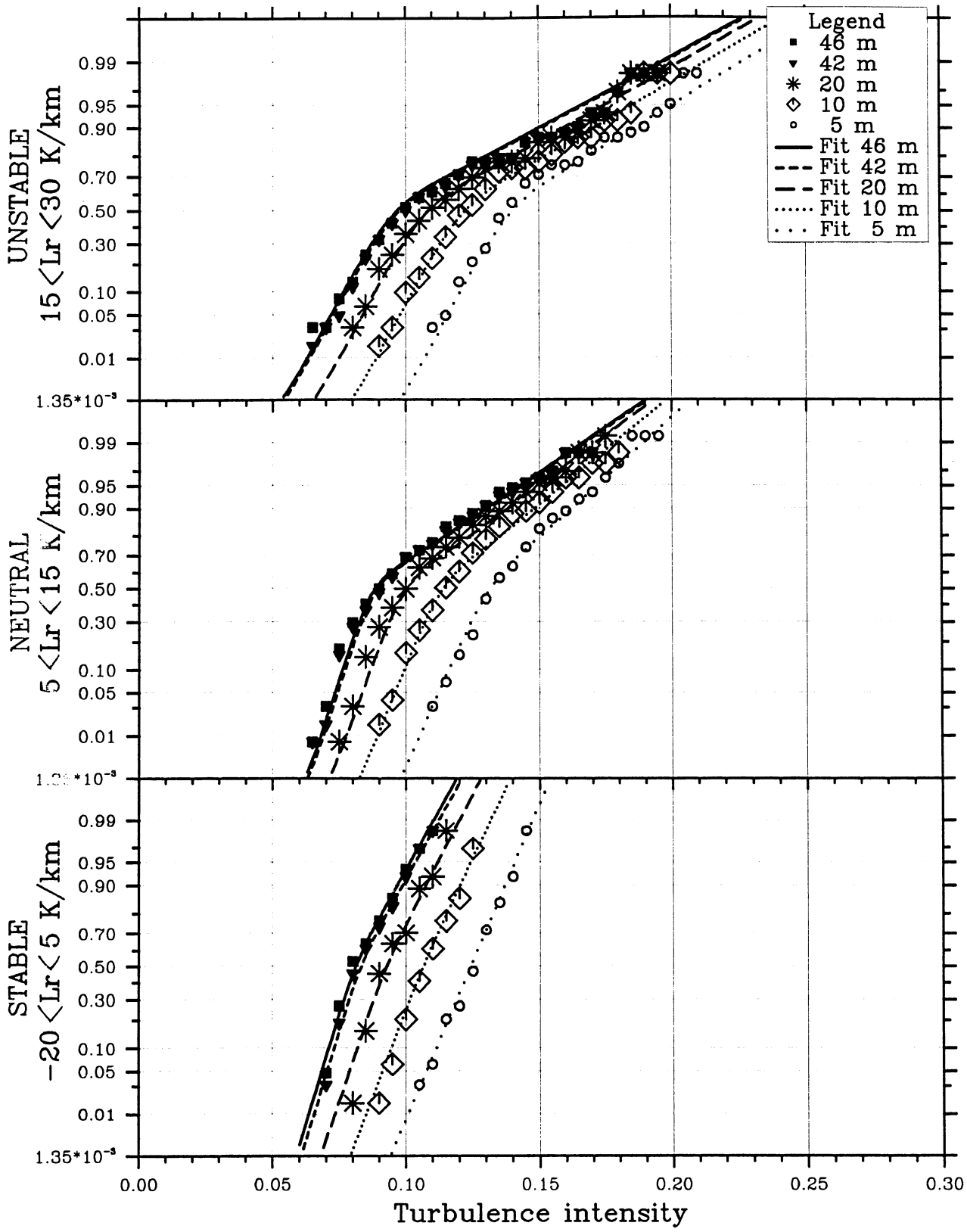

Fig. 4.5.3 Cumulative distribution of the turbulence intensity at 46, 42, 20, 10 and 5 m height at Sletringen for the reference wind speed range 14 - 18 m/s and 3 classes of lapse rate. See text for discussion.

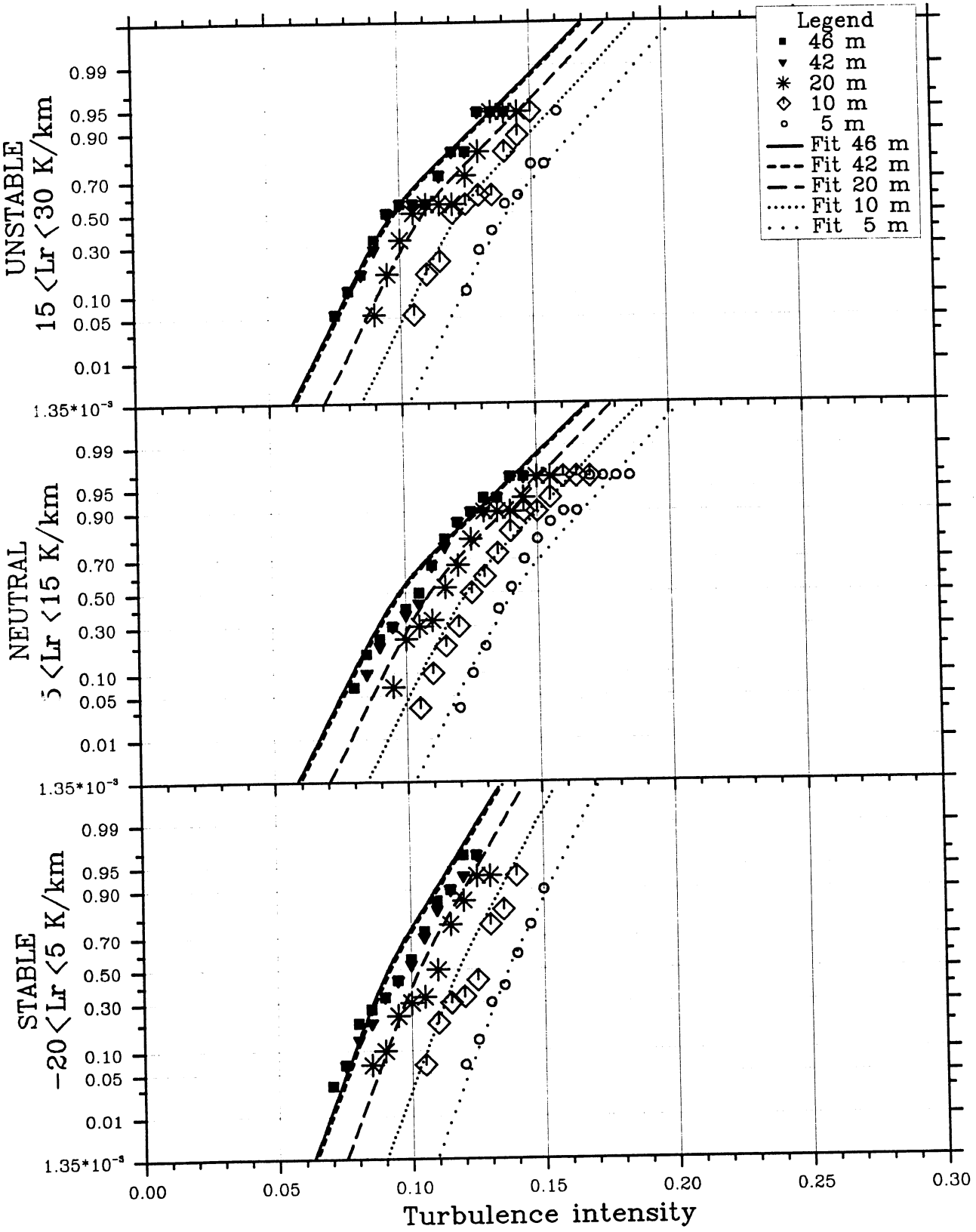

Fig. 4.5.4 As Fig. 4.5.3, but for the reference wind speed range 18 - 22 m/s.

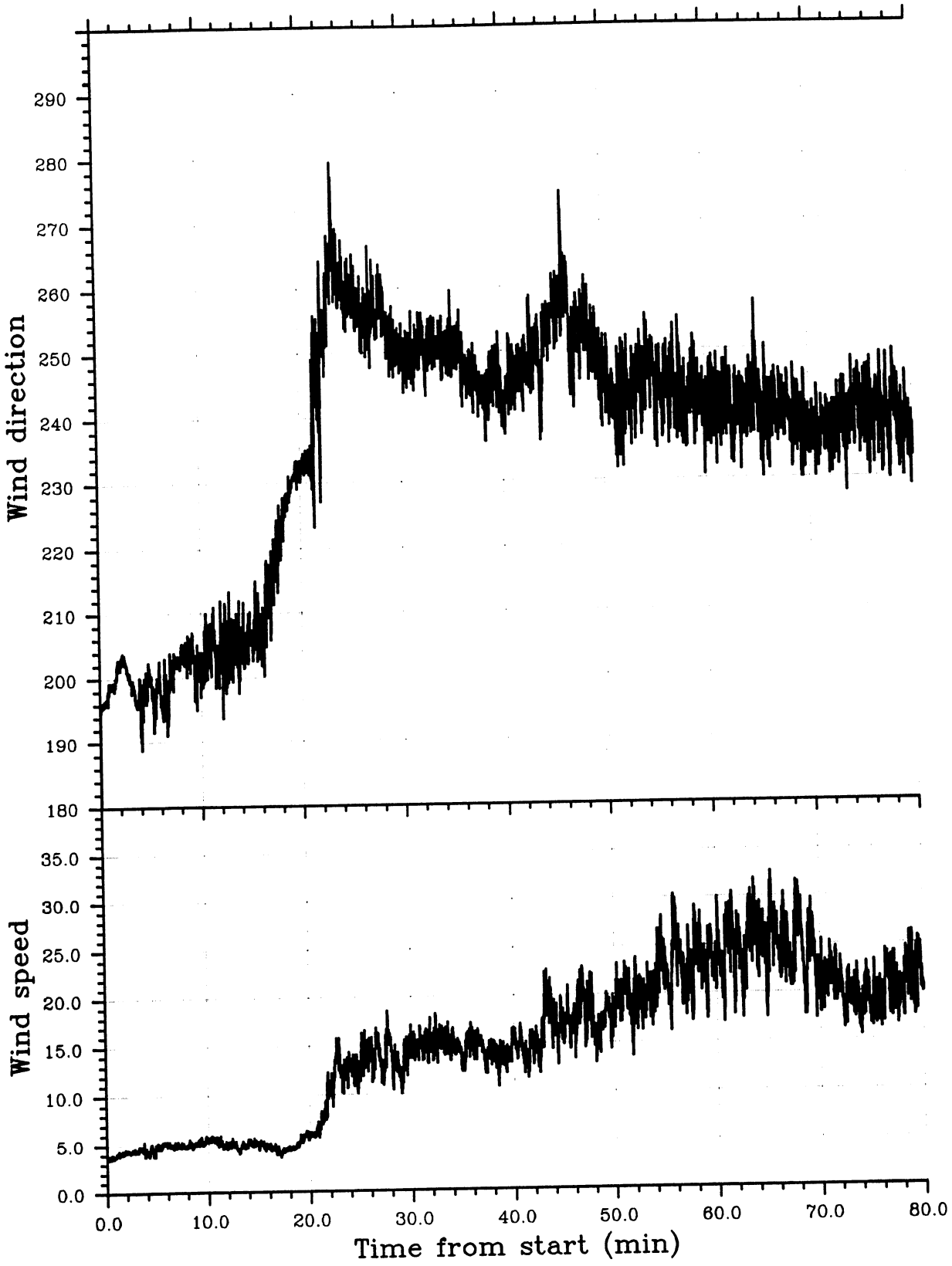

Fig. 4.6.1 Time series of wind direction at 45 m height (top) and reference wind speed (bottom) from Sletringen 1988.11.11, 6.40 - 8.00.

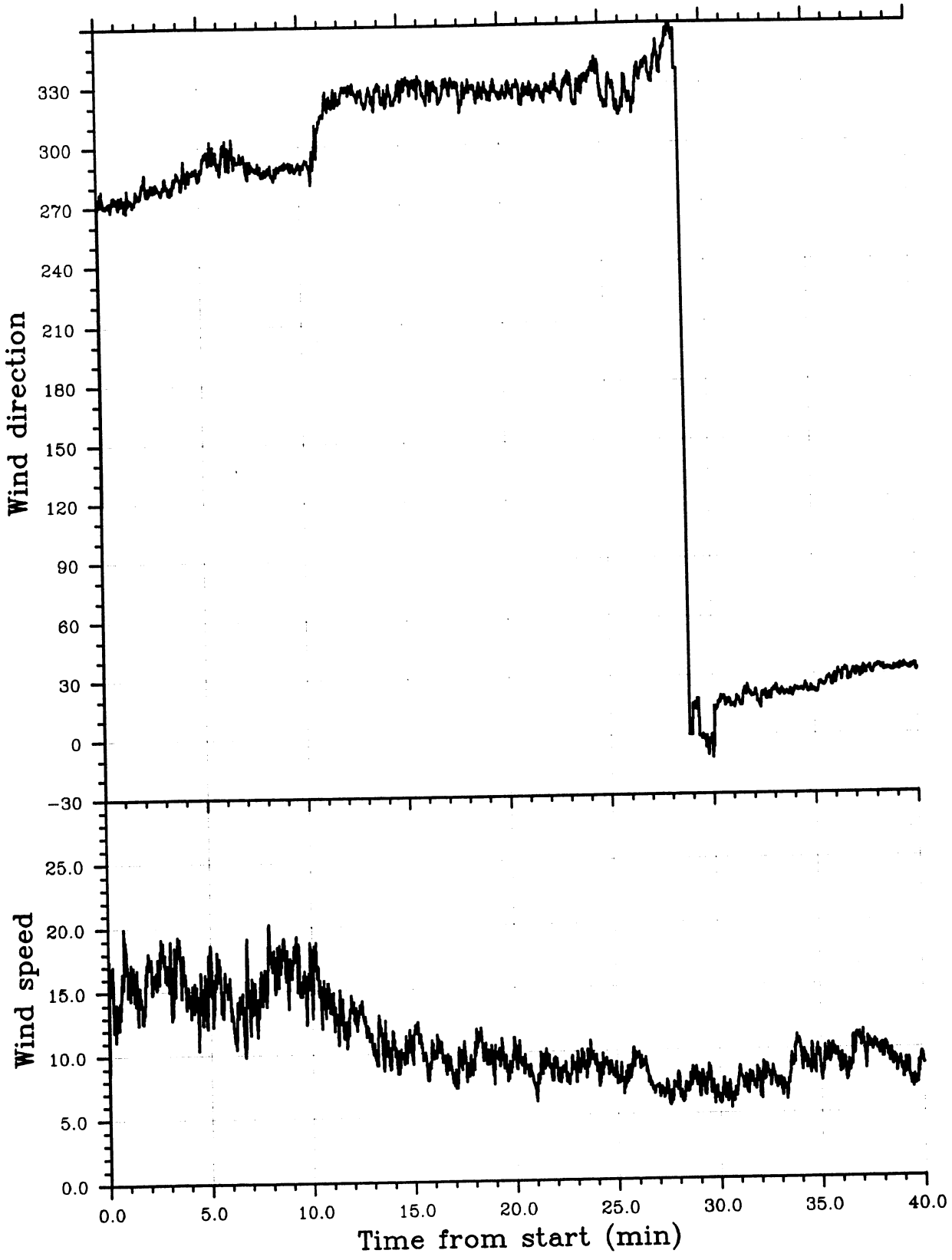

Fig. 4.6.2 Time series of wind direction at 100 m height (top) and reference wind speed (bottom) from Skipheia 1988.12.21, 6.00 - 6.40.

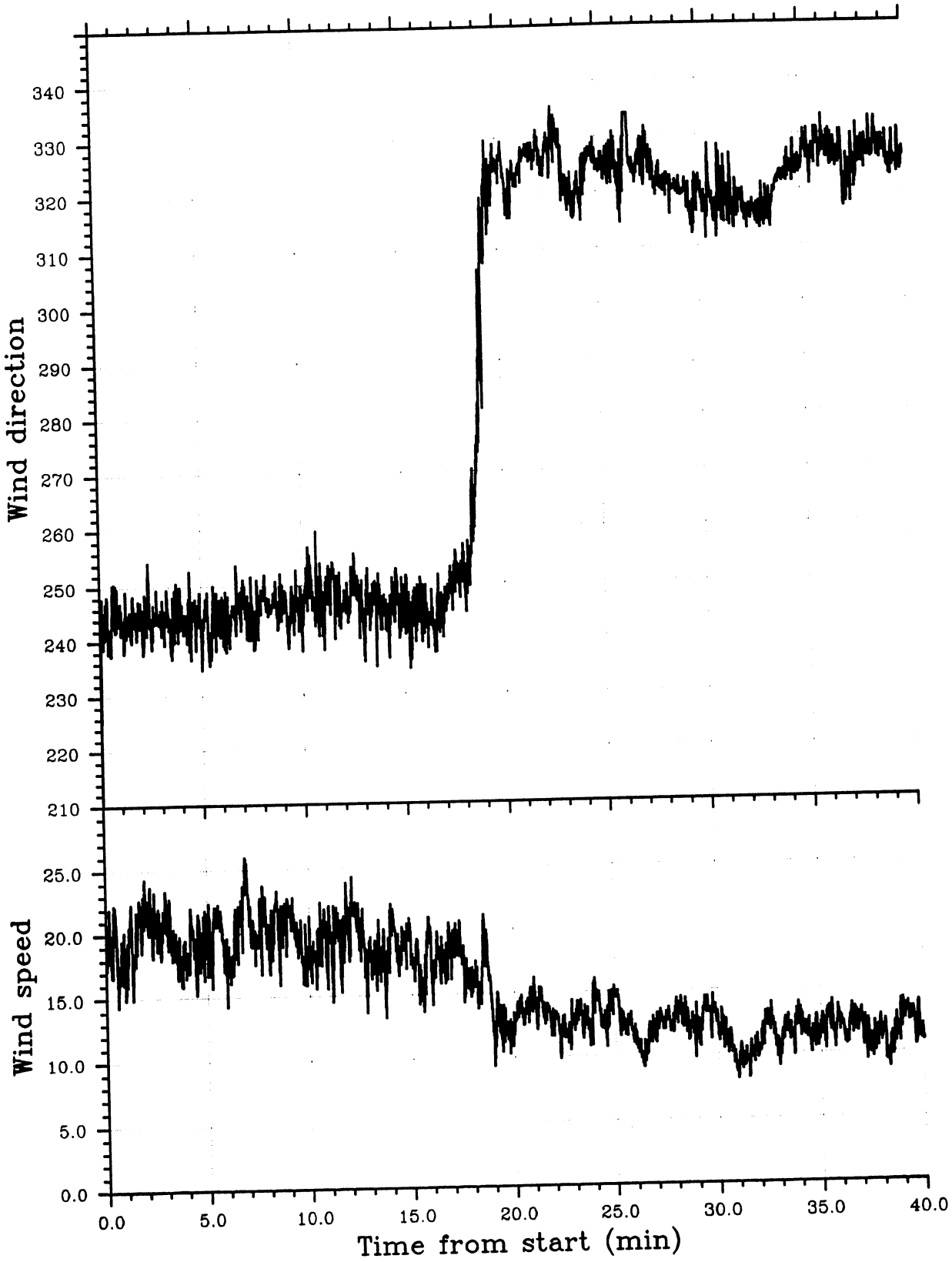

Fig. 4.6.3a Time series of wind direction at 45 m height (top) and reference wind speed (bottom) from Sletringen 1988.11.16, 12.40 - 13.20.

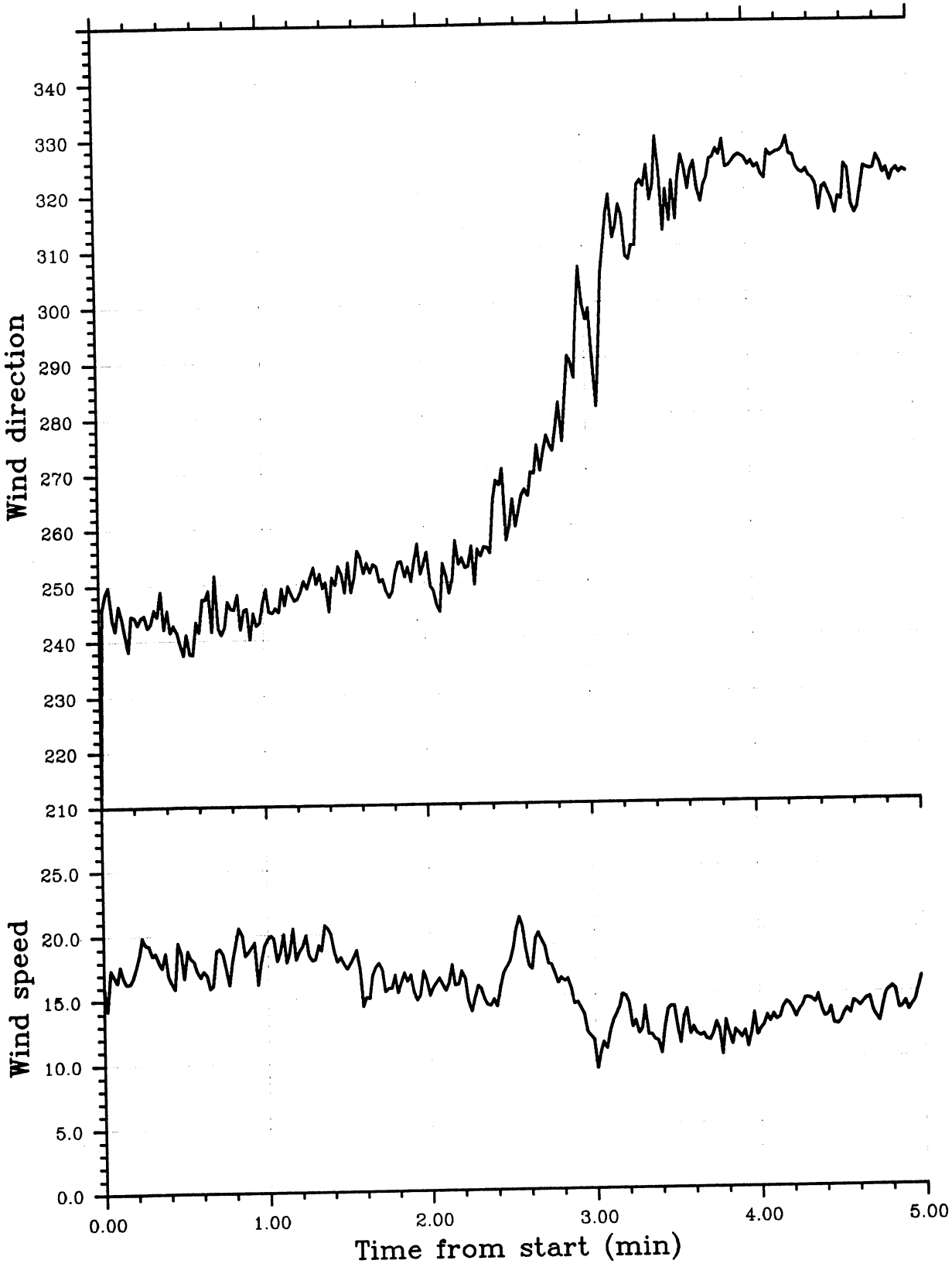

Fig. 4.6.3b As Fig. 4.6.3a, but with an expanded time scale for the period 13.06 - 13.11.

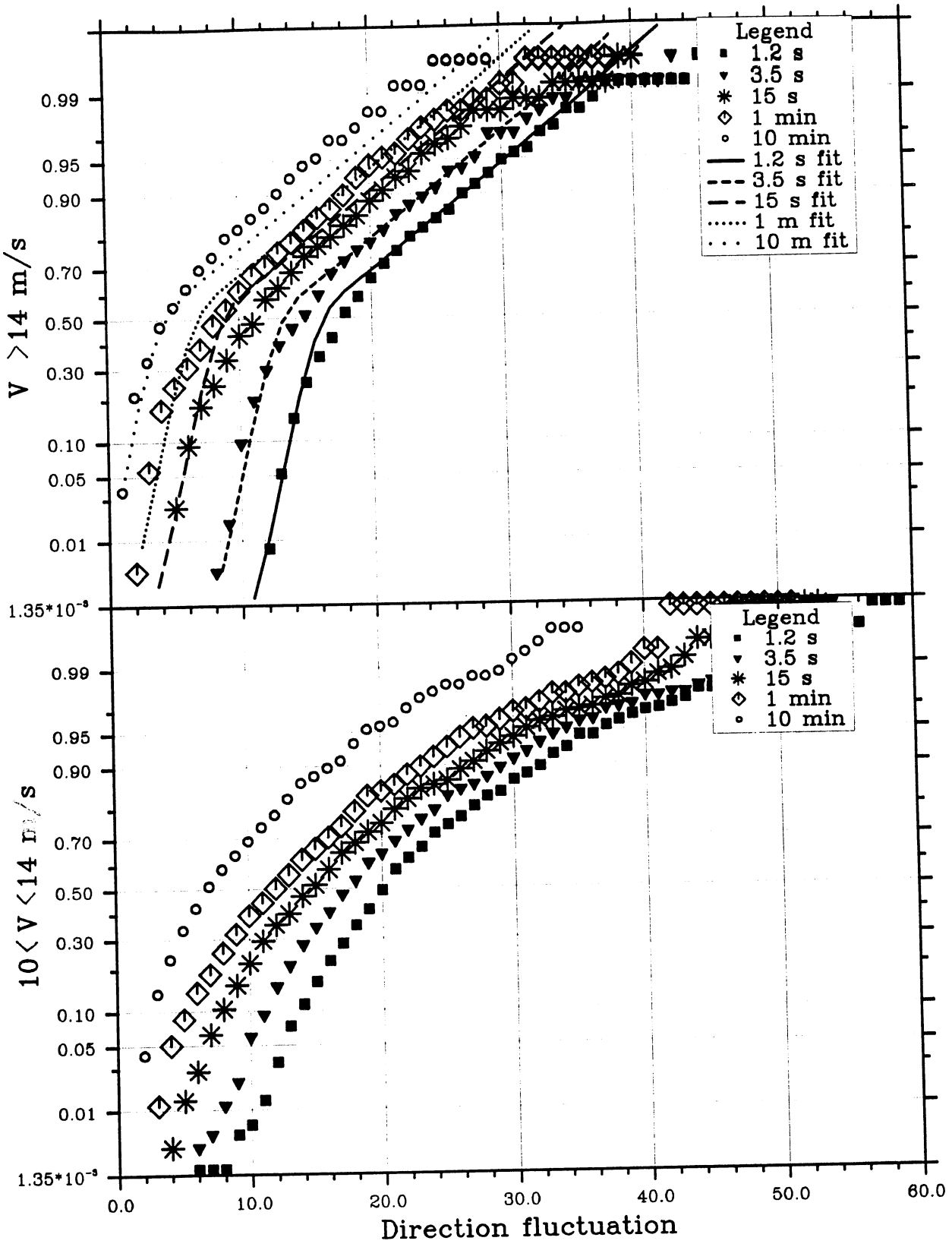

Fig. 4.6.4 Cumulative distributions of the maximum wind direction fluctuations for different averaging intervals at Sletringen. See text for further details.
Top: Reference wind speed exceeding 14 m/s.
Bottom: Reference wind speed in the range 10 - 14 m/s.

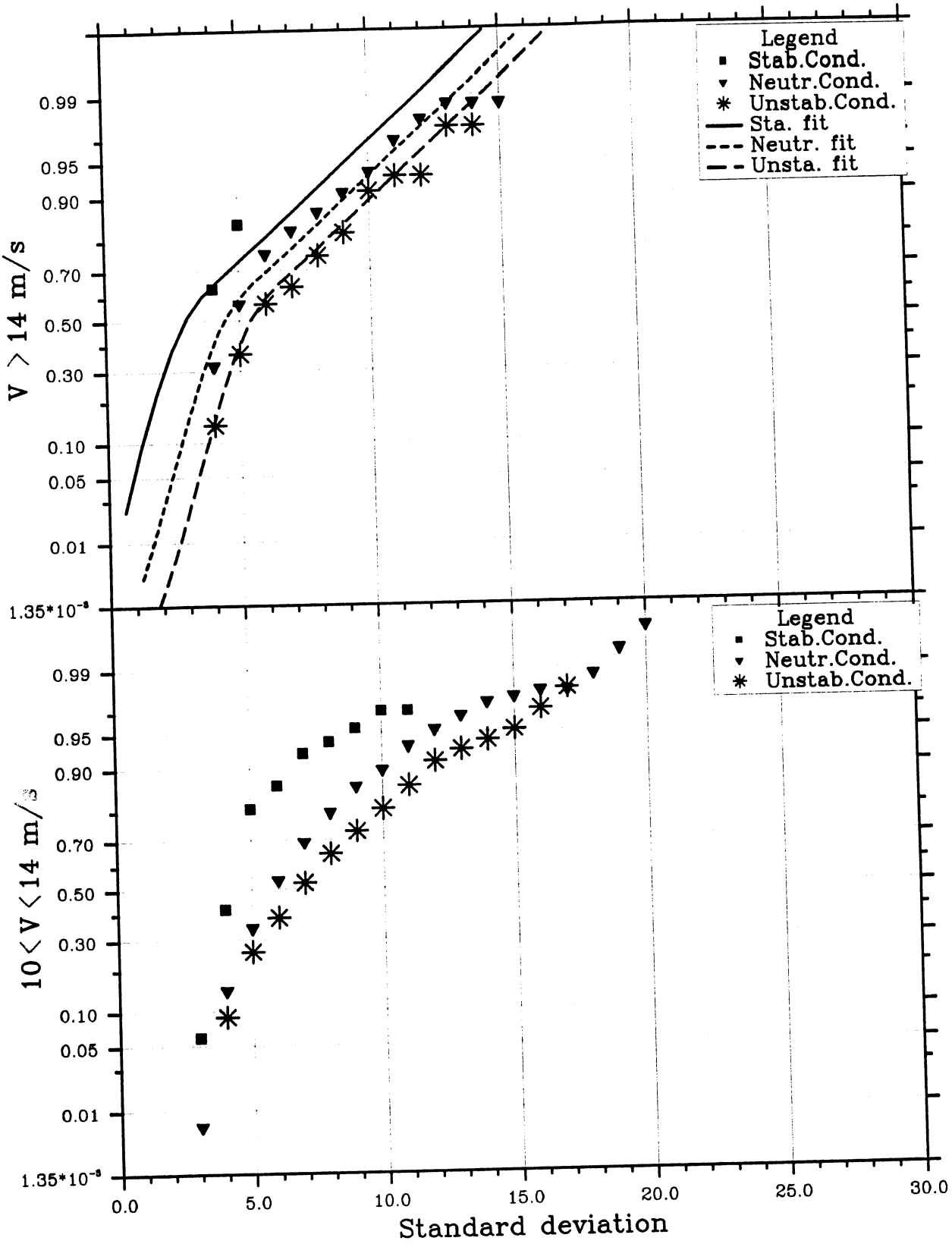

Fig. 4.6.5 Cumulative distributions of the 1 h standard deviation of wind direction for 2 ranges of reference wind speed and 3 ranges of lapse rate. The data shown are from 45 m height at Sletringen. See text for further details.

FIGURES FOR SECTION 5

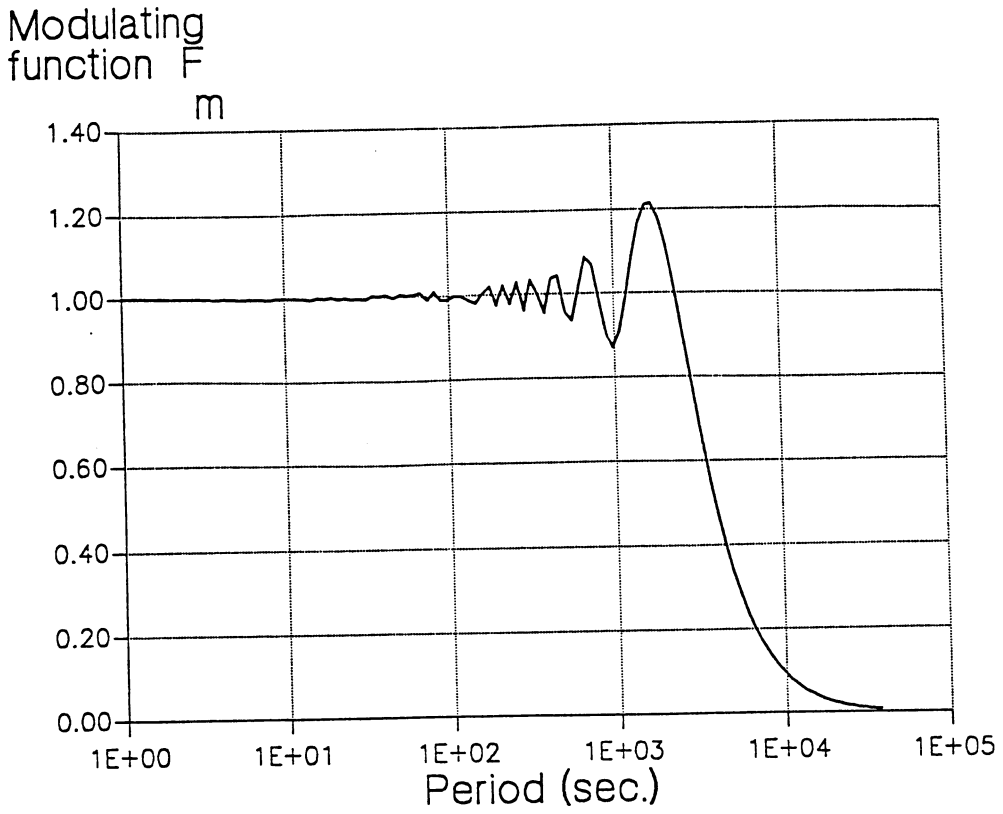

Fig. 5.2.1 The modulating function F_M in Eq. 2 versus period τ_m for T = 40 min.

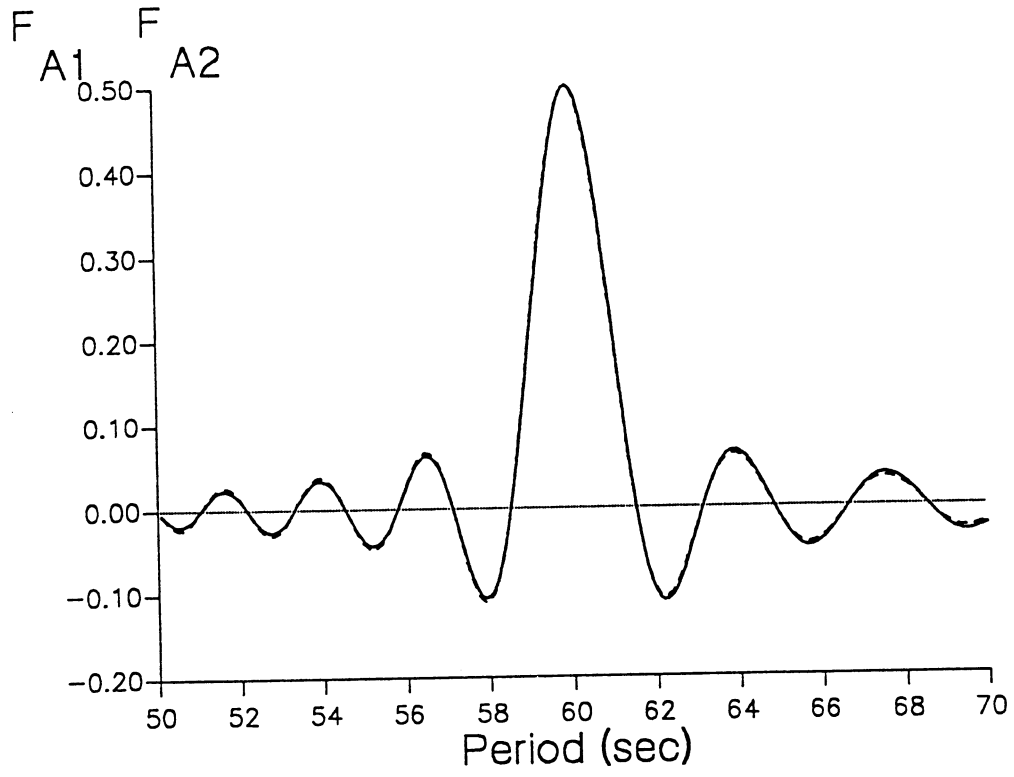

Fig. 5.2.2 Weight functions F_{A1} and F_{A2} for the 1 min Fourier-components (see Eq. 3b).

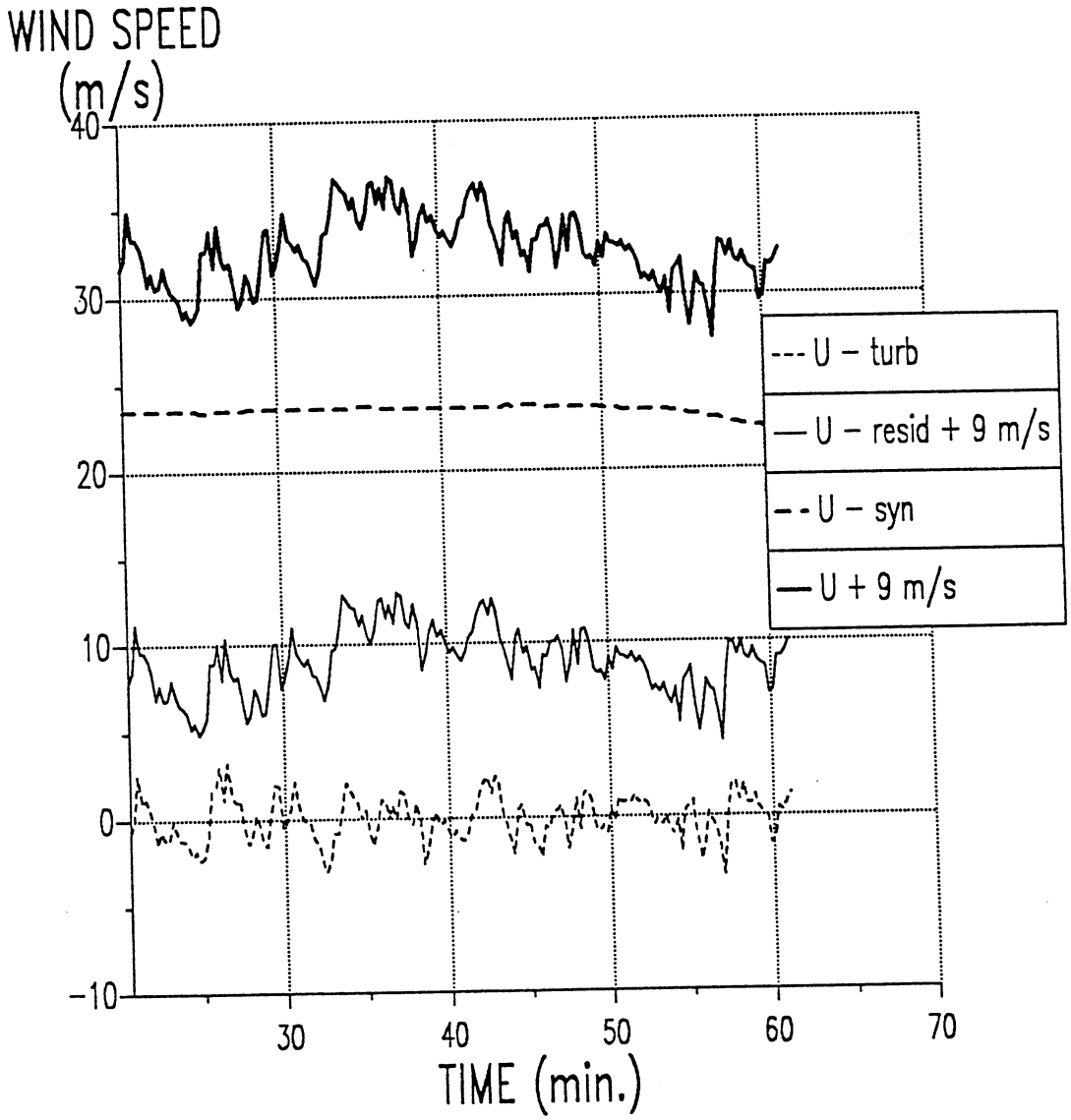

Fig. 5.2.3 Example of the basic, synoptic, residual and turbulent time series as defined.

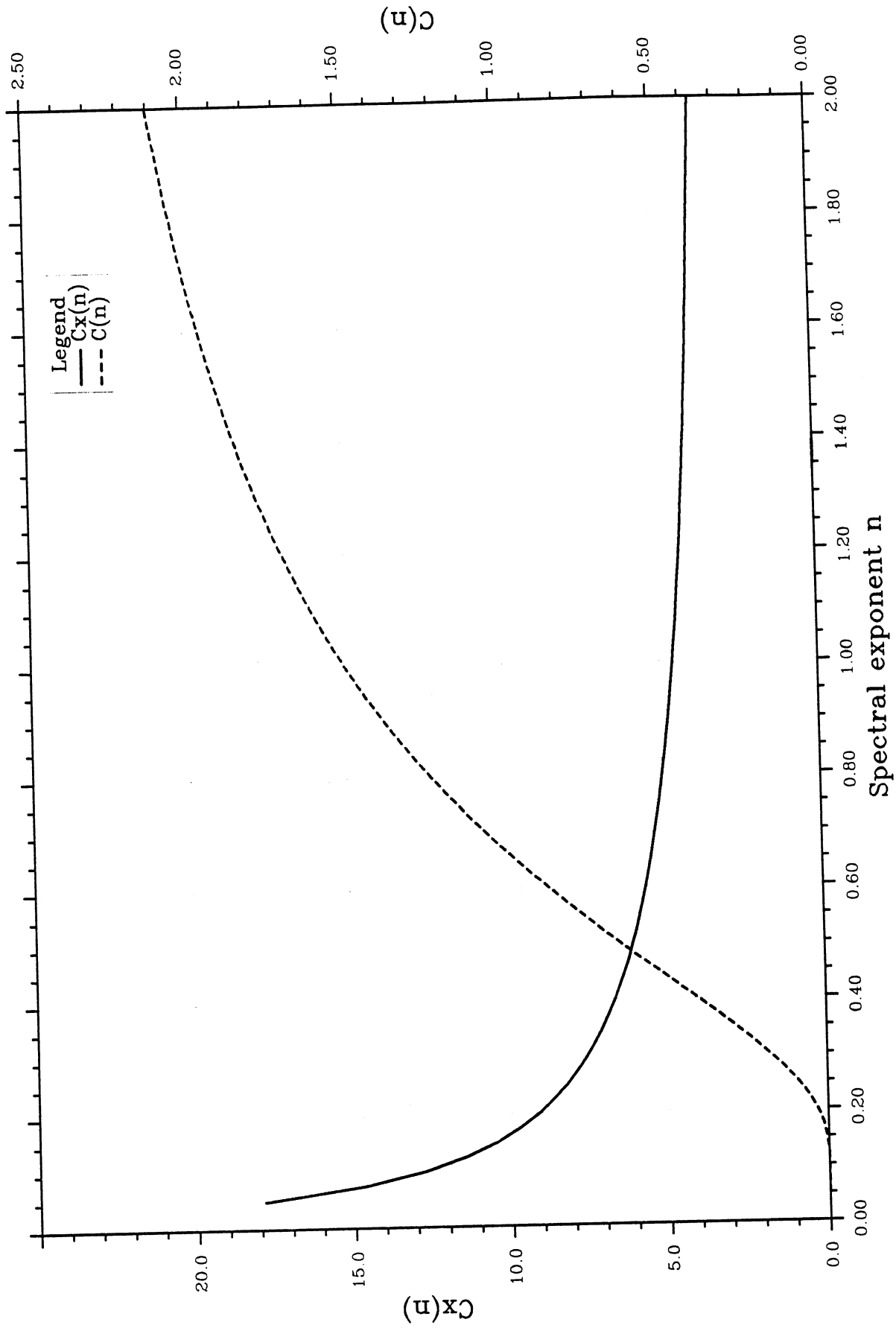

Fig. 5.3.1a The functions C(n) (dashed line) and Cx(n), which determines the total variance as a function of the spectral shape coefficient n. See text for further discussion.

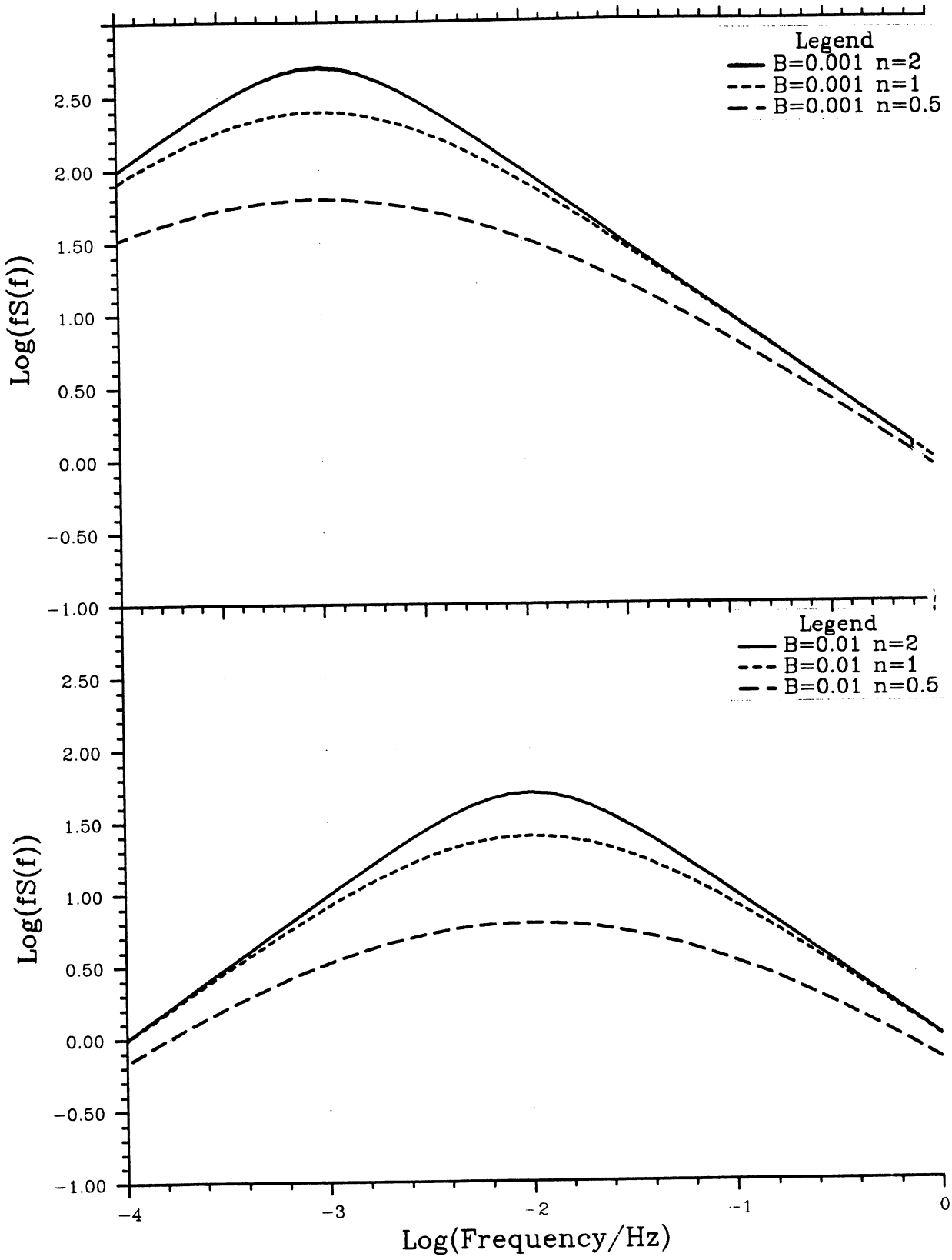

Fig. 5.3.1b Examples of the generalized spectral function, Eq. (7) for A=1 and values of B and n as indicated.

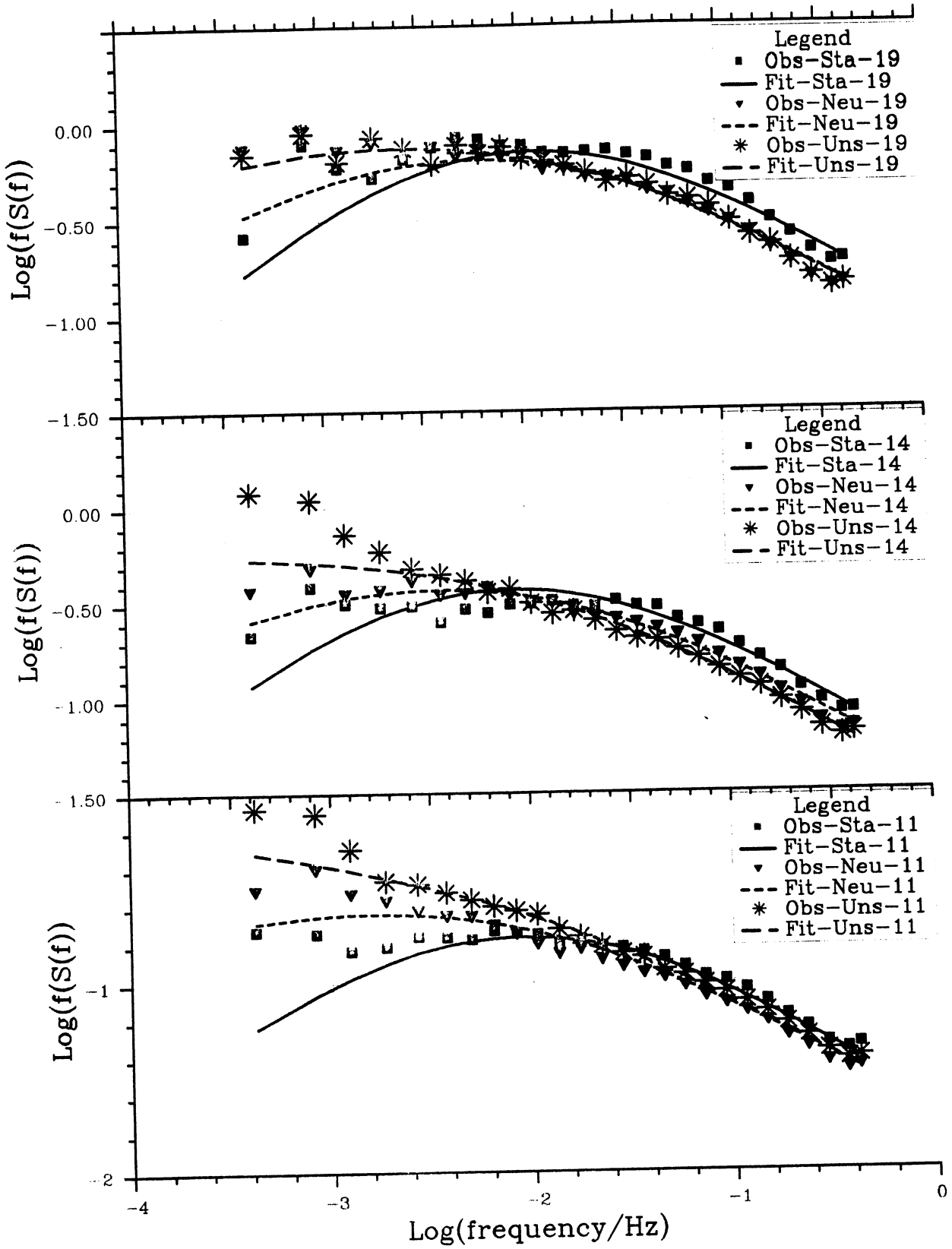

Fig. 5.3.2 Average spectra for the heights 46 and 42 m at Sletringen versus frequency for 3 classes of reference wind speed (the class mean is indicated) and 3 classes of lapse rate.

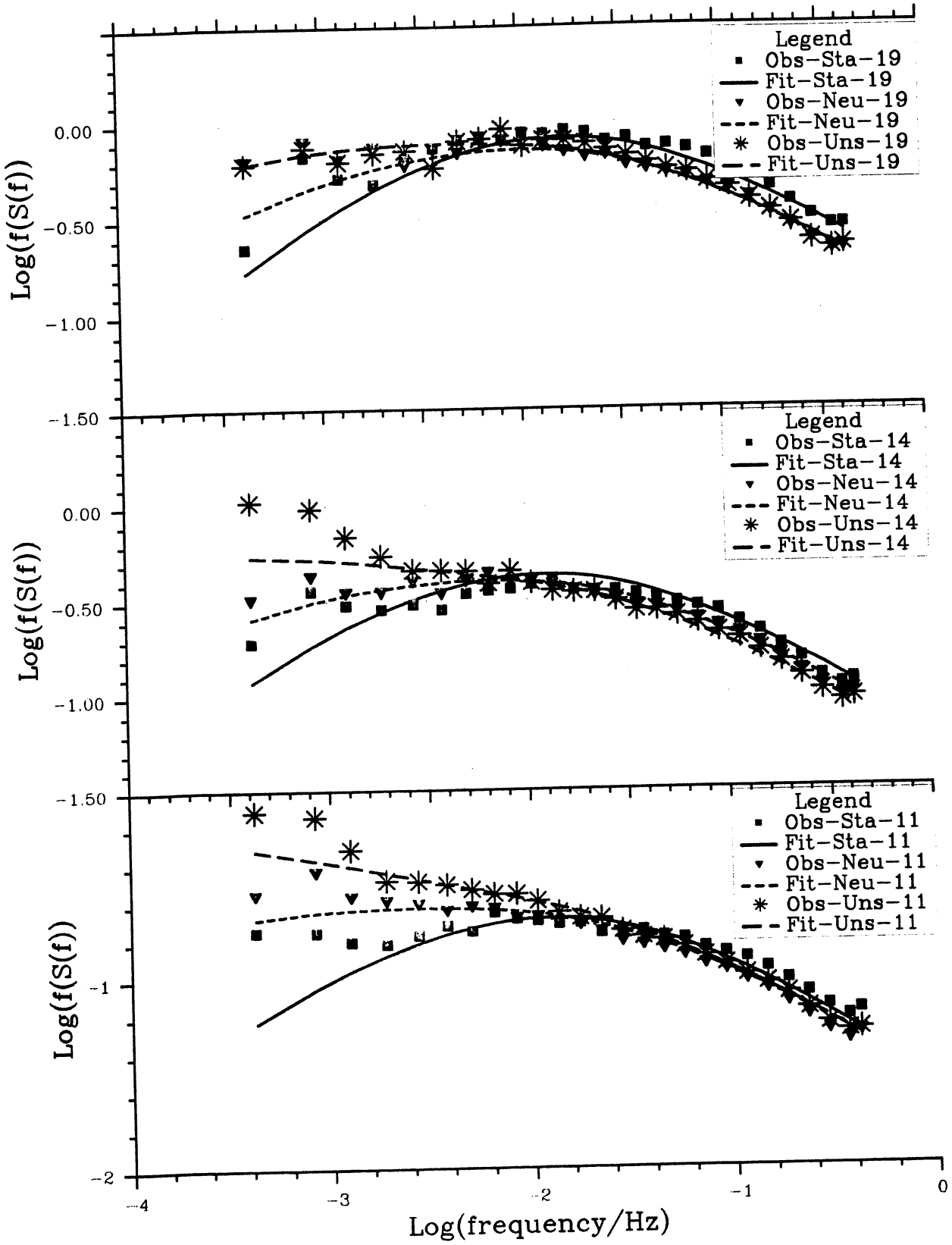

Fig. 5.3.3 As Fig. 5.3.2, but for 20 m height.

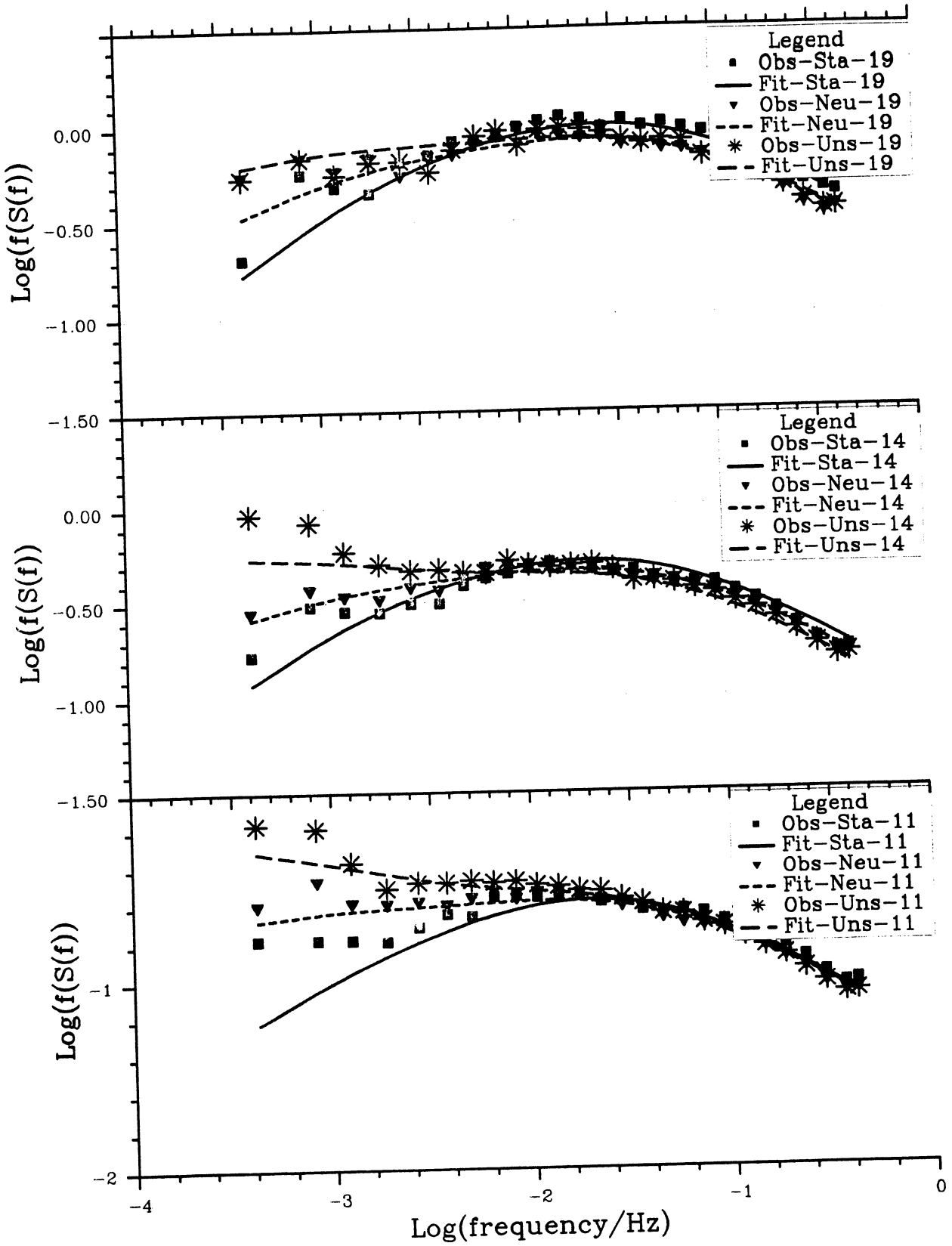

Fig. 5.3.4 As Fig. 5.3.2, but for 10 m height.

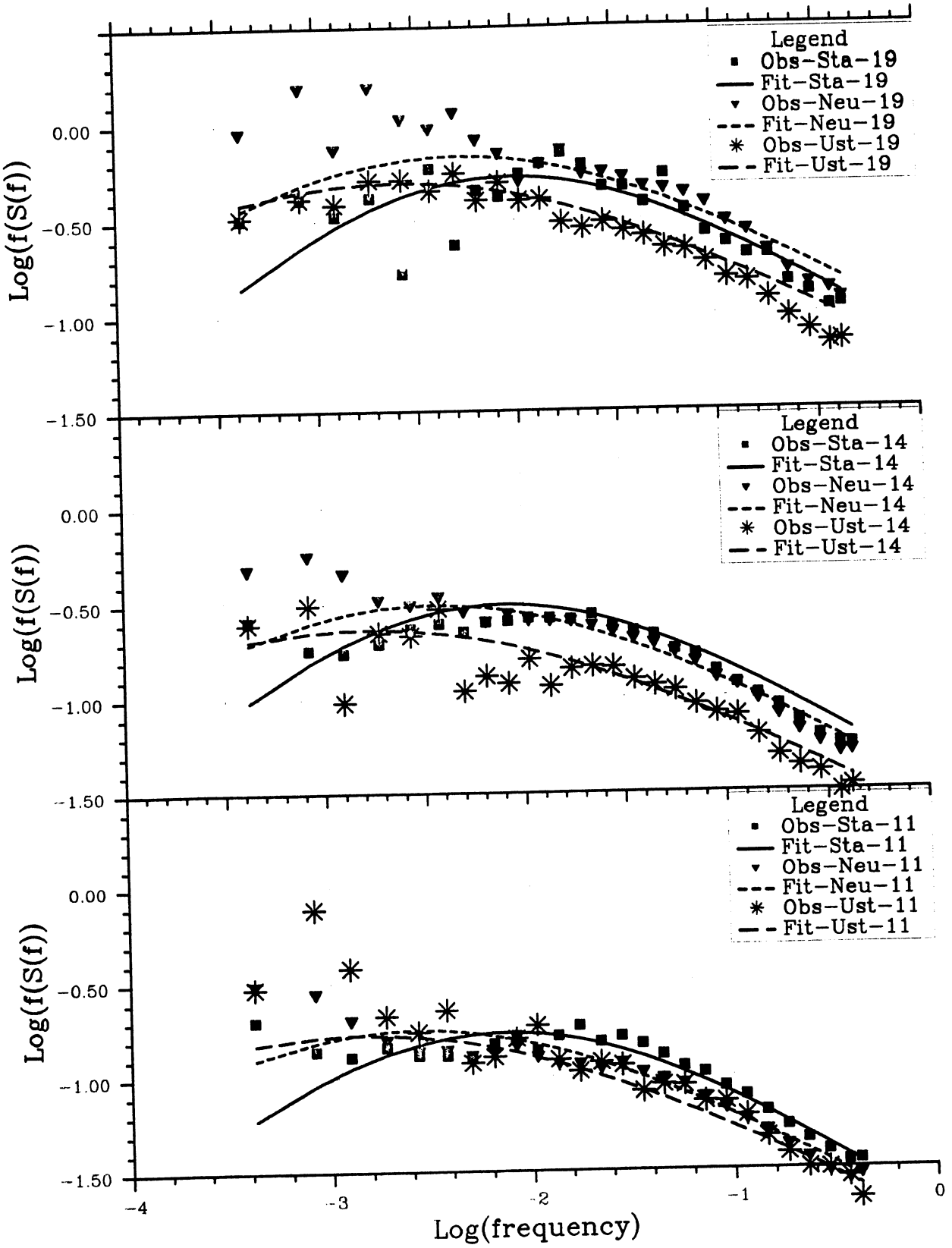

Fig. 5.3.5 As Fig. 5.3.2, but for 100 m height and maritime sector at Skipheia.

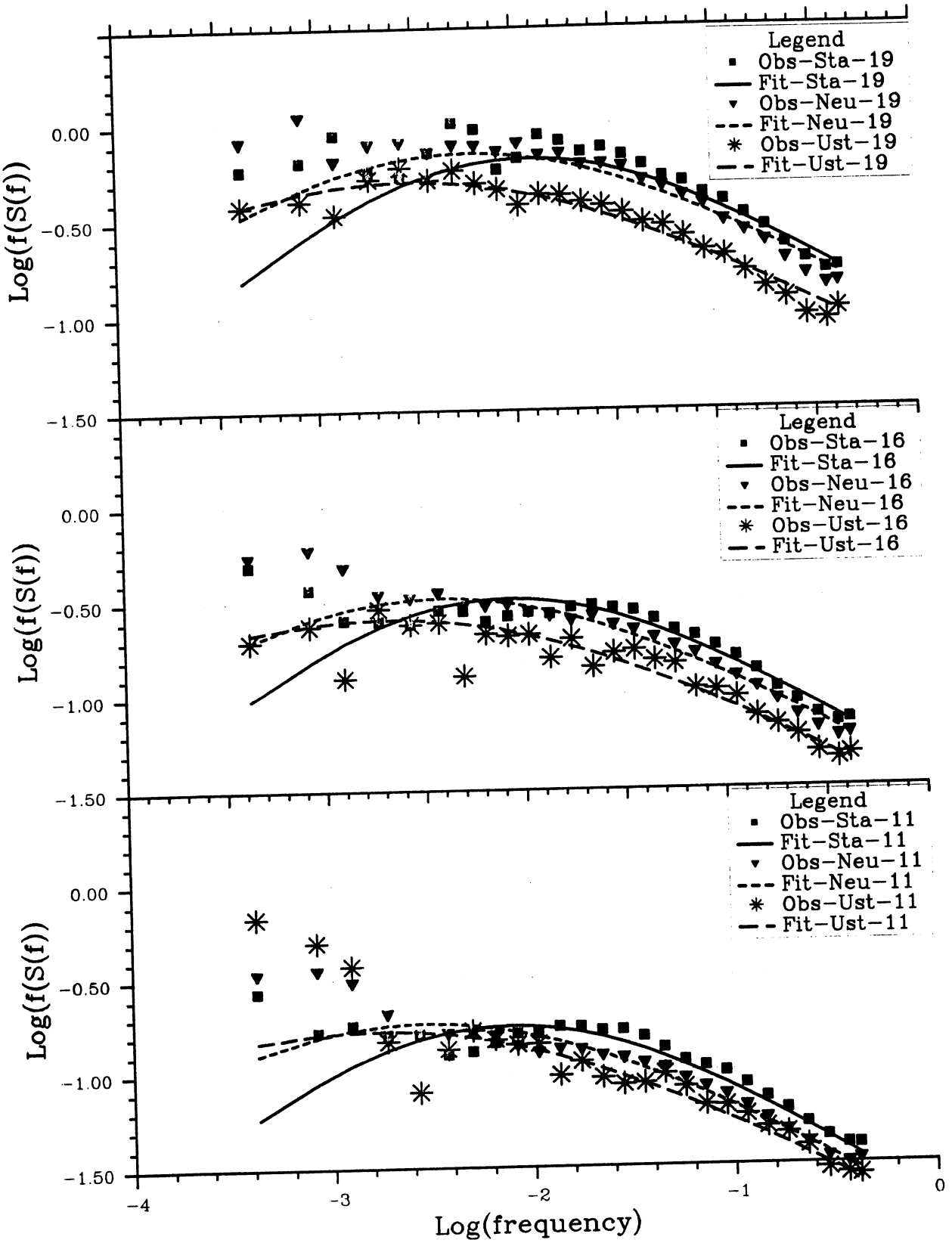

Fig. 5.3.6 As Fig. 5.3.2, but for 70 m height and maritime sector at Skipheia.

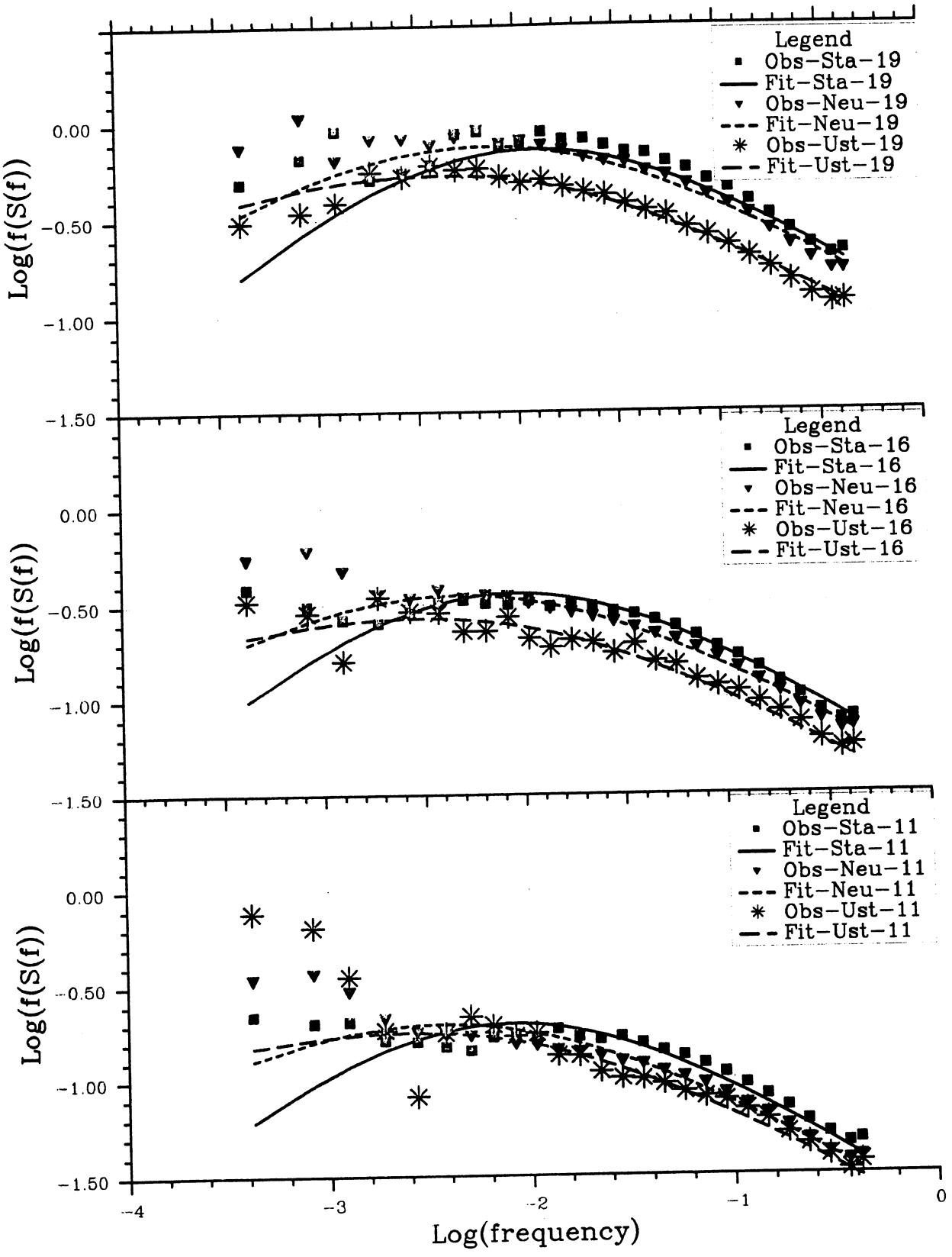

Fig. 5.3.7 As Fig. 5.3.2, but for 40 m height and maritime sector at Skipheia.

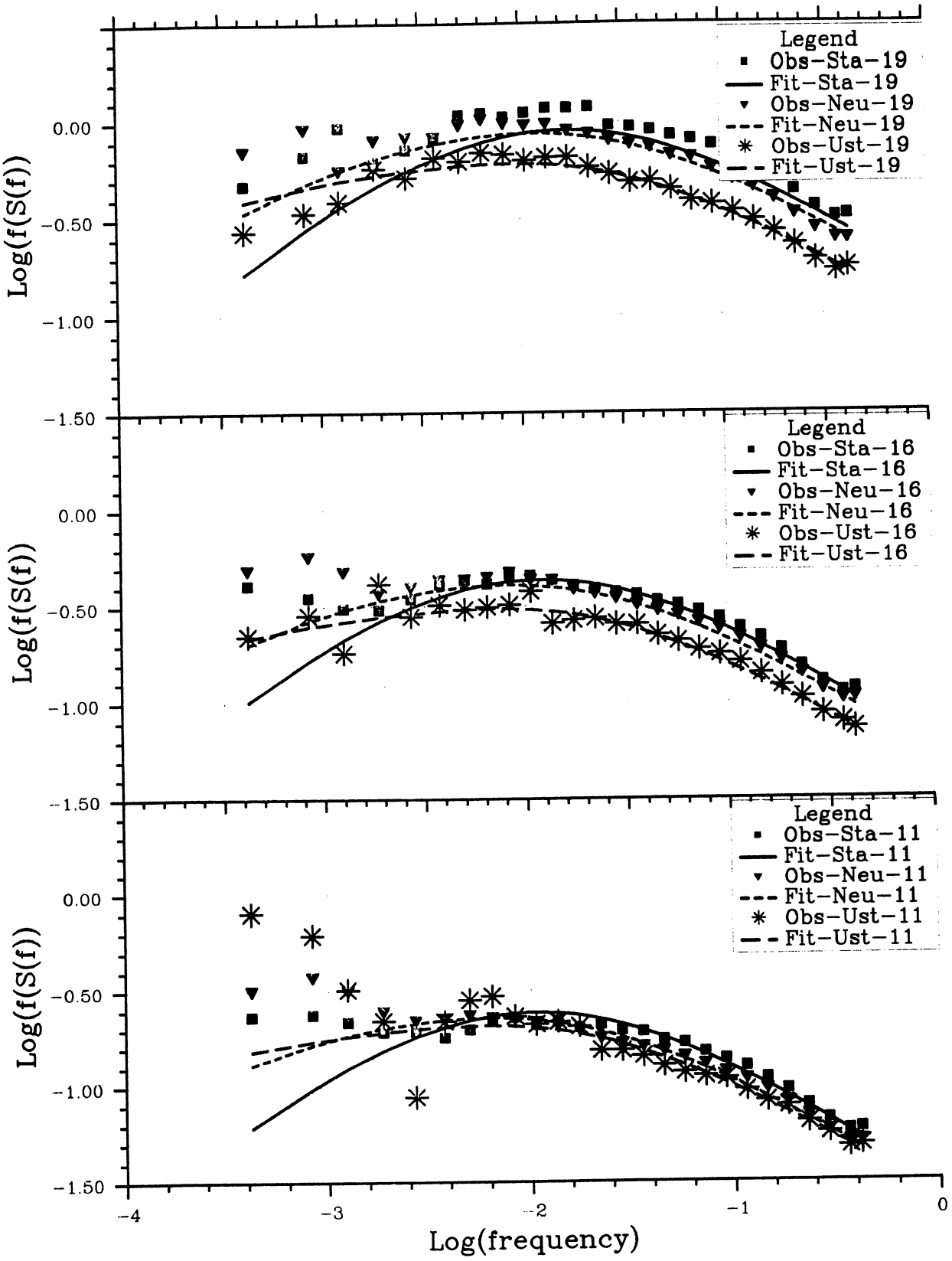

Fig. 5.3.8 As Fig. 5.3.2, but for 20 m height and maritime sector at Skipheia.

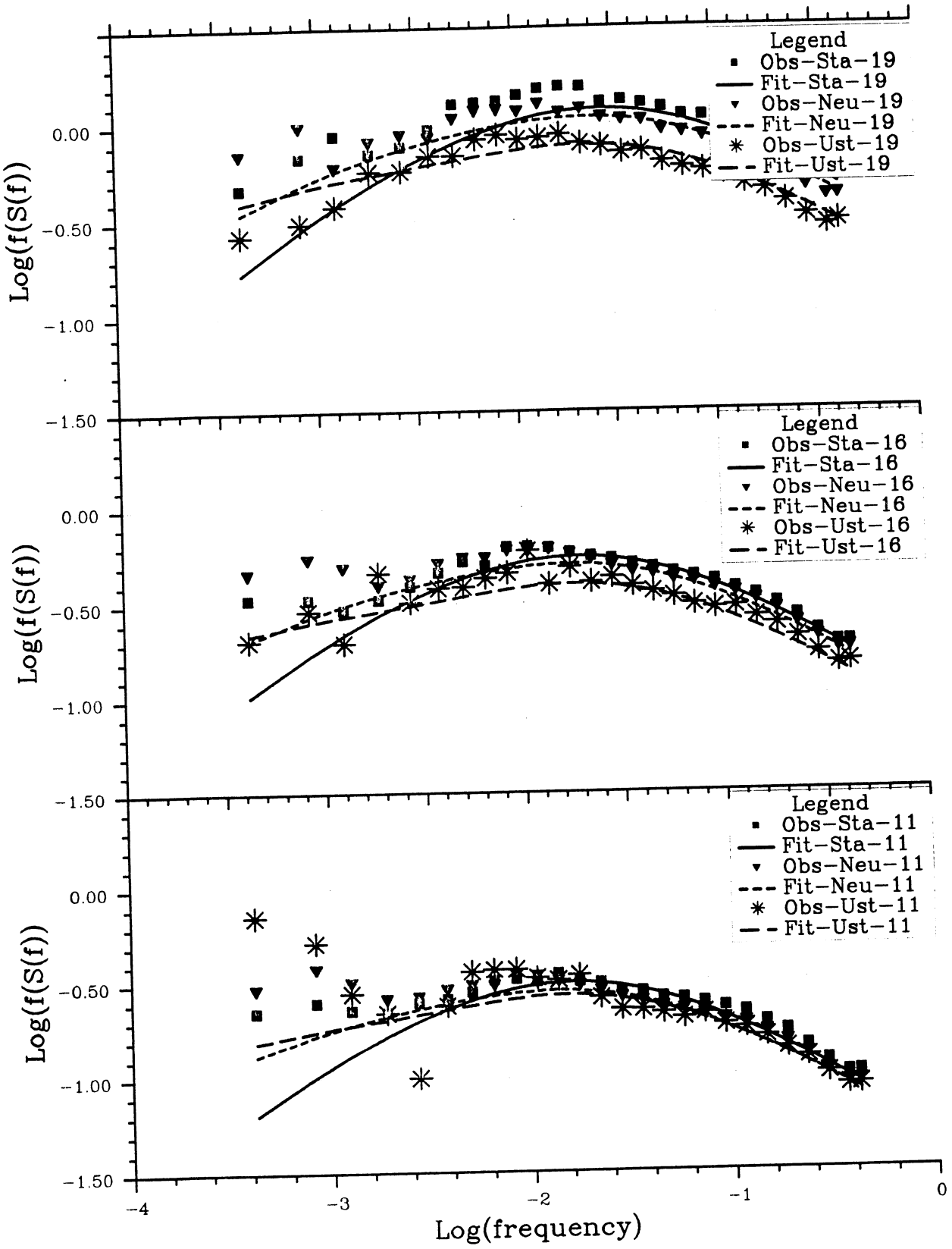

Fig. 5.3.9 As Fig. 5.3.2, but for 10 m height and maritime sector at Skipheia.

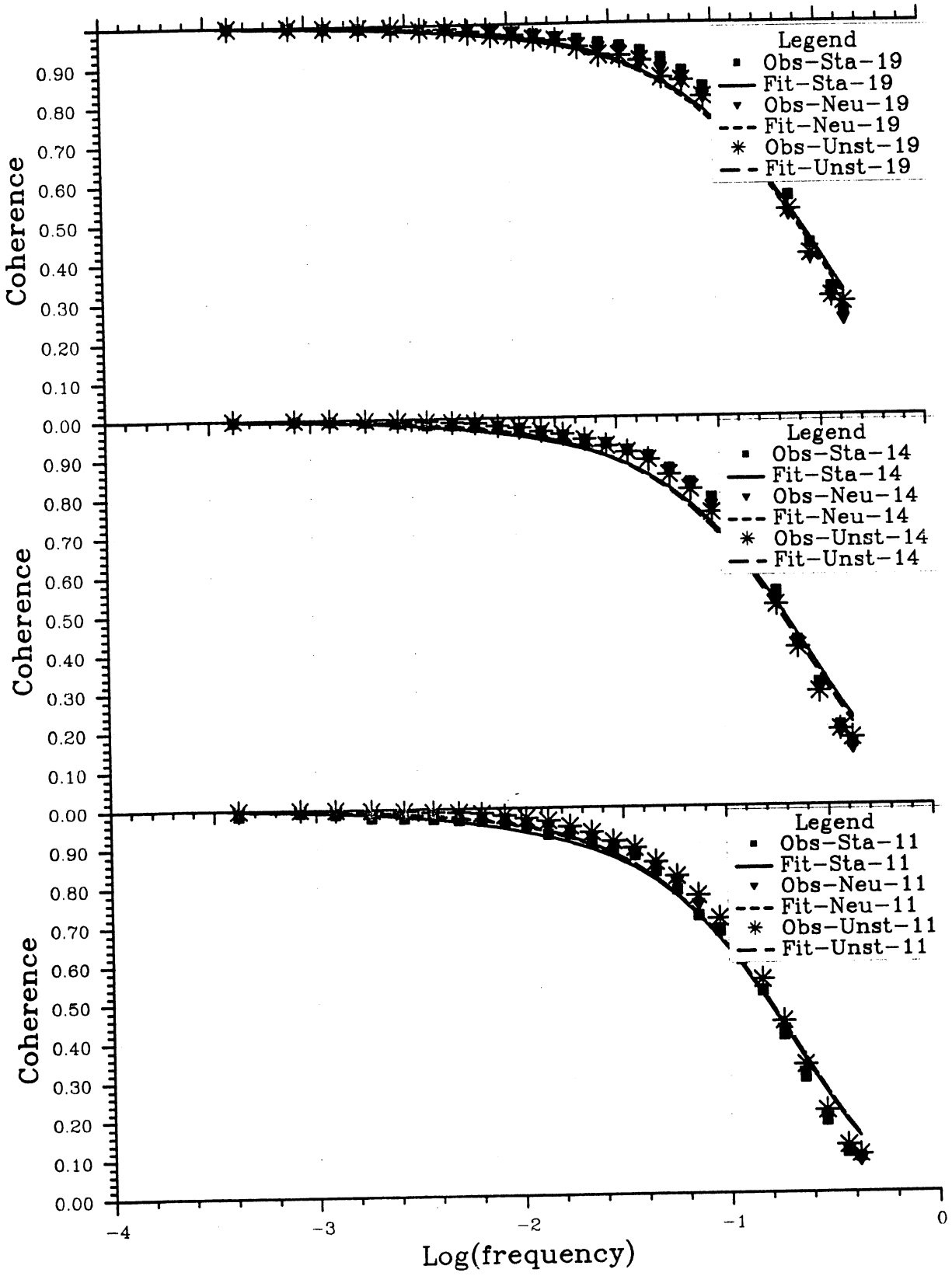

Fig. 5.4.1 Vertical coherence of wind speed between the heights 46 and 42 m at Sletringen versus frequency for 3 wind speed classes and 3 lapse rate classes as indicated.

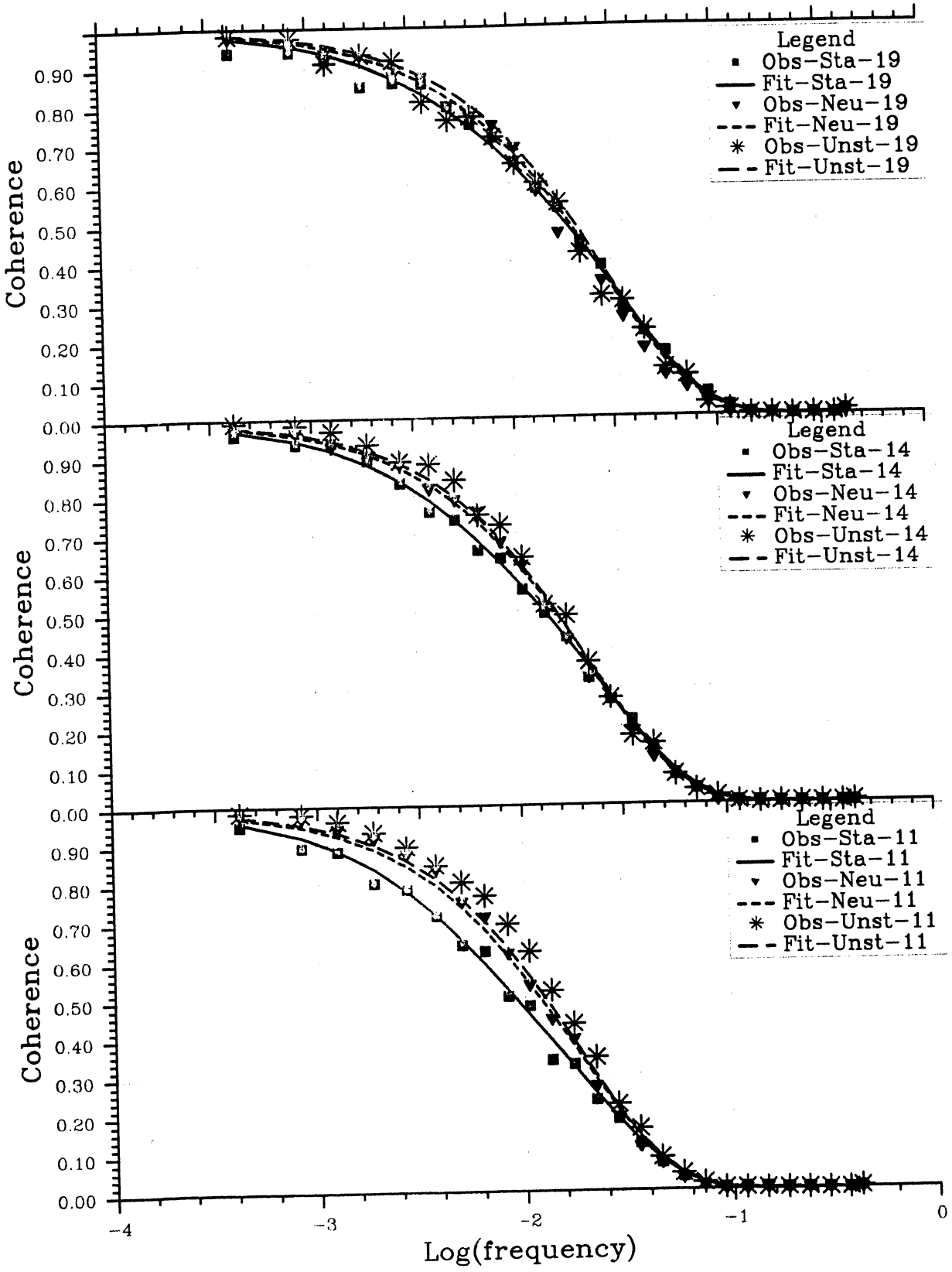

Fig. 5.4.2 As Fig. 5.4.1, but between the heights 46 and 20 m.

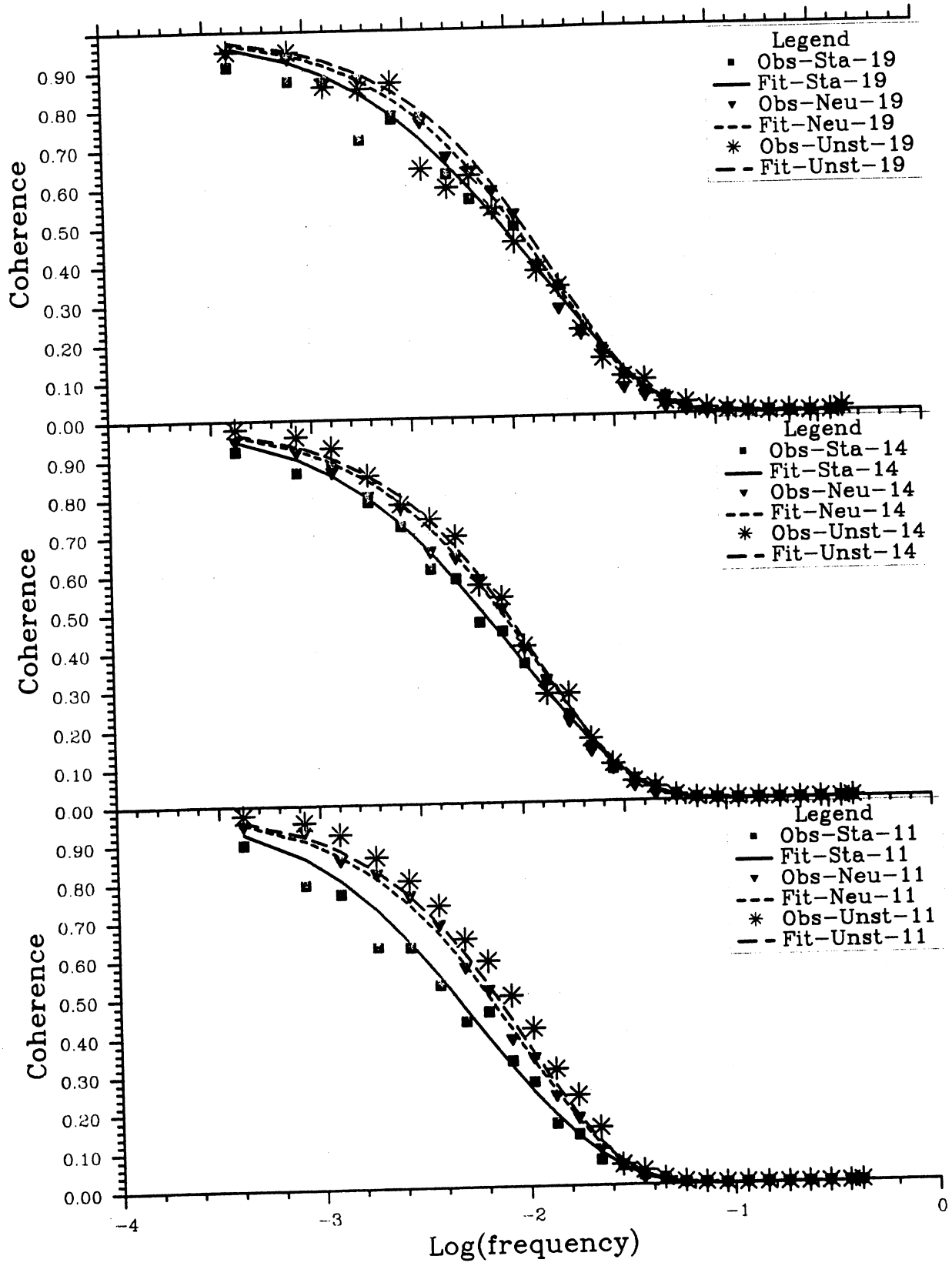

Fig. 5.4.3 As Fig. 5.4.1, but between the heights 46 and 10 m.

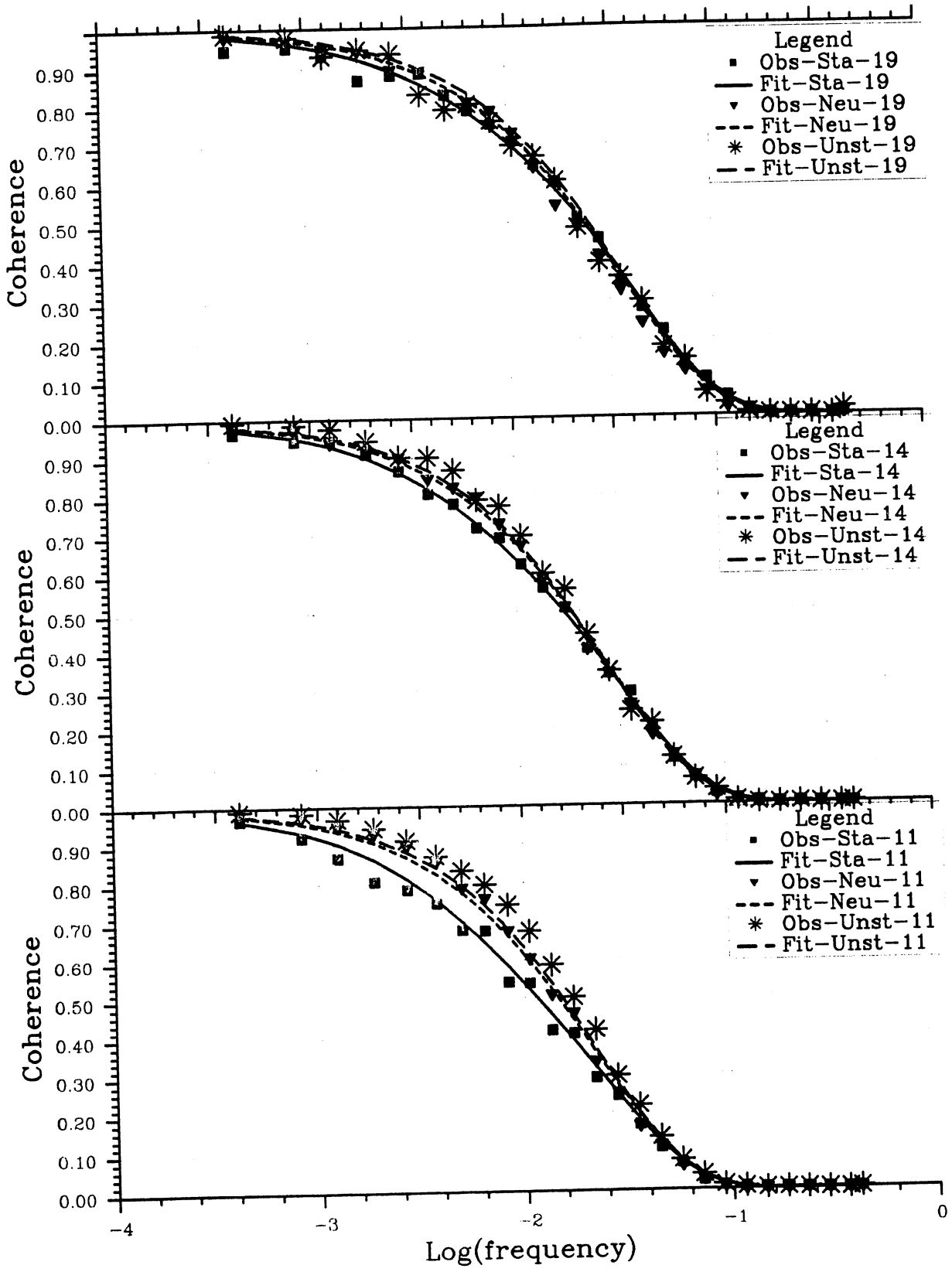

Fig. 5.4.4 As Fig. 5.4.1, but between the heights 42 and 20 m.

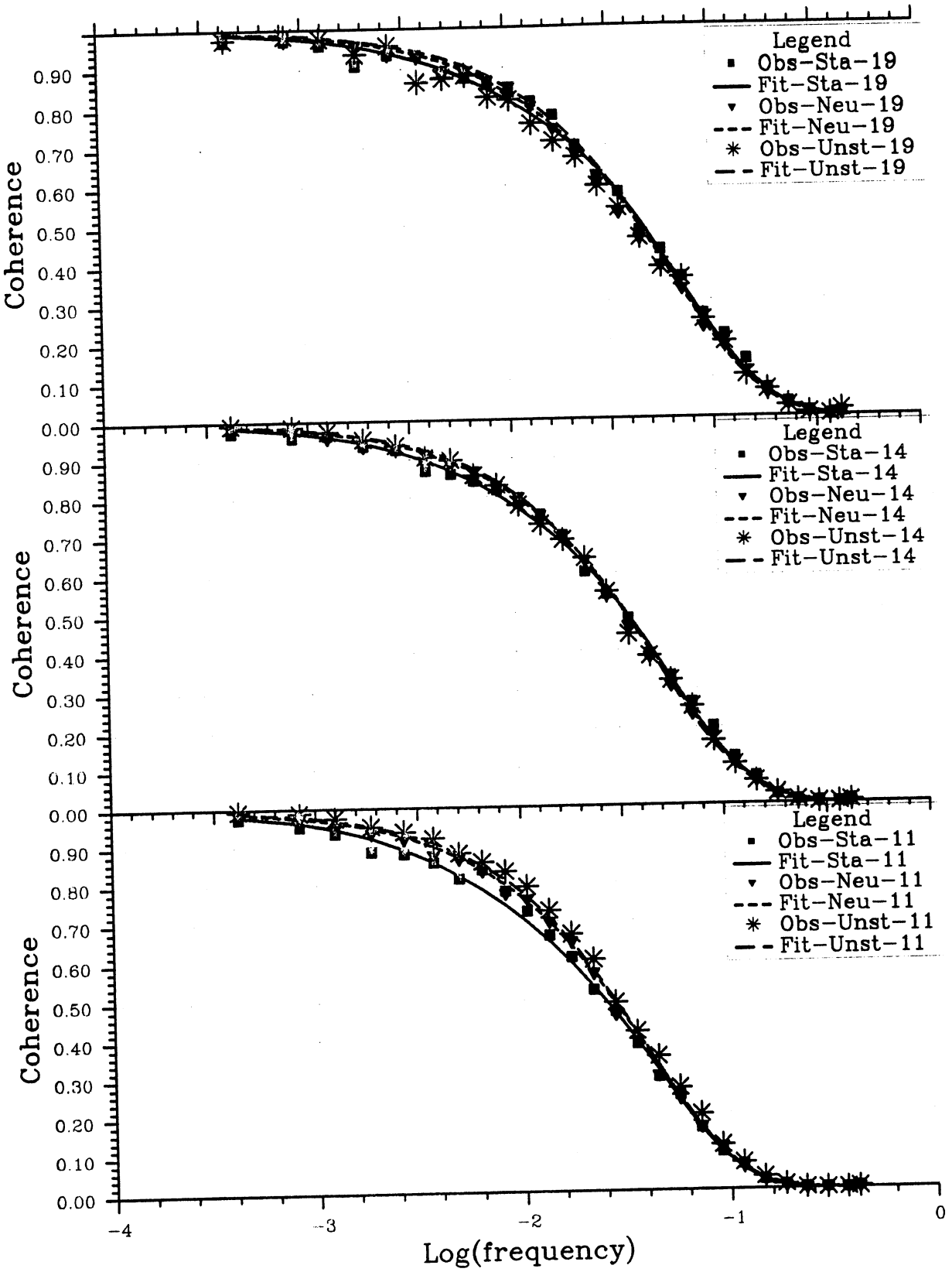

Fig. 5.4.5 As Fig. 5.4.1, but between the heights 20 and 10 m.

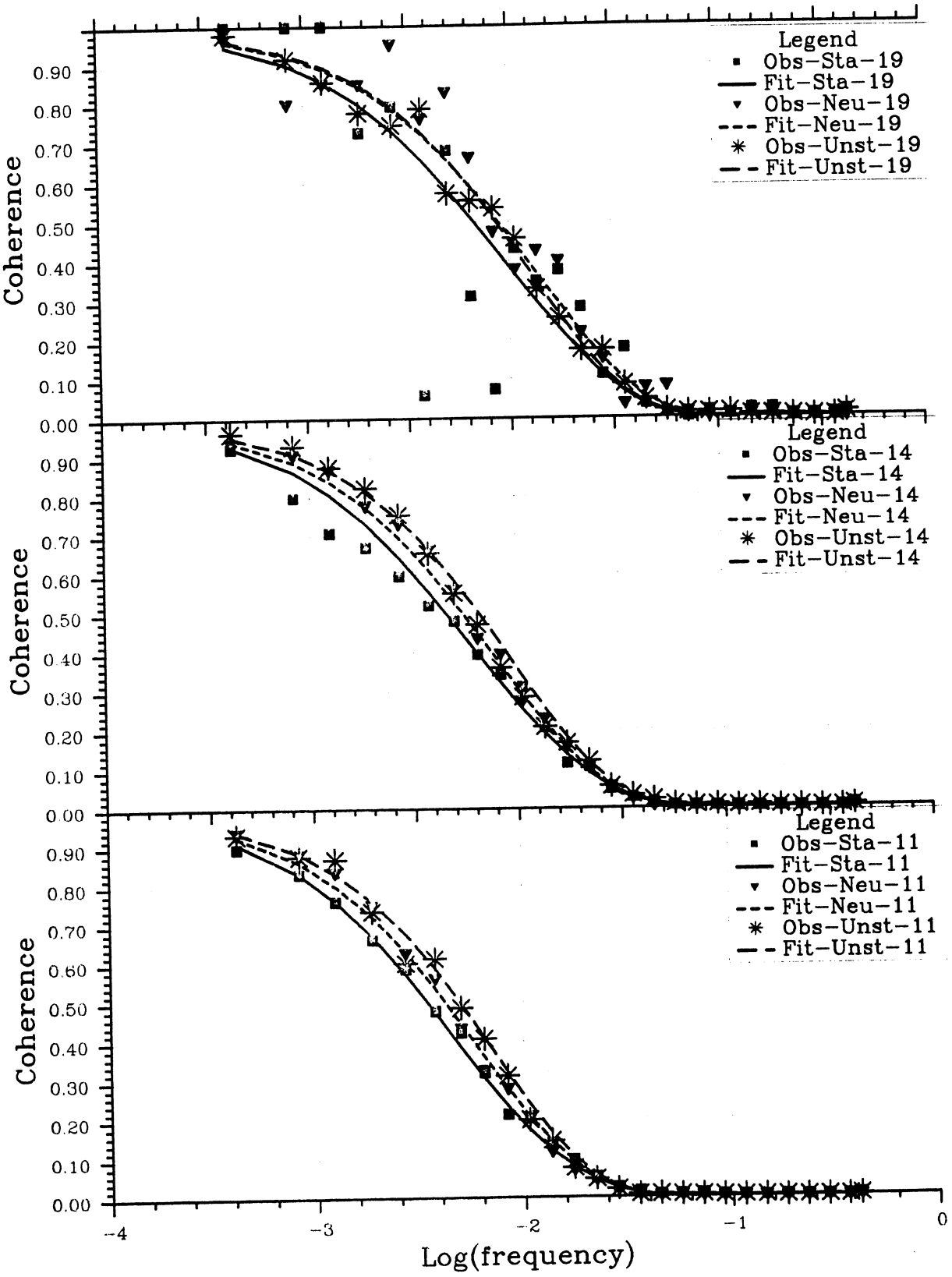

Fig. 5.4.6 As Fig. 5.4.1, but between the heights 100 and 40 m at Skipheia (mean for 2 masts).

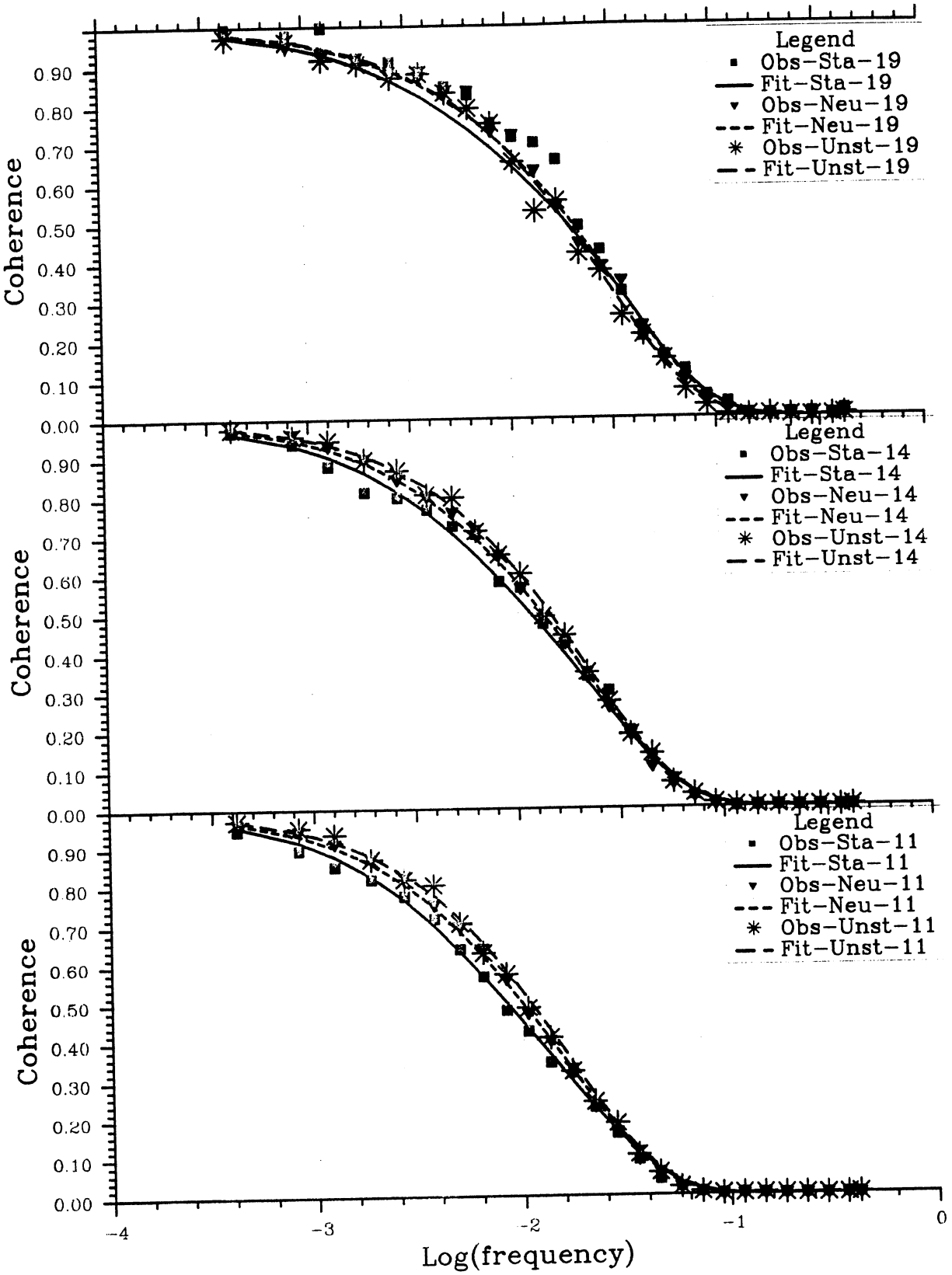

Fig. 5.4.7 As Fig. 5.4.1, but between the heights 70 and 40 m at Skipheia (1 mast).

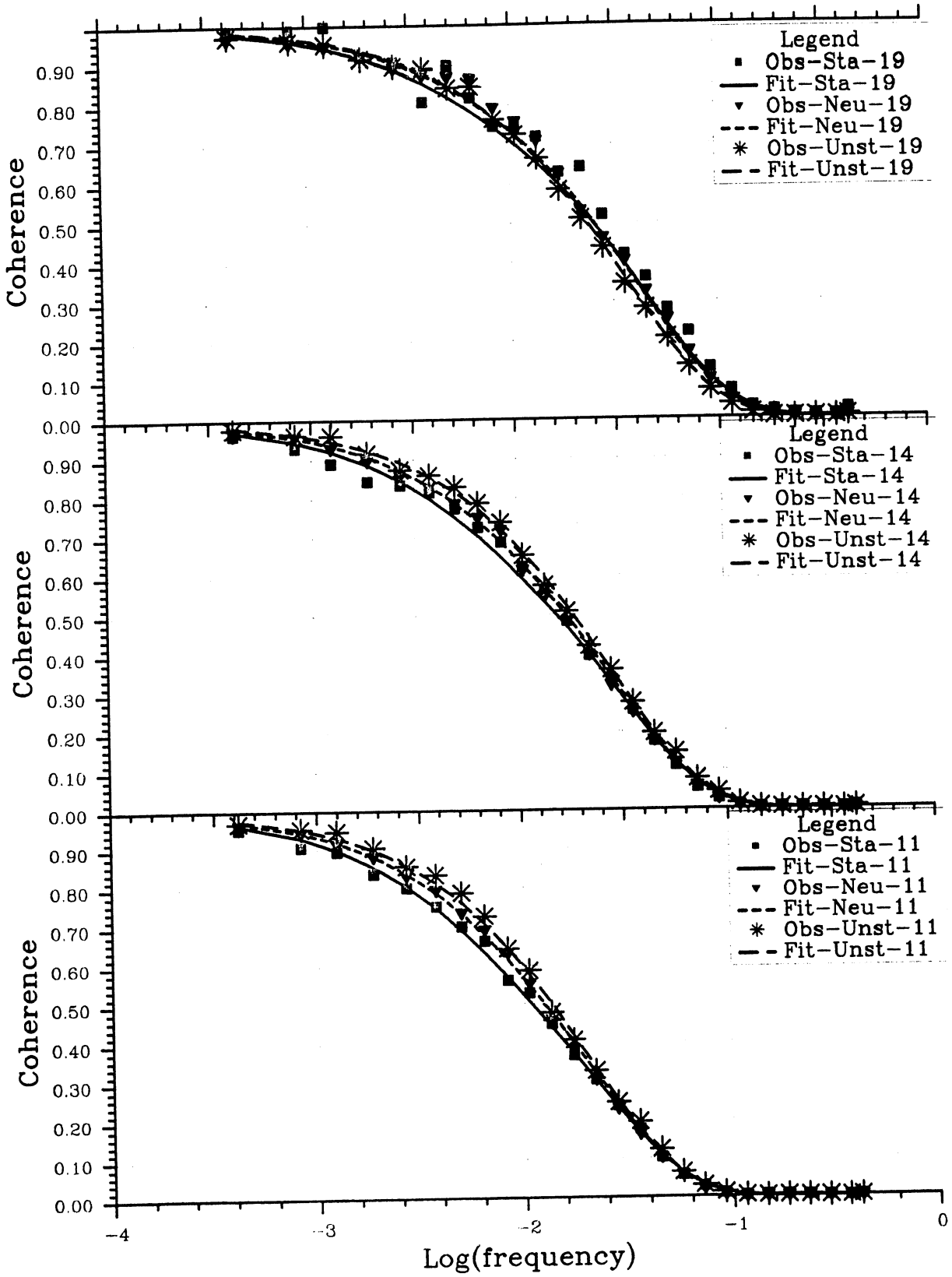

Fig. 5.4.8 As Fig. 5.4.1, but between the heights 40 and 20 m at Skipheia (mean for 3 masts).

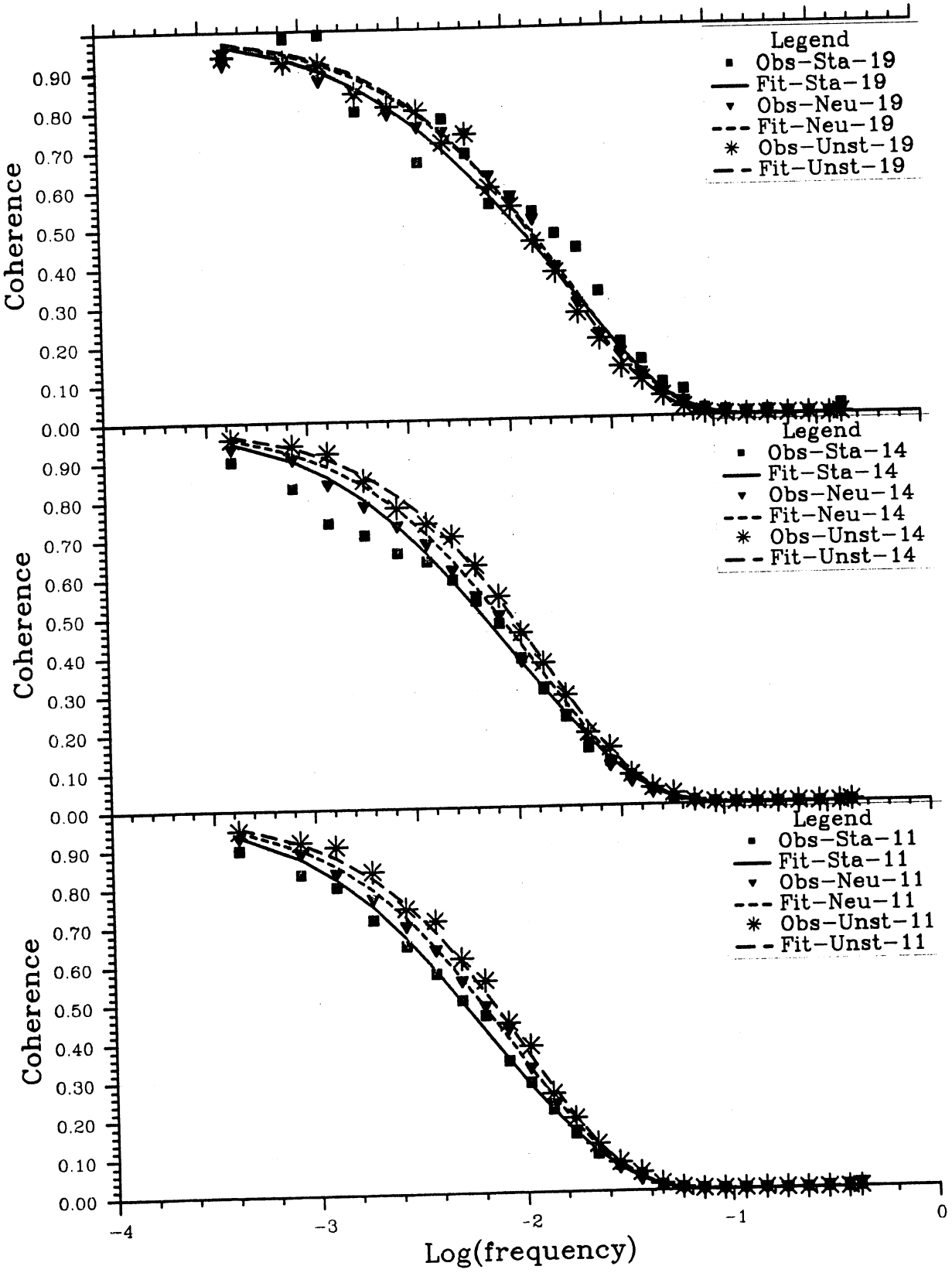

Fig. 5.4.9 As Fig. 5.4.1, but between the heights 40 and 10 m at Skipheia (mean for 3 masts).

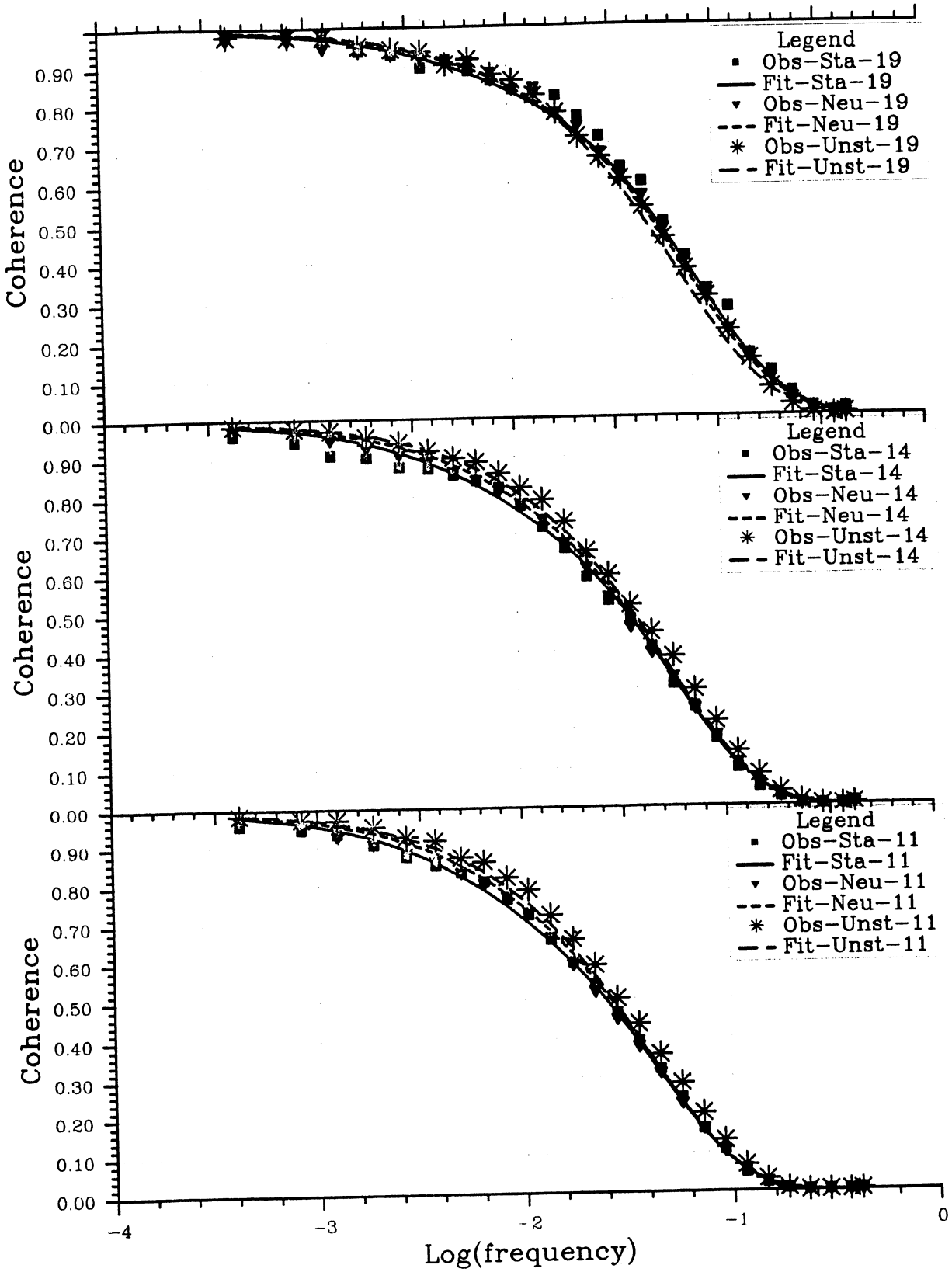

Fig. 5.4.10 As Fig. 5.4.1, but between the heights 20 and 10 m at Skipheia (mean for 3 masts).

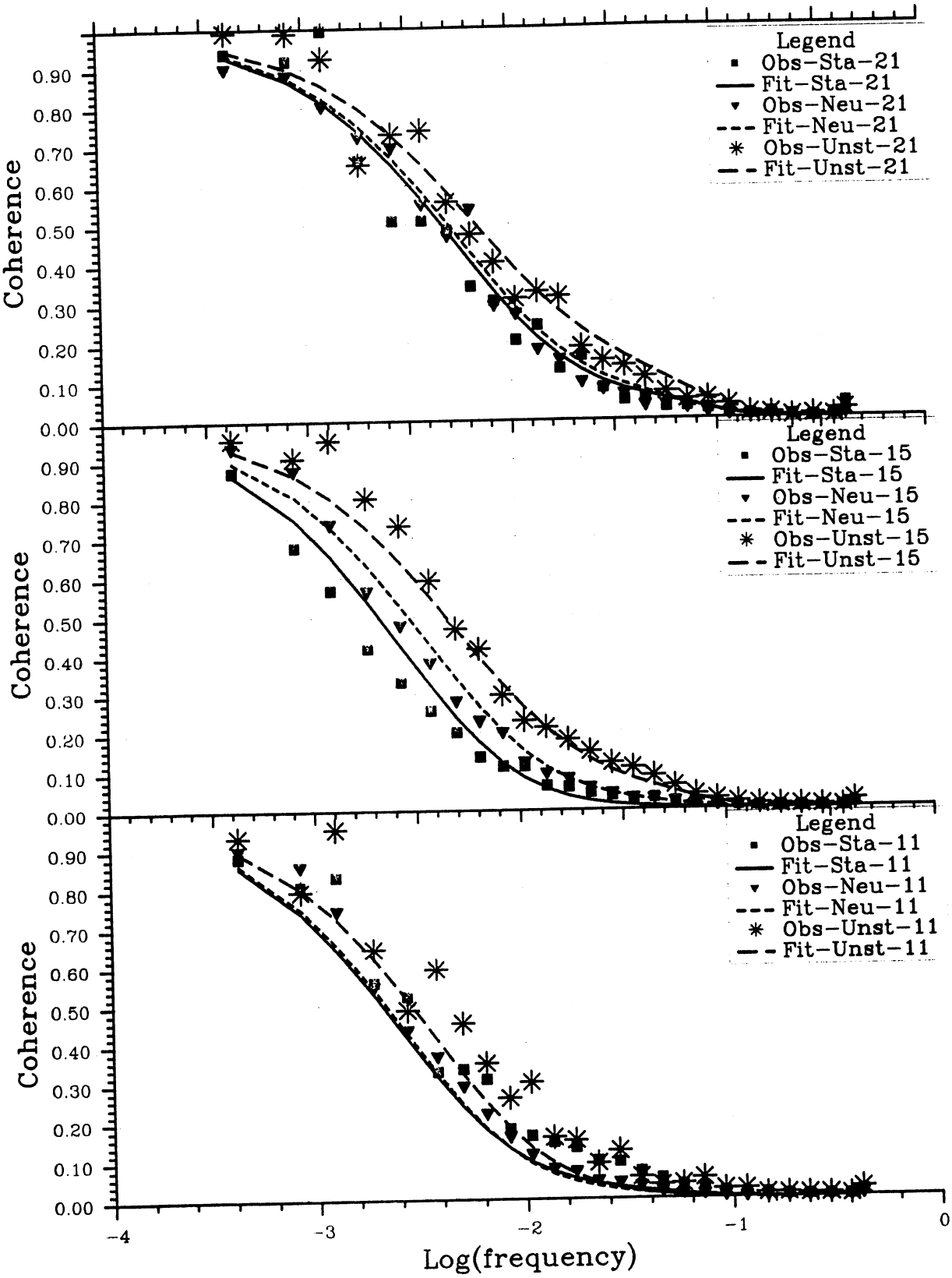

Fig. 5.4.11 Coherence of wind speed for horizontal separation versus frequency for 3 masts and 40 m height in the restricted maritime sector at Skipheia. Speed and lapse rate classes as indicated.

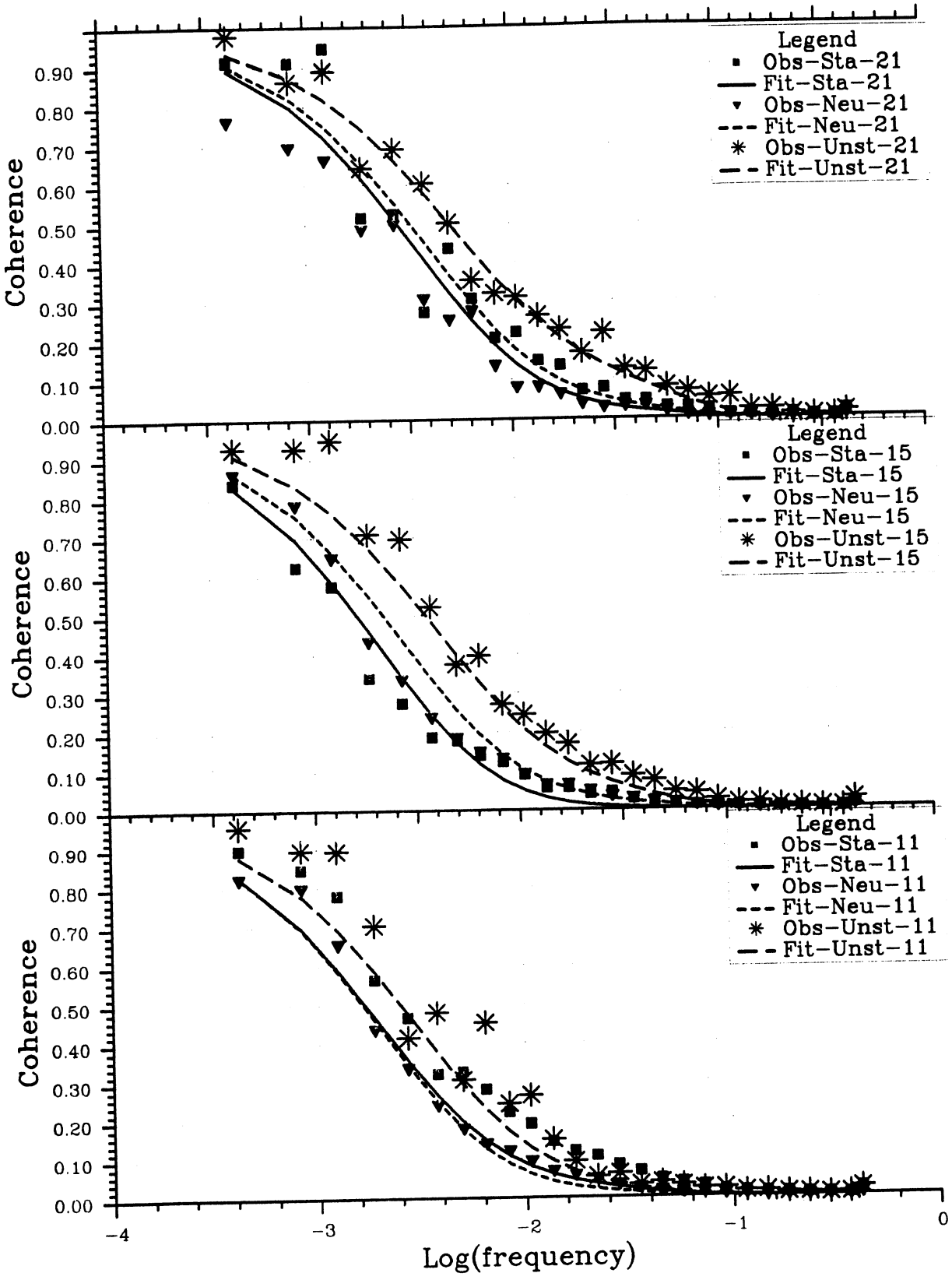

Fig. 5.4.12 As Fig. 5.4.11, but for 20 m height.

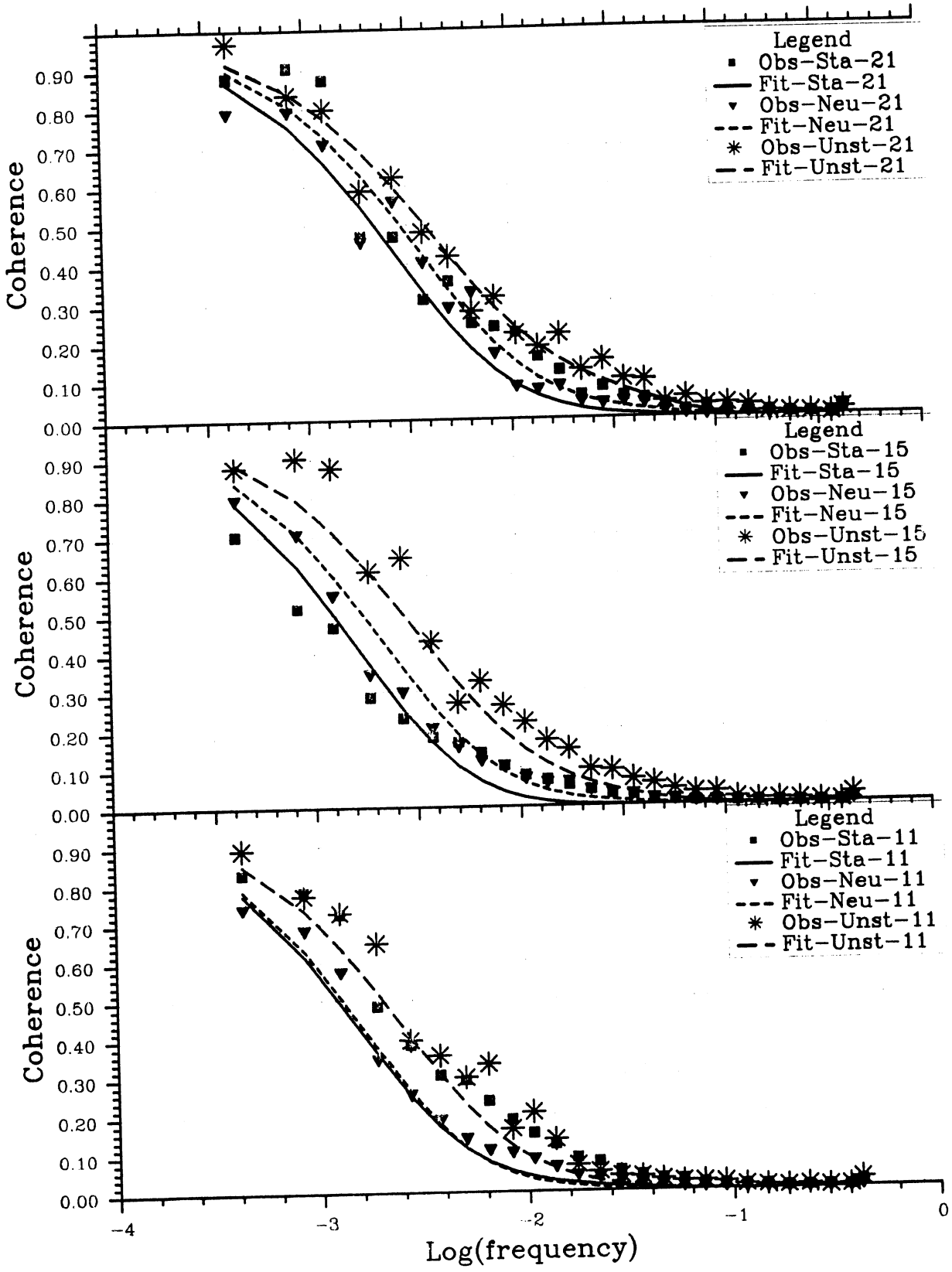

Fig. 5.4.13 As Fig. 5.4.11, but for 10 m height.

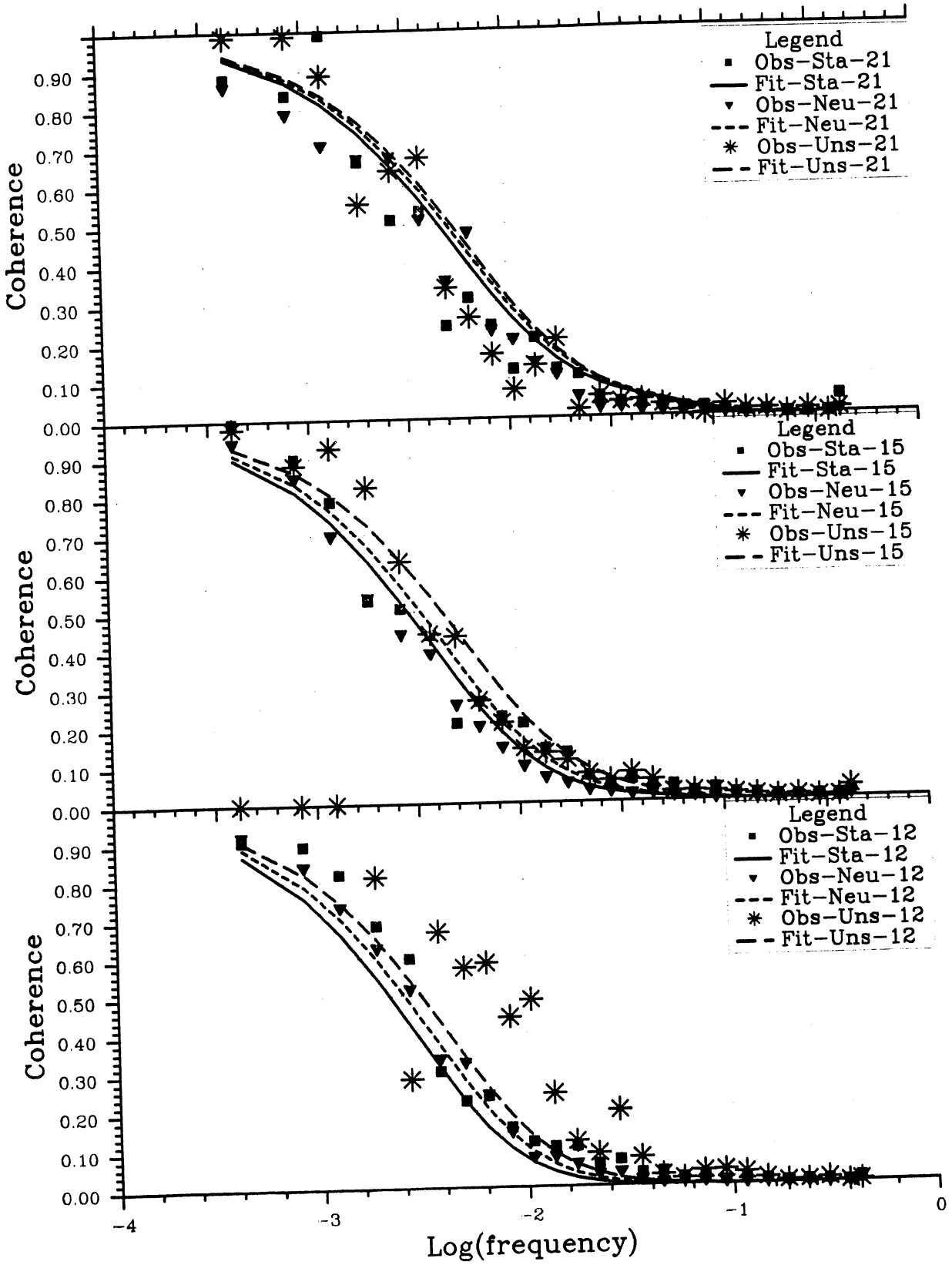

Fig. 5.4.14 Lateral coherence of wind speed versus frequency for 40 m height at Skipheia. Mast 2 - 4 data for the wind direction sector [198°,228°], approximally normal to the mast plane. Speed and lapse rate classes as indicated.

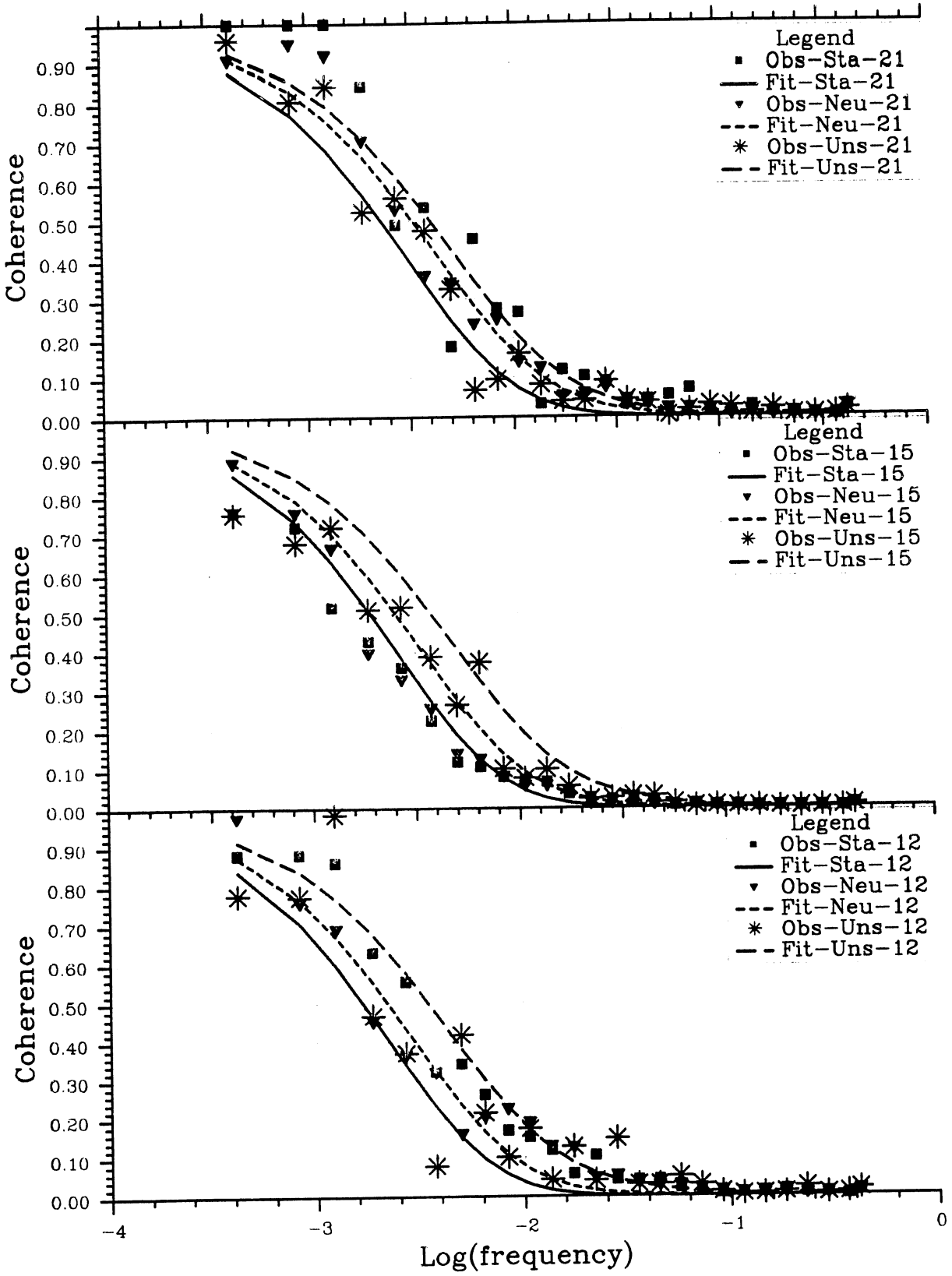

Fig. 5.4.15 As Fig. 5.4.14, but for 20 m height.

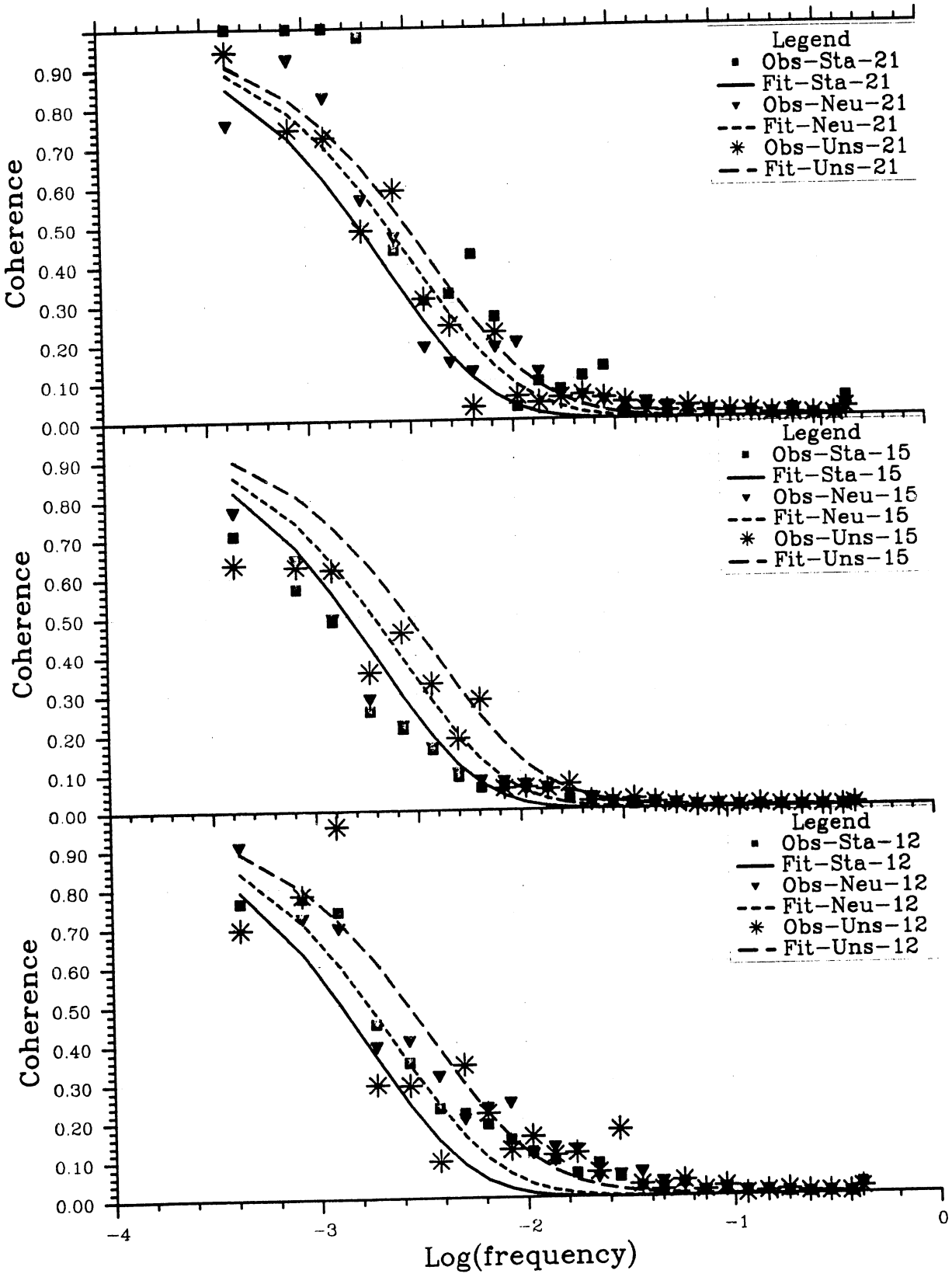

Fig. 5.4.16 As Fig. 5.4.14, but for 10 m height.

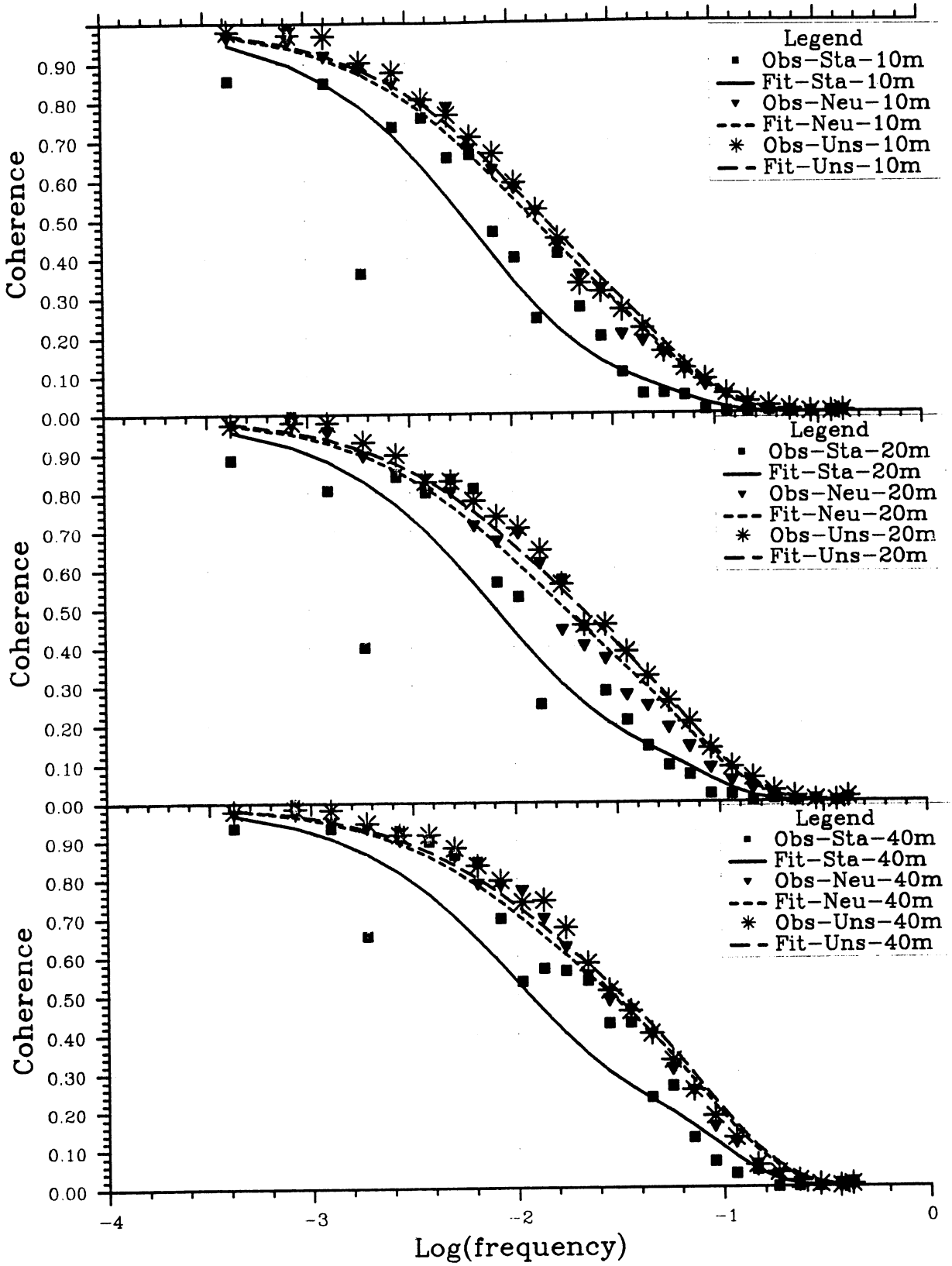

Fig. 5.4.17 Longitudinal coherence of wind speed for the heights 40, 20 and 10 m, 3 lapse rate classes and the lowest wind speed class versus frequency at Skipheia. Mast 2 - 4 data for the wind direction sector [288°,318°], along the mast plane.

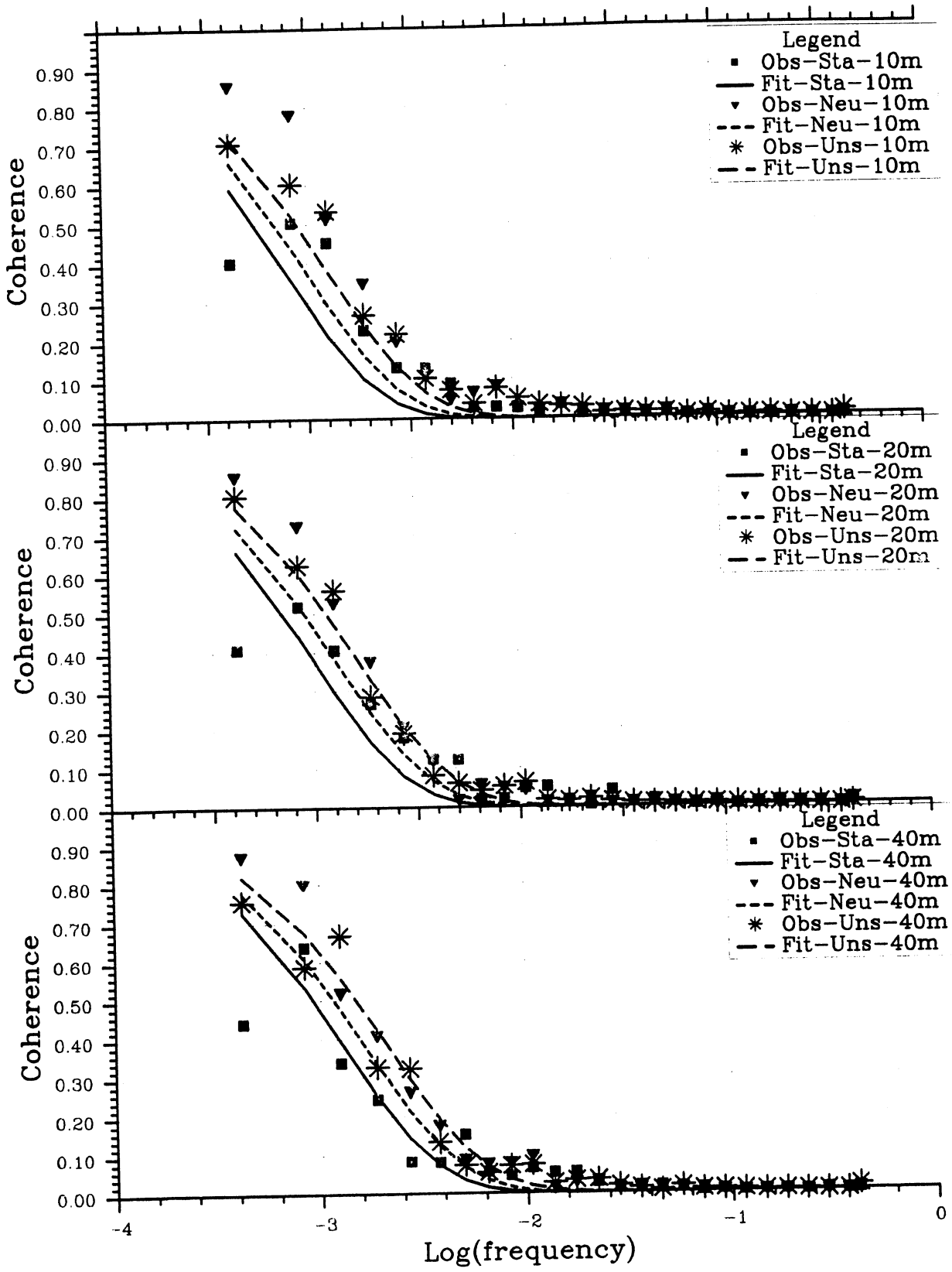

Fig. 5.4.18 Lateral coherence of wind speed for the heights 40, 20 and 10 m, 3 lapse rate classes and the lowest wind speed class versus frequency at Skipheia. Mast 2 - 3 data for the wind direction sector [277°,307°], approx. normal to the mast plane.

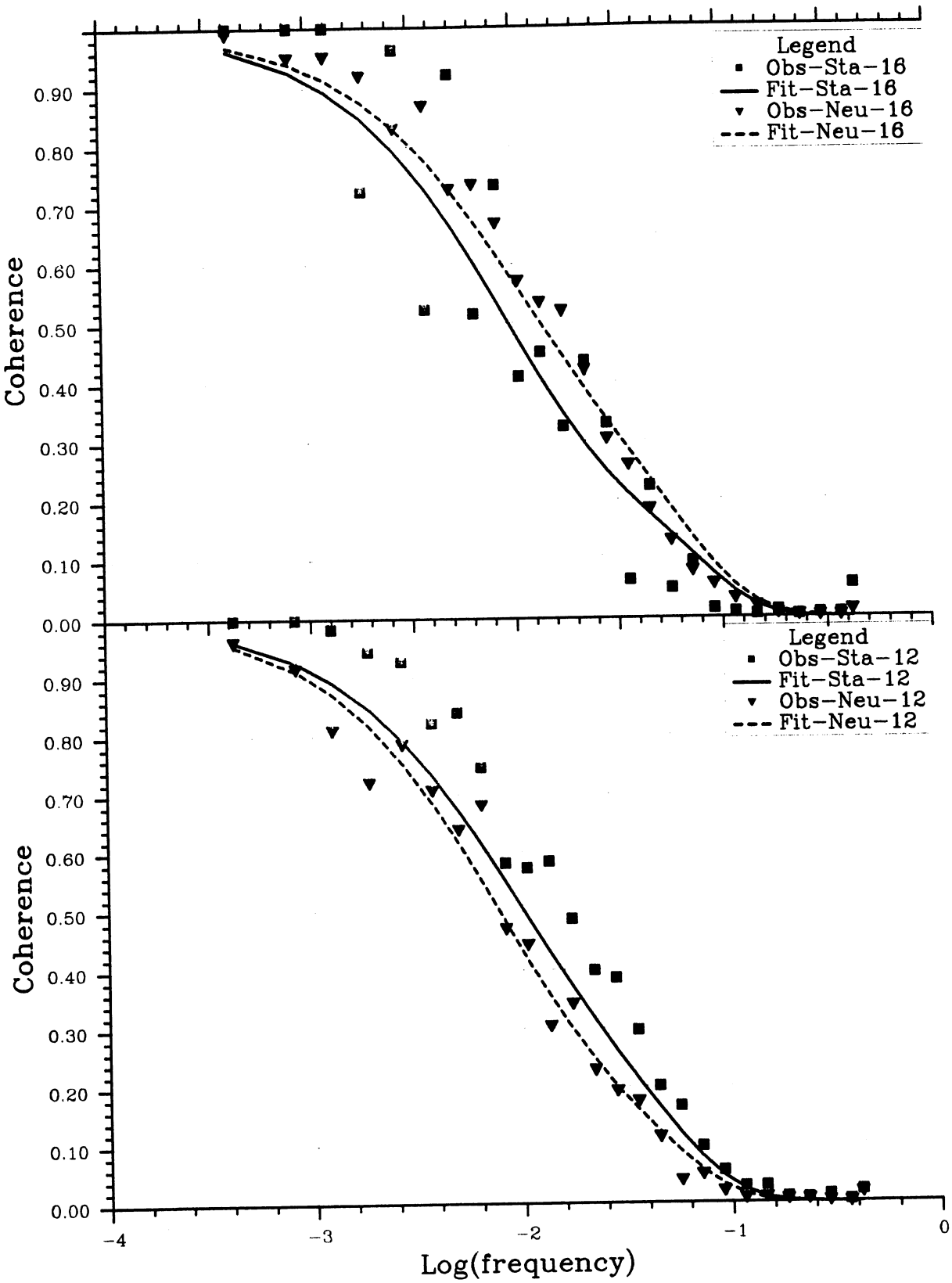

Fig. 5.4.19 Longitudinal coherence of wind speed for 40 m height, 2 lapse rate classes and 2 wind speed classes as indicated versus frequency at Skipheia. Mast 2 - 3 data for the wind direction sector [187°,217°], along the mast plane.

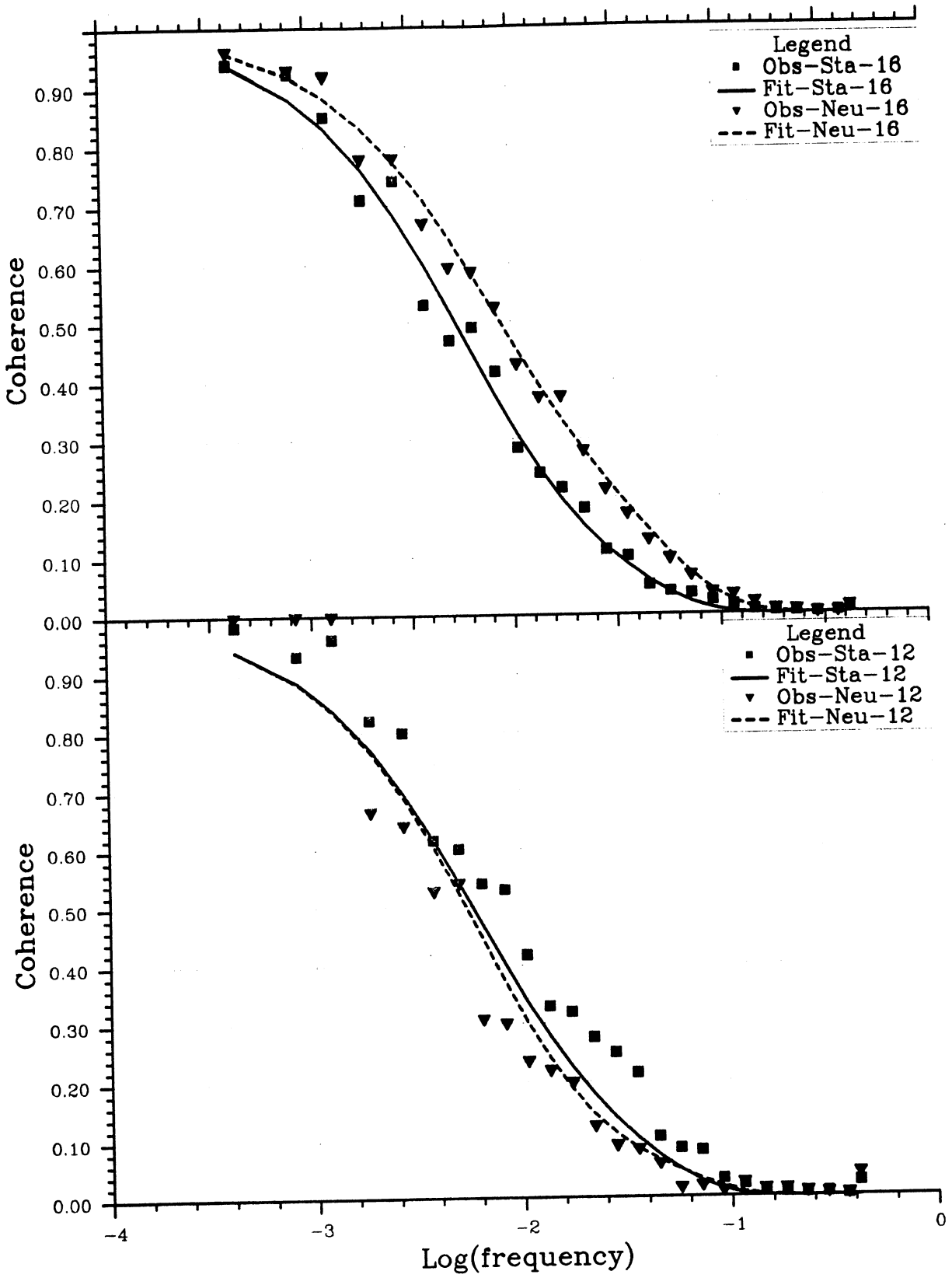

Fig. 5.4.20 As Fig. 5.4.19, but for 20 m height.

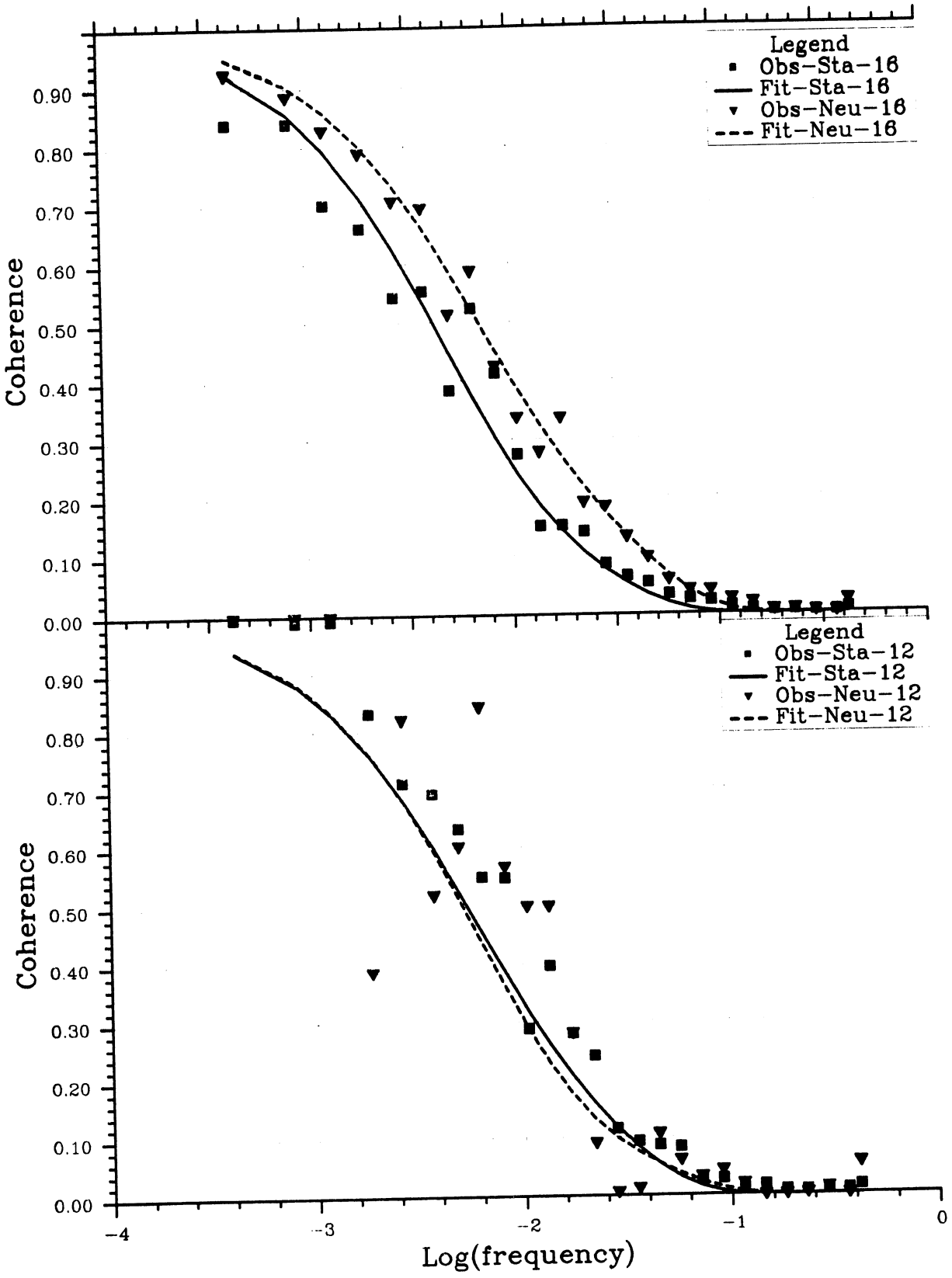

Fig. 5.4.21 As Fig. 5.4.19, but for 10 m height.

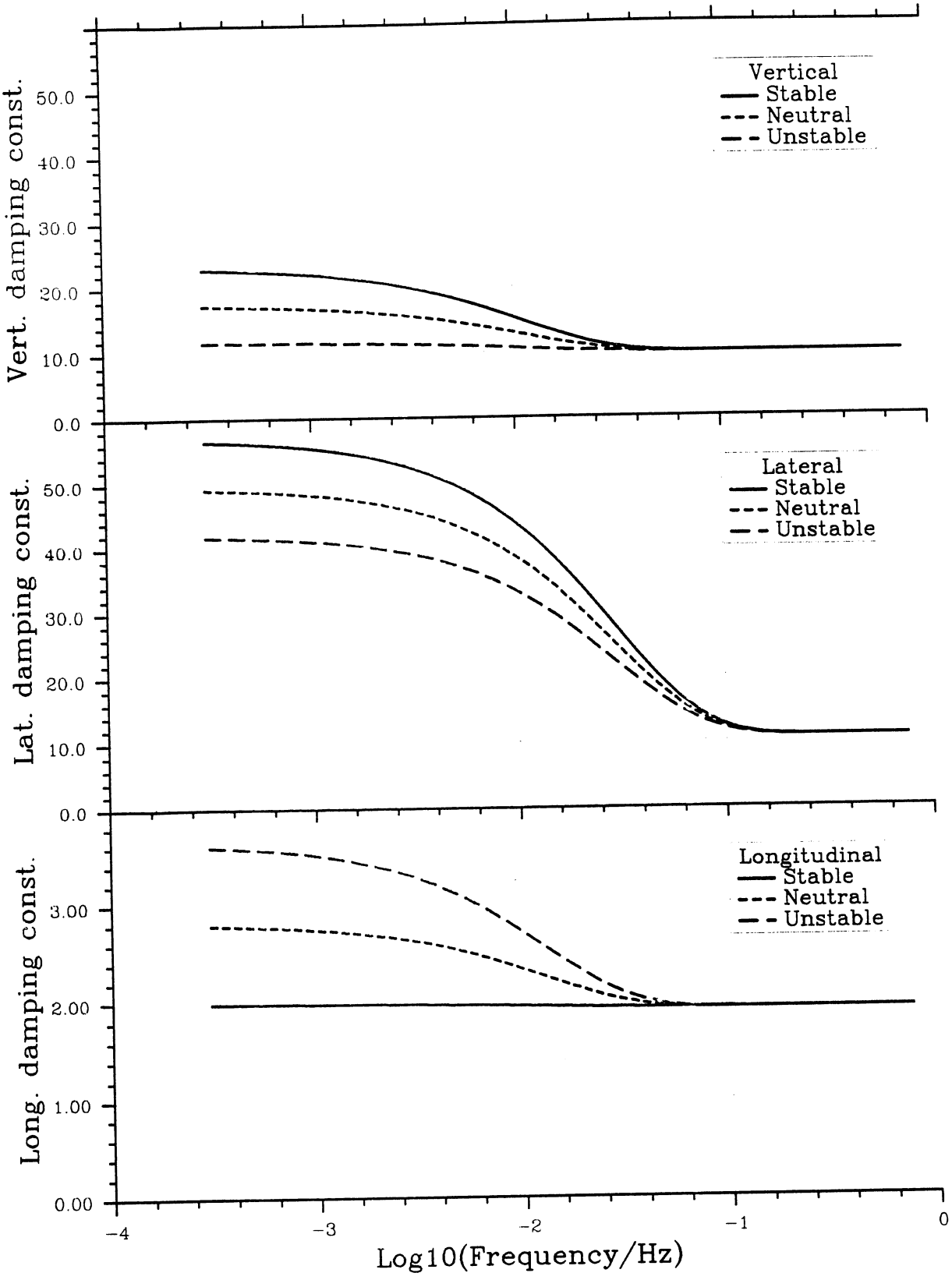

Fig. 5.4.22 The damping coefficients for vertical, lateral and longitudinal coherence versus frequency. The curves are calculated from the parameterizations discussed in the text for lapse rate values of 0 (stable), 10 (neutral) and 20 K/km (unstable atmosphere), and u_r = 20 m/s and z_g = 4.

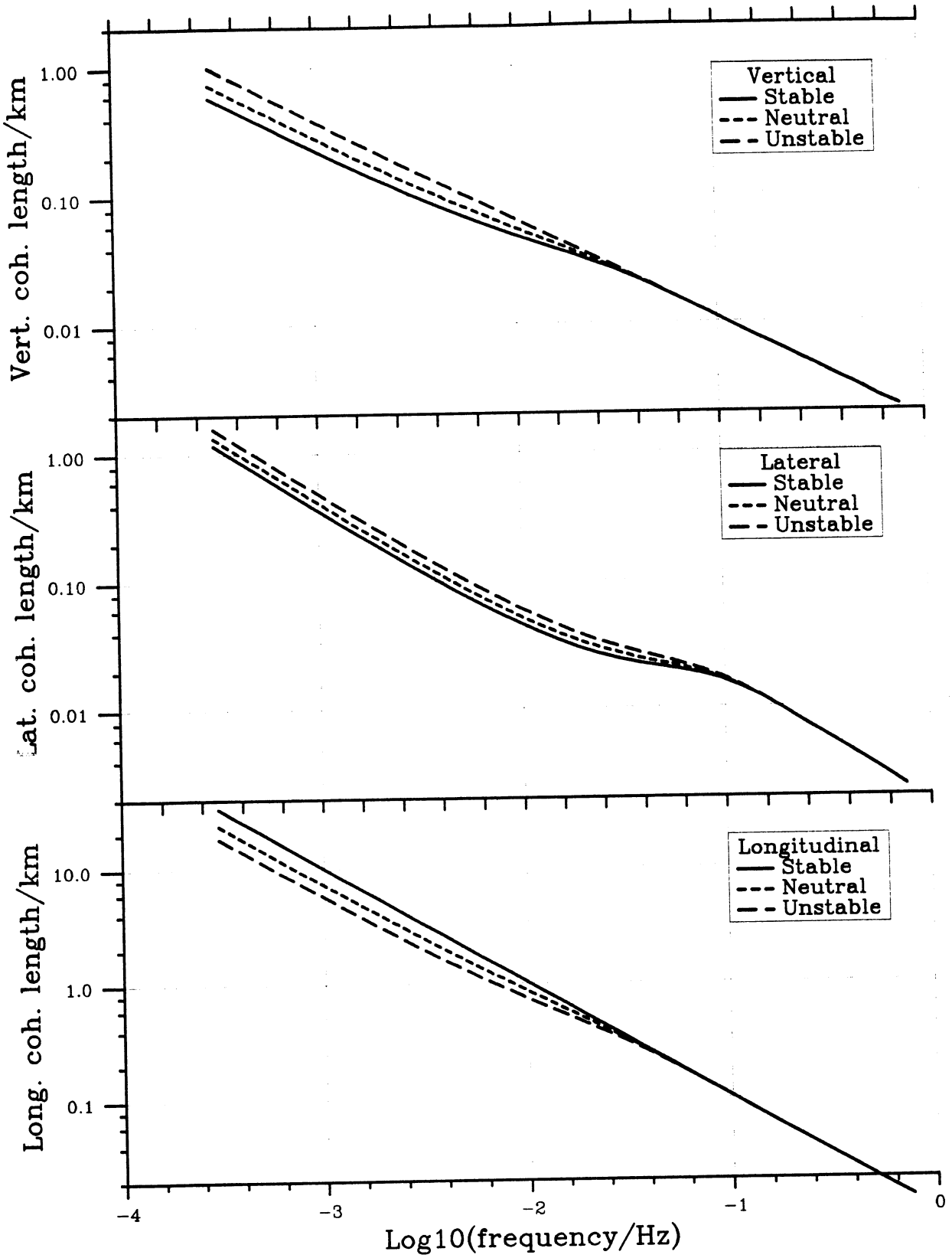

Fig. 5.4.23 Vertical, lateral and longitudinal coherence length versus frequency, for the same cases as in Fig. 5.4.22.

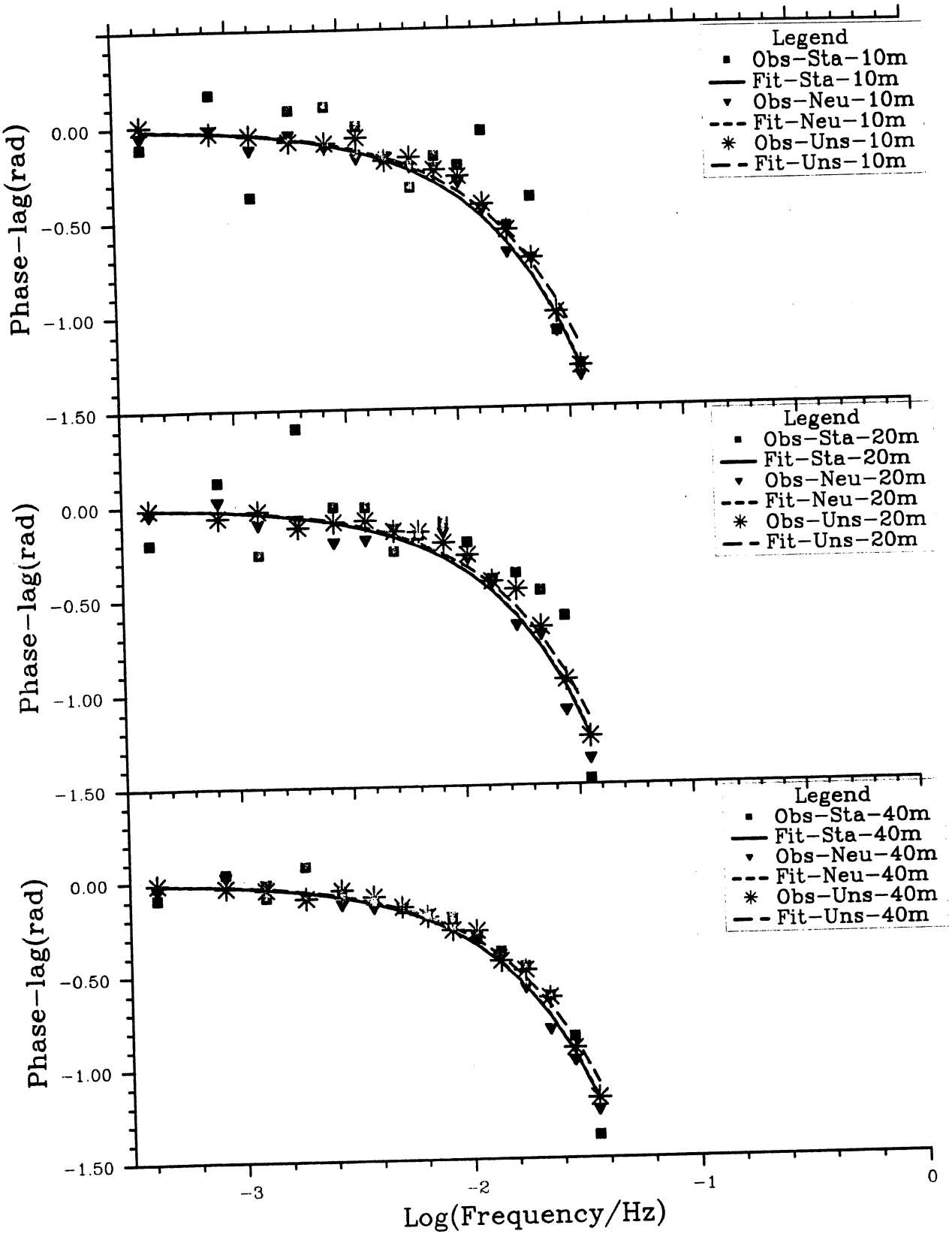

Fig. 5.4.24 Phase difference between sensors in mast 2 and 4 at Skipheia in a 30° sector along the masts (see text) versus frequency for the heights 40, 20 and 10 m, 3 lapse rate classes and the lowest wind speed class.

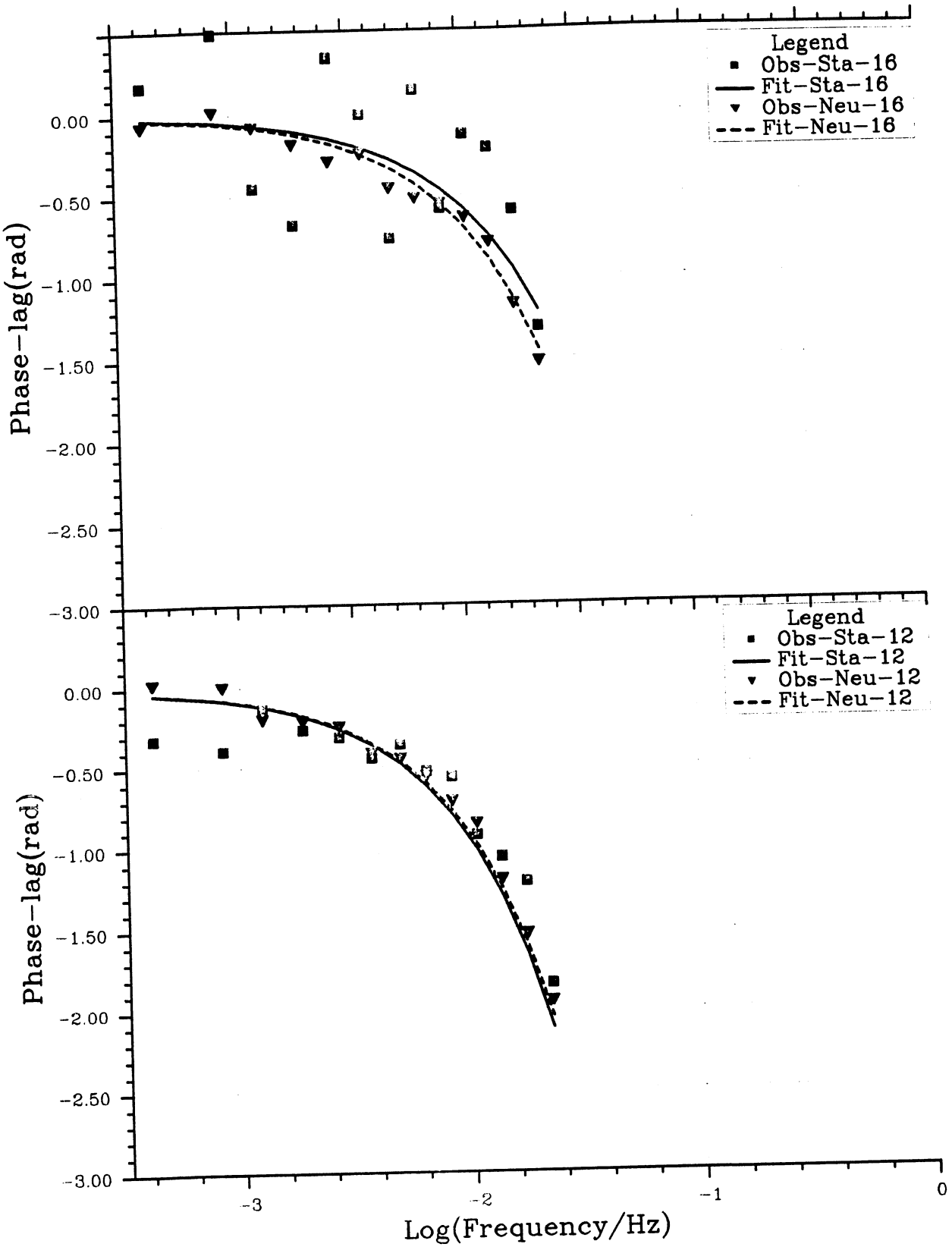

Fig. 5.4.25 Phase difference between sensors in mast 2 and 3 at Skipheia in a 30° sector along the masts (see text) versus frequency for the height 40 m, 2 lapse rate classes and 2 wind speed classes.

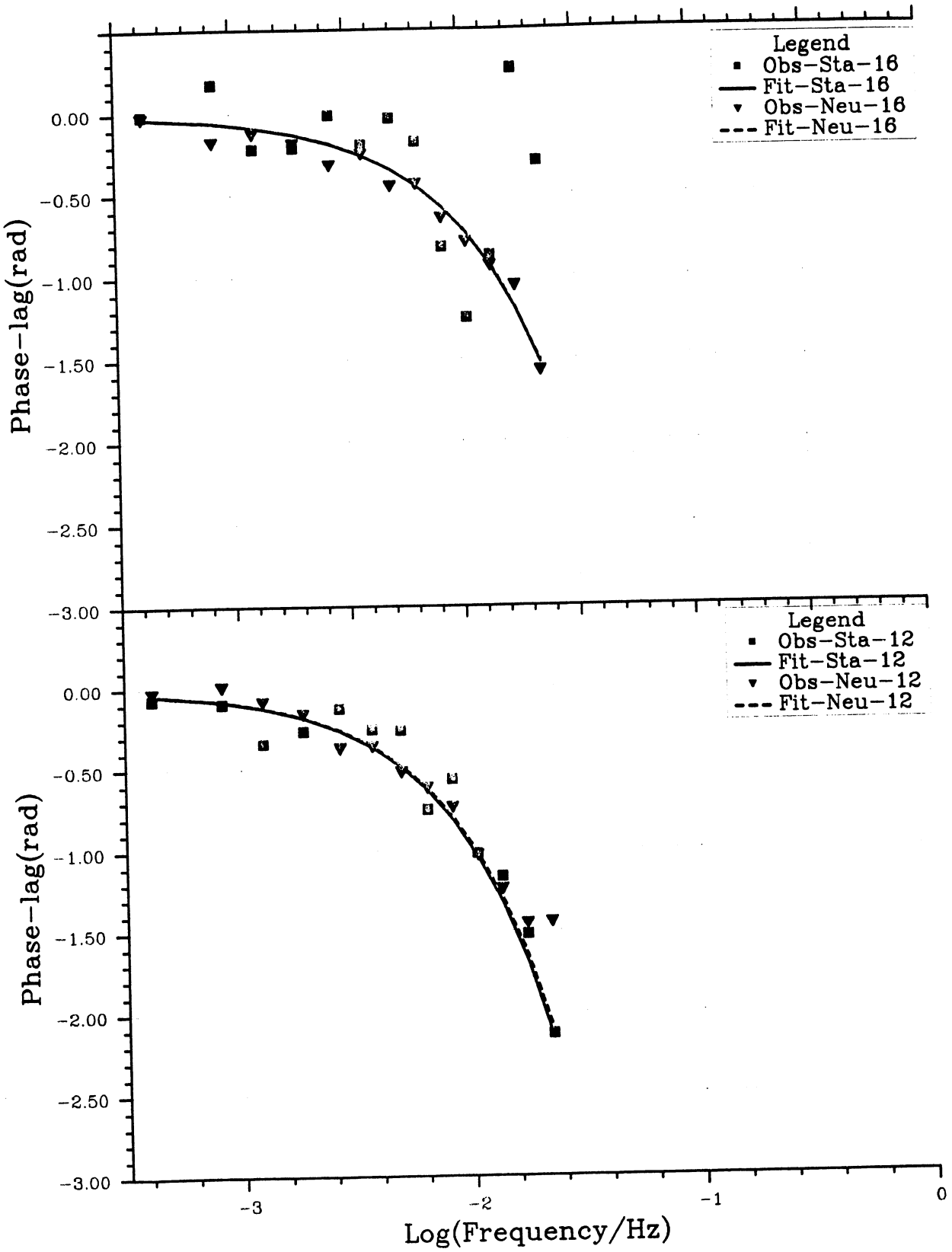

Fig. 5.4.26 As Fig. 5.4.25, but for 20 m height.

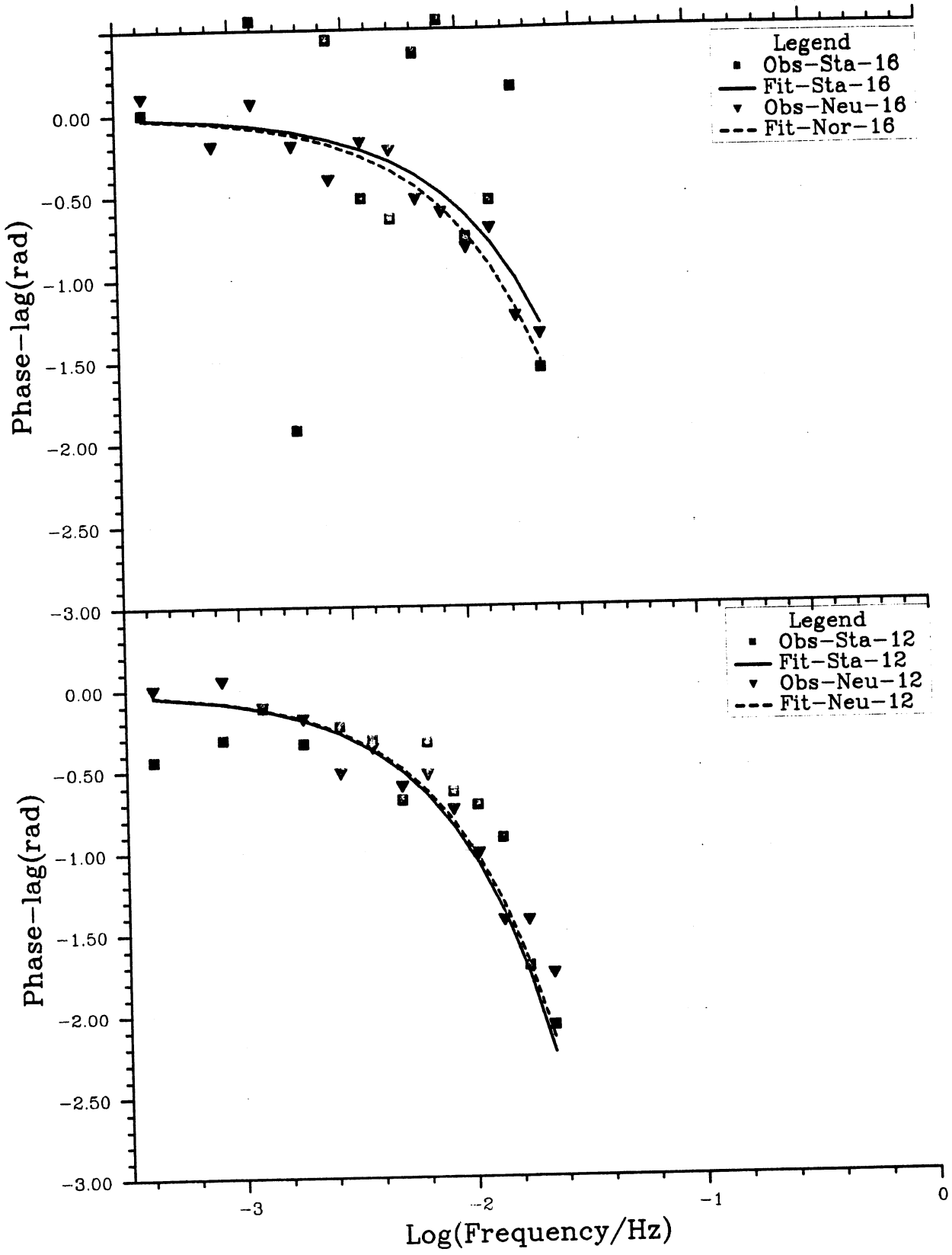

Fig. 5.4.27 As Fig. 5.4.25, but for 10 m height.

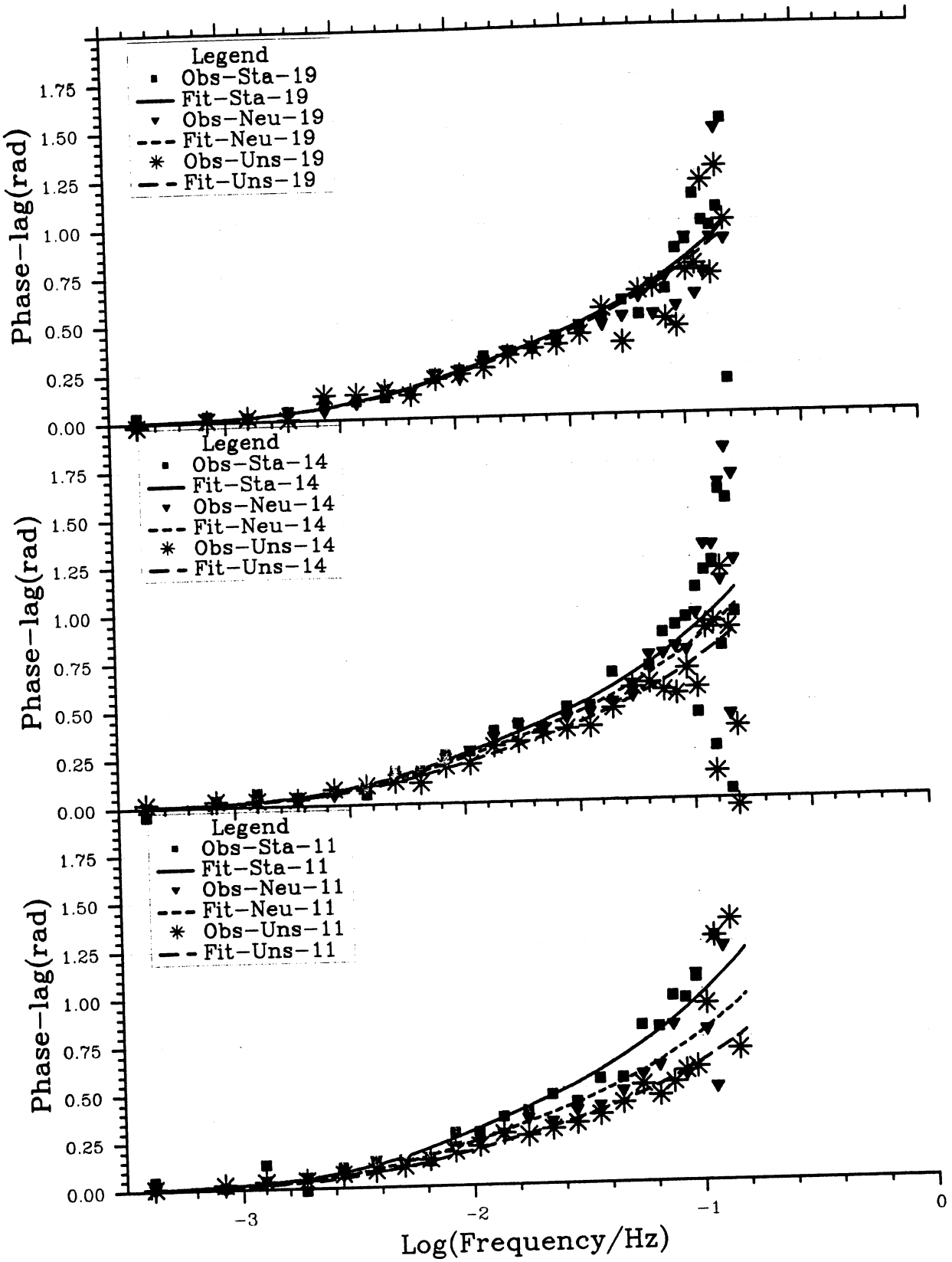

Fig. 5.4.28 Phase difference between sensors at 42 and 20 m height at Sletringen versus frequency for 3 lapse rate classes and 3 wind speed classes.

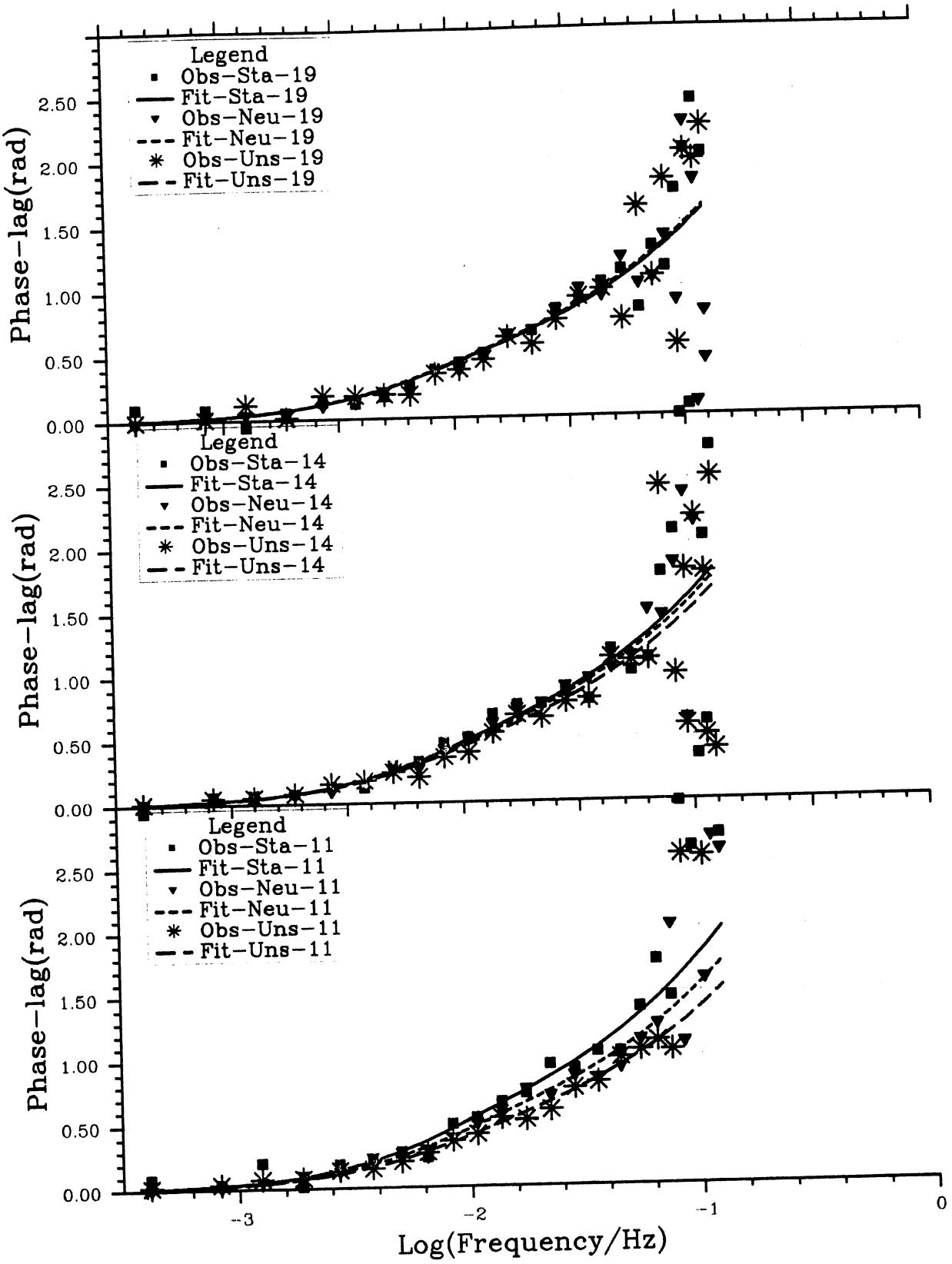

Fig. 5.4.29 As Fig. 5.4.28, but between 42 and 10 m height.

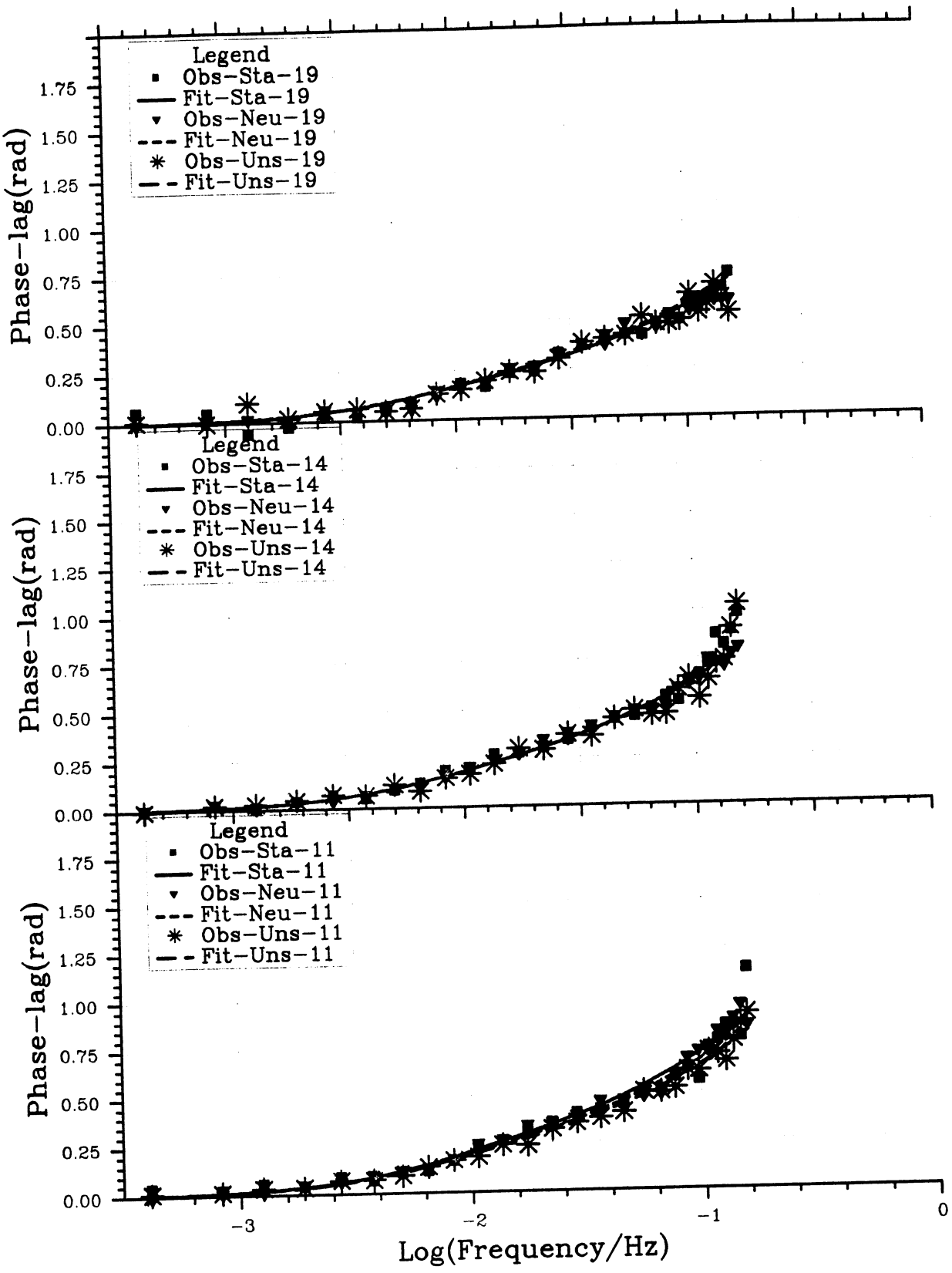

Fig. 5.4.30 As Fig. 5.4.28, but between 20 and 10 m height.

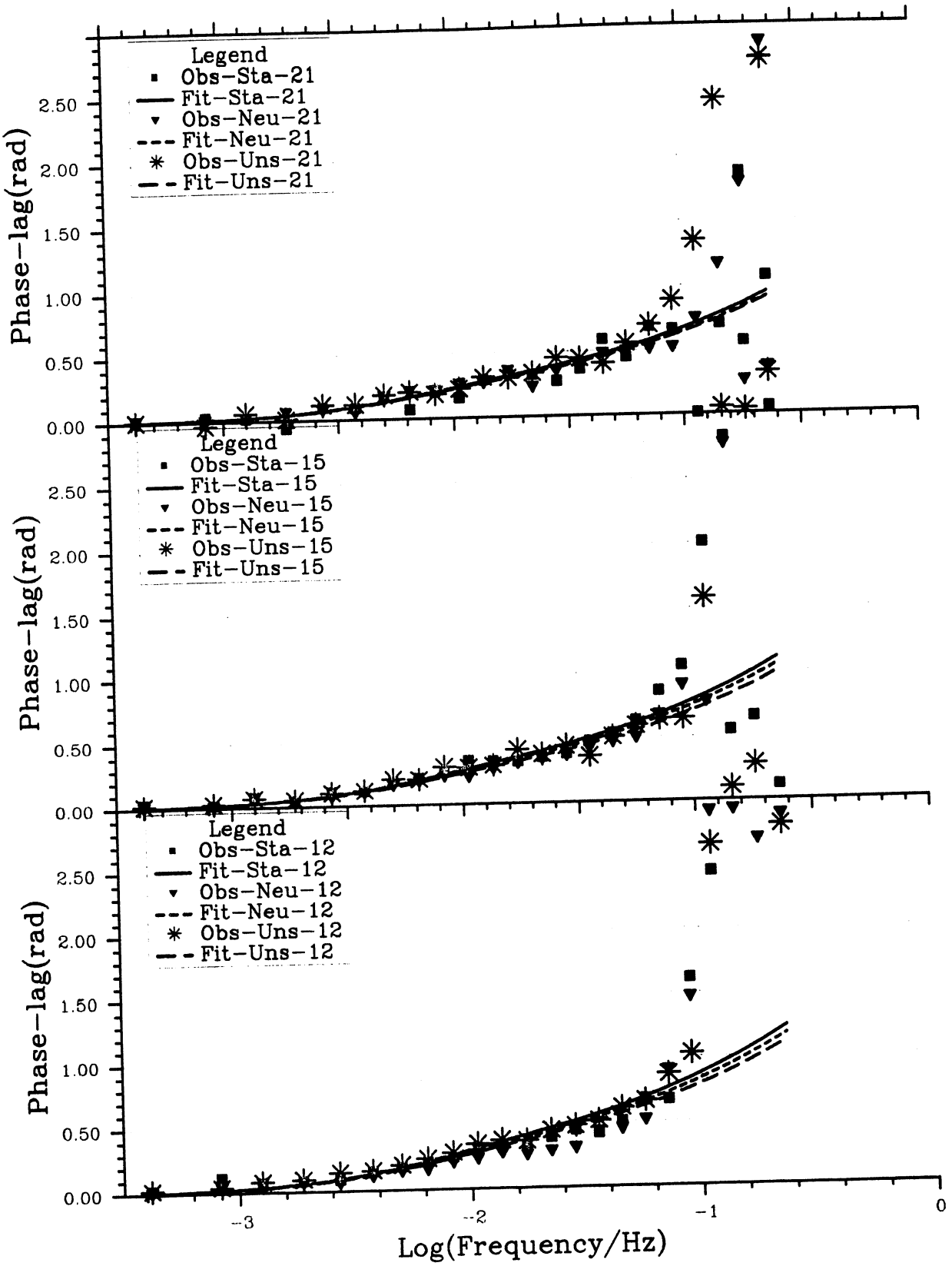

Fig. 5.4.31 As Fig. 5.4.28, but between 70 and 40 m height in mast 2 at Skipheia.

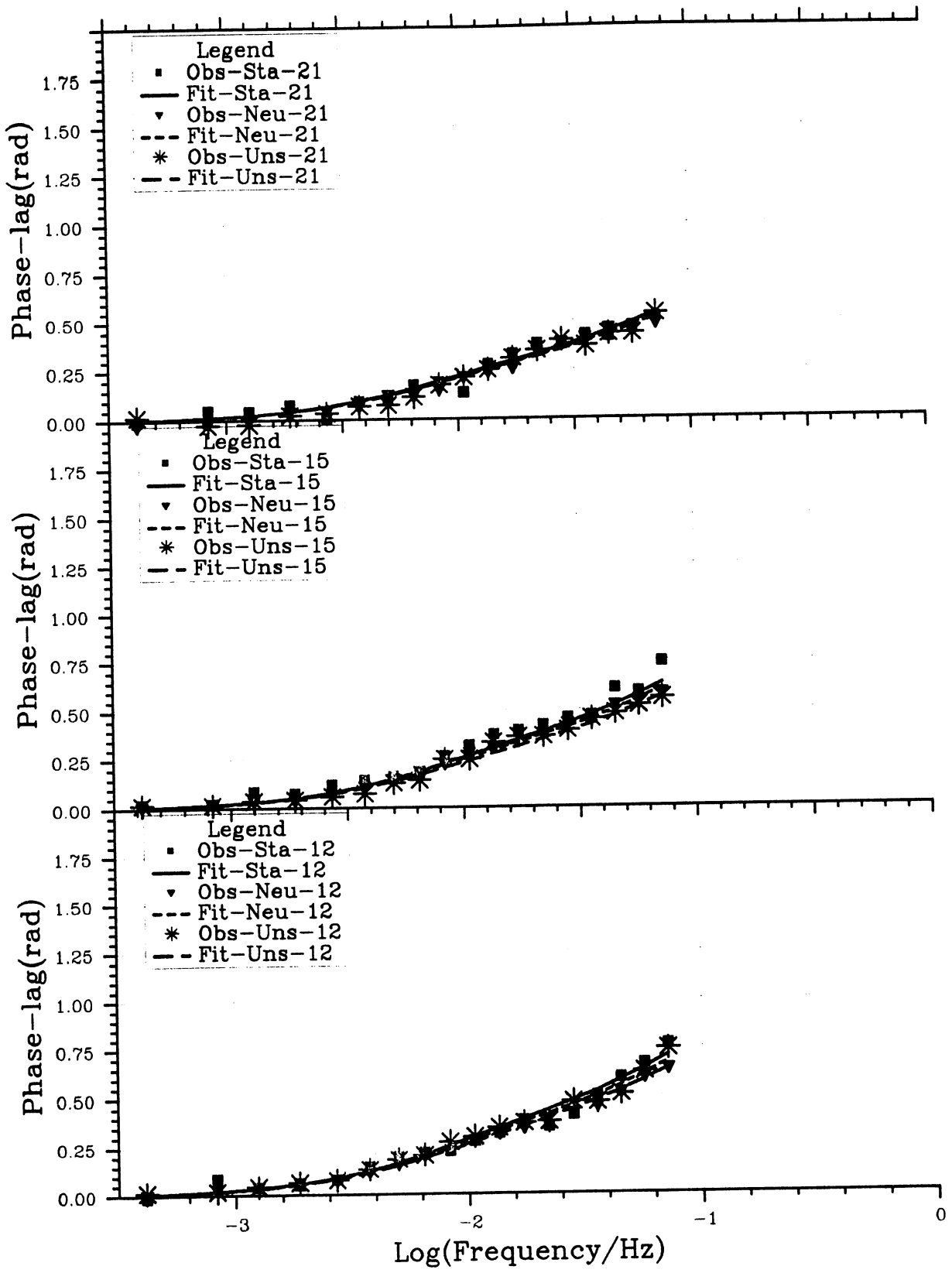

Fig. 5.4.32 As Fig. 5.4.28, but between 40 and 20 m height at Skipheia (mean values for 3 masts).

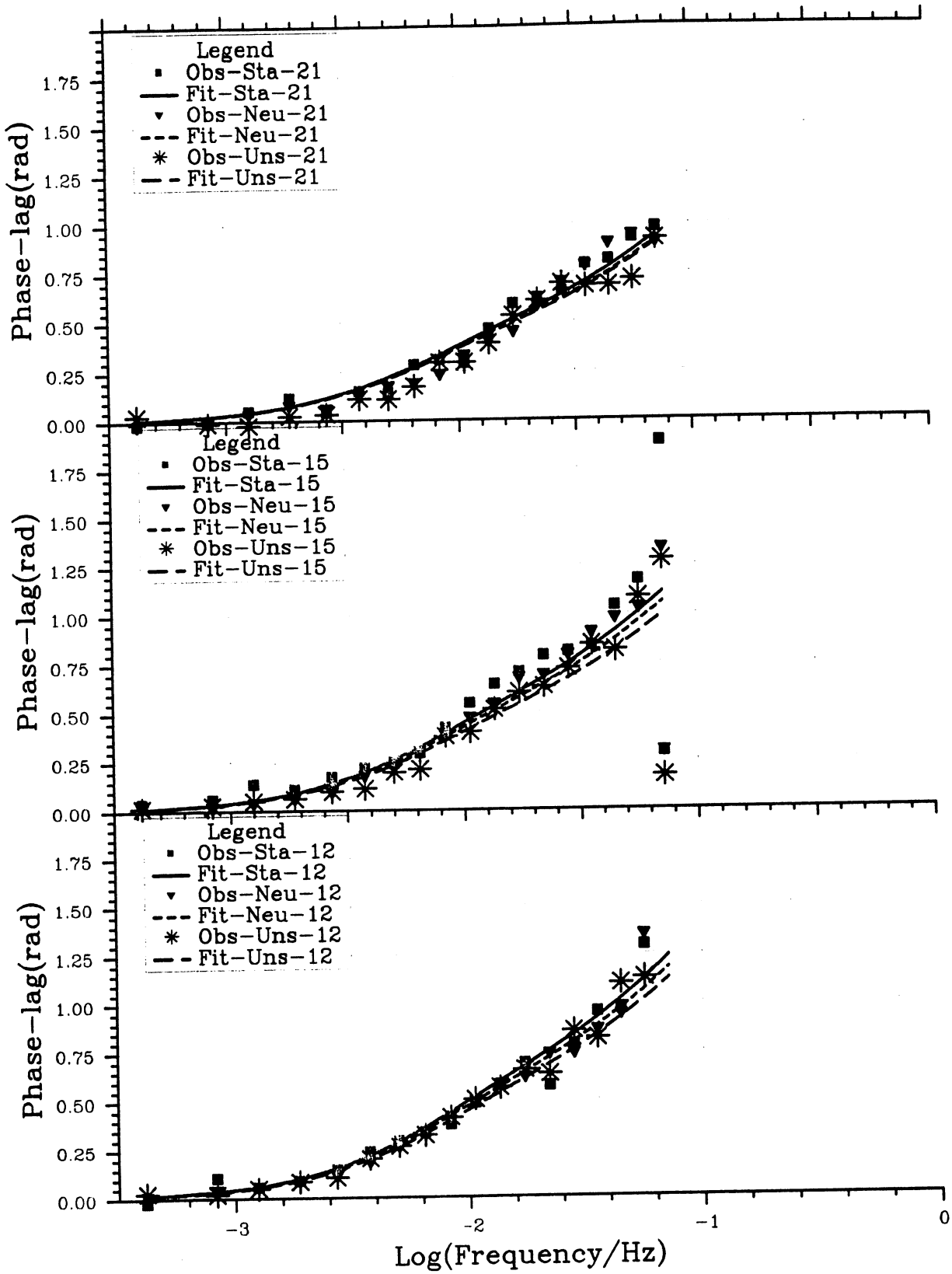

Fig. 5.4.33 As Fig. 5.4.28, but between 40 and 10 m height at Skipheia (mean values for 3 masts).

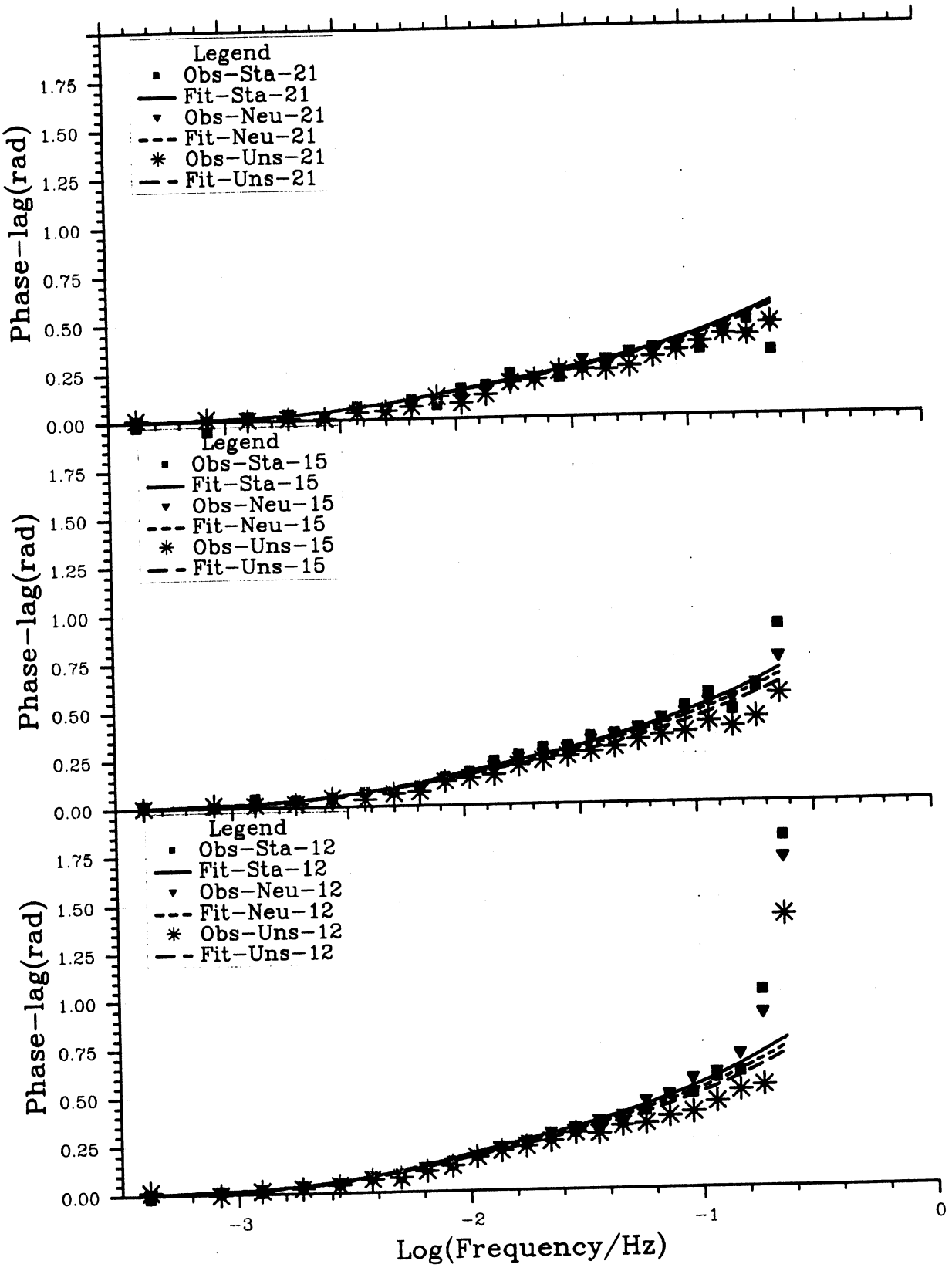

Fig. 5.4.34 As Fig. 5.4.28, but between 20 and 10 m height at Skipheia (mean values for 3 masts).